Universitätsmedizin Rostock

Klinik für Hals-Nasen-Ohrenheilkunde, Kopf- und Halschirurgie „Otto Körner“

Direktor: Univ.-Prof. Dr. med. Robert Mlynski

Neue Aspekte zu Mechanismus, Diagnostik und Therapie der altersbedingten Schwerhörigkeit

Kumulative Habilitationsschrift

Zur Erlangung des akademischen Grades

doctor medicinae habilitata (Dr. med. habil.)

der Universitätsmedizin Rostock

vorgelegt von

Dr. med. Lichun Zhang

geb. am 23.02.1985 in: Tongcheng, China

wohnhaft in Kavelstorf

Rostock, den 16.04.2025

https://doi.org/10.18453/rosdok_id00005289

Dieses Werk ist lizenziert unter einer
Creative Commons Namensnennung 4.0 International Lizenz.

Dekan: Prof. Dr. med. Bernd J. Krause

1. Gutachter: Prof. Dr. med. Robert Mlynski, Klinik und Poliklinik für Hals-Nasen-Ohrenheilkunde, Kopf- und Halschirurgie, Universitätsmedizin Rostock

2. Gutachter: Prof. Dr. med. Mark Praetorius, Klinik für Hals-, Nasen- und Ohrenheilkunde, UKE Hamburg

3. Gutachter: Prof. Dr. med. Friedrich Ihler, Klinik und Poliklinik für Hals-, Nasen-, Ohrenkrankheiten, Kopf- und Halschirurgie, Universitätsmedizin Greifswald

Jahr der Einreichung: 2025

Jahr der Verteidigung: 2026

Inhaltsverzeichnis

Verzeichnis der in dieser kumulativen Habilitationsschrift zusammengefassten Arbeiten 4

Abbildungsverzeichnis 5

Tabellenverzeichnis 7

Abkürzungsverzeichnis 8

Zusammenfassung 9

1. Einleitung 9

2. Cochleäre Synaptopathie bei Wüstenrennmäusen – neuer Aspekt zum Mechanismus 11

3. Diagnostische Ansätze 20

4. Therapieansätze 26

5. Schlussbetrachtung 34

6. Literaturverzeichnis 36

Anhang 41

Curriculum Vitae 41

Publikationsliste 45

Danksagung 53

Eidesstattliche Erklärung 55

Originalarbeiten 57

Verzeichnis der in dieser kumulativen Habilitationsschrift zusammengefassten Arbeiten

1. **Zhang L,** Engler S, Koepcke L, Steenken F, Köppl C. Concurrent gradients of ribbon volumen and AMPA-receptor patch volume in cochlear afferent synapses on gerbil inner hair cells. Hear Res. 2018;364:81-99. doi: 10.1016/j.heares.2018.03.028.

2. Heeringa AN, **Zhang L**, Ashida G, Beutelmann R, Steenken F, Köppl C. Temporal coding of single auditory nerve fibers is not degraded in aging gerils. J Neurosci. 2020;40(2):343-354. doi: 10.1523/JNEUROSCI.2784-18-2019. (**Co-Erstautor**).

3. Schmidt FH, Dörmann A, Ehrt K, Grossmann W, Mlynski R, **Zhang L**. The curvature quantification of wave I in auditory brainstem responses detects cochlear synaptopathy in human being. Eur Arch Otorhinolaryngol. 2024 May 4. doi: 10.1007/s00405-024-08699-6. Online ahead of print.

4. **Zhang L,** Mißler D, Ehrt K, Großmann W, Mlynski R, Schmidt FH. Can mismatch negativity be used as an indicator to predict central auditory deficits in individuals with normal hearing? Audiol. Res. 2025, 15(2), 43; https://doi.org/10.3390/audiolres15020043.

5. **Zhang L,** Schmidt FH, Cantre D, Brenzel R, Ehrt K, Großmann W, Langner S, Mlynski R. The predictive value of preoperative measurements of cochlear nerve diameters from MRT and postoperative speech perception in adult patients with cochlear implant. Otol Neurotol. 2024. doi: 10.1097/MAO0000000000004293. (**Co-Erstautor**).

6. Schmidt FH, **Zhang L,** Glabasnia MW, Schurzig D, Ehrt K, Cantre D, van Bonn-Ytrehus SM, Großmann W, Mlynski R. Systematic overestimation of the angular insertion depth of electrode arrays in cochlear implantation (CI) patients with small cochlea by imaging processing software. Otol Neurotol. Otol Neurotol. 2024. doi: 10.1097/MAO.0000000000004294. Online ahead of print. (**Co-Erstautor**)

7. Schmidt FH, Stauga P, Mißler D, Ehrt K, Großmann W, Mlynski R, Zhang L. Electrically evoked mismatch negativity from speech stimuli as an objective measure of cochlear implant performance. Front Neurosci. 2025. doi:10.1097/MAO0000000000004145.

Abbildungsverzeichnis

Abb. 1 Beispiel für die Bildanalyse eines immunmarkierten konfokalen Stapels ---- 13

Abb. 2 Streudiagramme des normalisierten Volumens der präsynaptischen Ribbons im Vergleich zum normalisierten Volumen ihres Co-lokalisierten postsynaptischen GluR2-Patches für einzelne identifizierte funktionelle Synapsen ---- 13

Abb. 3 Normalisierte Volumina funktioneller Synapsenelemente ---- 14

Abb. 4 Normalisierte Volumina funktioneller Synapsenelemente in Abhängigkeit von ihrer relativen Position entlang zweier Haarsinneszellachsen ---- 15

Abb. 5 Wüstenrennmäuse zeigen unterschiedliche Grade des altersbedingten Hörverlusts bei verschiedenem Alter. ---- 17

Abb. 6 Das Phasen-Locking auf Reintöne wird durch das Altern nicht beeinträchtigt. ---- 18

Abb. 7 Die Peakamplitude und Peakbreite aus 'DifCor' werden vom Alter nicht beeinflusst. 19

Abb. 8 Die Peakamplitude und Peakbreite aus 'SumCor' werden vom Alter nicht beeinflusst. ---- 19

Abb. 9 Die Spontanrate (SR) des Hörnervs nimmt mit altersbedingtem Hörverlust ab. ---- 20

Abb. 10 Beispiele zur Quantifizierung der Welle I in BERA-Aufzeichnungen ---- 21

Abb. 11 Hörschwellen aller Probanden im Frequenzbereich von 0,125 kHz bis 16 kHz ---- 22

Abb. 12 Die Korrelationsanalysen der Amplitude, Fläche und Krümmung der Welle I der BERA mit EHF-Schwellen ---- 22

Abb. 13 Die Korrelationsanalysen der Amplitude, Fläche und Kurvenkrümmung mit dem Alter ---- 23

Abb. 14 Der Vergleich der verschiedenen Parameter der Welle I mit wiederholter k-facher Kreuzvalidierung ---- 23

Abb. 15 Messung der Amplitude der Potentiale ---- 27

Abb. 16 Vergleich der kortikalen Potentiale in Bezug auf die MMN, berechnet als Differenz zwischen abweichenden und Standardreizen, bei Sprach- und Reintonbedingungen ---- 27

Abb. 17 Screenshot von 3D Slicer, der die Messung der Flächen des N. cochlearis (ACN), des N. facialis (AFN) und des inneren Gehörgangs (AIEC) in der parasagittalen Sektion zeigt. ---- 27

Abb. 18 Fläche des CN normalisiert auf die Fläche des Gesichtsnervs (ACN/AFN) und die Sprachverständlichkeit nach der anfänglichen Anpassung für vier Gruppen mit unterschiedlichem Grad des asymmetrischen Hörverlustes ---- 28

Abb. 19 Postoperatives Röntgenbild (Stenvers) zur Bestimmung des Insertionswinkels, veranschaulicht am Beispiel der Elektrode 6 aus einem FLEXsoft-Elektrodenarray --- 29

Abb. 20 Streudiagramm der Beziehung zwischen der geschätzten und gemessenen maxAID veranschaulicht ---- 29

Abb. 21 Die Optimierung der Schätzung der maximalen Insertionstiefe (maxAID) mithilfe von OTOPLAN beinhaltete die Anpassung des Offsets am runden Fenster (RW). ---- 30

Abb. 22 Darstellung der EEG-Antworten auf die verschiedenen Reize in der Kontroll- und der CI-Gruppe ---- 32

Abb. 23 Vergleich der Antworten auf die verschiedenen Reize zwischen der Kontrolle- und der CI-Gruppe ---------- 33

Abb. 24 Vergleich der EEG-Antworten auf die verschiedenen Reize zwischen der CI-Gruppe mit gutem und schlechtem postoperativen Sprachverstehen ---------- 33

Tabellenverzeichnis

Tab. 1 Statistische Analyse der Korrelation zwischen CN-Geometrie und WRS in verschiedenen Gruppen zu verschiedenen Zeitpunkten nach der Aktivierung des CI. ----------27

Abkürzungsverzeichnis

ACN	Querschnittsfläche des N. cochlearis
AFN	Fläche des N. facialis
AHLm	mäßiger asymmetrische Hörverlust
AIEC	Fläche des inneren Gehörgangs
AMPA	α-Amino-3-hydroxy-5-methyl-4-isoxazolpropionsäure
ANF	Hörnervfasern
BERA	Hirnstammaudiometrie
BF	*Beste Frequenz*
CDL	Länge des Ductus cochlearis
CI	*Cochlea-Implantate*
CN	*N. cochlearis*
EEG	Elektroenzephalografie
EHF	Extended high frequency
EHFT	Extended high-frequency threshold
FF	*Erstanpassung*
IHC	innere Haarsinneszelle
M	Modiolus
MA	mittelalte
maxAID	maximale Inerstionstiefe
MMN	Mismatch Negativität
nHL	normalisierte Hörschwelle
OL	*alte*
RMSE	Wurzel des mittleren Quadratischen Fehlers
RW	rundes Fenster
SAC	Shuffled-Autokorrelogramm
SR	*Spontanrate*
SSC	Oberer Bogengang
SSD	Einseitige Taubheit
V	Vestibulum
VM	Volumen des Modiolus
VS	*Vektor-Stärke*
WRS	Wortkennungstest
XAC	Kreuz-Stimulus-Autokorrelogramm
YO	*junge*

Zusammenfassung

1. Einleitung

Altersbedingte Schwerhörigkeit, auch als Presbyakusis bekannt, ist die häufigste Sinnesstörung beim älteren Menschen (1). Diese nimmt mit dem Alter zu und betrifft bis zu 84,3% der Patienten, die über 80 Jahre alt sind. Die geschätzte Prävalenz liegt bei über 500 Millionen betroffenen, die im Jahr 2025 über 60 Jahre alt sein werden (2). Altersbedingte Schwerhörigkeit tritt häufiger bei Männern auf als bei Frauen (2-4). Verschiedene potenzielle Faktoren können diese Unterschiede verursachen, wie z.B. Sexualhormone (Östrogen) oder Arbeitsrisiken mit Lärmexposition (5-8). Es ist bekannt, dass Östrogen vielen Organsystemen, einschließlich des Hörsystems, Schutz bietet, auch wenn der genaue Mechanismus bisher nicht geklärt ist. Es gibt jedoch viele indirekte Hinweise. Beispielsweise haben Frauen mit Turner-Syndrom, die normalweise an einem Östrogenmangel leiden, eine frühere altersbedingte Schwerhörigkeit im Vergleich zur Kontrollgruppe (9). Die Menopause ist oft mit mitochondrialer Dysfunktion, Neuroinflammation, synaptischen Funktionsstörungen, kognitiven Defiziten und erhöhten Risiken für altersbedingte Schwerhörigkeit verbunden. Zusätzlich ist bekannt, dass Männer bei der Arbeit häufiger Lärm ausgesetzt sind als Frauen (8).

Typischerweise klagen Patienten über eine zunehmende, irreversible, sensorineurale Schwerhörigkeit mit steigendem Alter. Diese beginnt meist im Hochtonbereich und schreitet langsam in die mittleren und niedrigen Frequenzbereiche fort (10). Pathologisch beeinflusst die altersbedingte Schwerhörigkeit nicht nur die Cochlea, sondern die gesamte Hörbahn (11). Neue Studien fokussieren sich hauptsächlich auf die frühen Stadien der altersbedingten Schwerhörigkeit, einschließlich Mechanismen, Diagnostik und Therapieplanung (11,12).

Im frühen Stadium der altersbedingten Schwerhörigkeit beklagen die Patienten am häufigsten ein eingeschränktes Sprachverständnis in Umgebungsgeräuschen. In der Klinik wird diese Diagnose normalerweise nicht durch Routine-Diagnostikmethoden festgestellt. Im letzten Jahrzehnt beschreibten Autoren dieses Phänomen als versteckten Hörverlust (Hidden hearing loss) (13-15). In Tiermodellen haben Studien gezeigt, dass eine Erkrankung der Verbindung zwischen inneren Haarsinneszellen und dem auditorischen Nerv, bekannt als cochleare Synaptopathie, die Ursache sein könnte (16). Beim Menschen ist eine direkte Untersuchung der cochlearen Synapsen nicht möglich. Daher versuchen viele Wissenschaftler neue diagnostische Methoden zur Feststellung des versteckten Hörverlusts zu entwickeln. Es gibt derzeit viele Studien, die das Felsenbein von verstorbenen Menschen untersuchen. Diese Studien zeigen, dass die Anzahl der cochleären Synapsen bei älteren Menschen deutlich geringer ist, als bei einer jüngeren Kontrollgruppe (17).

Die Amplitude der Welle I der Hirnstammaudiometrie (BERA) wurde bereits in Tiermodellen untersucht und hat gezeigt, dass eine Korrelation zwischen der cochleären Synaptopathie und der Amplitude der Welle I besteht. Bei Mäusen mit cochleärer Synaptopathie ist die Amplitude der Welle I der BERA geringer (16, 18-20). Allerdings sind die Wellen I beim Menschen relativ klein und variabel (21). Daher ist die Amplitude der Welle I der BERA für die Diagnose der cochleären Synaptopathie beim Menschen wenig geeignet.

Der Stapediusreflex, auch als akustischer Reflex oder Mittelohrreflex bekannt, bezeichnet die Kontraktion des M. stapedius im Mittelohr, die durch erhörte Schalldruckpegel ausgelöst wird, um das Innenohr vor Schäden zu schützen. Tierexperimentelle Studien haben gezeigt, dass der Stapediusreflex zur Diagnose der cochleären Synaptopathie eingesetzt werden kann (22). In einer Studie untersuchten Wissenschaftler Mäuse mit cochleärer Synaptopathie, die durch Lärmtraumata verursacht wurden und fanden heraus, dass die Schwelle des Stapediusreflexes erhöht war und die maximale Amplitude bei Mäusen mit cochleärer Synaptopathie abnahm (22). Der potenzielle Mechanismus könnte darin begründet sein, dass die für den Stapediusreflex hauptsächlich verantwortlichen afferenten Nervenfasern solche mit niedriger Spontanrate sind (22-24) und dass diese Nervenfasern anfälliger für die cochleäre Synaptopathie sind. Allerdings zeigte eine neue Studie an Menschen andere Ergebnisse. In dieser Studie fanden die Autoren keine Korrelation zwischen dem Stapediusreflex und Tinnitus, Sprachverstehen in Umgebungsgeräuschen oder Lärmtraumata bei Menschen mit normalen Hörschwellen im klinischen Audiogram, die jedoch an einer cochleären Synaptopathie leiden könnten (25).

Extended high-frequency threshhold (EHFT) ist eine relativ neue Methode zur Diagnose der cochleären Synaptopathie beim Menschen. Im Jahr 2016 rekrutierten Liberman et al. (26) junge Probanden. Alle Probanden hatten keine Hörprobleme und auch keine audiologische Vorgeschichte. Die klinische Untersuchung zeigte keine Auffälligkeiten und die klinische Audiometrie ergab normale Hörschwellen. Ein Fragebogen zu Problemen beim Sprachverstehen im Störgeräusch wurde durchgeführt und die Probanden wurden in zwei Gruppen eingeteilt: eine Gruppe ohne anamnestische Probleme beim Sprachverstehen im Störgeräusch und eine Gruppe mit Problemen beim Sprachverstehen im Störgeräusch. Anschließend untersuchten und analysierten die Wissenschaftler die Schwellen im erweiterten hochfrequenten Bereich und entdeckten, dass die Schwellen in der Gruppe mit Problemen beim Sprachverstehen im Störgeräusch signifikant höher waren, als in der Gruppe ohne Probleme beim Sprachverstehen im Störgeräusch (26). Es ist bekannt, dass die Deterioration der EHFT nicht von der cochleären Synaptopathie, sondern von Erkrankungen der äußeren Haarsinneszellenen verursacht wird. Frühere Tiermodelle haben jedoch gezeigt, dass die cochleäre Synapsen in der apikalen und mittleren Windung anfälliger sind als die äußeren Haarsinneszellenen in der basalen Windung (27, 28). Daher ist es möglich, dass die EHFT als indirekter Biomarker für die cochleäre Synaptopathie verwendet werden kann.

Im Jahr 2022 entwickelte Bao et al. eine neue Methode, die Analyze der Krümmung der Welle I der BERA, und verwendete diese in Mäusemodellen zur Diagnostik. Sie verglichen sie mit verschiedenen anderen Verfahren und entdeckten, dass die Krümmung der Welle I der BERA deutlich sensitiver und zuverlässiger ist im Vergleich dazu, insbesondere der Amplitude der Welle I (29). Wie diese Methode beim Menschen funktioniert, ist jedoch bis jetzt unklar. Zudem stellt sich die Frage, wie sich das zentrale auditive System im Alter verändert und ob es Biomarker gibt, die solche frühen Veränderungen erfassen können. Bisher gibt es darauf in der Literatur keine eindeutige Antwort.

Die konventionelle Therapie für altersbedingte Schwerhörigkeit ist die Hörrehabilitation mit Hörgeräten. Wenn sich die Hörschwelle weiter verschlechtert, können konventionelle Hörgeräte die normale Hörleistung nicht mehr verbessern. Cochlea-Implantate (CI) kommen dann zum Einsatz. Die moderne CI-Therapie zeigt im Durchschnitt ein sehr gutes postoperatives Sprachverstehen. Wenn jedoch der individuelle Patient betrachtet wird,

können die Ergebnisse stark variieren. Manche Patienten haben ein sehr gutes Sprachverstehen und können beispielsweise problemlos Musikhören, während andere nur Geräusche erkennen können, ohne offenes Sprachverstehen (30). Insgesamt gibt es viele Faktoren, wie z.B. Alter, die Dauer der Schwerhörigkeit, den Zustand des N. cochlearis, die das postoperative Sprachverstehen beeinflussen können (30-34). Wissenschaftler in diesem Bereich fokussieren sich hauptsächlich auf die präoperative Einschätzung des postoperativen Sprachverstehens, das intraoperative Monitoring der CI-Elektrodenlage und -funktion sowie postoperativen Anpassungen und zentrale Adaptionsprozesse zur Erklärung der variablen Ergebnisse.

2. Cochleäre Synaptopathie bei Wüstenrennmäusen – neuer Aspekt zum Mechanismus

Wie bereits zuvor diskutiert, ist eine direkte Untersuchung der cochleären Synapse beim Menschen nicht möglich. Daher wäre es wünschenswert, ein Tiermodell zu verwenden, das in dieser Eigenschaft dem Menschen ähnlich ist. Ältere Wüstenrennmäuse weisen sowohl ein ähnliches Audiogrammprofil als auch sehr ähnliche histologische Veränderungen in verhaltensbezogenen und physiologischen Aspekten wie beim Menschen auf. Daher sind sie gut als Tiermodell für die Studie der altenbedingten Schwerhörigkeit geeignet (35).

Zusätzlich haben Wüstenrennmäuse eine sehr kurze Lebensspanne von etwa 3 bis 4 Jahren. Während dieser kurzen Lebensdauer können altersbedingte Faktoren, die das Hörsystem beeinflussen, untersucht werden (36, 37). Dadurch sind diese Tiere noch besser für die Untersuchung der altersbedingten Schwerhörigkeit geeignet.

In anderen Modellen mit Katzen, Meerschweinchen und Mäusen haben Wissenschaftler entdeckt, dass der N. cochlearis aus verschiedenen Nervenfasern besteht, die in Fasern mit niedriger Spontanrate (SR< 0,5 Spikes/s), mittlerer Spontanrate (0,5 < SR < 18 Spikes/s) und hoher Spontanrate (> 18 Spikes/s) unterteilt werden können (38, 39).

Die Nervenfasern mit niedriger Spontanrate haben normalerweise höhere akustische Schwellen und sind für die Codierung der feinen temporalen Struktur des akustischen Stimulus, insbesondere für das Sprachverstehen in Umgebungsgeräuschen, zuständig. Diese Fasern sind sehr anfällig für externe Faktoren und degenerieren daher zuerst. Die Nervenfasern mit hoher Spontanrate haben hingegen niedrigere akustische Schwellen und sind für die Hörschwelle zuständig. Sie sind sehr stabil gegenüber äußeren Einflüssen (39, 40).

Aus anatomischer Sicht haben die Nervenfasern mit niedriger Spontanrate kleinere Axone, verlaufen auf der modiolaren Seite der inneren Haarsinneszellen (der neuronalen Seite) und besitzen große präsynaptische Ribbon-Strukturen sowie kleine postsynaptische Elemente. Die Nervenfasern mit hoher Spontanrate haben jedoch größere Axone, verlaufen auf der Pillar-Seite der inneren Haarsinneszellen (der abneuralen Seite) und besitzen kleine präsynaptische Ribbon-Strukturen sowie große postsynaptische Elemente (39, 41-45).

Es stellt sich deshalb die Frage: wie sehen die charakteristischen Eigenschaften der synaptischen Elemente in Wüstenrennmäusen aus?

Arbeit 1: Gleichzeitige Gradienten des Ribbon-Volumens und des α-Amino-3-hydroxy-5-methyl-4-isoxazolpropionsäure- (AMPA)-Rezeptor-Volumens in Cochlea-Afferenten-Synapsen der inneren Haarsinneszelle von Wüstenrennmäusen

In dieser Studie wurden präsynaptische und postsynaptische Elemente der cochleären Synapse in jungen Wüstenrennmäuse durch Antikörper markiert und mit konfokaler Mikroskopie untersucht. Anschließend wurde die Synapse dreidimensional rekonstruiert und quantitativ analysiert. Insgesamt wurden sieben Positionen von 0,5 bis 32 kHz erfasst. Die räumliche Position der Synapsen wurde in einem Koordinatensystem mit Bezug auf ihre jeweilige innere Haarsinneszelle (IHC) bestimmt (Abbildung 1). Insgesamt wurden die Synapsen von 147 IHC in 5 Tieren vollständig analysiert. Die gefundene Anzahl an Synapsen pro IHC entspricht früheren Publikationen, die von etwa 20 bis 22 Synapsen pro IHC berichten (40, 46-50).

Das Volumen der Ribbon-Synapsen (Interquartilsabstand von 0,067 bis 0,16 µm³, mit einem Median von 0,11 µm³) korreliert mit dem postsynaptischen AMPA-Element (Interquartilsabstand von 0,09 bis 0,31 µm³, mit einem Median von 0,17 µm³), wobei größere Ribbon-Synapsen auch größere postsynaptische AMPA-Elemente aufwiesen (Abbildung 2). Darüber hinaus variierten die Volumina sowohl der präsynaptischen Ribbons als auch der postsynaptischen Rezeptor-Patches entlang der modiolar-pillar und longitudinalen Achsen ihrer Haarsinneszellen (Abbildung 3 und 4). Die Gradienten im Ribbon-Volumen stimmen mit früheren Befunden bei Katze, Meerschweinchen, Maus und Ratten überein (39, 45, 51-53) und unterstützen weiterhin eine Rolle bei der Differenzierung der physiologischen Eigenschaften von Typ-I-Afferenzen. Die positive Korrelation zwischen den Volumina der prä- und postsynaptischen Elemente bei der Wüstenrennmaus unterscheidet sich jedoch von den entgegengesetzten Gradienten, die bei der Maus gefunden wurden, was auf rassenspezifische Unterschiede in den postsynaptischen AMPA-Rezeptoren hindeutet, die nicht mit den grundlegenden Klassen von Typ-I-Afferenzen zusammenhängen.

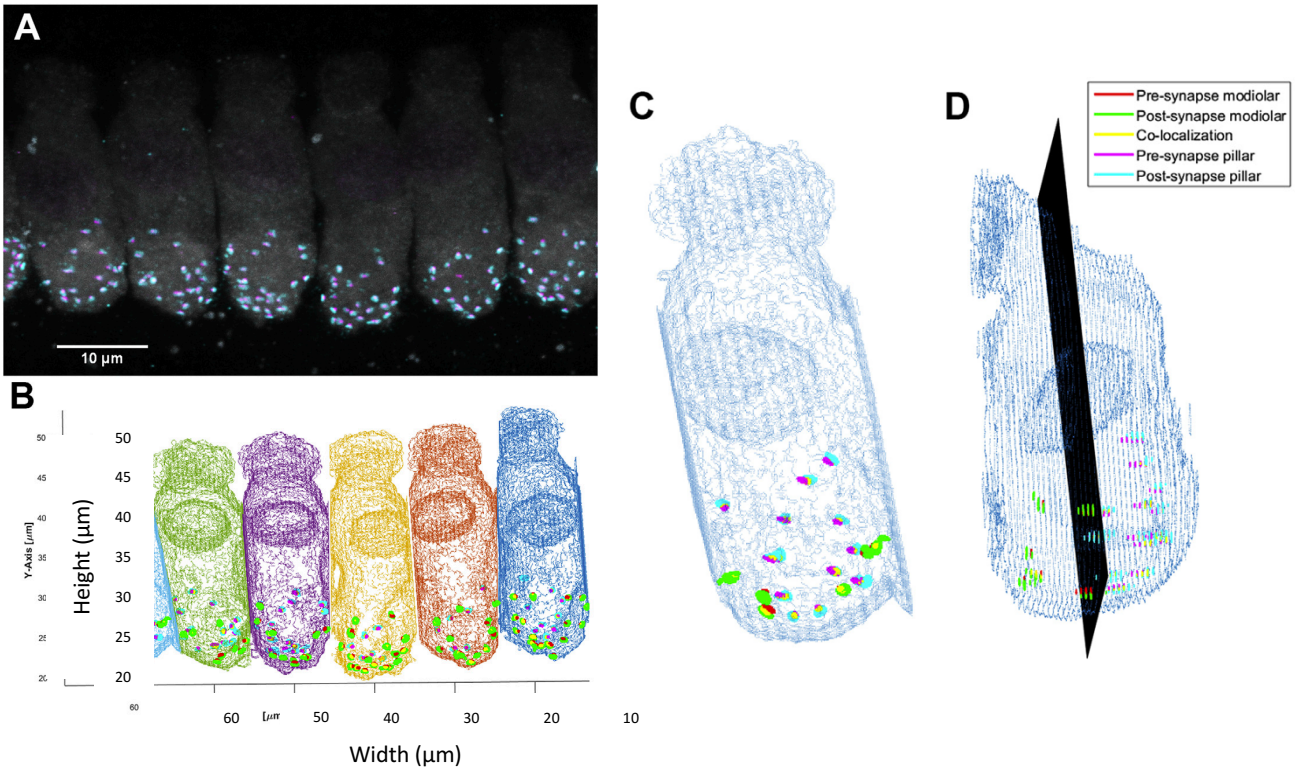


Abb. 1 Beispiel für die Bildanalyse eines immunmarkierten konfokalen Stapels. A: z-Projektion des konfokalen Stapels, der sechs IHC enthält. Grau: MyoVIIa-Markierung der Haarsinneszellen, Magenta: CtBP2-Markierung der präsynaptischen Ribbons, Cyan: GluR2-Markierung der postsynaptischen Rezeptoren. Die beiden Farbkanäle mit synaptischer Markierung wurden einer Dekonvolution unterzogen. Um diese Abbildung zu erstellen, wurde die Markierung aufgehellt und der Kontrast verstärkt. B: 3D-Mesh-Rekonstruktion der gleichen sechs IHC, einzeln abgegrenzt und durch unterschiedliche Farben hervorgehoben, zusammen mit allen erkannten funktionellen Synapsen. C, D: Eine der IHC wird in höherer Vergrößerung und aus zwei verschiedenen Blickwinkeln gezeigt, die sich um 90 Grad um die y-Achse unterscheiden. Die synaptischen Elemente sind farblich kodiert, wie in der Legende angegeben. Panel D zeigt auch die Ebene, die die modiolar-pillar-Hälfte der IHC definiert.

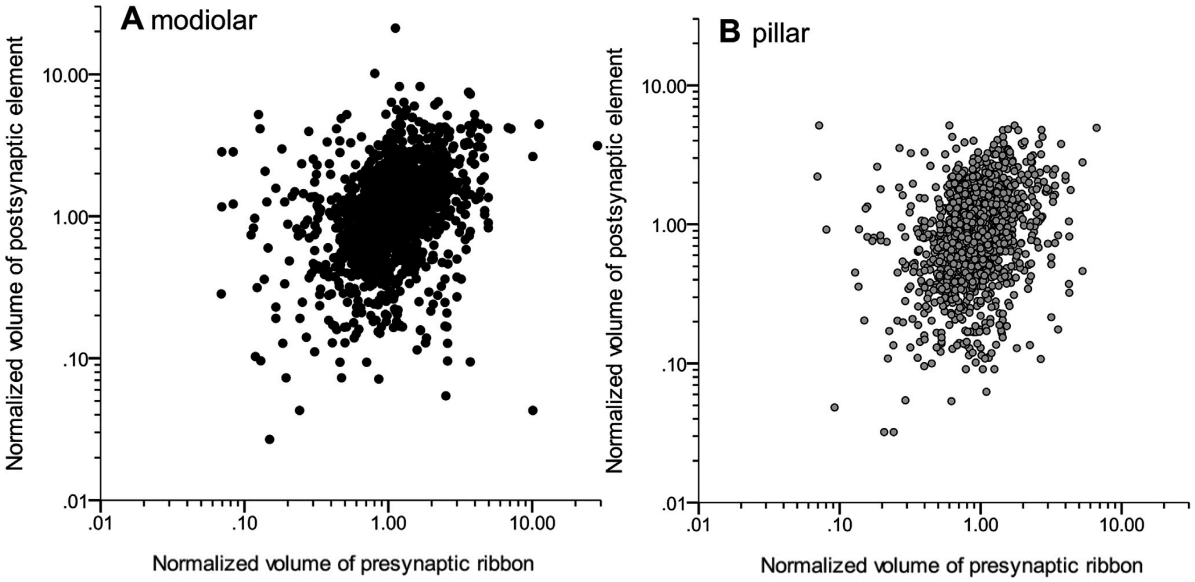


Abb. 2 Streudiagramme des normalisierten Volumens der präsynaptischen Ribbons im Vergleich zum normalisierten Volumen ihres Co-lokalisierten postsynaptischen GluR2-Patches für einzelne identifizierte funktionelle Synapsen. A: Nur Synapsen, die sich in der modiolar-Hälfte ihrer IHC befinden. B: Nur Synapsen, die sich in der pillar-Hälfte ihrer IHC befinden. Die Volumina der prä- und postsynaptischen Elemente sind in beiden Populationen positiv korreliert (Spearman-Rangkorrelation, $p < 0{,}001$, $r = 0{,}36$, $n = 1848$ für modiolar-Hälfte; $p < 0{,}001$, $r = 0{,}33$, $n = 1376$ für pillar-Hälfte).

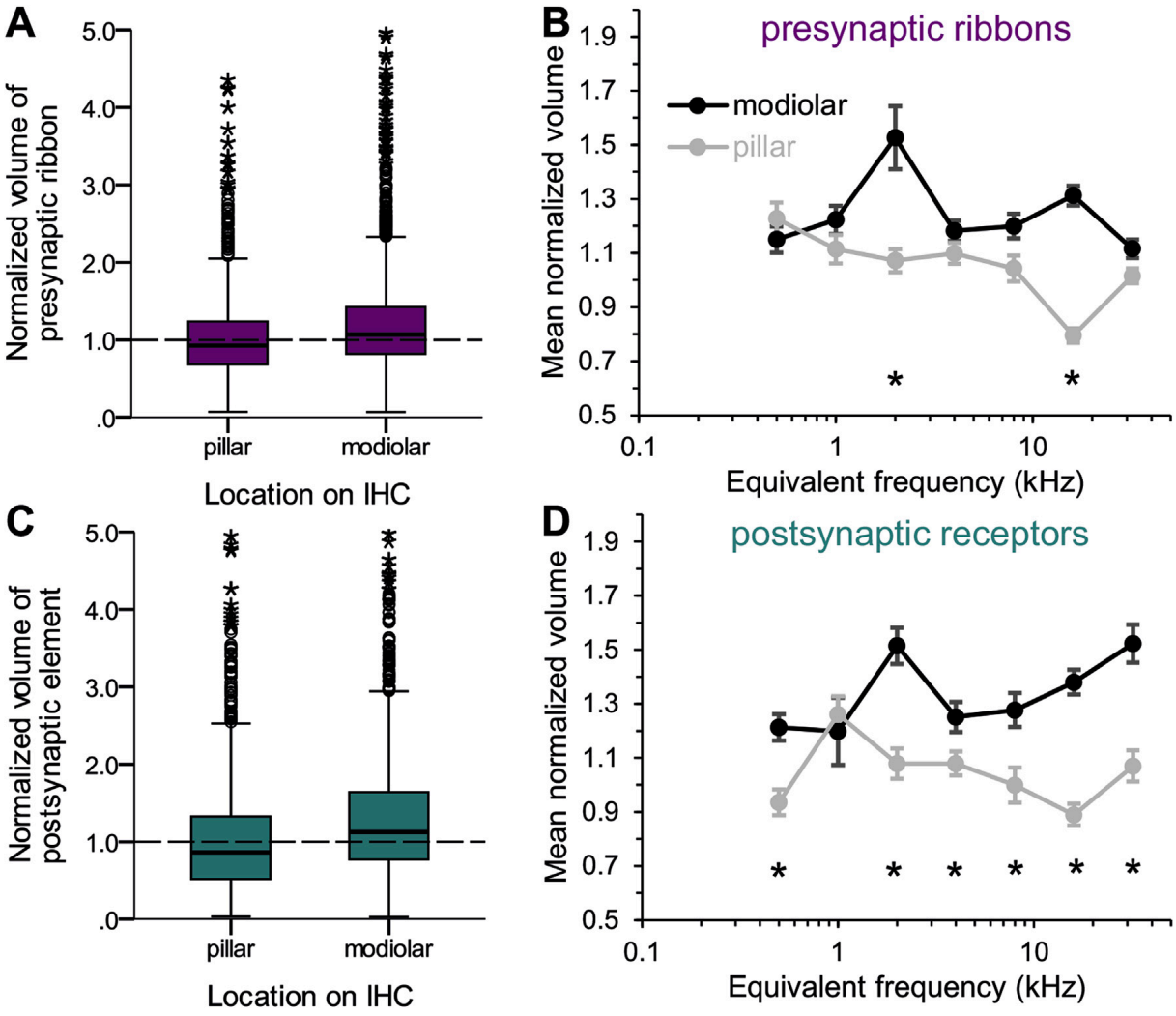


Abb. 3 Normalisierte Volumina funktioneller Synapsenelemente. A, C: Boxplots, die das normalisierte Volumen der präsynaptischen Ribbons (A) und der postsynaptischen GluR2-Patches (C) separat für Synapsen in den Pillar- und Modiolar-Hälften ihrer jeweiligen IHC zeigen. Zur besseren Übersichtlichkeit wurde die y-Achse begrenzt, wodurch bis zu sieben weiteren Ausreißern nicht dargestellt werden. B, D: Dieselben Daten, jedoch als Mittelwerte ± Standardfehler des Mittelwerts dargestellt und zusätzlich nach der Frequenzposition in der Cochlea aufgeschlüsselt (n = 1848 Synapsen in der modiolar-Hälfte, n = 1376 Synapsen in der pillar-Hälfte). Dieses Darstellungsformat wurde gewählt, um eine genaue Vergleichbarkeit mit veröffentlichen Daten von Mäusen (Liberman und Liberman, 2016; Liberman et al., 2015; Yin et al., 2014) zu gewährleisten. Die scheinbaren Ausreißer bei 2 und 16 kHz werden durch die Darstellung der Mittelwerte verstärkt. Asteriske kennzeichnen statistisch signifikante Unterschiede zwischen den modiolar und pillar Daten an spezifischen Orten (Mann-Whitney-U-Tests, $p < 0,01$).

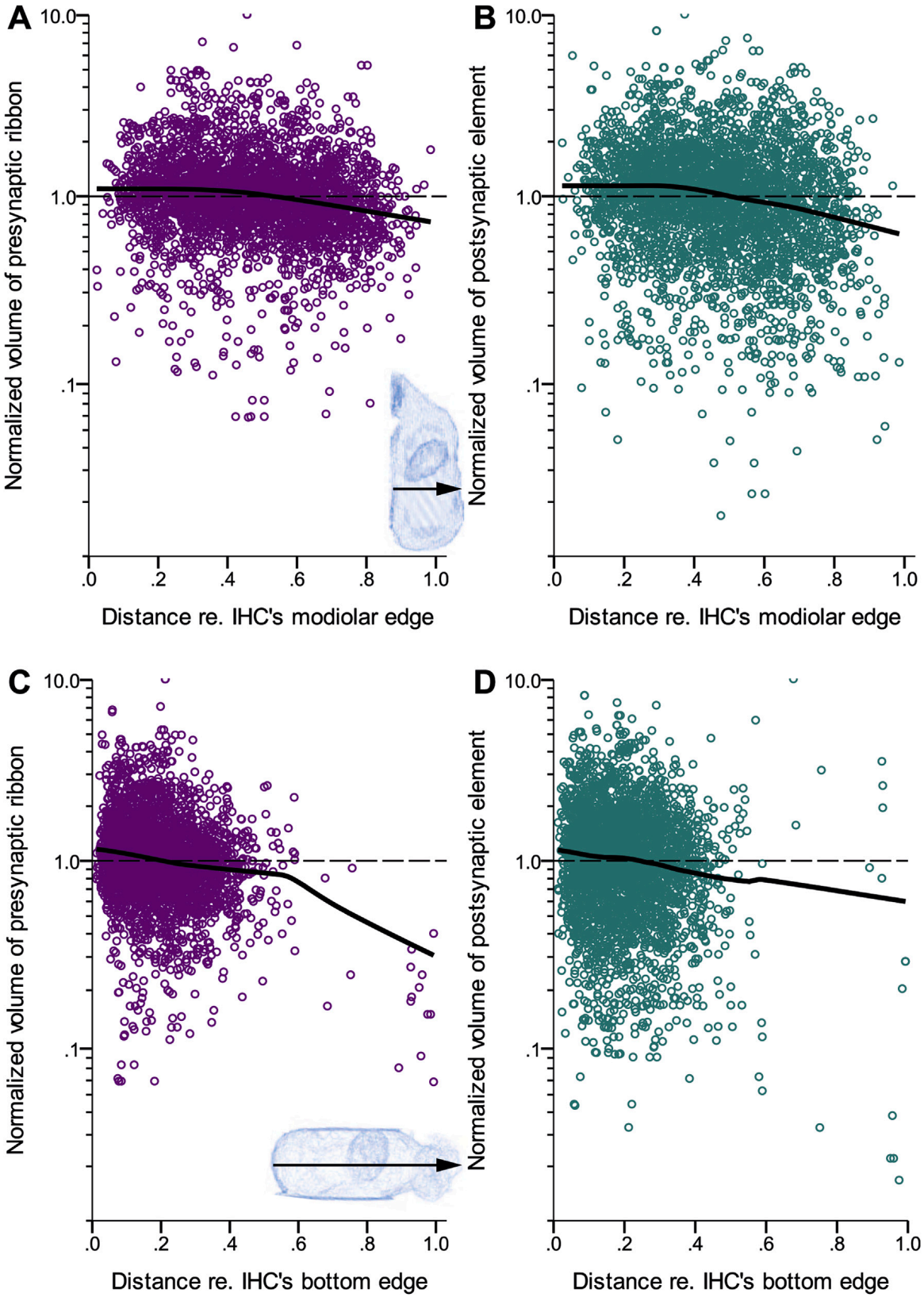


Abb. 4 Normalisierte Volumina funktioneller Synapsenelemente in Abhängigkeit von ihrer relativen Position entlang zweier Haarsinneszellenachsen. A, B: Normalisiertes Volumen des präsynaptischen Ribbons (A) oder postsynaptischen GluR2-Patches (B) in Abhängigkeit von der Position entlang der Modiolar-Pillar-Achse ihrer IHC. C, D: Dieselben Daten in Abhängigkeit von der Position entlang der longitudinalen Achse der IHC. Als visuelle Hilfsmittel zeigen die gestrichelten Referenzlinien das Medianvolumen in jedem Panel an, die dicken durchgezogen Linien repräsentieren lokal gewichtete Mittelwerte (Loess-Funktion von SPSS, wobei 50% der Datenpunkte werwendet werden). Cartoons der IHC in den Panels A und C veranschaulichen weiter die jeweiligen anatomischen Achsen, die dargestellt sind. Die Bereiche der y-Achsen in allen vier Panels werden auf einen einheitlichen wert begrenzt, wodurch 1-3 Datenpunkte in jedem Panel ausgeschlossen wurden.

Arbeit 2: Die temporale Kodierung einzelner Hörnervfasern ist bei alternden Wüstenrennmäusen nicht beeinträchtigt

In dieser Studie wurde untersucht, ob die zeitliche Kodierung bereits auf der Ebene des N. cochlearis beeinträchtigt ist. Einzelzellaufzeichnungen von Hörnervfasern (ANF) wurden bei 41 mongolischen Wüstenrennmäusen beider Geschlechter durchgeführt, die in junge, mittelalte und alte Tiere unterteilt wurden. Die Hörschwellen wurden unter Verwendung von durch Chirps hervorgerufenen auditorisch evozierten Potentialen (BERAs) bestimmt. Die mittelalten (MA) und alten (OL) Rennmäuse hatten signifikant höhere Hörschwellen als junge Rennmäuse (YO), unterschieden sich jedoch nicht signifikant voreinander ($H_{(2)} = 21{,}69$, $p = 1{,}95 \times 10^{-5}$; Mann-Whitney-U-Tests: YO vs. MA, $p = 1{,}60 \times 10^{-3}$, YO vs. OL, $p = 1{,}50 \times 10^{-4}$, MA vs. OL, $p = 0{,}23$) (Abbildung 5). Die Qualität der zeitlichen Kodierung wurde als Vektor-Stärke (VS) in Reaktion auf Töne bei der besten Frequenz (BF) bewertet und durch Konstruktion von Shuffled-Autokorrelogramm (SAC) und Kreuz-Stimulus-Autokorrelogramm (XAC) sowie durch Rückkorrelation aus Reaktionen auf 1-Sekunden-Rauschimpulse bei 10 - 30 dB [SPL] über dem Schwellenwert untersucht (54). Bei vergleichbaren Hörschwellen zeigten alle Messungen, dass die zeitliche Kodierung in den Hörnervfasern von alternden Wüstenrennmäusen nicht verändert war. Darüber hinaus blieben sowohl die zeitliche Feinstruktur als auch die Hüllenkodierung unbeeinträchtigt. Die zeitliche Feinstrukturkodierung wurde anhand der Peakamplitude und Peakbreite der ’DifCor’ beurteilt. ’DifCor’ wurden aus den Unterschieden zwischen SAC und XAC berechnet. Die zeitliche Hüllenkodierung wurde durch die Peakamplitude und Peakbreite der ’SumCor’ bewertet. ’SumCor’ wurden als Durchschnitt aus SAC und XAC berechnet. (Abbildung 6-8). Es wurde jedoch eine Reduktion der spontanen Feuerrate bei alten Rennmäusen festgestellt (Abbildung 9). Wichtig ist, dass trotz der erhöhten Hörschwellen die Frequenzabstimmung der Hörnervfasern nicht beeinträchtigt war. Diese Ergebnisse deuten darauf hin, dass altersbedingte Defizite in der zeitlichen Kodierung eher zentral auftreten, möglichweise aufgrund eines Verlusts von Hörnervfasern (oder deren peripheren Synapsen), aber nicht aufgrund qualitativer Änderungen in den Reaktionen der verbleibenden Hörnervfasern. Die reduzierte spontane Feuerrate, die erhöhten Hörschwellen aber jedoch die normale Frequenzabstimmung der alten Hörnervfasern, können durch die bekannte Reduktion des endokochleären Potentials aufgrund einer Strial-Dysfunktion bei alten Rennmäusen erklärt werden.

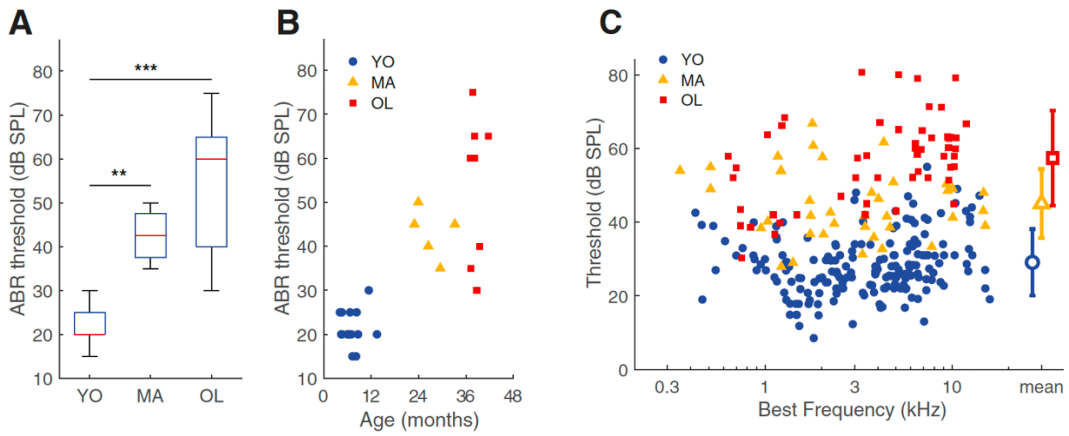


*Abb. 5 Wüstenrennmäuse zeigen unterschiedliche Grade des altersbedingten Hörverlusts bei verschiedenem Alter. A: Boxplots der Hörschwellen, die durch Chirps bei jungen (YO, n = 15), mittelalten (MA, n = 5) und alten (OL, n = 9) Rennmäuse bestimmt wurden. Asteriske zeigen einen signifikanten Unterschied zwischen zwei Gruppen nach post-hoc-Vergleichen an. **p < 0,01, *p < 0,001, Bonferroni-Holm-korrigiert. Boxplots zeigen den Median (horizontale rote Linie), das 25. und 75. Perzentil (blaues Kästchen) und die extremeren Datenpunkte, die nicht als Ausreißer betrachtet werden (Whisker). Datenpunkte werden als Ausreißer betrachtet, wenn sie höher als das 75. Perzentil + 1,5 x (75. - 25. Perzentil) oder niedriger als das 25. Perzentil – 1,5 x (75. – 25. Perzentil) sind, was ungefähr ± 2,7 x Standardabweichungen entspricht. Bei den Hörschwellenwerten der jungen Rennmäuse sind der Median und das 25. Perzentil der gleiche Wert und liegen daher übereinander. B: Die Hörschwelle von Chirps jedes Tieres in Abhängigkeit von seinem Alter in Monaten. C: Hörschwelle in Abhängigkeit von der BF der Hörnervenfasen bei jungen (blaue Kreise, n = 186), mittelalten (gelbe Dreiecke, n = 39) und alten (rote Quadrate, n = 54) Tieren. Durchschnittliche Hörschwellenwerte ± Standardabweichungen sind mit großen offenen Symbolen rechts dargestellt.*

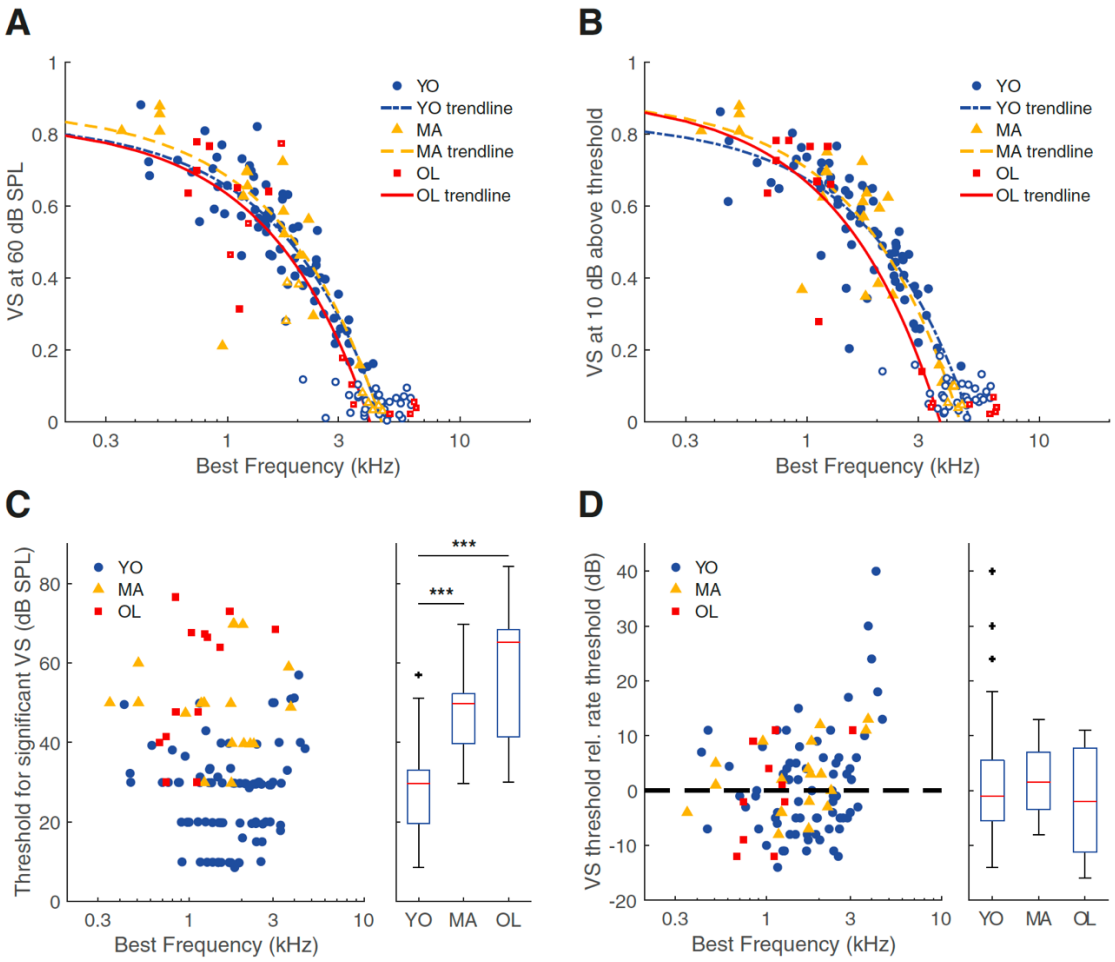


Abb. 6 Das Phasen-Locking auf Reintöne wurde durch das Altern nicht beeinträchtigt. A: VS der Antwort der Hörnervenfasen auf einen BE-Ton bei 60 dB SPL, in Abhängigkeit von BF, für junge (n = 74), mittelalte (n = 16) und alte (n = 7) Rennmäuse. Offene Symbole zeigen VS-Werte an, die nicht signifikant waren (p > 0,001 oder N < 50), die nicht in die Analyse einbezogen wurden. Die wenigen hohen, aber nicht signifikanten VS-Werte in der Gruppe der mittelalten und alten Rennmäuse stammen von Hörnervenfasen mit einer hohen Hörschwelle und somit einer geringen Anzahl von Spikes (N < 50). VS-Werte von Hörnervenfasen mit einer Feuerrate < 5 Spikes/s bei 60 dB SPL werden nicht gezeigt (MA: n = 1, OL: n= 5). Die Trendlinien zeigen lineare Regressionen, getrennt für junge, mittelalte und alte Rennmäuse.

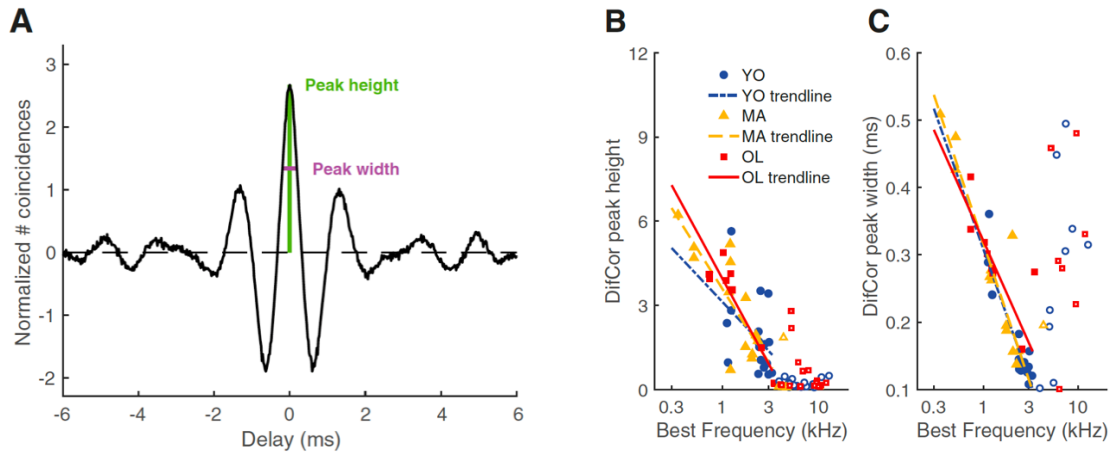


Abb. 7 Die Peakamplitude und Peakbreite aus 'DifCor' wurden vom Alter nicht beeinflusst. A: Beispiel der 'DifCor' für dieselbe Hörnervenfaser, die in Abbildung 4A gezeigt wird. Die Peakamplitude (bei einer Verzögerung von 0 ms, von der gestrichelten Referenzlinie aus) betrug 2,67 (dargestellt in Grün) und die Peakbreite betrug 0,38 ms (dargestellt in Magenta). B: 'DifCor'-Peakamplitude in Abhängigkeit von der BF für junge (blaue Kreise; n = 18), mittelalte (gelbe Dreiecke; n = 13) und alte (rote Quadrate; n = 9) Rennmäuse. Die Peakamplitude waren zwischen den verschiedenen Altersgruppen ähnlich, nahmen jedoch mit zunehmender BF ab. Logarithmische Regressionen sind als visuelle Hilfsmittel dargestellt. Offene Symbole in B und C zeigen Hörnervenfasern mit einer BF von 3,5 kHz an, die nicht in die Regressionsanalysen einbezogen wurden. C: Gleiche Daten und Format wie in B, aber jetzt wird die 'DifCor'-Peakbreite dargestellt.

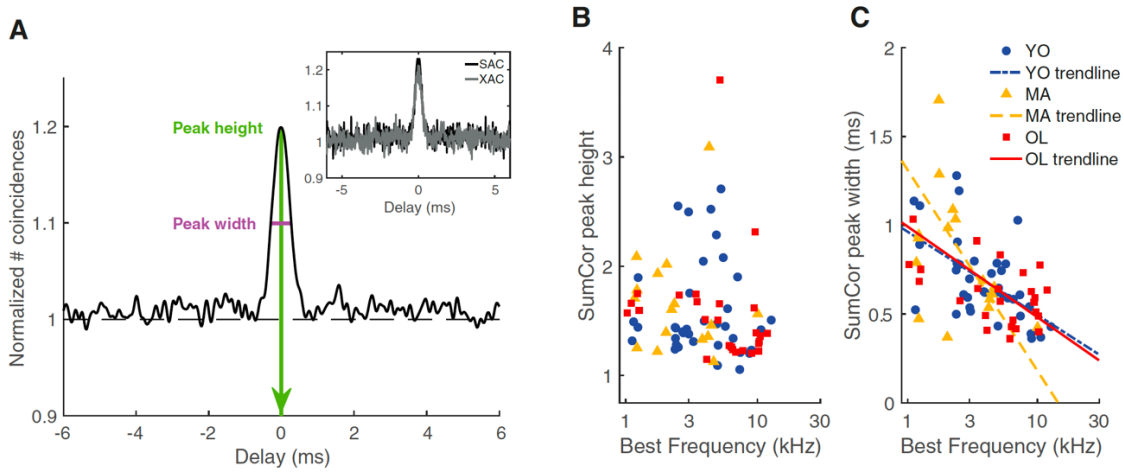


Abb. 8 Die Peakamplitude und Peakbreite aus 'SumCor' wurden vom Alter nicht beeinflusst. A: Beispiel der 'SumCor' einer Hörnervenfaser einer jungen Rennmaus (BF = 7,5 kHz). Im Einsatz: Die SAC und XAC derselben Hörnervenfaser (XAC/SAC-Verhältnis = 1,02). Die Peakamplitude (von 0) betrug 1,22 (grün) und die Peakbreite betrug 0,53 ms (magenta). B: 'SumCor'-Peakamplitude als Funktion der BF für junge (blaue Kreise; n = 38), mittelalte (gelbe Dreiecke; n = 19) und alte (rote Quadrate, n = 28) Rennmäuse. C: 'SumCor'-Peakbreite als Funktion der BF für die verschiedenen Altersgruppen. Logarithmische Regressionen sind als visuelle Hilfsmittel dargestellt.

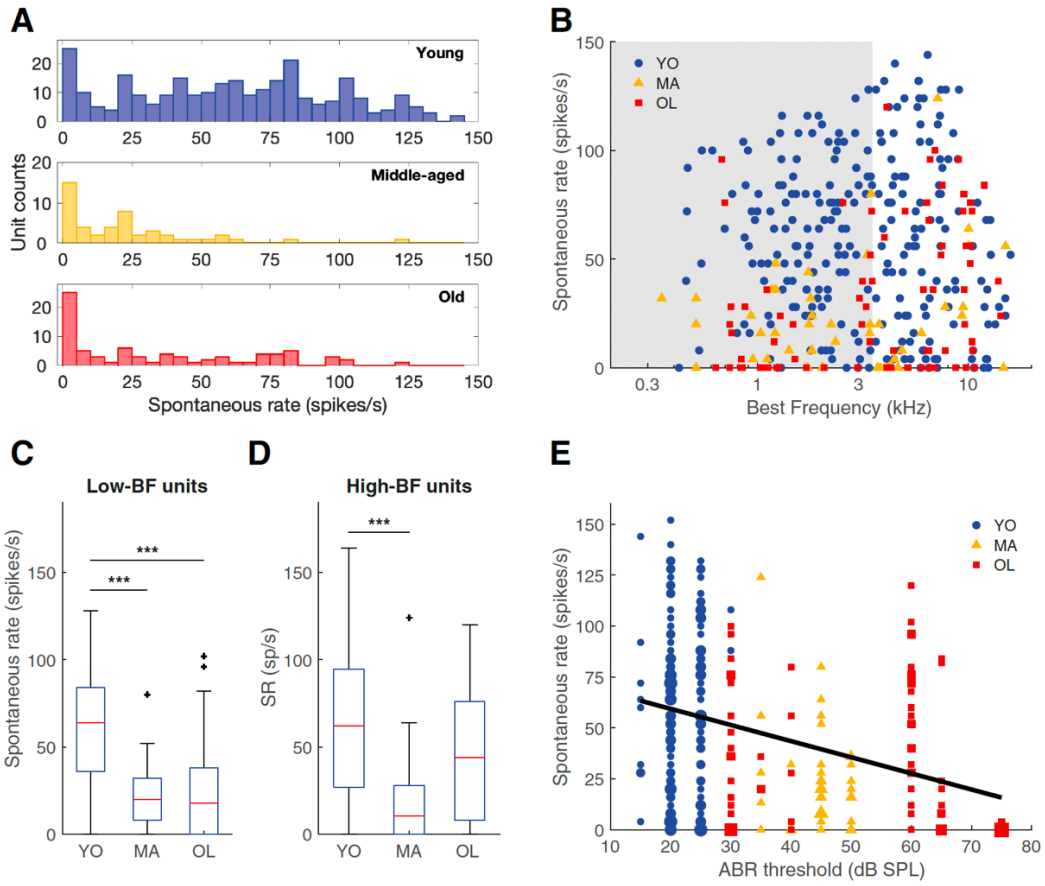


*Abb. 9 Die Spontanrate (SR) des Hörnervs nahm mit altersbedingtem Hörverlust ab. A: Die SR-Verteilung aller Hörnervenfasen, die von jungen (n = 272; blau), mittelalten (n = 48; gelb) und alten (n = 78; rot) Rennmäusen aufgezeichnet wurden. B: SR aufgetragen gegen BF bei jungen (blaue Kreise), mittelalten (gelbe Dreiecke) und alten (rote Quadrate) Tieren. Der grau schattierte Bereich zeigt Hörnervenfasen mit einer BF von mehr als 3,5 kHz an. C, D: Boxplots der SRs, getrennt für Hörnervenfasen mit niedriger BF (C; YO: n = 146, MA: n = 28, OL: n = 36) und hoher BF (D; YO: n = 137, MA: n = 20, OL: n = 44), sowie für junge (YO), mittelalte (MA) und alte (OL) Rennmäuse in jedem Diagramm. E: SR aufgetragen als Funktion der Hörschwelle für Klicks dieses Tieres (YO: n = 149, MA: n = 37, OL: n = 78). Die schwarze Trendlinie repräsentiert die lineare Regression zwischen Hörschwelle und SR. Die Markierungsgröße repräsentiert die Anzahl der überlappenden Datenpunkte. ***p < 0,001. Ausreißer sind als schwarze Kreuze dargestellt (+).*

3. Diagnostische Ansätze

Es gibt keinen Goldstandard für die Diagnose der cochleären Synaptopthie beim Menschen. Die neue entwickelte Methode bezüglich der Krümmung der Welle I der BERA wurde an Mäusen verwendet und zeigte, dass die Krümmung deutlich stabiler und zuverlässiger ist im Vergleich zur Amplitude der Welle I der BERA (29). Dieses Verfahren wurde in der folgenden Studie auf den Menschen übertragen und untersucht. Darüber hinaus kamen kortikale Potentiale im Rahmen der Mismatch-Negativität (MMN) zum Einsatz, die in der Lage sind, unterschiedliche Reize auf zentraler Ebene zu unterscheiden (55-57). Diese wurden bei normalhörenden Probanden verschiedener Altersgruppen eingesetzt, um zu prüfen, ob sich damit frühe Veränderungen der Hörbahn erkennen lassen.

Arbeit 3: Die Krümmungsquantifizierung der Welle I in der auditorischen Hirnstammaudiometrie erkennt die cochleären Synaptopathie beim Menschen

Das Studienprotokoll wurde von der Ethikkommission der Universitätsmedizin Rostock genehmigt (A 2022-0127). In diese Studie wurde 80 gesunde Probanden aufgenommen. Alle Probanden unterzogen sich einer Audiometrie mit Standard- und erweiterten hohen Frequenzen (EHF) im Bereich vom 0,125 bis 16 kHz und einer auditorischen Hirnstammaudiometrie mit einem Stimulus von 80 dB nHL-Klick. Die Peakamplitude, die Peaklatenz, die Krümmung am Peak und die Fläche unter der Kurve von Welle I der BERA wurden berechnet und analysiert (Abbildung 10). Die EHF-Hörschwelle der Probanden verschlechterte sich mit dem Alter (Abbildung 11). Die Pearson-Korrelationsanalyse zeigte eine signifikante, negative Korrelation zwischen der Krümmung und dem Alter sowie zwischen der Krümmung und der Schwelle der EHF (10-16 kHz). Darüber hinaus wurde die gleiche Korrelation zwischen Alter und Fläche sowie Alter und EHF-Schwelle beobachtet (Abbildung 12, 13). Der Modellvergleich zeigte, dass die Krümmung am Peak von Welle I die beste Metrik ist, die mit der EHF-Schwelle korreliert (Abbildung 14) und deshalb zur Erkennung der cochleären Synaptopathie beim Menschen in der Routinediagnostik angewendet werden, könnte um die frühzeitige Degeneration des Hörnervs zu erkennen.

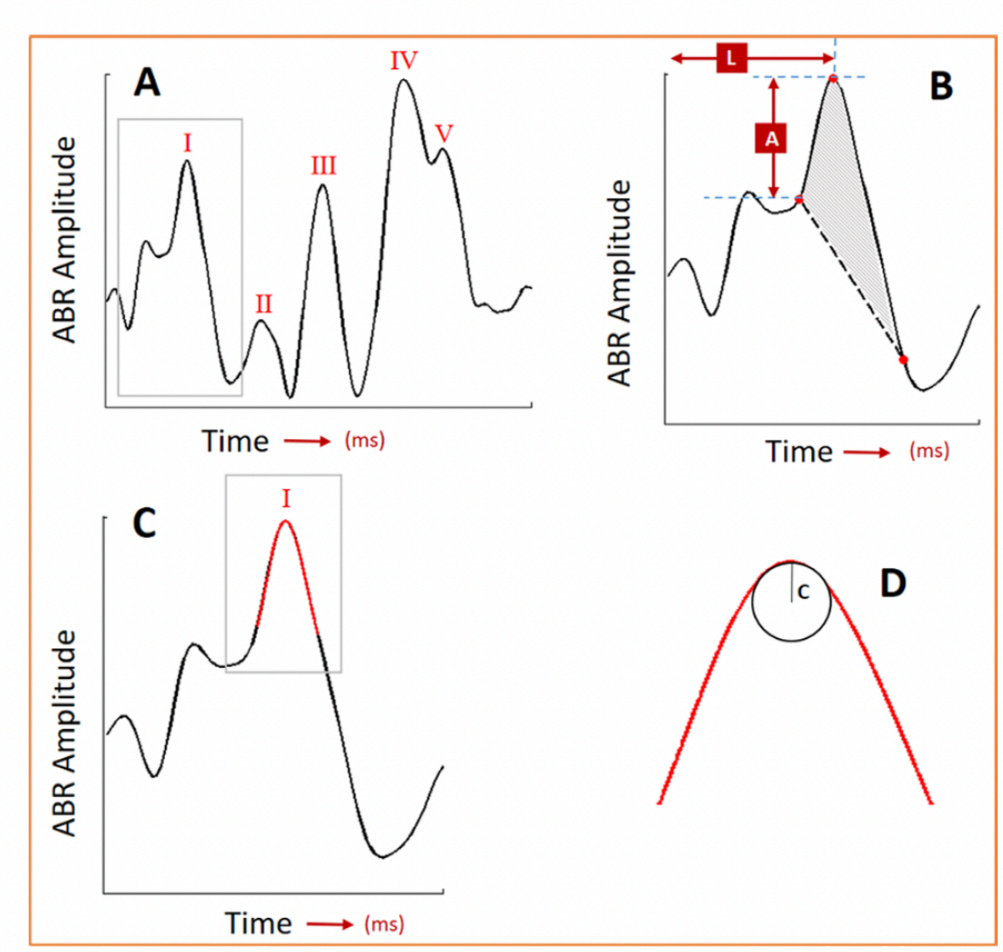


Abb. 10 Beispiele zur Quantifizierung der Welle I in BERA-Aufzeichnungen. A: BERA-Aufzeichnung von einem Probanden, bei der alle Wellen (I-V) markiert sind. Das graue Rechteck wurde verwendet, um die Welle I zu kennzeichnen. B: Die Welle I derselben Probanden wird zur Berechnung der Amplitude (A), der Peaklatenz (L) und der Fläche unter der Kurve (grauer Bereich) ausgewählt. C: Ein Polynom-Fit auf dieselbe Welle I angewendet, um die Krümmung zu quantifizieren. D: Die Krümmungsquantifizierung wird am Peak der Welle I berechnet.

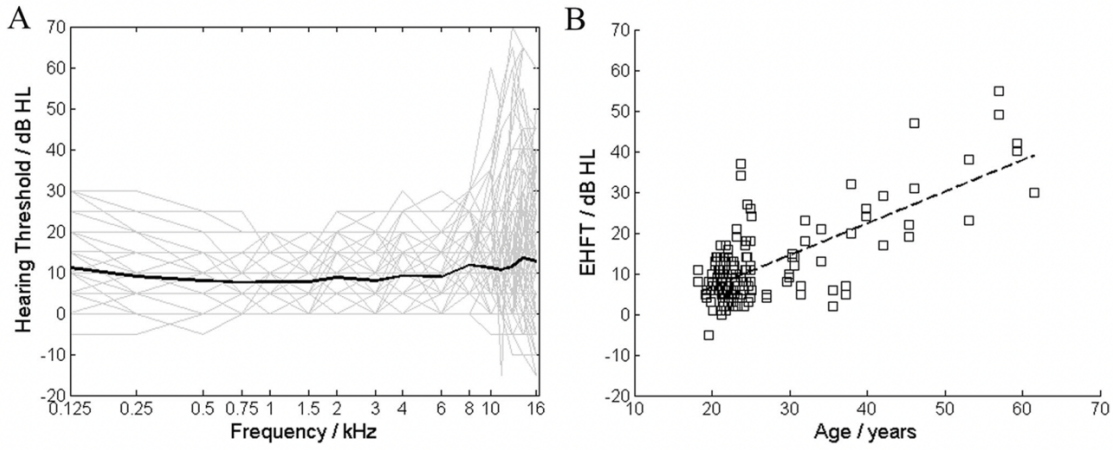


Abb. 11 A: Hörschwellen aller Probanden (graue Farbe) und der Durchschnitt (Schwarz) im Frequenzbereich von 0,125 kHz bis 16 kHz. Die Hörschwellen liegen im normalen Bereich von 0,125 bis 8 kHz, variieren also nicht um mehr als 30 dB, steigen jedoch bis zu 10 kHz an. B: Streudiagramm der durchschnittlichen EHF-Schwellen (von 10 bis 16 kHz) im Vergleich zum Alter bei allen Ohren der Probanden. Die Pearson-Korrelationsanalyse zeigt eine positive Korrelation mit R = 0,73.

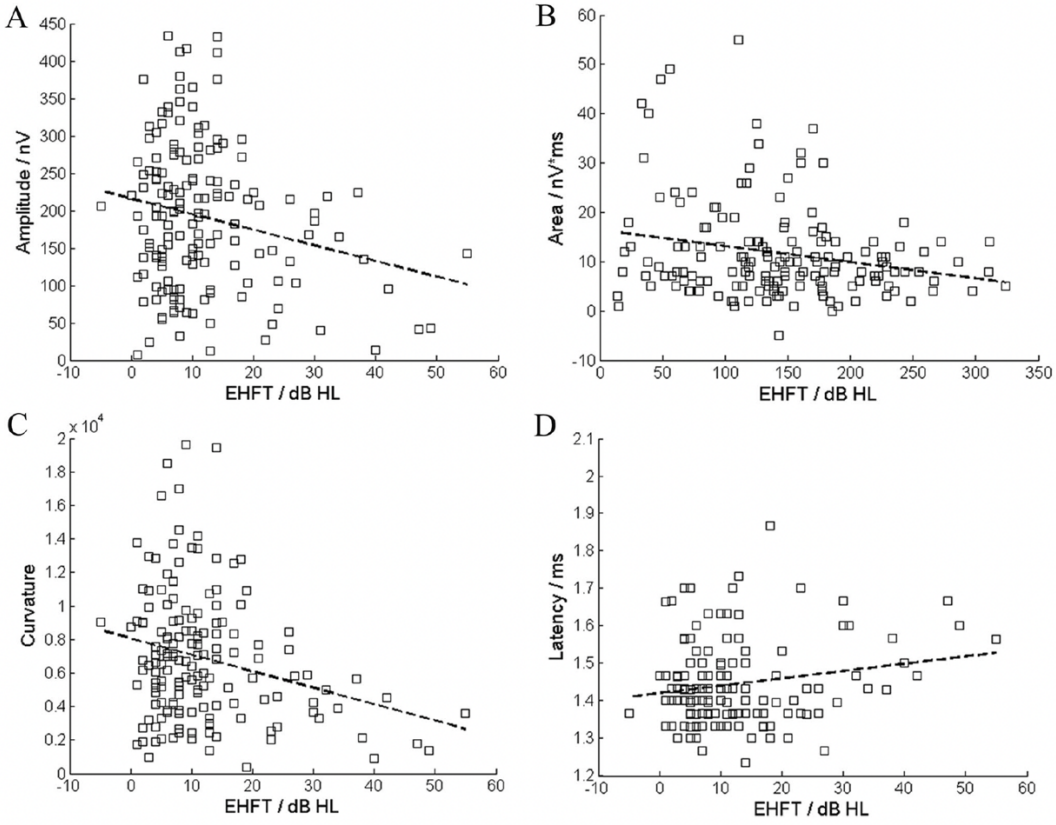


Abb. 12 Die Korrelationsanalysen der Amplitude (A), Fläche (B) und Krümmung der Welle I der BERA (C) mit EHF-Schwellen zeigen statistisch signifikante negative Korrelation zwischen Amplitude und EHF-Schwellen, zwischen Fläche und EHF-Schwellen sowie zwischen Krümmung der Welle I und EHF-Schwellen. Eine signifikante positive Korrelation ergab sich zwischen der Peaklatenz und EHF-Schwellen (D).

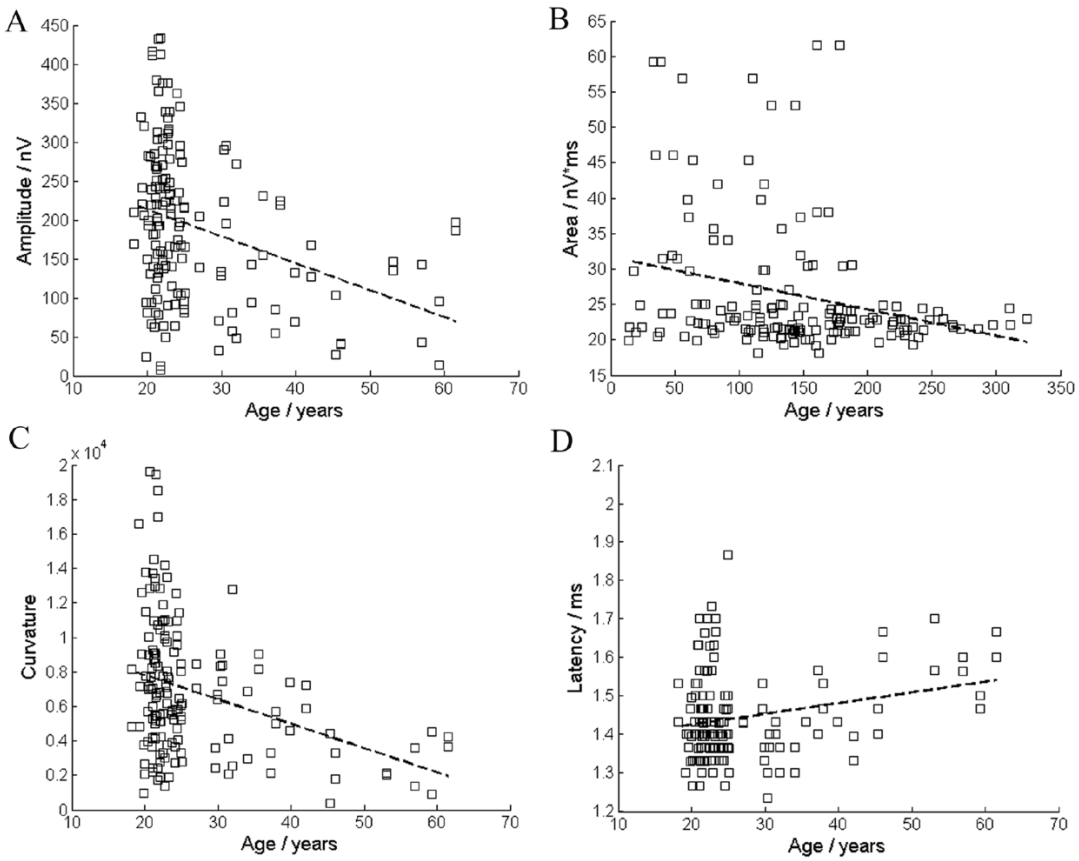


Abb. 13 Die Korrelationsanalysen der Amplitude (A), Fläche (B) und Kurvenkrümmung (C) mit dem Alter zeigen statistisch signifikante negative Korrelation zwischen Amplitude und Alter, Fläche und Alter sowie Kurvenkrümmung und Alter. Eine statistisch signifikante positive Korrelation ergab sich zwischen Peaklatenz und Alter (D).

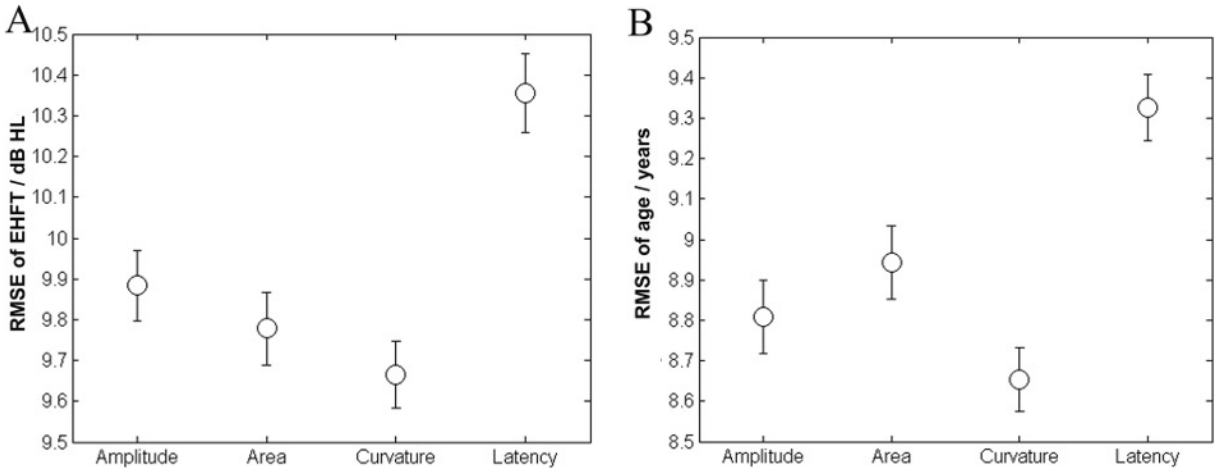


Abb. 14 Der Vergleich der verschiedenen Parameter der Welle I mit wiederholter k-facher Kreuzvalidierung zeigt, dass die Kurvenkrümmung die beste Metrik ist, um mit EHF-Schwellen (A) und Alter (B) zu korrelieren. (RMSE: Wurzel des mittleren quadratischen Fehlers)

Arbeit 4: Kann Mismatch-Negativität (MMN) als Indikator zur Vorhersage zentral-auditiver Defizite bei Personen mit normalem Hörvermögen verwendet werden?

Das Studienprotokoll wurde von der Ethikkommission der Universitätsmedizin Rostock genehmigt (A 2023-0010). In der Studie wurden 73 gesunde Probandinnen und Probanden eingeschlossen. Alle Teilnehmenden unterzogen sich einer Audiometrie mit Standardfrequenzen sowie erweiterten hohen Frequenzen (EHF) im Bereich vom 0,125 bis 16 kHz. Zusätzlich wurden zentrale kortikale Potentiale der MMN unter zwei verschiedenen Paradigmen erhoben: einem Sprachparadigma (ba/da) und einem Reintonparadigma (1/2 kHz). Die MMN-Amplitude und -Latenzen wurden von gemittelten Wellenformen berechnet (Abbildung 15). Die Ergebnisse zeigten, dass das Alter die Amplitude der MMN in Sprachparadigma signifikant beeinflusst (χ^2 = 13,0; p = 0,002). Bei der Einteilung der Probanden in Altersgruppen zeigte sich, dass die MMN-Amplitude im Sprachparadigma in der Altersgruppe 25–30 Jahre signifikant geringer war als in der Gruppe 20–25 Jahre (p = 0,0015; Cohen's d = 0,63) (Abbildung 16). Für die Latenzzeiten ergaben sich keine signifikanten Unterschiede. Dies galt ebenso für andere kortikale Potentiale, einschließlich P300. Darüber hinaus wurde der Einfluss der Schwellenwerte im Bereich der EHF untersucht. Es zeigte sich kein signifikanter Effekt der EHF-Schwellen auf MMN-Amplitude, -Latenz oder P300. Diese Studie zeigt, dass die Amplitude der MMN im Sprachparadigma als elektrophysiologische Messgröße zwar Einschränkungen bei der Diagnostik eines versteckten Hörverlusts aufweist, jedoch möglicherweise als Indikator für zentrale auditive Defizite verwendet werden kann.

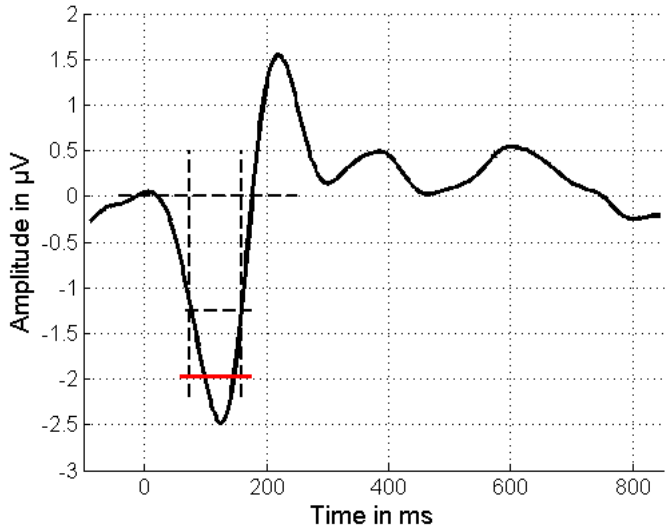


Abb. 15 Messung der Amplitude der Potentiale. Lange horizontale gestrichelte Linie: Basislinie; kurze horizontale gestrichelte Linie: 50% der Amplitude zwischen Spitze und Basislinie; vertikale gestrichelte Linien: Zeitfenster der kritischen Dauer, definiert durch die 50%-Amplitudenwerte der ansteigenden und abfallenden Flanke; rote Linie: durchschnittliche Amplitude über das kritische Zeitfenster.

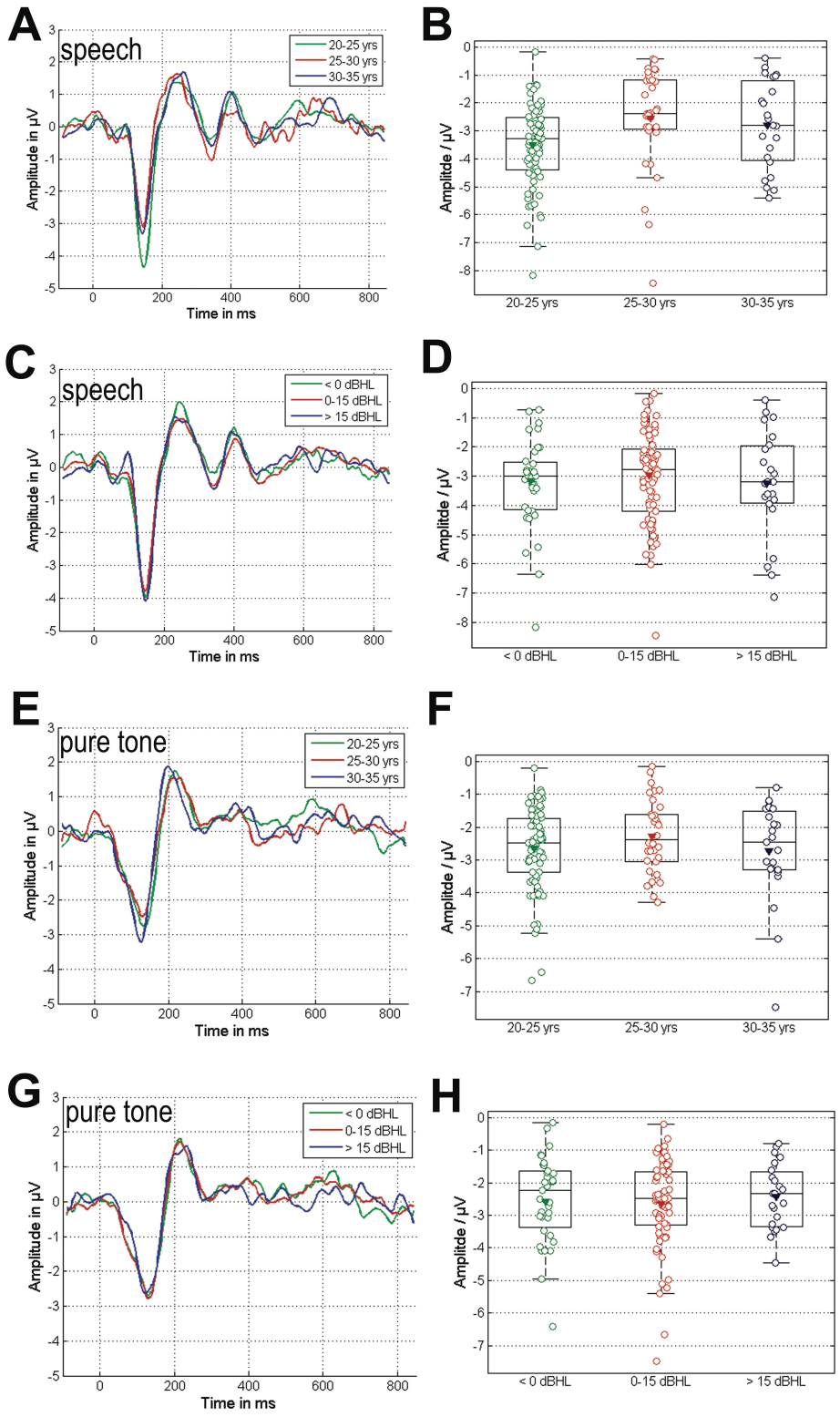


Abb. 16 Vergleich der kortikalen Potentiale in Bezug auf die MMN, berechnet als Differenz zwischen abweichenden und Standardreizen, bei Sprach- (A – D) und Reintonbedingungen (E – H). (A): gemittelte kortikale Potentiale auf Sprachreize, unterteilt nach Altersgruppen der Teilnehmenden: 20 – 25, 25 – 30 und 30 -35 Jahre. (B) Boxplot-Vergleich der MMN-Amplituden auf Sprachreize zwischen den Altersgruppen. (C): gemittelte kortikalen Potentiale auf Sprachreize, gruppiert nach EHF-Schwellen der Teilnehmenden: < 0 dB HL, 0 -15 dB HL, > 15 dB HL. (D): entsprechende Darstellung der MMN-Amplituden im Boxplot. (E): gemittelte kortikalen Potentiale auf Reintonreize, unterteilt nach Altersgruppen. (F): Boxplot-Vergleichen der MMN-Amplitude bei Reintonreizen zwischen den Altersgruppen. (G): gemittelte kortikale Potentiale auf Reintonreize, unterteilt nach EHF-Schwellen der Teilnehmenden. (H): entsprechende Vergleich der MMN-Amplituden bei Reintonreizen im Boxplot. Die Mittelwerte sind in allen Boxplots durch Dreiecke gekennzeichnet.

4. Therapieansätze

Bei ausgeprägter altersbedingter Schwerhörigkeit ist das CI derzeit der beste Therapieansatz. Die postoperative Performance ist vielversprechend, variiert aber teilweise stark individuell (30). Von klinischer Bedeutung ist, ob und wie das postoperative Sprachverstehen präoperativ individuell vorhergesagt werden kann und welche zugrunde liegenden Ursachen die Variabilität des postoperative Sprachverstehens erklären.

Arbeit 5: Der prädiktive Wert präoperativer Messungen des N. cochlearis-Nervendurchmessers mit MRT und der postoperativen Sprachwahrnehmung bei erwachsenen Patienten mit Cochlea-Implantat.

In dieser Studie wurde untersucht, ob objektive Messungen des N. cochlearis (CN), die aus präoperativen MRT-Bildern abgeleitet wurden, mit der postoperativen Sprachwahrnehmung bei CI-Patienten korrelieren. Es wurden 68 Patienten, die zwischen 2020 und 2023 eine Cochlea-Implantation erhielten, rekrutiert. Präoperative MRT-Bilder wurden verwendet, um das Volumen des Modiolus (VM), die Querschnittsfläche des N. cochlearis (ACN) sowie zur Normalisierung die Fläche des N. facialis (AFN) und die Fläche des inneren Gehörgangs (AIEC) zu messen (Abbildung 17). Die postoperative Sprachwahrnehmung wurde mithilfe von Wortkennungstests (WRS) unter Verwendung des Freiburger Einsilber- und Mehrsilbertests zu verschieden Zeitpunkten nach der Erstanpassung (FF) des CI-Prozessors bewertet: Unmittelbar nach FF, 1 Monat, 3 Monate und 6 Monate nach FF. Die Korrelationsanalyse zeigte eine statistisch signifikante positive Korrelation zwischen dem Verhältnis von ACN zu AFN (ACN/AFN) und WRS bei der Erstanpassung ($R = 0,36$, $p < 0,003$). Diese Korrelation verschwand jedoch bei den nachfolgenden Untersuchungen (Table 1; Abbildung 18). Darüber hinaus zeigte sich, dass die Korrelation hauptsächlich durch Patienten mit mäßigem bis schwerem asymmetrischem Hörverlust (AHLm) auf der kontralateralen Seite getrieben wurde ($R = 0,62$, $p = 0,0003$) (Abbildung 18). Die vorliegenden Ergebnisse deuten darauf hin, dass die Bewertung der Größe des N. cochlearis durch die MRT nur eine begrenzte prädiktive Aussagekraft für die postoperativen Sprachwahrnehmung bei CI-Beratungen besitzt. Bei Patienten mit AHLm ist allerdings eine Korrelation auf die anfängliche Aktivierungsphase nachweisbar.

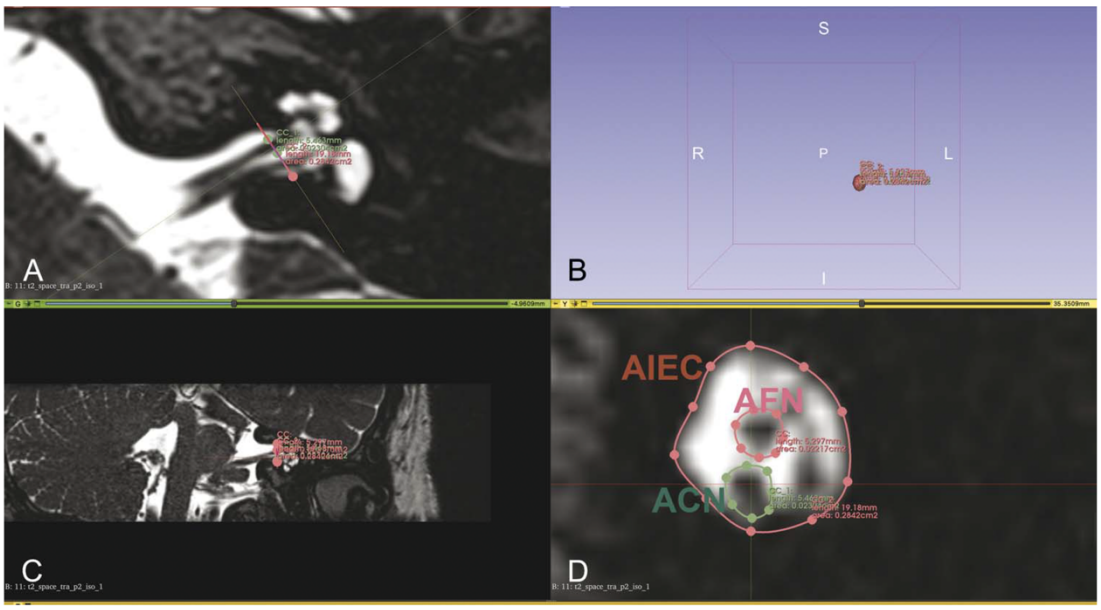


Abb. 17 Screenshot von 3D Slicer, der die Messung der Flächen des N. cochlearis (ACN), des N. facialis (AFN) und des inneren Gehörgangs (AIEC) in der parasagittalen Sektion zeigt. (A) axiale Ebene des Innengehörgangs, in der zwei Achsen dargestellt sind, die die Bewegung ermöglichen, um die Zielbilder in der coronalen Ebene (C) und der sagittalen Ebene (D) zu erzeugen. Die ausgewählte Ebene wird im dreidimensionalen Raum dargestellt (B).

		Pearson correlation				p-value			
WRS at time point	**CN metric**	**SSD**	**AHLm**	**AHLh**	**total**	**SSD**	**AHLm**	**AHLh**	**total**
First fitting	VM	0.15	-0.06	0.07	0.04	0.60	0.74	0.76	0.73
	ACN	0.22	0.03	0.10	0.09	0.44	0.87	0.67	0.47
	ACN / AFN	0.24	**0.62****	0.14	**0.36***	0.44	**0.0003**	0.533	**0.003**
	ACN / AIEC	-0.05	0.04	0.18	0.07	0.86	0.84	0.43	0.58
1 month	VM	-0.33	-0.08	0.29	0.04	0.26	0.65	0.16	0.72
	ACN	0.22	-0.07	0.15	0.07	0.48	0.70	0.48	0.58
	ACN / AFN	-0.3	0.34	0.03	0.08	0.34	0.08	0.89	0.70
	ACN / AIEC	-0.03	-0.04	0.08	0.01	0.91	0.81	0.72	0.91
3 months	VM	-0.21	-0.09	0.35	0.04	0.46	0.62	0.15	0.76
	ACN	0.07	-0.21	0	-0.08	0.82	0.27	0.98	0.56
	ACN / AFN	-0.43	0.11	0.29	0.05	0.14	0.60	0.24	0.70
	ACN / AIEC	-0.24	-0.15	0.13	-0.06	0.41	0.44	0.59	0.66
6 months	VM	-0.02	0.13	0.25	0.14	0.95	0.56	0.35	0.31
	ACN	0.18	-0.09	-0.01	0.01	0.57	0.66	0.96	0.95
	ACN / AFN	-0.05	0.30	0.11	0.14	0.88	0.20	0.70	0.36
	ACN / AIEC	-0.05	-0.29	0.08	-0.10	0.89	0.17	0.76	0.48

Tab. 1 Statistische Analyse der Korrelation zwischen CN-Metrik und WRS in verschiedenen Gruppen zu verschiedenen Zeitpunkten nach der Aktivierung des CI. (SSD: einseitige Taubheit; AHLh: hoher asymmetrischer Hörverlust)

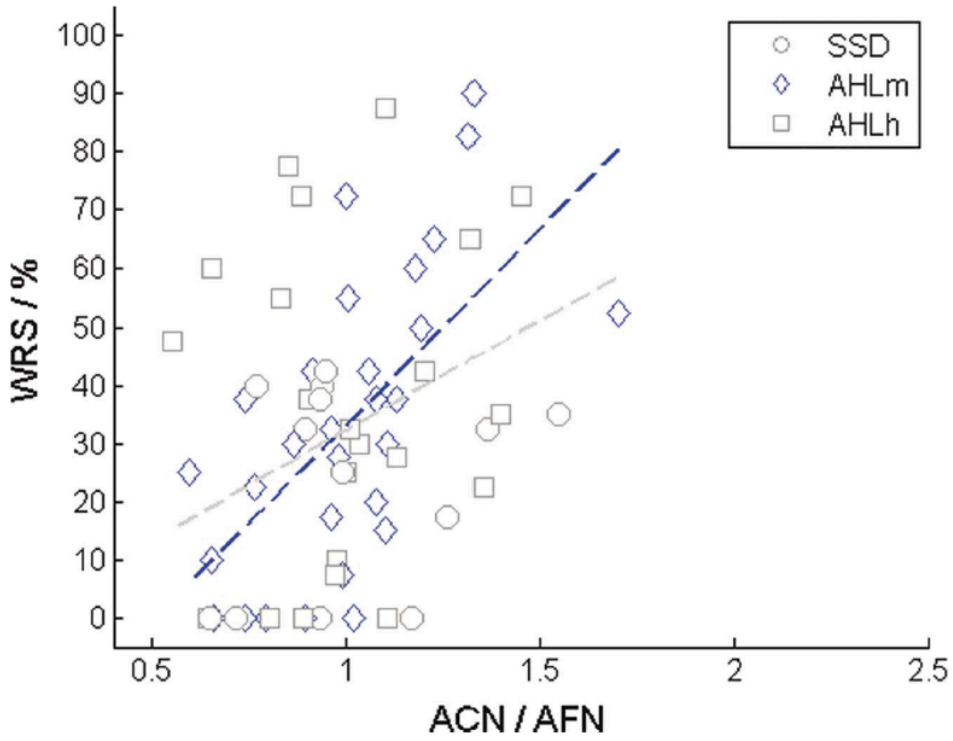


Abb. 18 Fläche des CN normalisiert auf die Fläche des Gesichtsnervs (ACN/AFN) und die Sprachverständlichkeit nach der Erstanpassung für vier Gruppen mit unterschiedlichem Grad des asymmetrischen Hörverlustes: einseitige Taubheit (SSD) (graue Kreise), moderater asymmetrischer Hörverlust (dunkelblaue Rauten) und hoher asymmetrischer Hörverlust (graue Quadrate). Die Pearson-Korrelationsanalysen zeigen eine positive Korrelation mit R = 0,36 in der gesamten Gruppe (graue gestrichelte Linie) und eine verstärkte Korrelation mit R = 0,62 in der Subgruppe der AHLm (dunkelblaue gestrichelte Linie).

Arbeit 6: Systemische Überschätzung der Winkelinsertionstiefe von Elektrodenarrays bei Cochlea-Implantat-Patienten mit kleiner Cochlea durch eine Bildverarbeitungssoftware

Die Schätzung der Länge des Ductus cochlearis (CDL) unterstützt CI-Teams bei der Auswahl der geeigneten Elektrodenarray-Länge vor der Cochlea-Implantation. Kommerzielle Software-Algorithmen, wie z.B OTOPLAN machen dies möglich und werden häufig verwendet. Hier stellt sich die Frage, wie genau diese kommerziellen Software-Algorithmen sind. In dieser Studie werden Patienten untersucht, die alle ein 31.5mm flexibles Elektrodenarray erhalten haben und bei denen im radiologischen Bild eine normale Cochlea befundet wurd. Insgesamt wurden 72 Ohren von Patienten, die sich zwischen Januar 2019 und Dezember 2022 einer Cochlea-Implantation unterzogen, eingeschlossen. Routinemäßig durchgeführte postoperative Stenvers-Röntgenaufnahmen zeigten in allen Fällen eine vollständige Insertion des Elektrodenarrays. Eine präoperative geschätzte maximale Insertionstiefe (maxAID) wurde mithilfe der kommerziellen Software-Algorithmen ermittelt. Die tatsächliche maxAID wurde anhand der Stenvers-Röntgenaufnahmen bestimmt (Abbildung 19). Die präoperative geschätzte maxAID zeigte eine Korrelation mit der postoperativ gemessenen maxAID ($R = 0,45$, $p < 0,001$), wich jedoch um 44,8° ± 8,4° ab (Abbildung 20). Es gibt eine systemische Überschätzung der Insertionstiefen durch die kommerziellen Software-Algorithmen für Werte, die 720° überschreiten. Um dies zu berücksichtigen, wurden ein optimaler Offset von 2,4 mm identifiziert, wenn dieser Parameter bei der Schätzung der maxAID für Tiefen über 720° berücksichtig wird (Abbildung 21). Diese Ergebnisse zeigen, dass OTOPLAN die AID bei CI-Patienten vorhersagt, jedoch bei kleinen Cochleae (CDL < 35 mm) abweicht.

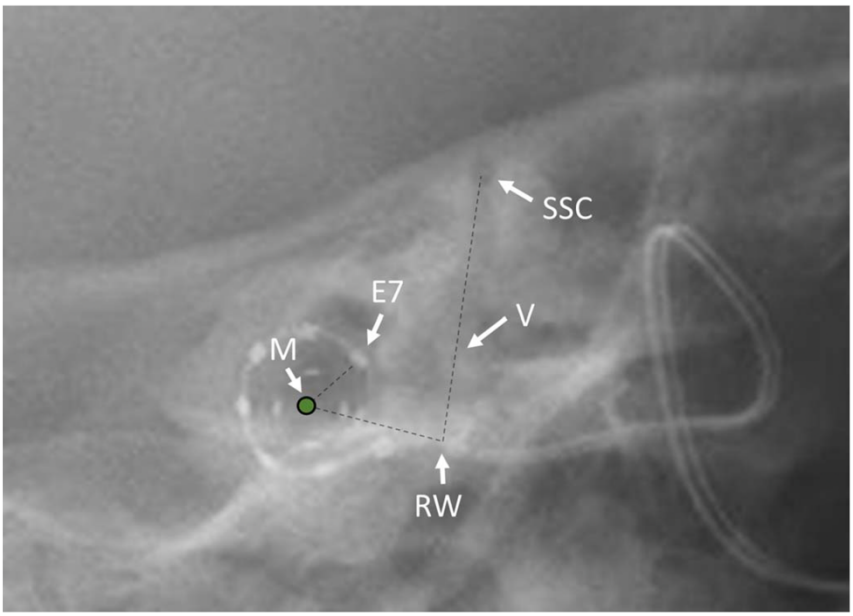


Abb.19 Postoperatives Röntgenbild (Stenvers) zur Bestimmung des Insertionswinkels, veranschaulicht am Beispiel der Elektrode 6 aus einem FLEXsoft-Elektrodenarray; SSC bezeichnet den oberen Bogengang; V: Vestibulum; M: Modiolus; 0°: Position des runden Fensters (RW).

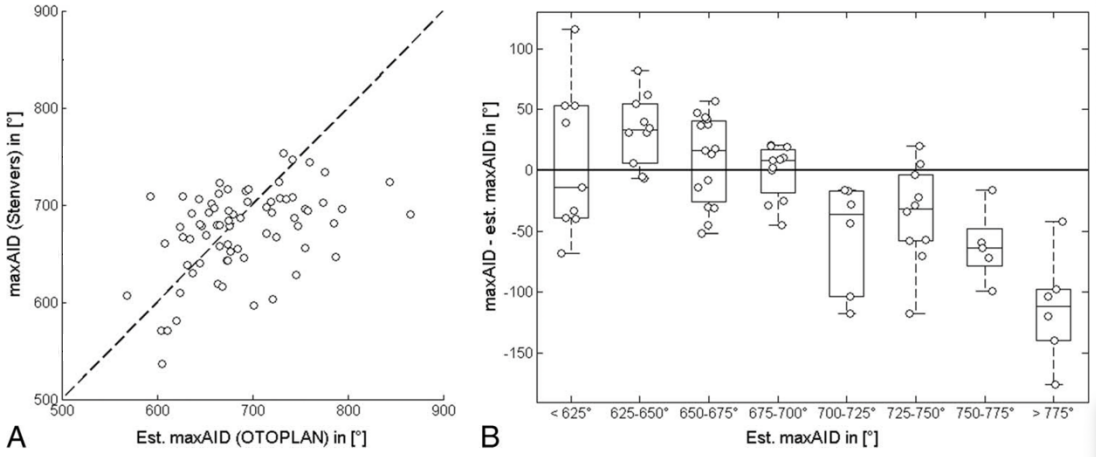


Abb. 20 (A) Streudiagramm, das die Beziehung zwischen der geschätzten und gemessenen maxAID veranschaulicht. (B) Abweichungen der geschätzten maxAID von den gemessenen Werten, gruppiert nach geschätzter Insertionstiefe. Vorhersagen im Bereich von 700°-725° und bei tieferen Insertionswinkeln zeigen eine zunehmend größere Abweichung von der tatsächlich gemessenen maxAID. Die negative Abweichung bedeutet eine Überschätzung der Insertionswinkel durch die kommerzielle Software.

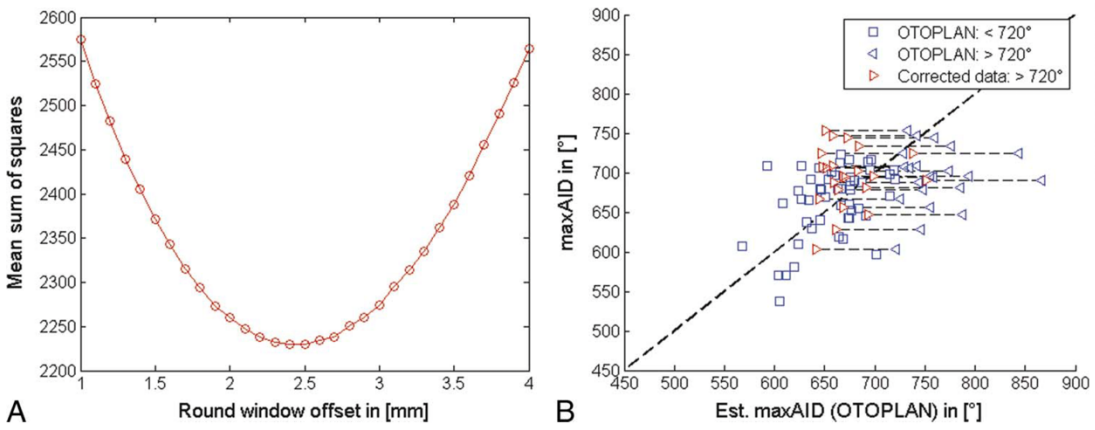


Abbildung 21 Die Optimierung der Schätzung der maximalen Insertionstiefe (maxAID) mithilfe von OTOPLAN beinhaltete die Anpassung des Offsets am runden Fenster (RW). (A): zeigt die Abweichung der geschätzten und gemessenen maxAID nach Feinabstimmung des RW-Offsets, wobei das Optimum bei 2,4 mm liegt. (B): Präsentiert eine Streudiagramm, dass die Korrelation zwischen der geschätzten und gemessenen maxAID darstellt, kategorisiert als Est. maxAID < 720° (blaue Quadrate), Est. Max.AID > 720° (blaue Dreiecke, nach links zeigend) und maxAID > 720° nach Korrektur unter Verwendung des optimalen RW-Offsets (rote Dreiecke, nach rechts zeigend).

Die richtige Position des Elektrodenarrays in der Cochlea ist die Voraussetzung für ein optimal funktionierendes CI. Derzeit verwenden die meisten Kliniken ein postoperatives radiologisches Röntgenbild, um die Elektrodenposition zu bestimmen. Wenn eine abnormale Position der Elektrode festgestellt wird, muss eine Revisionsoperation durchgeführt werden (58-60). Darüber hinaus erhöht die postoperative Bildgebung die Strahlenbelastung. Um eine Elektrodenfehllage und eine postoperative Bildgebung zu vermeiden, wäre ein intraoperatives, stabiles und zuverlässiges Echtzeit-Monitoring der Elektrodenlage wünschenswert.

Arbeit 7: Elektrisch evozierte Mismatch-Negativität (MMN) durch Sprachreize als objektiver Indikator zur Beurteilung der Leistung von Cochlea-Implantaten

Ziel dieser Studie, war die Untersuchung, ob das kortikale Potenzial der elektrisch evozierte MMN als objektiver Indikator zur Beurteilung der Leistung von CI verwendet werden kann. Es wurde Patienten eingeschlossen, die ein CI der Firma Med-EL erhielten. Zusätzlich wurde eine Gruppe junger normalhörender Personen als Kontrollgruppe rekrutiert. Das Sprachreiz-Paradigma bestand aus den Silben ba und da, die über eine Audioeingabe an den CI-Prozessor übertragen wurden, um eine MMN-Antwort abzuleiten. Bei den normalhörenden Probanden wurden die Sprachreize über einen In-Ear-Kopfhörer präsentiert. Das Sprachverstehen wurde mit der Worterkennungstests (WRS) unter Verwendung des Freiburger Einsilbertests gemessen. Insgesamt wurden 23 CI-Patienten und 35 normalhörende Personen untersucht. Die Ergebnisse zeigen, dass die MMN-Komponenten bei CI-Patienten denen normalhörender Probanden ähneln, insbesondere in Bezug auf die typischen Wellen N1, P2 und MMN. Allerdings war die Amplitude bei CI-Patienten signifikant reduziert und die Latenz verlängert (Abbildung 22, 23). Zudem zeigte sich eine signifikante Korrelation zwischen der elektrisch evozierten MMN und dem WRS ($R = 0{,}50$, $p = 0.01$) bei den CI-Patienten. Darüber hinaus wurden die CI-Patienten basierend auf ihrem WRS in zwei Gruppen eingeteilt: eine Gruppe mit gutem postoperativem Sprachverstehen und eine Gruppe mit schlechtem postoperativen Sprachverstehen. Die Ergebnisse zeigten, dass die Amplitude in der Gruppe mit gutem Sprachverstehen signifikant höher war als in der Gruppe mit schlechtem Sprachverstehen ($\chi^2 = 7.0$, $p = 0.008$). Zudem war die Latenz in der Gruppe mit gutem Sprachverstehen signifikant kürzer ($\chi^2 = 5{,}3$, $p = 0.02$) (Abbildung 24). Diese Studie zeigt, dass die elektrisch evozierte MMN als objektiver Indikator zur Beurteilung der Leistung von Cochlea-Implantaten verwendet werden kann. Die Methode hat das Potenzial, wertvolle Erkenntnisse für notwendige Anpassung im Anpassungsprozess zu liefern, insbesondere für Patienten, die keine subjektiven Tests durchführen können.

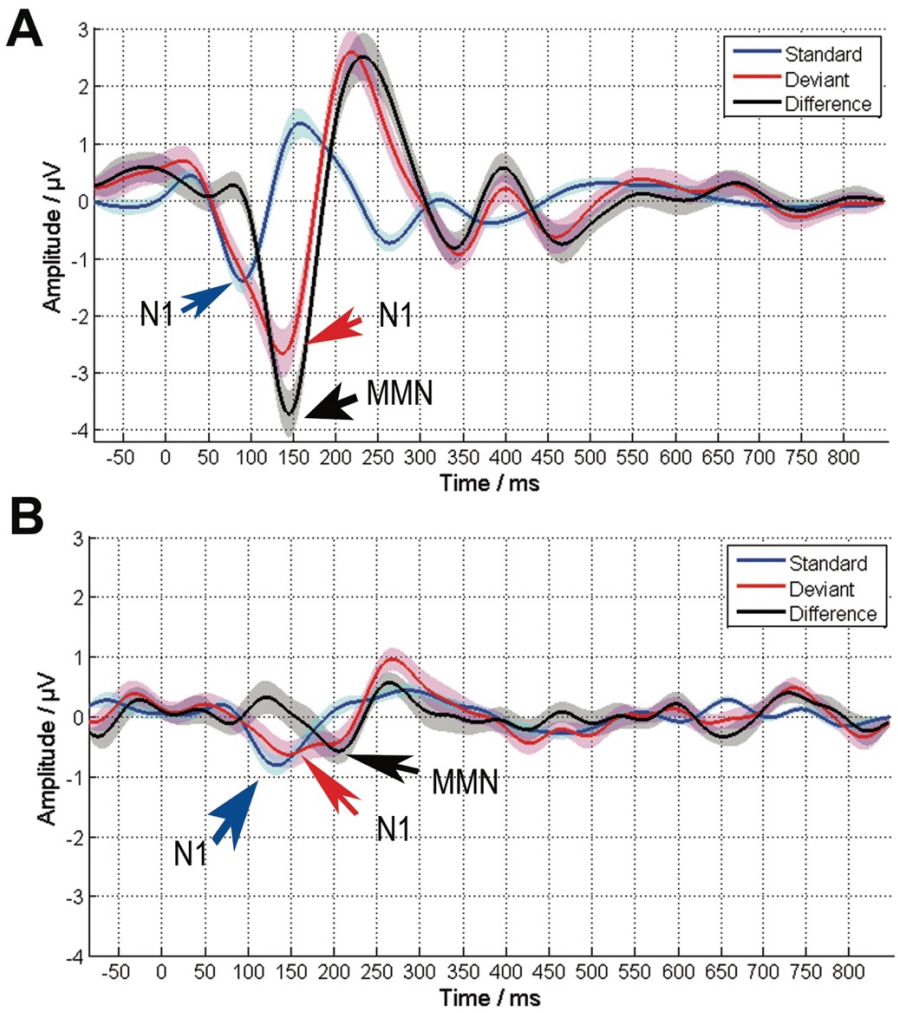


Abb. 22 Darstellung der EEG-Antwort auf den Standardreiz (blau), den abweichenden Reiz (rot) und die Differenz zwischen den beiden Reizen (schwarz) für Kontrollgruppe (A) und die CI-Gruppe (B). Die durchgezogenen Linien repräsentieren die durchschnitte Antwort, während die schattierte Fläche den Standardfehler anzeigt. Die Pfeile heben die N1-Antworten auf sowohl den Standard- als auch den abweichenden Reiz sowie die MMN-Antwort auf deren Differenz hervor. Sowohl der Standard- als auch der abweichende Reiz zeigen eine ähnliche kortikale Antwort, die durch eine ausgeprägte N1, die zwischen 120 ms und 150 ms ihren Höhepunkt erreicht, sowie eine markante P2, deren Gipfel zwischen 250 ms und 300 ms liegt, gekennzeichnet ist. Dennoch wird die kortikale Antwort auf den abweichenden Reiz (rot), der sowohl N1- als auch P2-Ableitungen umfasst, von der MMN überschattet, die durch die Analyse der Differenz zwischen dem Standard- und dem abweichenden Reiz (Schwarz) unterscheidbar ist. Der Peak tritt dabei zwischen 140 ms und 210 ms auf.

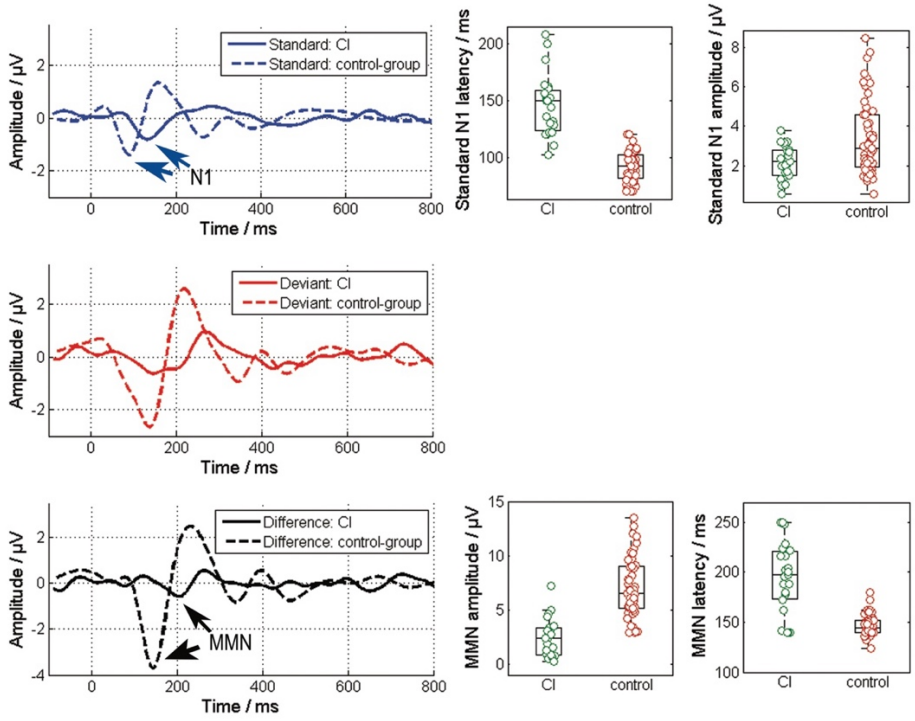


Abbildung 23 Vergleich der Antworten auf den Standardreiz (blau), den abweichenden Reiz und die Differenz ihrer kortikalen Antworten zwischen der CI-Gruppe und der Kontrollgruppe. Die linke Spalte zeigt die grand-average Antwort, während die rechte Spalte die Amplitude und Latenzen der spezifischen Potenziale innerhalb dieser EEG-Antworten im Detail darstellt. Die N1- und MMN-Antworten werden durch die Pfeile hervorgehoben. (Standard: N1-P2-Amplitude und N1-Peak-Latenz; Differenz: MMN-Amplitude von Peak zu Peak und MMN-Peak-Latenz)

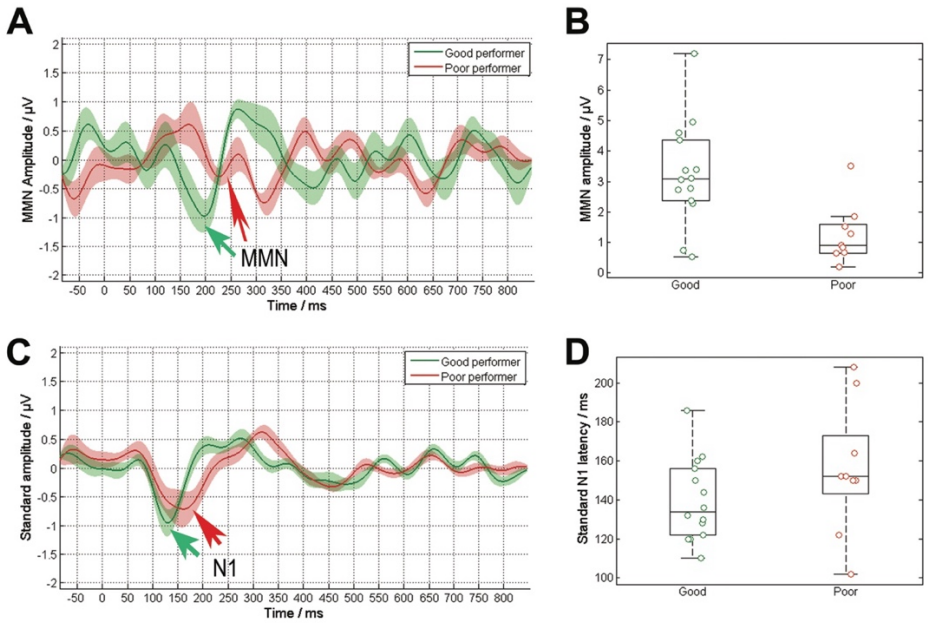


Abb. 24 Vergleich der Kortikalen Antworten auf den abweichenden Reiz (A) und den Standardreiz (C), basierend auf den gruppierten Daten, die nach Sprachverstehen eingeteilt wurden (guter Performer: WRS ≥ 65%, schlechte Performer: WRS < 65%). Die durchgezogenen Linien repräsentieren die durchschnittliche Antwort, während die schattierte Fläche den Standardfehler anzeigt. Die Pfeile heben die N1-Antworten auf beide Standardreize und die MMN-Antwort auf deren Differenz hervor. Der abweichende Reiz zeigte bemerkenswerte Unterschiede in der Amplitude der MMN-Antwort (B). Schlechte Performer wiesen eine reduzierte MMN-Amplitude auf. Der Standardreiz zeigte keine signifikanten Unterschiede in der N1-Latenz (D), wobei verzögerte Latenzen bei den schlechten Performern beobachtet wurden.

5. Schlussbetrachtung

Altersbedingte Schwerhörigkeit betrifft meistens Menschen mit einem Alter über 80 Jahre und verursacht Kommunikationsprobleme, Isolation sowie kognitive Einschränkungen (61-62). Im Laufe des Alterungsprozesses gibt es zudem viele andere Faktoren, die das Hörvermögen beeinflussen können, wie z.B. Lärmbelastung oder ototoxische Medikamente. Solche Faktoren sind schwer zu kontrollieren und können in der Analyse nicht vollständig erfasst werden. Daher sind Experimente in Tiermodellen notwendig, um die Mechanismen zu untersuchen, da hier diese Faktoren während der kurzen Lebensspanne besser kontrolliert werden können. In der ersten Studie wurden Wüstenrennmäuse als Tiermodell verwendet, um diese potenziellen Mechanismen zu untersuchen. Die Arbeit untersuchte die grobe Morphologie der Synapsen bei jungen Rennmäusen sowie die Funktion der noch erhaltenen Nervenfasern bei alten Rennmäusen. Die morphologische Studie zeigte, dass die Gradienten im Ribbon-Volumen mit früher publizierten Befunden übereinstimmen und weiterhin eine Rolle bei der Differenzierung der physiologischen Eigenschaften von Typ-I-Afferenzen unterstützen (39, 45, 51-53). Die physiologische Studie zeigte, dass die zeitliche Kodierung der erhaltenen Nervenfasern nicht abnimmt. Dies deutet darauf hin, dass altersbedingte Defizite in der zeitlichen Kodierung eher zentral auftreten, möglichweise aufgrund eines Verlusts von Hörnervfasern (oder deren peripheren Synapsen), jedoch nicht aufgrund qualitativer Änderungen in den Reaktionen der verbleibenden Hörnervfasern. Diese Ergebnisse bilden die Grundlage für zukünftige Untersuchungen zu den morphologischen und physiologischen Veränderungen der Synapsen im Alter sowie dazu, welche Ebenen der Hörbahn sich verschlechtern oder verändern.

Die frühe Erkennung altersbedingter Schwerhörigkeit, insbesondere im Hinblick auf versteckten Hörverlust, ist sehr schwierig. Es gibt derzeit keinen Goldstandard für die Bestimmung des versteckten Hörverlustes. Es gibt einige Methoden, einschließlich BERA, Sprachverstehen im Umgebungsgeräusch, Stapediusreflex-Messung, EHFT-Schwelle und Krümmung der Welle I der BERA die unterschiedlich gut mit verstecktem Hörverlust korrelieren. Die vorliegenden Arbeiten zur temporalen Kodierung in Abhängigkeit vom Alter und zur Quantifizierung der Welle I Krümmung befassen sich mit der Entwicklung eines optimalen und zuverlässigen Verfahrens. Mit der Krümmungsberechnung der Welle I steht möglicherweise erstmals ein zuverlässiges Verfahren für die Erfassung der altersbedingten Synaptopathie zur Verfügung. Auf zentraler Ebene verwendet die vorliegende Arbeit elektrophysiologische Untersuchungen kortikaler Potentiale im Rahmen der MMN. Die Ergebnisse zeigen, dass die Amplitude der MMN im Sprachparadigma signifikant altersabhängig ist. Diese deutet darauf hin, dass die Sprachinduzierte MMN-Amplitude als potenzieller Indikator für frühe Veränderungen der zentralen Hörbahn herangezogen werden kann.

Die medikamentöse Therapie der altersbedingten Schwerhörigkeit ist bisher nicht sehr erfolgreich (63). Derzeit sind Hörgeräte und CIs die gängigsten Therapiemöglichkeiten für diese Erkrankung. CIs haben vielversprechende Ergebnisse gezeigt. Viele Faktoren können das postoperative Ergebnis beeinflussen. Die Auswahl geeigneter Patienten ist der erste Schritt zur Planung eines CI. Zahlreichende Studien haben die Prognosekriterien kontinuierlich verbessert, was die postoperative Leistung weiter steigert. Zusätzlich spielt eine optimale Elektrodenposition in der Cochlea eine große Rolle für das bestmögliche Sprachverstehen. Die bisher vorgestellte Methode der radiologischen Bildgebung liefern wertvolle Informationen

über das Elektrodenarray und dessen Lage in der Cochlea. Die exakte Interpretation der Messwerte ermöglicht eine präzise Anpassung der Cochlea-Implantation an die individuellen Frequenzspezifikation. Zusätzlich ermöglicht das hier präsentierte objektive Maß zur Beurteilung des postoperativen Sprachverstehens die Evaluierung von CI-Patienten, die keine subjektiven Tests durchführen können. Diese objektiven Methoden liefert ebenfalls wertvolle Erkenntnisse für notwendige Anpassung im Anpassungsprozess.

6. Literaturverzeichnis

1. Wang J and Puel JL. Presbycusis: An update on cochlear mechanisms and therapies. J Clin Med. 2020;9(1):218. doi: 10.3390/jcm9010218.
2. Addressing the rising prevalence of hearing loss; World Health Organization: Geneva, Switzerland, 2018.
3. Helzner EP, Cauley JA, Pratt SR, Wisniewski SR, Zmuda JM, Talbott EO, de Rekeneire N, Harris TB, Rubin SM, Simonsick EM, Tylavsky FA, Newmann AB. Race and sex differences in age-ralted hearing loss: the health, aging and body composition study. J Am Geriatr Soc. 2005;53(12):2119-27. doi: 10.1111/j.1532-5415.2005.00525.x.
4. Pearson JD, Morrell CH, Gordon-Salant S, Brant LJ, Metter EJ, Klein LL, Fozard JL. Gender differences in a longitudinal study of age-associated hearing loss. J Acoust Soc Am. 1995;97(2):1196-205. doi:10.1121/1.412231.
5. Charitidi K, Meltser I, Tahera Y, Canlon B. Functional responses of estrogen receptors in the male and female auditory system. Hear Res. 2009;252(1-2):71-78. doi: 10.1016/j.heares.2008.12.009.
6. Delhez A, Lefebvre P, Pequeux C, Malgrange B, Delacroix L. Audiotry function and dysfunction: Estrogen makes a difference. Cell Mol Life Sci. 2020;77(4):619-635. doi: 10.1007/s00018-019-03295-y.
7. Williamson T, Zhu X, Pineros J, Ding B, Frisina RD. Understanding hormone and hormone therapies' impact on the auditory system. J Neurosci Res. 2020;98(9):1721-1730. doi: 10.1002/jnr.24588.
8. Helfer KS. Gender, age and hearing. Semin Hear. 2001;22(3):271-286.
9. Hederstierna C, Hultcrantz M, Rosenhall U. Estrogen and hearing from a clinical point of view; chearactersitics of auditory function in women with Turner syndrome. Hear Res. 2009;252(1-2):3-8.
10. Bowl MR, Dawson SJ. Age-related hearing loss. Cold Spring Harb Perspect Med. 2019;9(8):a033217. doi:10.1101/cshperspect.a033217.
11. Wang W, Zhao X, Chai R, Fan J. Progress on mechanisms of age-related hearing loss. Front Neurosci. 2023;17:1253574. doi:10.3389/fnins.2023.1253574.
12. Xiong W, Yu S, Liu K, Gong S. Loss of cochlear ribbon synapses in the early stage of aging causes initial hearing impairment. Am J Transl Res. 2020;12(11):7354-7366.
13. Schaette R, McAlpine D. Tinnitus with a normal audiogram: physiological evidence for hidden hearing loss and computational model. J Neurosci Off J Soc Nurosci. 2011; 31:13452-13457.
14. Bajin MD, Dahm V, Lin VYW. Hidden hearing loss: current concepts. Curr Opin Otolaryngol Head Neck Surg. 2022;30(5):321-325. doi: 10.1097/MOO.0000000000000824.
15. C Kohrman D, Wan G, Cassinotti L, Corfas G. Hidden hearing loss: A disorder with multiple etiologies and mechanisms. Cold Spring Harb Perspect Med. 2020;10(1):a035493. doi:10.1101/cshperspect.a035493.
16. Sergeyenko Y, Lall K, Liberman MC, Kujawa SG. Age-related cochlear synaptopathy: an early-onset contributor to auditory functional decline. J Neurosci 2013; 33(34):13686-13694.
17. Viana LM, O'Malley JT, Burgess BJ, Jones DD, Oliveria CA, Santos F, Merchant SN, Liberman LD, Liberman MC. Cochlear neuropathy in human presbycusis: confocal analysis of hidden hearing loss in post-mortem tissue. Hear Res. 2015;327:78-88. doi: https://doi.org/10.1016/j.heares.2015.04.014.

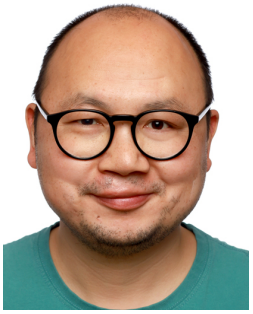
18. Kujawa SG, Libermann MC. Adding insult to injury: cochlear nerve degeneration after 'temporary' noise-induced hearing loss. J Neurosci. 2009; 29(45):14077–14085. https:// doi. org/10. 1523/ JNEUR OSCI. 2845- 09. 2009.
19. Kujawa SG, Liberman MC (2015) Synaptopathy in the noiseexposed and aging cochlea: primary neural degeneration in acquired sensorineural hearing loss. Hear Res 330(Pt B):191–199. https:// doi. org/ 10. 1016/j. heares. 2015. 02. 009
20. Shaheen LA, Valero MD, Liberman MC. Towards a diagnosis of cochlear neuropathy with envelope following responses. J Assoc Res Otolaryngol. 2015; 16(6):727-745. https:// doi. org/ 10. 1007/s10162- 015- 0539-3.
21. Bramhall NF. Use of the auditory brainstem response for assessment of cochlear synaptopathy in humans. J Acoust Soc Am. 2021;150(6):4440. https:// doi. org/ 10. 1121/ 10. 00074 84.
22. Valero MD, Hancock KE, Liberman MC. The middle ear muscle reflex in the diagnosis of cochlear neuropathy. Hear Res. 2016;332:29-38. doi: 10.1016/j.heares.2015.11.005.
23. Mepani AM, Kirk SA, Hancock KE, Bennett K, de Gruttola V, Liberman MC, Maison SF. Middle ear muscle reflex and word recognition in ‚normal-hearing' adults: evidence for cochlear sanpatopathy? Ear Hear. 2020;41(1):25-38. doi: 10.1097/AUD0000000000000804.
24. Bharadwaj HM, Mai AR, Simpson JM, Choi I, Heinz MG, Shinn-Cunningham BG. Non-invasive assays of cochlear synaptopathy – candidates and considerations. Neuroscience. 2019;407:53-66. doi: 10.1016/j.neuroscience.2019.02.031.
25. Guest H, Munro KJ, Plack CJ. Acoustic Middle-Ear-Muscle-Reflex thresholds in humans with normal audiograms: no relations to tinnitus, speech perception in noise, or noise exposure. Neuroscience. 2019;407:75-82. doi: 10.1016/j.neuroscience.2018.12.019.
26. Liberman MC, Epstein MJ, Cleveland SS, Wang H, Maison SF. Toward a differential diagnosis of hidden hearing loss in humans. PLoS ONE 2016; 11(9):e0162726. https:// doi. org/ 10. 1371/journ al. pone. 0162726.
27. Liberman MC, Liberman LD, Maison SF. Effect feedbackslows cochlear aging. J Neurosci. 2014;34(13):4599–4607. https:// doi.org/ 10. 1523/ JNEUR OSCI. 4923- 13. 2014.
28. Maison SF, Usubuchi H, Liberman MC. Efferent feedback minimizes cochlear neuropathy from moderate noise exposure. J Neurosci 2013;33(13):5542–5552. https:// doi. org/ 10. 1523/ JNEUROSCI. 5027- 12. 2013.
29. Bao J, Jegede SL, Hawks JW, Dade B, Guan Q, Middaugh S, Qiu Z, Levina A, Tsai TH. Detecting cochlear synaptopathy through curvature quantification of the auditory brainstem response. Front Cell Neurosci. 2022;16:851500. https://doi.org/10.3389/fncel.2022.851500.
30. Lee J, Nadol JB Jr., Eddington DK. Depth of electrode insertion and postoperative performance in humans with cochlear implants: a histopathologic study. Audiol Neurootol. 2010;15:323–31.
31. Blamey P, Artieres F, Başkent D, et al. Factors affecting auditory performance of postlinguistically deaf adults using cochlear implants: an update with 2251 patients. Audiol Neurootol. 2013;18:36–47.
32. Pisoni DB, Kronenberger WG, Harris MS, Moberly AC. Three challenges for future research on cochlear implants. World J Otorhinolaryngol Head Neck Surg. 2018;23:240–54.
33. Peng KA, Kuan EC, Hagan S, Wilkinson EP, Miller ME. Cochlear nerve aplasia and hypoplasia: predictors of cochlear implant success. Otolaryngol Head Neck Surg. 2017;157:392–400.

34. Chung J, Jang JH, Chang SO, et al. Does the width of the bony cochlear nerve canal predict the outcomes of cochlear implantation? Biomed Res Int. 2018;21:5675848.
35. Schmiedt RA (2010): The physiology of cochlear presbycusis. In: The aging auditory system. London: Springer.
36. Mills JH, Schmiedt RA and Kulish LF. Age-related changes in auditory potentials of Mongolian gerbils. Hear Res. 1990. 46:201-210.
37. Hamann I, Gleich O, Klump GM, Kittel MC, Boettcher FA, Schmiedt RA and Strutz J: Behavioral and evoked-potential thresholds in young and old Mongolian gerbils (meriones unguiculatus). Hear Res. 2002;171:82-95.
38. Liberman MC: 1982b. Single-neuron labeling in the cat auditory nerve. Science 216:1239-1241.
39. Furman AC, Kujawa SG, Liberman MC. Noise-induced cochlear neuropathy is selective for fibers with low spontaneous rates. J Neurophysiol. 2013;110(3):577-586.
40. Bourien J, Tang Y, Batrel C, Huet A, Lenoir M, Ladrech S, Desmadryl G, Nouvian R, Puel JL., Wang J. Contribution of auditory nerve fibers to compound action potential of the auditory nerve. J Neurophysiol. 2014;112:1025-1039.
41. Liberman, MC. Single-neuron labeling in the cat auditory nerve. Science 1982;216:1239e1240.
42. Merchan-Perez, A, Liberman, MC. Ultrastructural differences among afferent synapses on cochlear hair cells: correlations with spontaneous discharge rate. J. Comp. Neurol. 1996; 371, 208e221.
43. Gilels, F, Paquette, ST, Zhang, J, Rahman, I, White, PM. Mutation of Foxo3 causes adult onset auditory neuropathy and alters cochlear synapse architecture in mice. J. Neurosci. 2013;33, 18409e18424.
44. Liberman, LD, Wang, H, Liberman, MC. Opposing gradients of ribbon size and AMPA receptor expression underlie sensitivity differences among cochlearnerve/ hair-cell synapses. J. Neurosci. 2011;31, 801e808.
45. Kalluri, R, Monges-Hernandez, M. Spatial gradients in the size of inner hair cell ribbons emerge before the onset of hearing in rats. J Assoc Res Otolaryngol. 2017;18, 399e413.
46. Bartrel, C, Huet, A, Hasselmann, F, Wang, J, Desmadryl, G, Nouvian, R, Puel, JL, Bourien, J. Mass potentials recorded at the round window enable the detection of low spontaneous rate fibers in gerbil auditory nerve. Plos One. 2017;12:e0169890.
47. Gleich, O, Semmler, P, Strutz, J. Behavioral auditory thresholds and loss of ribbon synapses at inner hair cells in aged gerbils. Exp. Gerontol. 2016;84:61e70.
48. Johnson, SL, Forge, A, Knipper, M, Munkner, S, Marcotti, W. Tonotopic variation in the calcium dependence of neurotransmitter release and vesicle pool replenishment at mammalian auditory ribbon synapses. J. Neurosci. 2008;28:7670e7678.
49. Meyer, AC, Frank, T, Khimich, D, Hoch, G, Riedel, DMCN, Yarin, YM, Harke, B, Hell, SW, Egner, A, Moser, T. Tuning of synapse number, structure and function in the cochlea. Nat. Neurosci. 2009;12:444e453.
50. Slepecky, NB, Galsky, MD, Swartzentruber-Martin, H, Savage, J. Study of afferent nerve terminals and fibers in the gerbil cochlea: distribution by size. Hear Res. 2000;144:124e134.
51. Liberman, LD, Suzuki, J, Liberman, MC. Dynamics of cochlear synaptopathy after acoustic overexposure. JARO J. Assoc. Res. Otolaryngol. 2015;16:205e219.
52. Song, Q, Shen, P, Li, XW, Shi, LJ, Liu, LJ, Wang, JP, Yu, ZP, Stephen, K, Aiken, S, Yin, S, Wang, J. Coding deficits in hidden hearing loss induced by noise: the nature and impacts. Sci. Rep. 2016;6.

53. Yin, Y, Liberman, LD, Maison, SF, Liberman, MC. Olivocochlear innervation maintains the normal modiolar-pillar and habenular-cuticular gradients in cochlear synaptic morphology. J Assoc Res Otolaryngol. 2014;15:571e583.
54. Joris PX, Louage DH, Cardoen L, van der Heijden M. Correlation index: a new metric to quantify temporal coding. Hear Res. 2006;216–217:19–30.
55. Näätänen R, Gaillard A, Mäntysalo S. Early selective-attention effect on evoked potential reinterpreted. Acta Psychol. 1978;42:313-329.
56. Näätänen R. The mismatch negativity; A powerful tool for cognitive neuroscience. Ear Hear. 1995;16:6-18.
57. Näätänen R, Petersen B, Torppa R, Lonka E, Vuust P. The MMN as a viable and objective marker of auditory development in CI users. Hear. Res. 2017;353:57-75.
58. Hoppe U, Brademann G, Stoever T, et al. Evaluation of a transimpedance matrix algorithm to detect anomalous cochlear implant electrode position. Audiol Neurootol 2022;27:347–55.
59. Gabrielpillai J, Burck I, Baumann U, et al. Incidence for tip foldover during cochlear implantation. Otol Neurotol 2018;39:1115–21.
60. Noble AR, Christianson E, Norton SJ, et al. Reliability of measuring insertion depth in cochlear implanted infants and children using cochlear view radiography. Otolaryngol Head Neck Surg 2020;163:822–8.
61. Chern A and Golub JS. Age-related hearing loss and dementia. Alzheimer Dis Assoc Disord. 2019;33(3):285-290.
62. Su P, Hsu CC, Lin HC, Huang WS, Yang TL, Hsu WT, Lin CL, Hsu CY, Chang KH, Hsu YC. Age-related hearing loss and dementia: a 10-year national population-based study. Eur Arch Otorhinolaryngol. 2017;274(5):2327-2334.
63. Michels TC, Duffy MT, Rogers DJ. Hearing loss in adults: differential diagnosis and treatment. Am Fam Physician. 2019;100(2):98-108.

Anhang

Curriculum Vitae



Persönliche Daten

- **Name:** Dr. med. Lichun Zhang
- **Geburtsdatum:** 23.02.1985
- **Geburtsort:** Tongcheng, Anhui, China

Beruflicher Werdegang

- **07/2021:** Ernennung zum Oberarzt, Klinik und Poliklinik für Hals-Nasen-Ohrenheilkunde, Kopf- und Halschirurgie "Otto Körner", Universitätsmedizin Rostock, Prof. Dr. med. R. Mlynski
- **01/2021 – 06/2021:** Assistenzarzt/Facharzt, Universitätsklinik für Hals-Nasen-Ohren-Heilkunde, Evangelisches Krankenhaus Oldenburg, Medizinischer Campus, Universität Oldenburg, Prof. Dr. med. A. Radeloff
- **09/2018 – 12/2020:** Assistenzarzt, Klinik für Hals-, Nasen-, Ohrenheilkunde, Charité – Universitätsmedizin Berlin, Prof. Dr. med. H. Olze
- **05/2018 – 08/2018:** Assistenzarzt, Abteilung für Hals-, Nasen-, Ohrenheilkunde, Sankt Getrauden Krankenhaus, Berlin, Prof. Dr. med. O. Kaschke
- **12/2016 – 04/2018:** Assistenzarzt, Klinik für Hals-, Nasen-, Ohrenheilkunde, Klinikum Oldenburg, Medizinischer Campus, Univerität Oldenburg, Prof. Dr. med. F. Hoppe
- **12/2014 – 04/2018:** Postdoc, Abteilung für Neurowisschenschaften, Exzellenzcluster "Hearing4all".
- **09/2010 – 11/2014:** Assistenzarzt, Abteilung für HNO-Heilkunde, Krankenhaus für Augen-, Ohren-, Nasen- und Halskrankheiten der Fudan Universität, Shanghai, China
- **09/2007 – 06/2010:** Assistenzarzt, Abteilung für Radiologie, Krankenhaus für Augen-, Ohren-, Nasen- und Halskrankheiten der Fudan Universität, Shanghai, China.

Akademischer Werdegang

- **12/2014 – 04/2018:** Postdoc, Abteilung für Neurowisschenschaften, Exzellenzcluster "Hearing4all". Forschungsprojekte: 1). Aufnahme der Einzeleinheiten des N. vestibulocochlearis in alternden Rennmäusen; 2). Veränderungen der cochleären Synapsen der alternden Rennmäuse

- **11/2012 – 04/2014:** Postdoc und Gastarzt, Abteilung für HNO-Heilkunde, Universitätskrankenhaus Iowa, Iowa City, USA. Prof. M. Hansen
- **01/2012 – 01/2014:** Medizinische Lizenzprüfungen in den USA (USMLE): 1). Schritt 1, 2 und 3. 2). ECFMG-Zertifikat: 26.08.20013
- **07/2013:** Promotion zum Thema „Knochenleitungshörvermögen bei Mikrotie- Patienten“, Themenvergabe von Prof. Tianyu Zhang, Krankenhaus für Augen-, Ohren-, Nasen- und Halskrankheiten der Fudan Universität
- **02/2012 – 08/2012:** wissenschaftlicher Mitarbeiter in der Klinik für Ohren-, Nasen-, Hals- und Gesichtschirurgie, Universitätsspital Zürich. Prof. Dr. med. A. Huber. Thema: Mittel- und Innenohr-Mechanik.
- **03/2013 – 04/2013:** Famulatur in der Inneren Medizin, Cleveland Clinic Ohio, USA.
- **09/2010 – 06/2013:** Doktorarbeit, Abteilung für HNO-Heilkunde, Fudan Universität, Shanghai, China
- **09/2007 – 06/2010:** Masterarbeit, Abteilung für Radiologie, Fudan Universität, Shanghai, China.
- **09/2002 – 06/2007:** Studium der Humanmedizin, Medical College der Universät Shihezi

Zusätzliche Qualifikationen und Tätigkeiten

- DEGUM -Stufe II für das Gebiet Kopf/Hals-Diagnostik, Deutsche Gesellschaft für Ultraschall in der Medizin e.V.

Klinische & Wissenschaftliche Schwerpunkte

- Otologie und Neurotologie

Drittmittel

- CTNR Young Neuroscientist Programme, Universitätsmedizin Rostock 2023 „Einfluss des retrocochleären Status des auditorischen Systems auf die postoperativen Sprachverständlichkeit bei Patienten mit Cochlea-Implantat“, Bewerber: Frau Dana Kathrin Dohr, Mentor: Prof. Dr. med. Robert Mlynski, Leitung: Dr. med. Lichun Zhang / Dr. rer. nat. Florian Schmidt, Fördervolumen: Förderhöhe für Personal: Postdoc, TV-L E 13.3 40 Stunden/Woche; Förderungsdauer: 12 Monate.
- FORUN Nachwuchsförderung, Universitätsmedizin Rostock 2024, „Verbesserung der

Klangqualität beim Hören mit einem Cochlea Implantat durch Berücksichtigung der Tonhöhenwahrnehmung und der Elektrodenposition“, Leitung: Dr. rer. nat. Florian Schmidt / Dr. med. Lichun Zhang, Fördervolumen 12 000 €

- FORUN Nachwuchsförderung, Universitätsmedizin Rostock 2022, „Korrelation der präoperativen MR-Neurographie des N. vestibulocochlearis und der postoperativen Sprachverständlichkeit bei Patienten mit Cochlea-Implantat“ Leitung: Dr. med. Lichun Zhang, Fördervolumen 19.617,08 €

Dr. med. Lichun Zhang

Rostock, der 16.04.2025

Publikationsliste

Originalarbeiten

- **Zhang L**, Mißler D, Ehrt K, Großmann W, Mlynski R, Schmidt FH. Can mismatch negativity be used as an indicator to predict central auditory deficits in individuals with normal hearing? Audiol. Res. 2025, 15(2),43: https://doi.org/10.3390/audiolres15020043.
    a. **Impact Factor: 2.1**

- **Zhang L**, Stauga P, Mißler D, Ehrt K, Großmann W, Mlynski R, Schmidt FH. Eletrically evoked mismatch negativity from speech stimuli as an objective measure of cochlear implant performance. Front Neurosci. 2025 Feb 26:19:1559141. doi: 10.3389/fnins.2025.1559141.
    a. **Impact Factor: 3.2**

- **Zhang L**, Schmidt FH, Cantre D, Brenzel R, Ehrt K, Großmann W, Langner S, Mlynski R.The predictive value of preoperative measurements of cochlear nerve diameters from MRT and postoperative speech perception in adult patients with cochlear implant. Otol Neurotol. 2024 Sep. 6 doi: 10.1097/MAO.0000000000004293. online ahead of print.
    a. **Impact Factor: 1.9**

- Schmidt FH*, **Zhang L***, Glabasnia MW, Schurzig D, Ehrt K, Cantre D, van Bonn-Ytrehus SM, Großmann W, Mlynski R. Systematic overestimation of the angular insertion depth of electrode arrays in cochlear implantation (CI) patients with small cochlea by imaging processing software. Otol Neurotol. 2024 Aug. 2. doi: 10.1097/MAO.0000000000004294. **(* geteilte Erstautorenschaft**)
    a. **Impact Factor: 1.9**

- Schmidt FH, Dörmann A, Ehrt K, Grossmann W, Mlynski R, **Zhang L**. The curvature quantification of wave I in auditory brainstem responses detects cochlear synaptopathy in human beings. Eur Arch Otorhinolaryngol. 2024 Sep; 281(9):4735-4746. doi: 10.1007/s00405-024-08699-6. (**Letzteautor**)
    a. **Impact Factor: 1.9**

- **Zhang L**, Schmidt FH, Oberhoffner T, Ehrt K, Cantre D, Großmann W, Schraven SP, Mlynski R. Transimpedance matrix can be used to estimate electrode positions intraoperatively and to monitor their positional changes postoperatively in cochlear implant (CI) patients. Otol Neurotol. 2024 Apr 1;45(4):e289-e296. doi: 10.1097/MAO0000000000004145.
    a. **Impact Factor: 1.9**

- Ji H*, **Zhang L***, Hussain HMJ, Aftab A, Yu H, Xiao M. Novel cis compound heterozygous variants in MYO6 causes early onset of non-syndromic hearing loss in a Chinese family. Front Genet. 2024 Jan 11:14:1275633. doi: 10.3389/fgene.2023.1275633. **(* geteilte Erstautorenschaft**).
    a. **Impact Factor: 2.8**

- Heeringa AN[*], **Zhang L[*],** Ashida G, Beutelmann R, Steenken F, Köppl C. Temporal coding of single auditory nerve fibers is not degraded in aging gerbils. J. Neurosci. 2020 Jan 8; 40(2):343-354. doi: 10.1523/JNEUROSCI.2784-18.2019 **([*] geteilte Erstautorenschaft**)
    a. **Impact Factor: 6.074**

- **Zhang L**, Engler S, Koepcke L, Steenken F, Koeppl C. Concurrent gradients of ribbon volume and AMPA-receptor patch volume in cochlear afferent synapses on gerbil inner hair cells. Hear Res. 2018 Jul;364:81-89. doi: 10.1016/j.heares.2018.03.028.
    a. **Impact Factor: 2.064**

- **Zhang L**, Gao N, Yin Y, Yang L, Chen Y, Dai P, Zhang T. The bone conduction hearing in congenital aural atresia. Eur Arch Otorhinolaryngol. 2016(273) 7:1697-1703. doi: 10.1007/s00405-015-3727-1.
    a. **Impact Factor: 1.678**

- **Zhang L,** Tong B, Wang Z, Sha Y, Zhang F, Lao Z, Zhang T. A comparison. Of three MDCT-processing protocols: preoperative assessment of the ossicular chain in otitis media. Eur Arch Otorhinolaryngol. 2014 Mar;271(3):445-54. doi: 10.1007/s00405-013-2415-2.
    a. **Impact Factor: 2.391**

- Schmidt FH, Hocke T, **Zhang L**, Großmann W, Mlynski R. Tone decay reconsidered: preliminary results of a prospective study in hearing-aid users with moderate to severe hearing loss. J Clin Med. 2024 Jan 16;13(2):500. doi: 10.3390/jcm13020500.
    a. **Impact Factor: 3.9**

- Tuft B, **Zhang L**, Xu L, Hangartner A, Hansen M, Guymon A. Matrial stiffness effects on neurite alignment to photopolymerized micropatterns. Biomacromolecules. 2014, 15:3717-3727. doi: 10.1021/bm501019s.
    a. **Impact Factor: 5.750**

- Steenken F, Herringa AN, Beutelmann R, **Zhang L**, Bovee S, Klump GM, Köppl C. Age-related decline in cochlear ribbon synapses and ist relation to different metrics of auditory-nerve activity. Neurobiol Aging. 2021;108:133-145. doi: 10.1016/j.neurobiolaging.2021.08.019.
    a. **Impact Factor: 5.133**

- **Zhang L**, Chen Y, Zhang T. Three-stage surgery of combining auricule reconstruction, meatoplasty and tympanoplasty for patients with congenital micro-atresia. Chin J Otorhinolaryngo Head Neck Surg. 2015;50(3):197-202. PMID:26268491. (**Chinesisch**)
    a. **Impact Factor: 0.166**

- **Zhang L**, Kang H, Zhang T. Sha Y, Chi F, Tan L, Fu Y, Jin L. Uncommon thyroglossal duct cyst with inward tendency: a recommendation regarding ingrowth type. Int J Pediatr Otorhinolaryngol. 2012 Mar;76(3):322-6. doi: 10.1016/j.ijporl.2011.11.006.
    a. **Impact Factor: 1.731**

- **Zhang L**, Zhang T, Sha Y, Lin Y, Chen Q. Lingual thyroglossal duct cyst with recurrence after cystectomy or marsupialization under endoscopy: diagnosis and modified Sistrunk surgery. Laryngoscope. 2011 Sep;121(9): doi: 10.1002/lary.21909.
    a. **Impact Factor: 1.473**

- **Zhang L**, Sha Y, Wang Z, Luo D, Huang W, Dai P, Zhang T. 3D image of the middle ear ossicles: three protocols of post-processing based on multislice computed tomography. Eur Arch Otorhinolaryngol. 2011 May;268(5):677-83. doi: 10.1007/s00405-010-1441-6.
    a. **Impact Factor: 1.682**

- Tong B, **Zhang L**, Fang R, Sha Y, Chi F. 3D images based on MDCT in evaluation of patients with suspected foreign body aspiration. Eur Arch Otorhinolaryngol. 2013 Mar;270(3):1001-7. doi: 10.1007/s00405-012-2279-x.
    a. **Impact Factor: 1.608**

- **Zhang L**, Hong R, Dai C, Chi F, Sha Y. CT multiplane reconstruction images of superior semicircular canal dehiscence syndrome. Chin J Otorhinolaryngol Head Neck Surg, 2009 Sep;44(9):736-8. PMID: 20079096. (**Chinesisch**)
    a. **Impact Factor: -**

- **Zhang L**, Sha Y, Hong R, et al. The characteristic of superior semicircular canal dehiscence syndrome of multi-slice CT. Chin J Radiol, 2009;43(10):1027-1030. (**Chinesisch**)
    a. **Impact Factor: -**

- **Zhang L,** Hong R, Wang Z, et al., The evaluation of the integrity of the ossicles of the otitis media using MSCT volume rendering. Chinese Journal of Ophthamology and Otorhinolaryngology. 2010;10(3):150-151. (**Chinesisch**)
    a. **Impact Factor: -**

- Hong R, **Zhang L,** Wang Z, and et al. The Value of Multi-plannnar reformation HRCT in displaying the ossicles destroyed by chronic otitis media with cholesteatoma. Chineses Journal of Ophthamology and Otorhinolaryngology. 201;10(3):152-153. (**Chinesisch**)
    a. **Impact Factor: -**

Case Reports:

- Bassiouni M, **Zhang L**, Olze H, Dommerich S. Incus dislocation and traumatic tympanic membrane perforation as a complication of middle cranial fossa repair of tegmen dehiscence. Ear Nose Throat J. 2020 May;101(4):224-225. doi: 10.1177/0145561320950595.
    a. **Impact Factor: 1.3**

- Stölzel K, **Zhang L**, Borowski T, Olze H, Schroeder T, Eckardt KU, Nee J. Sepsis nach elektiver Septumplastik und Nasenmuschelverkleinerung. Laryngo-Rhino-Otol. 2019;98:517-574. doi: 10.1055/a-0889-8532 (**Deutsch**).
    a. **Impact Factor: 1.0**

- Skusa C, Skusa R, **Zhang L**. Cervikal necrotizing fasciitis of odontogenic origin. Dtsch Arztebl Int 2022;119:631. doi: 10.3238/arztebl.m2022.0159. (**Deutsch**).
    a. **Impact Factor:**

- Rafaelian A, Won S-Y, Trnovec S, Behmanesh B, Barz S, Busjahn C, Reuter DA, **Zhang L**, Mlynski R, Freiman T, Gessler F, Dubinski D. Otogenic brain abscess and concomitant acute COVID 19 infection – case report and review of the literature. J Neuro Surg A Cent Eur Neurosurg. 2024 Nov 20. doi: 10.1055/a-2479-5462.
    a. **Impact Factor: 0.9**

- **Zhang L**, Sha Y, Dai C. Another etiology for vertigo due to idiopathic lateral semicircular canal bony defect. Auris Nasus Larynx. 2011 Jun;38(3):402-5. doi: 10.1016/j.anl.2010.11.003.
    a. **Impact Factor: 0.761**

- **Zhang L**, Zhang F, Sha Y. Differential diagnosis of the tumor involving foramen jugulare. Journal of Clinical Radiology. 2009;(8):1170-1173. (**Chinesisch**).
    a. **Impact Factor: -**

- Zhang F, Sha Y, **Zhang L**, and et al. CT and MRI diagnosis of primary middle ear carcinoma invading jugular foramen. Chin J Radiol. 2011;45(11):1028-1031. (**Chinesisch**).
    a. **Impact Factor: -**

Peer Reviews:

- **Zhang L**, Zhang T, Dai P, Luo D. Titanium versus non-titanium prostheses in ossiculoplasty: a meta-analysis. Acta Otolaryngol. 2011 Jul;131(7):708-15. doi: 10.3109/00016489.2011.556662.
    a. **Impact Factor: 0.830**

Buchkapitel:

1. **Zhang L,** et al. in Sha Y, Luo D, Li H, Wang Z, Xian J (Eds), Kopf and Hals Bild, People's Medical Publishing House, Peking 2013, 54-70, 122-131. ISBN 978-7-117-19090-0/R.18091. (**Chinesisch**)
    a. **Impact Factor: -**

Zitierfähige Abstracts

- Stauga P, Schmidt F, Zhang L, Ehrt K, van Bonn-Ytrehus SM, Großmann W, Mlynski R. (2024). "Objektive Beurteilung des Sprachverstehens von CI-Patienten durch Ableitung der Mismatch Negativity" Laryngo-Rhino-Otologie. 103. doi: 10.1055/s-0044-1784249.
- Glabasnia MW, Schmidt FH, Zhang L, Ehrt K, van Bonn-Ytrehus SM, Großmann W, Mlynski R. (2024). "Using OTOPLAN to estimate the angular insertion depth for patients with a FLEXsoft electrode array from MED-EL." Laryngo-Rhino-Otologie. 103. doi: 10.1055/s-0044-1784842.
- Mißler D, Zhang L, Schmidt FH, Ehrt K, Großmann W, Mlynski R. (2024). "Kann die sprachinduzierte Mismatch-Negativität als Biomarker für Hidden hearing loss bei erwachsenen Menschen dienen?" Laryngo-Rhino-Otologie. 103. doi: 10.1055/s-0044-1784273.
- Schmidt FH, Bonk H, Zhang L, Ehrt K, van Bonn-Ytrehus SM, Großmann W, Mlynski R. (2024). "Wahrnehmung des Tieftonbereichs nach Cochlea Implantat Versorgung mit hoher cochleärer Abdeckung." Laryngo-Rhino-Otologie. 103. doi: 10.1055/s-0044-1784245.
- Zhang L, Brenzel R, Schmidt FH, Ehrt K, Cantre D, Großmann W, Mlynski R. (2024). "The preoperative measurements of auditory nerve diameters from MRT predict postoperative speech perception in adult patients with cochlear implantation (CI)." Laryngo-Rhino-Otologie. 103. doi: 10.1055/s-0044-1784543.
- Glabasnia MW, Schmidt FH, Zhang L, Ehrt K, van Bonn-Ytrehus SM, Großmann W, Mlynski R. (2024). "Schätzugng der angularen Insertionstiefe durch OTOPLAN für den FLEXsoft-Elektrodenträger von MED-EL." Laryngo-Rhino-Otologie. 103. doi: 10.1055/s-0044-1784202.
- Großmann W, Gommlich L, Zhang L, Schmidt FH, Mlynski R. (2024). "Evaluating cochlear implant outcome- which factors influence the subjective hearing impairment?" Laryngo-Rhino-Otologie. 103. doi: 10.1055/s-0044-1784844.
- Schmidt FH, Bonk H, Zhang L, Ehrt K, van Bonn-Ytrehus SM, Großmann W, Mlynski R. (2024). "Pitch perception at low frequency range in patients after cochlear implantation (CI) with high cochlear coverage" Larngo-Rhino-Otologie. 103. doi: 10.1055/s-0044-1784893.
- Zhang L, Schmidt FH, Dörmman A, Ehrt K, Mlynski R. (2023). "Die Krümmungsberechunung der Welle I in der BERA detektiert eine versteckte cochleäre Synaptopathie." Laryngo-Rhino-Otologie. 102. doi: 10.1055/s-0043-1766822.
- Ehrt K, Schmidt FH, Zhang L, Glabasnia WM, Schraven S, Mlynski R. (2023). "Bietet OTOPLAN wesentliche Vorteile für die präoperative chirurgische Planung einer Cochlea-Implatation?" Laryngo-rhino-Otologie. 102. doi: 10.1055/s-0043-1766719.
- Schmidt FH, Zhang L, Ehrt K, Schraven S, Mlynksi R. (2023). "Verwendung der Transimpedanzmatrix zur intraoperativen Schätzung der Elektrodenposition und zum postoeprativen Monitoring von Lageveränderungen." Larngo-Rhino-Otologie. 102. doi: 10-1055/s-0043-1766766.
- Wakonig KM, Arens P, Lerchbaumer M, Zhang L, Fischer T, Olze H, Dommerich S. (2021). "The role of multimodal ultrasound in the characterization of partoid gland lesions." Laryngo-Rhino-Otologie. 100. doi: 10.1055/s-0041-1727662.

Kongressvorträge

- Zhang L, Schmidt FH, Böhlke YBR, Ehrt Karsten, Grossman W, Mlynski R. (2025). "Diagnostic methods for potential cochlear synaptopathy in humans" Poster, 48th Annual ARO

MidWinter Meeting, Orlando, FL, USA, Feb. 2025

- Zhang L, Schmidt FH, Siemers T, Glabasnia MW, Ehrt K, Großmann W, Mlynski R. (2025). "Einfluss der Querschnittsfläche des Nervus cochlearis auf elektrisch evozierte Summenaktionspotentiale." Vortrag, 27. Jahrestagung der DGA & Frühjahrstagung der ADANO, Göttingen, März 2025.
- Zhang L, Schmidt FH, Glabasnia MW, Ehrt K, van Bonn-Ytrehus SM, Großmann W, Mlynski R. (2024). "Application of voltage matrix from the cochlear implant electrode array to predict cochlear coverage." Poster, 7th International Symposium Interface Biology of Implants, Rostock, June 2024
- Zhang L, Brenzel R, Schmidt FH, Ehrt K, Cantre D, Großmann W, Mlynski R. (2024). "Prognose des postoperativen Sprachverstehens bei Patienten mit CI-Versorgung durch die Vermessung des Nervus cochlearis." Visual Abstract/Poster mit Erläuterung, 95. Jahresversammlung der deutschen Gesellschaft für Hals-Nasen-Ohren-Heilkunde, Kopf- und Hals-Chirurgie e.V., Essen, Mai 2024.
- Zhang L, Schmidt FH, Mißler D, Ehrt Karsten, Grossman W, Mlynski R. (2024). "Can speech induced mismatch negativity be used as a biomarker for the hidden hearing loss in human adults?" Poster, 47th Annual ARO MidWinter Meeting, Anaheim, CA, USA, Feb. 2024
- Zhang L, Schmidt FH, Cantre D, Ehrt Karsten, Brenzel R, Großmann W, Mlynski R. (2023). "Die präoperative Nervengröße des Nervus cochlearis beeinflusst das postoperative Sprachverstehen bei Patienten mit Cochlea Implantat bei der Erstanpassung." Vortrag, Herbsttagung – ADANO, Greifswald, September 2023.
- Zhang L. (2023). "Listening again, Cochlea Implants" Vortrag, Head and Necak Imaging, Constanza, Rumänien, June 2023.
- Zhang L, Schmidt FH, Dörmann A, Ehrt K, Mlynski R. (2023). "Die Krümmungsberechnung der Welle I der BERA detektiert eine versteckte cochleäre Synaptopathie." Gesetzter Vortrag, 94. Jahresversammlung der deutschen Gesellschaft für Hals-Nasen-Ohren-Heilkunde, Kopf- und Hals-Chirurgie e.V, Leipzig, Mai 2023.
- Zhang L. (2023). "The curvature quantification of wave I in auditory brainstem responses detects cochlear synaptopathy in the elderly." Vortrag, CTNR Winter School 2023, Rostock & Gut Gremmelin, Germany, January 2023.
- Zhang L, Schmidt FH, Dörmann A, Ehrt K, Großmann W, Mlynski R. (2023). "The curvature quantification of wave I in auditory brainstem responses detects cochlear synaptopathy in the elderly." Poster, 46th Annual ARO MidWinter Meeting, Orlando, Florida, February 2023.
- Zhang L. (2018). "Spatial distribution of number and volumes of cochlear ribbon synapses on inner hair cells of young adult gerbils." Poster, 41th Annual ARO MidWinter Meeting, San Diego, CA, USA. February 2018.
- Zhang L. (2017). "Coding of temporal information in the auditory nerve of aging gerbils". Vortrag, Tagung des Forschungszentrums Neurosensorik im Hanse- Wissenschaftskolleg in Delmenhorst, November 2017.
- Zhang L. (2017). "Coding of temporal information in the audiotry nerve of aging gerbils". Poster, 40th Annual ARO MidWinter Meeting, Baltimore, MD USA, February 2017.
- Zhang L. (2016). "Synaptopathy in ageing gerbils". Vortrag. The 2016 Basic Auditory Science Meeting, Cambridge, UK, September 2016
- Zhang L. (2016). "Loss of inner hair cell synapse results in age-related hearing loss in gerbils." Poster, 39th Annual ARO MidWinter Meeting, San Diego, CA, USA, February 2016.
- Zhang L. (2014). "Loss of spiral ganglion neuron synaptic contact in associated with hearing

loss after acute high intensity intracochlear electrical stimulation in hearing mice." Poster, 37th Annual ARO MidWinter Meeting, San Diego, CA, USA, February 2014.

- Zhang L. (2010). "3D image of ossicles: three approaches of post-processing based on multslice computed tomography." Vortrag, the 26th International Congress of Radiology (ICR) 2010, Shanghai, China, Aprial 2010
- Zhang L (2010). "The evaluation of the integrity of the ossicles of the otitis media using MSCT volume rendering." Vortrag, the 26th International Congress of Radiology (ICR 2010), Shanghai, China, April 2010.
- Zhang L. (2009). "Diagnosis of superior semicircular canal dehiscence by MPR." Vortrag, the 8th Chinese Conference on Advances in Head and Neck Imaging, Yantai, Shandong, China, August 2009.

Danksagung

Ein großer Dank geht an meinen Betreuer, Gutachter und Mentor Herrn Prof. Robert Mlynski. Seit dem ersten Tag, an dem ich in Rostock als forschender Kliniker tätig bin, hat er mich fachlich unterstützt und nachhaltig geprägt. Danke, ich habe sehr viel von Ihnen gelernt. Meinen Kolleginnen und Kollegen sowie Doktorandinnen und Doktoranden an der Universitätsmedizin danke ich für die Zusammenarbeit und den inspirierenden Austausch. Es ist eine Freude, mit euch zu arbeiten und voreinander zu lernen.

Zusätzlich möchte ich meiner ersten wissenschaftlichen Mentorin nach der Promotion, Prof. Christine Köppl, meinen Dank aussprechen. Seit meiner Ankunft in Deutschland im Jahr 2014 hat sie mich fachlich unterstützt. Durch sie habe ich meine neurowissenschaftliche Arbeit erlernt. Ein besonderer Dank gilt auch meinem ersten klinischen Chef, Prof. Florian Hoppe. Sie haben mir die erste Chance gegeben, als Arzt in Deutschland zu arbeiten, und mich auf meinem Weg als Otologe tatkräftig unterstützt.

Ein weiterer Dank geht an Herrn Dr. Florian Schmidt. Zusammen haben wir Schritt für Schritt unsere Arbeitsgruppe aufgebaut. Nach unzähligen intensiven gemeinsamen Arbeitsphasen haben wir mittlerweile viele Forschungsprojekte und Publikationen erreicht.

Ein besonderer Dank gebührt meiner Familie in China und Deutschland, die immer an mich geglaubt und mir den Rückhalt und die Motivation gegeben hat. Meinen Freunden danke ich dafür, dass sie stets ein offenes Ohr für mich hatten und mich ermutigt haben, wenn es schwierig wurde.

Ich bin dankbar für die Unterstützung, die ich auf meinem Weg zur Habilitation erhalten habe. Es war eine anspruchsvolle, aber auch erfüllende Reise, und ich freue mich darauf, die nächsten Schritte auf meinem wissenschaftlichen Weg zu gehen.

Mit herzlichem Dank und großer Wertschätzung.

Lichun Zhang

Eidesstattliche Erklärung

Ich erkläre hiermit an Eides statt, dass ich die vorliegende Arbeit selbstständig und ohne unerlaubte fremde Hilfe angefertigt und keine anderen als die angegebenen Quellen benutzt habe. Die aus fremden Quellen direkt oder indirekt übernommenen Stellen sind als solche kenntlich gemacht. Die Arbeit wurde bisher in gleicher oder ähnlicher Form keinem anderen Prüfungsamt vorgelegt und auch nicht veröffentlicht.

Dr. med. Lichun Zhang

Kavelstorf, der 16.04.2025

Arbeit 1:

ARTICLE IN PRESS

Hearing Research xxx (2018) 1–9

Contents lists available at ScienceDirect

Hearing Research

journal homepage: www.elsevier.com/locate/heares

Research Paper

Concurrent gradients of ribbon volume and AMPA-receptor patch volume in cochlear afferent synapses on gerbil inner hair cells

Lichun Zhang [a, 1], Sina Engler [a, 2], Lena Koepcke [b], Friederike Steenken [a], Christine Köppl [a, *]

[a] Cluster of Excellence "Hearing4all" and Research Centre Neurosensory Science, Department of Neuroscience, School of Medicine and Health Science, Carl von Ossietzky University Oldenburg, 26129 Oldenburg, Germany
[b] Department of Neuroscience, Computational Neuroscience, Carl von Ossietzky University Oldenburg, 26129 Oldenburg, Germany

ARTICLE INFO

Article history:
Received 13 December 2017
Received in revised form
26 February 2018
Accepted 28 March 2018
Available online xxx

Keywords:
Auditory
Cochlea
Immunolabeling
Presynaptic
Postsynaptic
Ribbon synapse

ABSTRACT

The Mongolian gerbil is a classic animal model for age-related hearing loss. As a prerequisite for studying age-related changes, we characterized cochlear afferent synaptic morphology in young adult gerbils, using immunolabeling and quantitative analysis of confocal microscopic images. Cochlear wholemounts were triple-labeled with a hair-cell marker, a marker of presynaptic ribbons, and a marker of postsynaptic AMPA-type glutamate receptors. Seven cochlear positions covering an equivalent frequency range from 0.5 – 32 kHz were evaluated. The spatial positions of synapses were determined in a coordinate system with reference to their individual inner hair cell. Synapse numbers confirmed previous reports for gerbils (on average, 20–22 afferents per inner hair cell). The volumes of presynaptic ribbons and postsynaptic glutamate receptor patches were positively correlated: larger ribbons associated with larger receptor patches and smaller ribbons with smaller patches. Furthermore, the volumes of both presynaptic ribbons and postsynaptic receptor patches co-varied along the modiolar-pillar and the longitudinal axes of their hair cell. The gradients in ribbon volume are consistent with previous findings in cat, guinea pig, mouse and rat and further support a role in differentiating the physiological properties of type I afferents. However, the positive correlation between the volumes of pre- and postsynaptic elements in the gerbil is different to the opposing gradients found in the mouse, suggesting species-specific differences in the postsynaptic AMPA receptors that are unrelated to the fundamental classes of type I afferents.

© 2018 Elsevier B.V. All rights reserved.

1. Introduction

Acoustic information is mainly carried by the type I afferent fibers that contact inner hair cells (IHCs) and transmit to the ascending auditory system (review in Heil and Peterson, 2015). The connections between IHCs and the primary auditory neurons are formed by a specialized synapse, termed a ribbon synapse. Like any other chemical synapse, a functional ribbon synapse consists of a presynaptic active zone and a postsynaptic density (review in Schnee and Ricci, 2017), which are closely aligned. However, the presynaptic element is an ellipsoid dense body, the ribbon (Fuchs et al., 2003; Nouvian et al., 2006), located at the base of the hair cell, which is anchored to the plasma membrane via lamellar sheets (Piatigorsky, 2001). In addition, every ribbon is surrounded by many vesicles that contain the excitatory neurotransmitter glutamate (Meyer et al., 2009). Ribbon synapses are able to maintain a high and sustained neurotransmitter release (Meyer et al., 2009; Moser et al., 2006a, 2006b; Safieddine and Wenthold, 1999). The postsynaptic side exhibits glutamate receptors of the AMPA-type, which are accumulated in the area of the postsynaptic density (Meyer et al., 2009). On release into the synaptic cleft, glutamate activates receptors and depolarizes the type I afferent fibers, which then transmit the acoustic signal to the central auditory system

Abbreviations: ANOVA, analysis of variance; BSA, bovine serum albumin; CtBP2, C-terminal binding protein 2; IHC, inner hair cell; PBS, phosphate-buffered saline; SR, spontaneous discharge rate; TEM, transmission electron microscope

* Corresponding author. Department of Neuroscience, Carl von Ossietzky University, Carl-von-Ossietzky-Str. 9-11, 26129 Oldenburg, Germany.
E-mail address: christine.koeppl@uol.de (C. Köppl).
[1] Present address: ENT Department, Klinikum Oldenburg, Medical Campus, Carl von Ossietzky University Oldenburg, 26133 Oldenburg, Germany.
[2] Present address: Department of Otorhinolaryngology, University Medical Center Groningen, Netherlands.

https://doi.org/10.1016/j.heares.2018.03.028
0378-5955/© 2018 Elsevier B.V. All rights reserved.

Please cite this article in press as: Zhang, L., et al., Concurrent gradients of ribbon volume and AMPA-receptor patch volume in cochlear afferent synapses on gerbil inner hair cells, Hearing Research (2018), https://doi.org/10.1016/j.heares.2018.03.028

(Glowatzki and Fuchs, 2002; Moser et al., 2006b).

Classic studies in cats suggested that afferent neurons synapsing at different positions around the IHC have systematically different physiological and morphological characteristics: Fibers contacting the "pillar face" (abneural side) of the IHC, i.e., closer to the outer hair cells, had smaller presynaptic elements (ribbons) and axons of larger diameter, as well as lower thresholds to acoustic stimulation and higher spontaneous discharge rates (SRs). Those on the opposite "modiolar face" of the IHC (neural side) had larger ribbons and smaller axons, as well as higher acoustic thresholds and low SRs (Liberman, 1982; Merchan-Perez and Liberman, 1996). Similar spatial gradients in ribbon size have since been observed in other mammalian species, including different strains of mice (Gilels et al., 2013; Liberman et al., 2011, 2015; Yin et al., 2014), guinea pigs (Furman et al., 2013) and rats (Kalluri and Monges-Hernandez, 2017). In mice, an additional gradient in postsynaptic glutamate receptor patch size and/or density was reported that runs in the opposite direction, such that larger ribbons tend to face smaller postsynaptic receptor fields and vice versa (Liberman et al., 2011, 2015; Yin et al., 2014).

The Mongolian gerbil (*Meriones unguiculatus*) is a popular animal model for studies of aging in the auditory system, as it combines good low-frequency sensitivity similar to humans (Ryan, 1976), a relatively short life span (36 months; Cheal, 1986), and easy husbandry in a noise-controlled environment. A basic characterization of afferent synapse morphology in young gerbils is therefore an important prerequisite for studies on synaptopathy with age. So far, quantitative data are available on synaptic counts from different cochlear positions, primarily based on immunolabeled presynaptic ribbons (Gleich et al., 2016; Meyer et al., 2009), and to a lesser extent based on double-labeled pre- and postsynaptic pairs (Bourien et al., 2014; Batrel et al., 2017). There is only one study to date that examined spatial gradients in the size of afferent nerve terminals contacting the different sides of IHCs in young gerbils, using transmission electron microscopy (TEM) (Slepecky et al., 2000), which found no clear spatial gradients in the size of terminals around the IHCs (Slepecky et al., 2000). Using serial reconstructions from ultrathin sections, their sample was naturally limited, to 8 IHCs, and they did not consider any presynaptic elements. We present here a quantitative volumetric analysis of both pre- and postsynaptic elements of afferent synapses on gerbil IHC obtained from immunolabeled cochleae, which will serve as a fundamental database for future studies.

2. Materials and methods

2.1. Animals

Nine cochleae from 5 Mongolian gerbils (*Meriones unguiculatus*) of both sexes, and aged from 80 to 219 days (~2.5–7.5 months) were used for histological evaluation. All animals were born in the animal facility of the University of Oldenburg and raised in a controlled, quiet environment. All protocols and procedures were approved by the authorities of Lower Saxony, Germany, permits AZ 33.12-42502-04-10/0107 and AZ 33.19-42502-04-15/1828. Animals were euthanized by an overdose of sodium pentobarbital ("Narcoren", Merial GmbH, Hallbergmoos, Germany; intraperitoneal), then perfused intracardially with phosphate buffered saline (PBS; 137 mM NaCl, 10 mM phosphate and 2.7 mM KCl), with added heparin (ratiopharm, 25,000 IE/5 ml; 0.2 ml/100 ml), at pH 7.4 and room temperature, followed by 4% paraformaldehyde in PBS (pH 7.4) at room temperature. The cochleae were removed after perfusion, the oval window was opened through removal of the middle ear bones, and a tiny hole was carefully made at the very apex with a 30G needle, to allow fluid penetration. The samples were then transferred to 0.5 M EDTA in PBS and gently shaken at 8 °C for 1–2 days until the bone was completely decalcified.

2.2. Immunolabeling

The cochleae were subsequently treated with 1% Triton X-100 in PBS at room temperature for 1 h, then rinsed with 0.2% Triton in PBS three times at 5 min intervals. Three percent bovine serum albumin (BSA) with 0.2% Triton in PBS for 1 h at room temperature was used to block unspecific protein binding sites. An anti-CtBP2 (C-terminal binding protein 2) antibody (IgG1 monoclonal mouse; BD Biosciences; cat. no. 612044; RRID: AB_399431) at a concentration 1:400 was used to label presynaptic ribbons. An anti-GluR2 antibody (IgG2a monoclonal mouse; Millipore; cat. no. MAB 397; RRID: AB_2113875) at a concentration 1:200 labeled postsynaptic receptors. An anti-Myosin VIIa antibody (IgG polyclonal rabbit; Proteus Biosciences; cat. no. 25–6790; RRID: AB_10015251) at a concentration of 1:200 labeled hair cells. All 3 primary antibodies were diluted in the blocking solution and the cochleae were incubated in this mix at 37 °C overnight. Subsequently, cochleae were rinsed in PBS with 0.2% Triton, 5 times at 5 min intervals. Three secondary antibodies, matching the hosts of the primary antibodies - goat anti-mouse (IgG1)-AF 488 (Molecular Probes; cat. no. A21121; RRID: AB_141514) at a concentration of 1:500, goat anti-mouse (IgG2a)-AF568 (Invitrogen; cat. no. A-21134; RRID: AB_10393343) at a concentration of 1:200, and donkey anti-rabbit-AF647 (polyclonal secondary antibody; Life technologies-Molecular Probes; cat. no. A-31573; RRID: AB_162544) at a concentration of 1:500 - were used to bind specifically to the 3 primary antibodies. Cochleae were incubated with the secondary antibodies diluted in blocking solution at 37 °C for 2 h. After finally rinsing 3x in PBS, the cochleae were cut into 5–8 segments under a stereomicroscope (following the procedure of a video tutorial from the Eaton-Peabody Laboratories: https://www.masseyeandear.org/research/otolaryngology/investigators/laboratories/eaton-peabody-laboratories/epl-histology-resources/video-tutorial-for-cochlear-dissection) and mounted on slides using Vectashield Mounting Medium (Vector Laboratories, H-1000).

2.2.1. Image acquisition and processing

Every cochlear segment was examined and documented using a Nikon epi-florescence microscope system (Nikon 90i with NIS Elements software, Version 4.30), and a 4x objective. The length of the entire cochlea was then measured from these images by drawing a line along the row of inner hair cells using the NIS software. Seven different cochlear locations, at 1.39, 2.51, 3.8, 5.19, 6.64, 8.13 and 9.63 mm from the apex, corresponding to 0.5, 1, 2, 4, 8, 16 and 32 kHz respectively (Müller, 1996) were selected for the synapse analysis. These locations were examined with a confocal microscope (Leica Microsystem CMS GmbH, Leica TCS SP8 system), using an oil-immersion objective (63x, numerical aperture 1.40). The 488-nm (OPSL), 522-nm (OPSL) and 638-nm (Diode) lasers were used to excite the three antibody-labeled fluorescent channels. Image stacks were acquired at 0.08–0.10 µm/pixel resolution and using 0.3 µm steps in the z-dimension, with sequential scanning of the three channels for each z-layer and a hybrid detector in photon counting mode. Detector bandwidths for every channel were carefully adjusted to exclude crosstalk between the fluorescent channels. This was verified by control specimens labeled with only one of the three standard antibody labels. In an initial study phase, two cochleae (gerbil 3) were scanned at larger 0.5 µm steps in the z-dimension and using PMT detectors. Note that although specimens were mounted in a consistent way on slides, the hair cells were variably flattened, confocal scan direction was varied and we used both left and right cochleae. As a result, the analyzed

Please cite this article in press as: Zhang, L., et al., Concurrent gradients of ribbon volume and AMPA-receptor patch volume in cochlear afferent synapses on gerbil inner hair cells, Hearing Research (2018), https://doi.org/10.1016/j.heares.2018.03.028

stacks showed a range of different orientations of hair cells relative to the confocal z-axis (modiolar-to-pillar and the reverse, IHC-top-to-bottom and the reverse, as well as oblique orientations).

All confocal stacks were subjected to deconvolution (Hyugens Essentials, Version 15.10, SVI, Hilversum, Netherlands) with default settings (maximum iterations: 80; Signal to noise ratio: 10; Quality threshold: 0.01), using a theoretical point-spread function.

2.3. Image analysis

Manual counts were carried out with the aid of the ImageJ-based imaging package Fiji (http://fiji.sc/Fiji; Schindelin et al., 2012). Only double-labeled elements, where a presynaptic ribbon was judged to be juxtaposed to a postsynaptic GluR-patch, were counted.

A custom-written image analysis software (MATLAB version 2015a, The MathWorks, Inc., Natick, Massachusetts, United States) was used to determine the numbers and volumes of synaptic elements. In a first step, the sum of all labeled channels was used to define the overall area-of-interest. The borders of individual hair cells were then interactively delineated, and their anatomical axes individually defined in the cochlear apex-to-base, modiolar-pillar and hair-cell top-to-bottom dimensions. Next, the synaptic elements were detected by intensity thresholding, separately for the presynaptic CtBP2-channel and the postsynaptic GluR2 channel. This could optionally be refined in several ways and was guided by 3D displays of hair cells and binarized synaptic elements. Typically, a minimum voxel count of 5 was defined (corresponding to a volume of about 0.003 μm^3), and several elements that appeared to be two or more merged ribbons or GluR patches were interactively split.

Colocalization of pre- and postsynaptic immunolabel was used as the definition of a functional synapse. Our colocalization criterion was distance-based. Histograms of the distances between every possible pair of pre- and postsynaptic elements suggested that colocalized elements nearly always overlapped or at least touched at their nearest points. Choosing a more generous criterion led to increasing numbers of synaptic clusters comprised of more than two partners. We thus consistently required a minimal distance of zero between the nearest points of colocalized elements.

To develop and validate the image analysis, most stacks were initially analysed by 2–3 different observers (SE, LCZ, CK) separately, and results subsequently compared using the manual counts as a target guideline for developing image analysis criteria. Once the principal analysis was established, the resulting numbers of functional synapses were very consistent across repeated analyses. Regarding volumes of synaptic elements, we compared analyses of the same stack by different observers, as well as analyses by the same observer, using the raw confocal data and the data after deconvolution. In no case were the principal results affected; any differences were primarily in the absolute synaptic volumes. Deconvolution tended to reduce synaptic volumes; however, this difference was well within the variation between different users that applied different thresholding criteria. Normalization to the median volume within a particular confocal stack (after Liberman et al., 2011) eliminated these differences. For the final data shown here, two of the authors (LCZ and CK) contributed about half of the analyses each and all data were median-normalized. Pre- and postsynaptic elements were normalized separately, to their respective medians, and only colocalized elements contributed to the median.

2.4. Statistics

All statistical procedures were carried out with the use of IBM SPSS Statistics version 24. We used non-parametric statistics wherever possible. For the parametric analysis of variance, the assumptions of normality and homogeneity of variances were judged using both descriptive plots and standard tests (Kolmogorov-Smirnov, Levene). Data were transformed (either logarithmic or arcsine transformation) if this significantly improved compliance with the assumptions. However, we were unable to completely satisfy all assumptions.

3. Results

Manual synaptic counts were carried out for a total of 264 IHC from 9 different cochleae (see Supplementary Table 1a for an overview of the numbers of IHC evaluated at the different cochlear locations in different specimens). For the more extensive image analysis, a subset of confocal stacks was selected, such that each cochlear location was only represented once from each animal, either from its left or from its right cochlea, selected for the best structural preservation and orientation on the slide. This resulted in approximately equal numbers of IHC evaluated from each cochlear location, and 165 IHC in total (Supplementary Table 1b). Synapses in most of the IHC subjected to the full image analysis were also counted manually ($n = 147$).

We included cochleae from gerbils up to 219 days (about 7 months) of age. Across the ages included, there was no significant change in overall numbers of synapses per IHC (Kruskal-Wallis test, $p > 0.05$). We thus considered gerbils up to at least 7 months of age as representative for the normal young adult cochlea. Thresholds in quiet begin to deteriorate much later, from about 2 years of age, in gerbils (Henry et al., 1980; Mills et al., 1990).

3.1. Number of functional synapses per IHC along the tonotopic gradient

Synapse numbers varied only little, but significantly, across the tonotopic locations (Kruskal-Wallis test, $p \leq 0.001$ for both manual and image analysis counts; Fig. 1). Pairwise comparisons (Mann-Whitney U test) between all cochlear locations revealed that

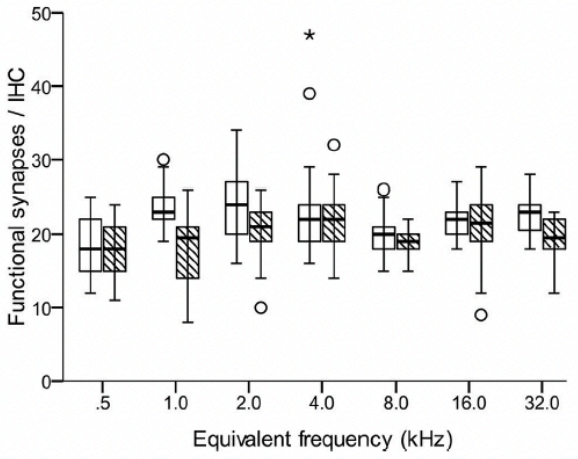


Fig. 1. Boxplot showing medians (thick horizontal line), interquartile ranges (boxes) and 1.5 times the interquartile ranges (whiskers) for the counts of functional synapses per IHC at different frequency positions along the gerbil cochlea. Empty boxes represent manual counts, hatched boxes the numbers derived from image analysis. Circles and stars indicate outliers beyond 1.5 times (circles) or 3 times (stars) the interquartile range (for numbers of IHC analyzed, see Table S1).

Please cite this article in press as: Zhang, L., et al., Concurrent gradients of ribbon volume and AMPA-receptor patch volume in cochlear afferent synapses on gerbil inner hair cells, Hearing Research (2018), https://doi.org/10.1016/j.heares.2018.03.028

primarily the 0.5 and 8 kHz positions had a lower synaptic count compared to the other frequency locations. However, the difference was small and only consistently significant against the other locations in the larger sample of manual counts. Overall, there was thus no convincing, systematic variation of synaptic numbers per IHC with tonotopic location. The overall median was 22 synapses/IHC in manual counts, and 20 synapses/IHC for image analysis counts. For individual IHC also, the manual count tended to be higher than the number of synapses detected by image analysis (Wilcoxon signed ranks test, $p < 0.001$, $n = 147$). The median difference was 6%.

3.2. Volumes of synaptic elements

Absolute volumes of synaptic elements derived from confocal images of immunolabeled tissue depend on the brightness of the label and thus on a number of technical variables, such as antibody concentration, tissue thickness, laser power and photodetector sensitivity and gain settings. These are difficult to maintain consistently across specimens. As expected, we observed considerable variation in synaptic volumes across different confocal stacks. The overall median was 0.11 μm^3 (interquartile range 0.067–0.16 μm^3) for presynaptic ribbons and 0.17 μm^3 (interquartile range 0.09–0.31 μm^3) for postsynaptic GluR2 receptor patches ($n = 3224$). The centers of gravity of colocalized pre- and postsynaptic partners were typically 0.17–0.29 µm apart (interquartile range); the median value was 0.21 µm. There was no systematic change in this colocalization distance along the tonotopic gradient.

For the remainder of the manuscript, we use volumes normalized to the median value of the respective confocal stack (see Methods). Note that this is an open-ended scale, where a value of 1 corresponds to the median volume. Elements smaller than the median have values below 1, and elements larger than the median values lie above 1.

3.3. Definition of hair-cell coordinates

Fig. 2 illustrates a typical example of an analysis; 6 IHC were individually defined in this case. Due to the histological processing and dissection, hair cells were occasionally bent into an unnatural shape. This was clearly noticable in the 3D mesh reconstructions that were derived during the first steps of our analysis, but much less obvious in the confocal images. An extreme case is illustrated in the supplementary figure. In such cases, we defined the anatomical axes relative to the hair cell's basal (synaptic) pole. The relative positions of synaptic elements along the IHC's longitudinal axis were then corrected posthoc to the analysis, using an estimate of the cell's true length. Overall, the IHCs of our sample had a median length of 35 µm, with no systematic variation along the tonotopic gradient.

3.4. Differential spatial distribution of synaptic volumes

We first asked whether any differential spatial distribution of functional synapses existed, based on the volumes of their pre- and postsynaptic elements. A plane was interactively defined for each individual IHC that separated its pillar from its modiolar half, and its functional synapses were assigned to one of those, depending on where the bulk of their respective volume was located (example in Fig. 2). Synapses were distributed nearly equally to both sides, with 1848 (57%) located in the modiolar halves and 1376 (43%) in the pillar halves of their respective IHC. Both presynaptic ribbons and postsynaptic GluR2 patches were significantly larger on the modiolar side (Mann-Whitney *U* test, $p < 0.001$). However, the difference was small: median values for normalized presynaptic ribbon volumes were 1.07 for modiolar locations and 0.93 for pillar locations (Fig. 3A); for postsynaptic GluR2 patches, the median

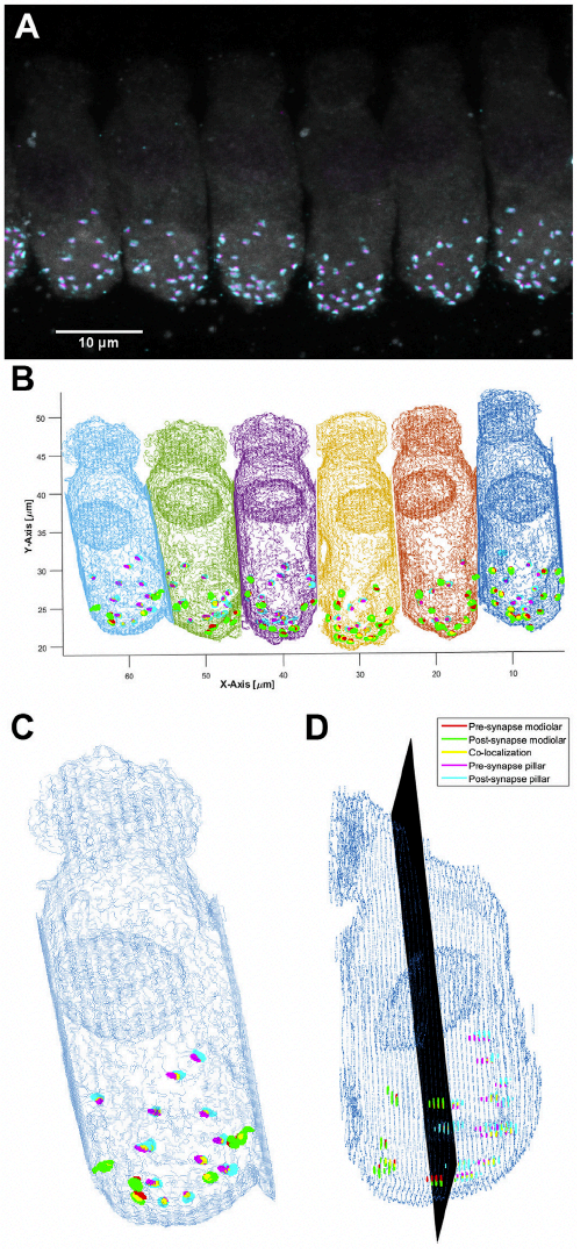


Fig. 2. Example for image analysis of one immunolabeled confocal stack. A: z-projection of the confocal stack containing 6 IHC. Gray: MyoVIIa label of hair cells, magenta: CtBP2-label of presynaptic ribbons, cyan: GluR2-label of postsynaptic receptors. The two color channels with synaptic label were subjected to deconvolution (see Methods); note also that the label was brightened and contrast-enhanced to produce this figure. B: 3D mesh reconstruction of the same 6 IHC, individually delineated and highlighted by different colors, together with all functional synapses detected. C, D: One of the IHC shown at higher magnification and from two different viewpoints, differing by 90° around the y-axis. The synaptic elements are color coded as indicated in the legend. Panel D also displays the plane that defined the IHC's modiolar and pillar halves.

Please cite this article in press as: Zhang, L., et al., Concurrent gradients of ribbon volume and AMPA-receptor patch volume in cochlear afferent synapses on gerbil inner hair cells, Hearing Research (2018), https://doi.org/10.1016/j.heares.2018.03.028

normalized volumes were 1.12 and 0.86, respectively (Fig. 3C). Fig. 3B and D show the data separately for each tonotopic location. Here, the volumes of postsynaptic receptor patches on the modiolar and pillar sides differed more consistently across all but one cochlear location, while the presynaptic ribbons more often proved to be of similar volume, i.e. not significantly different.

The distinction between pillar and modiolar had been guided by previous work in other species. However, the precise orientation of the dividing axis varies between studies (Liberman et al., 2011; Kalluri and Monges-Hernandez, 2017). In order to explore more open-mindedly for differential spatial distributions along more than one axis, a multivariate analysis of variance (ANOVA) was carried out, using normalized pre- and postsynaptic volumes as dependent variables, animal, cochlear location and confocal scan direction as fixed factors, and the relative positions along two of the hair-cell axes (pillar-modiolar and top-bottom) as covariate factors. The hair cell's apex-base dimension was not included, because its values drastically violated the assumptions of normality and homogeneity of variances. All factors, except scan direction, proved to significantly influence synaptic volumes ($p < 0.01$). However, their effect sizes were generally small, i.e. explained little of the variation of synaptic volumes. The two factors with the largest effect sizes were the position along the hair cell's pillar-modiolar axis (partial $\eta^2 = 0.046$) and position along the hair cell's longitudinal axis (partial $\eta^2 = 0.036$), followed by tonotopic location and animal, with very minor effect sizes (partial $\eta^2 = 0.005$ and 0.004, respectively). Differentiating between the effects on pre- and postsynaptic volumes (univariate analysis of variance for each dependent variable) revealed that the presynaptic ribbons varied slightly more along the hair cell's longitudinal axis (partial $\eta^2 = 0.031$) than along its pillar-modiolar dimension (partial $\eta^2 = 0.023$), whereas the reverse was true for the postsynaptic GluR2 patches (partial $\eta^2 = 0.014$ and 0.036, respectively).

The small effect sizes were also graphically obvious as very minor trends in the face of large variation (Fig. 4). Furthermore, the trends were in the same directions for both pre- and postsynaptic elements, indicating both larger ribbons and larger GluR2 receptor patches towards the modiolar side (Fig. 4A and B) and towards the base (Fig. 4C and D) of each hair cell.

Thus, both methods of analysis suggested a minor spatial variation in the volumes of presynaptic ribbons and postsynaptic receptor patches. Importantly, both pre- and postsynaptic elements

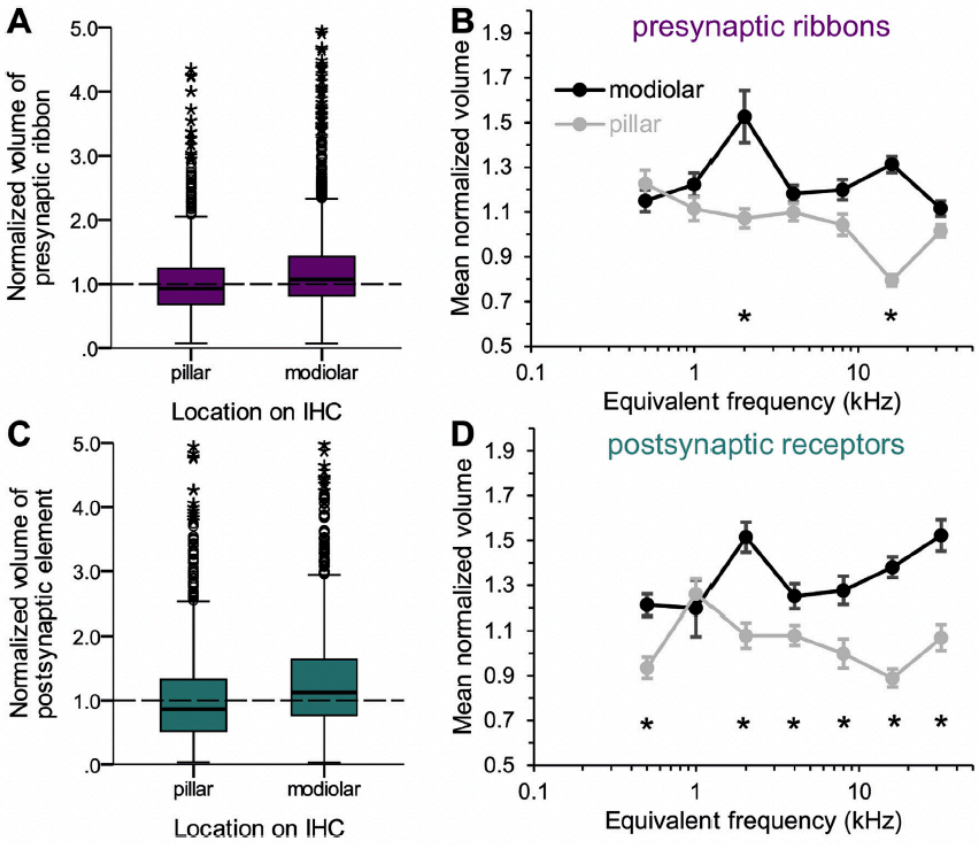


Fig. 3. Normalized volumes of functional synapse elements. A, C: Boxplots showing the normalized volume of presynaptic ribbons (A) or postsynaptic GluR2-patches (C), separately for synapses in the pillar and modiolar halves of their respective IHCs. Boxplot format is the same as in Fig. 1, but note that the y-axis range was limited for clarity, such that up to 7 further outliers are not shown. B, D: The same data, but now plotted as means ± standard errors of the mean, and additionally separated according to cochlear frequency position. Note that this display format was chosen to be exactly comparable to published data from mouse (Liberman and Liberman, 2016; Liberman et al., 2015; Yin et al., 2014). Note also that the apparent outliers at the 2 and 16 kHz positions are exaggerated by the choice of showing means; medians (which would be more appropriate for representing our positively skewed data distributions) showed less variability between cochlear locations. Stars indicate statistically significant differences between modiolar and pillar data at specific locations (Mann-Whitney U tests, $p \leq 0.01$).

Please cite this article in press as: Zhang, L., et al., Concurrent gradients of ribbon volume and AMPA-receptor patch volume in cochlear afferent synapses on gerbil inner hair cells, Hearing Research (2018), https://doi.org/10.1016/j.heares.2018.03.028

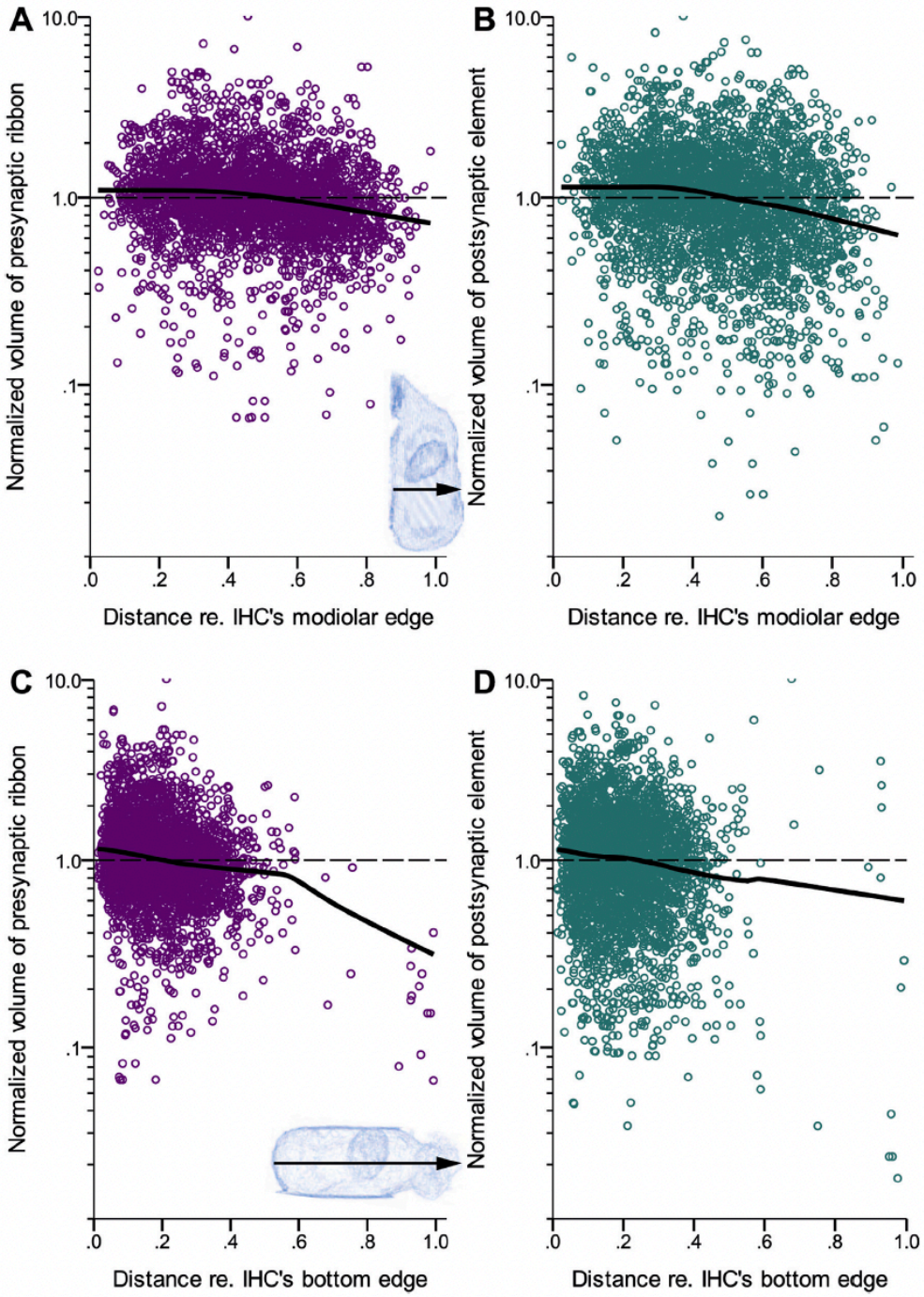


Fig. 4. Normalized volumes of functional synapse elements, as a function of their relative positions along two hair-cell axes. A, B: Normalized volume of presynaptic ribbons (A) or postsynaptic GluR2-patches (B), as a function of position along their IHC's modiolar-pillar axis. C, D: the same data, as a function of position along their IHC's longitudinal axis. As visual aids, the dashed reference lines indicate the median volume in each panel, the thick solid lines represent locally weighted averages (SPSS loess function, using 50% of data points). Cartoons of IHC in panels A and C further illustrate the respective anatomical axis plotted. Note that the y-axis ranges were limited to a uniform value for all 4 panels, which eliminated 1–3 data points in each.

Please cite this article in press as: Zhang, L., et al., Concurrent gradients of ribbon volume and AMPA-receptor patch volume in cochlear afferent synapses on gerbil inner hair cells, Hearing Research (2018), https://doi.org/10.1016/j.heares.2018.03.028

varied concurrently, from larger volumes on the modiolar side and at the bottom of each hair cell, to smaller volumes on the pillar side and higher up the IHC.

3.5. Correlations between the volumes of pre- and postsynaptic elements

For the mouse, opposing spatial gradients have been suggested for presynaptic ribbons and postsynaptic GluR2 receptor patches, such that synapses comprised of relatively small ribbons and relatively large postsynapses are located preferentially towards the hair cells' pillar side and vice versa (Liberman et al., 2011, 2015; Yin et al., 2014). The gerbil data described above is not compatible with that finding. We explored this further, reasoning that such opposing gradients, if present, should be revealed at the individual synapse level, regardless of whether they segregate spatially in any way. A plot of presynaptic versus postsynaptic volume for every functional synapse would then be expected to show a negative correlation. If there is also a spatial segregation, modiolar and pillar data points would be expected to cluster predominantly in separate quadrants. None of these predictions held for our gerbil data. Instead, there was a moderate, but highly significant, positive correlation between the volumes of pre- and postsynaptic elements, i.e. larger ribbons correlated with larger postsynaptic GluR2 patches (Spearman rank correlation, $p < 0.001$, $\rho = 0.37$, $n = 3224$). This correlation remained unchanged when modiolar and pillar synapse populations were tested separately (Fig. 5A and B). The same correlation also held after separating data from the different cochlear locations, except for the 0.5 kHz location, at which no significant correlation was found ($p = 0.15$, $n = 364$).

In summary, in the gerbil, we observed a predominantly positive correlation between the volumes of presynaptic ribbons and postsynaptic GluR2 receptor patches: larger ribbons correlated with larger receptor patches, and smaller ribbons with smaller receptor patches. This was found at all tonotopic locations, except at the most apical 0.5 kHz position, where no correlation was observed. Furthermore, as summarized in the previous section, both pre- and postsynaptic elements tended to be slightly larger on the modiolar side and at the bottom of the IHC, and slightly smaller on the pillar side and higher up the IHC.

4. Discussion

4.1. Innervation density of IHC along the tonotopic gradient in young gerbils

In this study, we compared manual counts of synapses to the numbers derived from our detection and colocalization analysis. Both methods gave very similar results and agreed well with previously-published counts from gerbil IHC. Typical numbers reported for the gerbil are around 20 synapses/IHC (Batrel et al., 2017; Bourien et al., 2014; Gleich et al., 2016; Johnson et al., 2008; Meyer et al., 2009; Slepecky et al., 2000). Of the studies that sampled across more than 2 cochlear locations, only Meyer et al. (2009) and Batrel et al. (2017) observed significant variation, in the form of a broad maximum between about 20% and 80% of the cochlear length (corresponding to about 1–25 kHz; Müller, 1996), and a reduction in synaptic numbers towards both ends. However, they also included samples from locations at the extreme apical and basal ends of the gerbil cochlea, whereas Gleich et al. (2016) and the present study may conceivably have undersampled those terminal regions.

Importantly, numbers reported for paired pre- and postsynaptic elements, presumed to be functional synapses (Bourien et al., 2014; Batrel et al., 2017; this study), for ribbons alone (Gleich et al., 2016; Johnson et al., 2008; Meyer et al., 2009), or just for afferent terminals (Slepecky et al., 2000), do not appear to differ systematically. For the gerbil, this confirms the typically mammalian, tight association of only one presynaptic ribbon for each afferent terminal, and a very low proportion of "orphaned" ribbons, similar to previous reports in mice and guinea pigs (Furman et al., 2013; Sergeyenko et al., 2013).

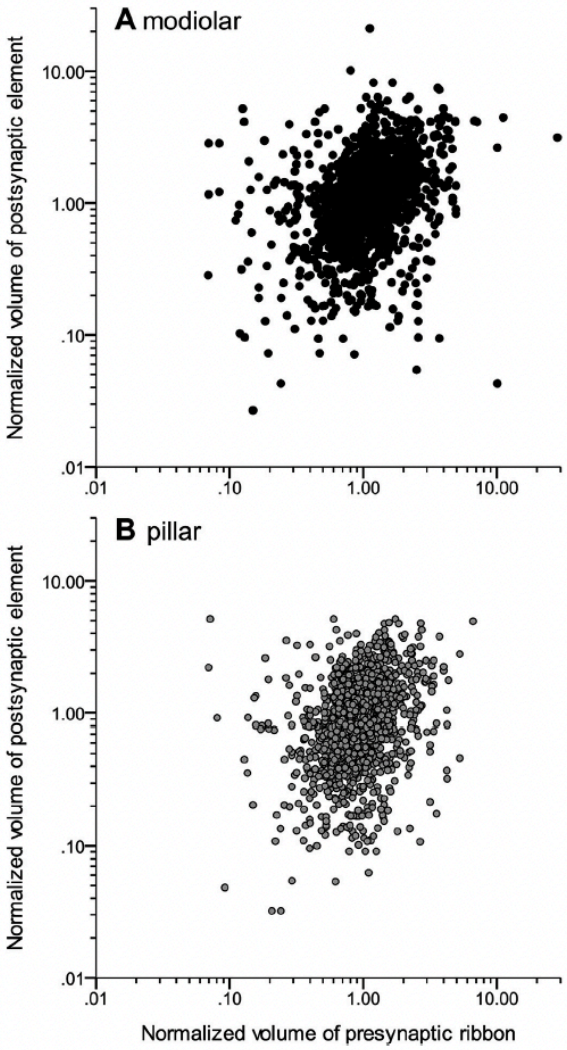


Fig. 5. Scatterplots of normalized volume of presynaptic ribbon versus the normalized volume of its colocalized postsynaptic GluR2 patch, for individual functional synapses identified. A: only synapses located in the modiolar half of their IHC. B: only synapses located in the pillar half of their IHC. The volumes of pre- and postsynaptic elements are positively correlated in both populations (Spearman rank correlation, $p < 0.001$, $\rho = 0.36$, $n = 1848$ for modiolar; $p < 0.001$, $\rho = 0.33$, $n = 1376$ for pillar).

4.2. Spatial gradients of presynaptic ribbon size across species

Our and other immunohistochemical studies used an antibody against CtBP2 to visualize presynaptic ribbons. This antibody recognizes a domain of CtBP2 shared with RIBEYE, which is the major

Please cite this article in press as: Zhang, L., et al., Concurrent gradients of ribbon volume and AMPA-receptor patch volume in cochlear afferent synapses on gerbil inner hair cells, Hearing Research (2018), https://doi.org/10.1016/j.heares.2018.03.028

structural component of the ribbon (Schmitz et al., 2000). Immunostaining is therefore widely assumed to provide a reliable reflection of ribbon size, at least after normalizing for variations in overall labeling brightness between samples, as in the present study.

Significant gradients in the sizes of presynaptic ribbons within a given IHC have now been observed in the mature cochlea of all mammalian species that were investigated: cat (Merchan-Perez and Liberman, 1996), different strains of mouse (Gilels et al., 2013; Liberman et al., 2011), guinea pig (Furman et al., 2013), rat (Kalluri and Monges-Hernandez, 2017) and gerbil (present study). Typically, ribbons facing the modiolar side of the IHCs are larger than ribbons facing the pillar side. In the mouse, which has been most thoroughly quantified, an additional gradient exists along the longitudinal axis of the IHC, such that ribbons tend to decrease in volume from the modiolar-basal domain towards the pillar-cuticular domain (Liberman et al., 2011, 2015; Yin et al., 2014). In the present study in the gerbil, the same trends in ribbon volume along the two IHC axes were qualitatively observed, but were considerably weaker quantitatively. Whereas in the mouse, normalized mean volumes on the modiolar side typically show values above 1.5, and are as low as 0.5 on the pillar side (Liberman and Liberman, 2016; Liberman et al., 2015; Yin et al., 2014), the variation in the gerbil was considerably less (Fig. 3B). Subtle differences in how the analyses were carried out may partly account for this. Yin et al. (2014) showed that the modiolar-pillar gradient in ribbon volume was actually attenuated in the mouse when synapses were classified relative to their location in individual hair cells (in their case, by basing the assignment on the polarity of pre- and postsynapse), instead of relative to a global axis for the entire confocal stack that matched each IHC less well. In our procedure for the gerbil, all synaptic positions were referenced to the coordinates of the individual hair cell.

The functional correlates of different ribbon volumes are believed to be the different physiological types of auditory-nerve fibers that are typical for mammals. This was directly shown in the cat by labeling single physiologically characterized fibers, tracing them back to their individual synapses on IHC, and reconstructing their dimensions from serial TEM sections (Merchan-Perez and Liberman, 1996). It was found that fibers with low SR always contacted their IHC on the modiolar side and tended to face larger ribbons, whereas high-SR fibers mostly synapsed on the IHC's pillar side and were associated with smaller ribbons. Since then, the morphological gradient in ribbon size has been a robust finding in both TEM and immunolabeled material across species (Furman et al., 2013; Kalluri and Monges-Hernandez, 2017; Liberman et al., 2011, 2015; Song et al., 2016; Yin et al., 2014), and the functional correlation is thus commonly assumed. Studies primarily differ in the extent to which this gradient is seen and the gerbil appears to have one of the weakest trends (but see also Kantardzhieva et al., 2013). The functional implications of this remain unclear, because it is an open question whether and how ribbon size is causally related to afferent physiology. Indeed, it is often pointed out that the association of smaller ribbons with the more highly active nerve fibers (and vice versa) is counter-intuitive (e.g., Merchan-Perez and Liberman, 1996; Wichmann and Moser, 2015). Recent work on mouse IHC showed that ribbon size is correlated with number and voltage dependence of presynaptic Ca^{2+} channels in the associated active zone and that the Ca^{2+} channel properties can explain different postsynaptic firing rates and sensitivity in the expected direction (Ohn et al., 2016). In zebrafish lateral-line hair cells, mutual regulatory interaction between RIBEYE and the presynaptic Ca^{2+} channels has been shown (Sheets et al., 2011, 2012), which could thus also provide a link between ribbon size and in-vivo physiological type of IHC afferents, albeit indirectly.

4.3. Spatial gradients of postsynaptic structures across species

Postsynaptic structures also vary within afferents connecting to the same IHC, again correlated with the *in vivo* physiological type. Classic work in cat and guinea pig established that high-SR fibers have larger axonal diameters than low-SR fibers (Liberman, 1982; Gleich and Wilson, 1993; Tsuji and Liberman, 1997). Furthermore, thinner, modiolar fibers (likely to be of the low-SR type), had a lower mitochondrial content than the larger fiber population (Liberman, 1980). However, terminal size and the area of the postsynaptic density did not appear to differ between the fiber types (Merchan-Perez and Liberman, 1996). Similarly, in the gerbil, no systematic distribution of terminal sizes around the IHC was observed, even though a segregration of axon diameters in the osseous spiral lamina is present, albeit less prominent than in the cat (Slepecky et al., 2000).

More recently, morphological gradients in postsynaptic GluR2 receptor volume were explored in immunostained material, with mixed results. In guinea pig and rat, no systematic variation was found along the pillar-modiolar axis (Furman et al., 2013; Kalluri and Monges-Hernandez, 2017). In contrast, in CBA/CaJ mice, a robust gradient was reported, which runs opposite to the ribbon volume variation, such that postsynaptic receptor patches tend to be larger on the pillar side and higher up on the IHC (Liberman et al., 2011, 2015; Yin et al., 2014). Our findings in the gerbil do not conform to these patterns. In our data, the postsynaptic receptor patch volume varied in the same direction, and along the same spatial axes, as the presynaptic ribbon volume. As pointed out by Yin et al. (2014), volume measurements from fluorescent immunolabeled material may be confounded by variations in GluR2 receptor density, as this will also influence the brightness of label (the detection criterion). Thus, some of the observed gradients may actually not be in volume but in receptor density, or a combination of both. Nonetheless, postsynaptic GluR2 receptors appear to vary less clearly with position on the IHC, and less consistently across different species.

4.4. Relationship between presynaptic ribbon and postsynaptic receptor patch volumes at the level of individual synapses

Opposing spatial gradients of ribbon and postsynaptic receptor patch volumes are robustly observed in CBA/CaJ mice that are at least 28d old (Liberman and Liberman, 2016; Liberman et al., 2011; Yin et al., 2014). Interestingly, the inverse relationship that is suggested by those data has barely been explored at the level of individual synapses. In the gerbil, using normalized volumes, we found a highly significant positive correlation that was consistent with the matching spatial gradients of pre- and postsynaptic elements. Importantly, the correlation at the level of individual synapses was clearly stronger, i.e. explained more of the total variance, than any of the relatively weak spatial trends. This suggests that larger presynaptic ribbons predominantly associate with larger (and/or denser) postsynaptic receptor patches, regardless of where they are located on the IHC in gerbils.

5. Conclusions

In summary, a more or less subtle spatial gradient in presynaptic ribbon volume along the pillar-modiolar axis of the IHC is a consistent finding across species and techniques. Ribbon volume also has some known physiological correlates - number and voltage dependence of presynaptic Ca^{2+} channels, spontaneous discharge rate of the postsynaptic fiber — although a causal relationship

Please cite this article in press as: Zhang, L., et al., Concurrent gradients of ribbon volume and AMPA-receptor patch volume in cochlear afferent synapses on gerbil inner hair cells, Hearing Research (2018), https://doi.org/10.1016/j.heares.2018.03.028

remains to be shown. Regarding postsynaptic structures, a similar spatial differentiation of axon diameters and mitochondrial content has been observed across different species, again with a likely physiological correlate in spontaneous discharge rate. The size of the afferent terminals contacting the IHC have only been quantified in cat and gerbil, but did not show any spatial or other differentiation in either case, again suggesting consistency across species. In contrast to this, the findings regarding volume of the postsynaptic GluR2 receptor patches differ strikingly across species. While no spatial differentiation was seen in guinea pig and rat, an inverse gradient to that seen for presynaptic ribbon volume was observed in the CBA/CaJ mouse, and a moderately strong positive correlation in the gerbil. There is no obvious explanation for this, except species differences. However, the presence of the different physiological classes of type I afferents that differ in spontaneous rate, threshold and dynamic range, is a universal characteristic of mammalian cochleae (reviews in Heil and Peterson, 2015; Huet et al., 2016). Species-specific variation in postsynaptic receptor volume and/or density thus suggests that this particular parameter does not contribute to the fundamental differentiation in the physiological properties of type I afferents.

Acknowledgements

This work was supported by the DFG Cluster of Excellence EXC 1077/1 "Hearing4all". We are grateful to STELS-OL (Scientific and Technical English Language Services, Oldenburg, Germany) for English language editing.

Appendix A. Supplementary data

Supplementary data related to this article can be found at https://doi.org/10.1016/j.heares.2018.03.028.

References

Bartrel, C., Huet, A., Hasselmann, F., Wang, J., Desmadryl, G., Nouvian, R., Puel, J.L., Bourien, J., 2017. Mass potentials recorded at the round window enable the detection of low spontaneous rate fibers in gerbil auditory nerve. Plos One 12, e0169890.
Bourien, J., Tang, Y., Batrel, C., Huet, A., Lenoir, M., Ladrech, S., Desmadryl, G., Nouvian, R., Puel, J.L., Wang, J., 2014. Contribution of auditory nerve fibers to compound action potential of the auditory nerve. J. Neurophysiol. 112, 1025–1039.
Cheal, M.L., 1986. The gerbil: a unique model for research on aging. Exp. Aging Res. 12, 3–21.
Fuchs, P.A., Glowatzki, E., Moser, T., 2003. The afferent synapse of cochlear hair cells. Curr. Opin. Neurobiol. 13, 452–458.
Furman, A.C., Kujawa, S.G., Liberman, M.C., 2013. Noise-induced cochlear neuropathy is selective for fibers with low spontaneous rates. J. Neurophysiol. 110, 577–586.
Gilels, F., Paquette, S.T., Zhang, J., Rahman, I., White, P.M., 2013. Mutation of Foxo3 causes adult onset auditory neuropathy and alters cochlear synapse architecture in mice. J. Neurosci. 33, 18409–18424.
Gleich, O., Semmler, P., Strutz, J., 2016. Behavioral auditory thresholds and loss of ribbon synapses at inner hair cells in aged gerbils. Exp. Gerontol. 84, 61–70.
Gleich, O., Wilson, S., 1993. The diameters of Guinea pig auditory nerve fibers: distribution and correlation with spontaneous rate. Hear. Res. 71, 69–79.
Glowatzki, E., Fuchs, P.A., 2002. Transmitter release at the hair cell ribbon synapse. Nat. Neurosci. 5, 147–154.
Heil, P., Peterson, A.J., 2015. Basic response properties of auditory nerve fibers: a review. Cell Tissue Res. 361, 129–158.
Henry, K.R., McGinn, M.D., Chole, R.A., 1980. Age-related auditory loss in the Mongolian gerbil. Arch. Oto-Rhino-Laryngol. 228, 233–238.
Huet, A., Batrel, C., Tang, Y., Desmadryl, G., Wang, J., Puel, J.L., Bourien, J., 2016. Sound coding in the auditory nerve of gerbils. Hear. Res. 338, 32–39.
Johnson, S.L., Forge, A., Knipper, M., Munkner, S., Marcotti, W., 2008. Tonotopic variation in the calcium dependence of neurotransmitter release and vesicle pool replenishment at mammalian auditory ribbon synapses. J. Neurosci. 28, 7670–7678.
Kalluri, R., Monges-Hernandez, M., 2017. Spatial gradients in the size of inner hair cell ribbons emerge before the onset of hearing in rats. J Assoc Res Otolaryngol 18, 399–413.
Kantardzhieva, A., Liberman, M.C., Sewell, W.F., 2013. Quantitative analysis of ribbons, vesicles, and cisterns at the cat inner hair cell synapse: correlations with spontaneous rate. J. Comp. Neurol. 521, 3260–3271.
Liberman, L.D., Liberman, M.C., 2016. Postnatal maturation of auditory-nerve heterogeneity, as seen in spatial gradients of synapse morphology in the inner hair cell area. Hear. Res. 339, 12–22.
Liberman, L.D., Wang, H., Liberman, M.C., 2011. Opposing gradients of ribbon size and AMPA receptor expression underlie sensitivity differences among cochlear-nerve/hair-cell synapses. J. Neurosci. 31, 801–808.
Liberman, L.D., Suzuki, J., Liberman, M.C., 2015. Dynamics of cochlear synaptopathy after acoustic overexposure. JARO J. Assoc. Res. Otolaryngol. 16, 205–219.
Liberman, M.C., 1980. Morphological differences among radial afferent fibers in the cat cochlea: an electron-microscopic study of serial sections. Hear. Res. 3, 45–63.
Liberman, M.C., 1982. Single-neuron labeling in the cat auditory nerve. Science 216, 1239–1240.
Merchan-Perez, A., Liberman, M.C., 1996. Ultrastructural differences among afferent synapses on cochlear hair cells: correlations with spontaneous discharge rate. J. Comp. Neurol. 371, 208–221.
Meyer, A.C., Frank, T., Khimich, D., Hoch, G., Riedel, D.,M.,C.N., Yarin, Y.M., Harke, B., Hell, S.W., Egner, A., Moser, T., 2009. Tuning of synapse number, structure and function in the cochlea. Nat. Neurosci. 12, 444–453.
Mills, J.H., Schmiedt, R.A., Kulish, L.F., 1990. Age-related changes in auditory potentials of Mongolian gerbil. Hear. Res. 46, 201–210.
Moser, T., Brandt, A., Lysakowski, A., 2006a. Hair cell ribbon synapses. Cell Tissue Res. 326, 347–359.
Moser, T., Neef, A., Khimich, D., 2006b. Mechanisms underlying the temporal precision of sound coding at the inner hair cell ribbon synapse. Journal of Physiology-London 576, 55–62.
Müller, M., 1996. The cochlear place-frequency map of the adult and developing Mongolian gerbil. Hear. Res. 94, 148–156.
Nouvian, R., Beutner, D., Parsons, T.D., Moser, T., 2006. Structure and function of the hair cell ribbon synapse. J. Membr. Biol. 209, 153–165.
Ohn, T.-L., Rutherford, M.A., Jing, Z., Jung, S., Duque-Afonso, C.L., Hoch, G., Picher, M.M., Scharinger, A., Strenzke, N., Moser, T., 2016. Hair cells use active zones with different voltage dependence of Ca2+ influx to decompose sounds into complementary neural codes. Proc. Natl. Acad. Sci. U.S.A. E4716–E4725.
Piatigorsky, J., 2001. Dual use of the transcriptional repressor (CtBP2)/ribbon synapse (RIBEYE) gene: how prevalent are multifunctional genes? Trends Neurosci. 24, 555–557.
Ryan, A., 1976. Hearing sensitivity of the Mongolian gerbil, Meriones unguiculatis. J. Acoust. Soc. Am. 59, 1222–1226.
Safieddine, S., Wenthold, R.J., 1999. SNARE complex at the ribbon synapses of cochlear hair cells: analysis of synaptic vesicle- and synaptic membrane-associated proteins. Eur. J. Neurosci. 11, 803–812.
Schindelin, J., Arganda-Carreras, I., Friese, E., Kaynig, V., Pietzsch, T., Preibisch, S., Rueden, C., Saalfeld, S., Schmid, B., Tinevez, J.-Y., White, D.J., Hartenstein, V., Elceiri, K., Tomancak, P., Cardona, A., 2012. Fiji: an open-source platform for biological-image analysis. Nat. Methods 9, 676–682.
Schmitz, F., Königstorfer, A., Südhof, T.C., 2000. RIBEYE, a component of synaptic ribbons: a protein's journey through evolution provides insight into synaptic ribbon function. Neuron 28, 857–872.
Schnee, M.E., Ricci, A., 2017. Hair cells and their synapses. In: Manley, G.A., Gummer, A.W., Popper, A.N., Fay, R.R. (Eds.), Understanding the Cochlea. Springer International Publishing AG, Cham, Switzerland, pp. 183–213.
Sergeyenko, Y., Lall, K., Liberman, M.C., Kujawa, S.G., 2013. Age-related cochlear synaptopathy: an early-onset contributor to auditory functional decline. J. Neurosci. 33, 13686–13694.
Sheets, L., Kindt, K.S., Nicolson, T., 2012. Presynaptic CaV1.3 channels regulate synaptic ribbon size and are required for synaptic maintenance in sensory hair cells. J. Neurosci. 32, 17273–17286.
Sheets, L., Trapani, J.G., Mo, W., Obholzer, N., Nicolson, T., 2011. Ribeye is required for presynaptic CaV1.3a channel localization and afferent innervation of sensory hair cells. Development 138, 1309–1319.
Slepecky, N.B., Galsky, M.D., Swartzentruber-Martin, H., Savage, J., 2000. Study of afferent nerve terminals and fibers in the gerbil cochlea: distribution by size. Hear. Res. 144, 124–134.
Song, Q., Shen, P., Li, X.W., Shi, L.J., Liu, L.J., Wang, J.P., Yu, Z.P., Stephen, K., Aiken, S., Yin, S., Wang, J., 2016. Coding deficits in hidden hearing loss induced by noise: the nature and impacts. Sci. Rep. 6.
Tsuji, J., Liberman, M.C., 1997. Intracellular labeling of auditory nerve fibers in Guinea pig: central and peripheral projections. J. Comp. Neurol. 381, 188–202.
Wichmann, C., Moser, T., 2015. Relating structure and function of inner hair cell ribbon synapses. Cell Tissue Res. 361, 95–114.
Yin, Y., Liberman, L.D., Maison, S.F., Liberman, M.C., 2014. Olivocochlear innervation maintains the normal modiolar-pillar and habenular-cuticular gradients in cochlear synaptic morphology. J Assoc Res Otolaryngol 15, 571–583.

Please cite this article in press as: Zhang, L., et al., Concurrent gradients of ribbon volume and AMPA-receptor patch volume in cochlear afferent synapses on gerbil inner hair cells, Hearing Research (2018), https://doi.org/10.1016/j.heares.2018.03.028

Arbeit 2:

Systems/Circuits

Temporal Coding of Single Auditory Nerve Fibers Is Not Degraded in Aging Gerbils

Amarins N. Heeringa,* Lichun Zhang,* Go Ashida, Rainer Beutelmann, Friederike Steenken, and Christine Köppl
Cluster of Excellence "Hearing4all" and Research Centre Neurosensory Science, Department of Neuroscience, School of Medicine and Health Science, Carl von Ossietzky University Oldenburg, 26129 Oldenburg, Germany

People suffering from age-related hearing loss typically present with deficits in temporal processing tasks. Temporal processing deficits have also been shown in single-unit studies at the level of the auditory brainstem, midbrain, and cortex of aged animals. In this study, we explored whether temporal coding is already affected at the level of the input to the central auditory system. Single-unit auditory nerve fiber recordings were obtained from 41 Mongolian gerbils of either sex, divided between young, middle-aged, and old gerbils. Temporal coding quality was evaluated as vector strength in response to tones at best frequency, and by constructing shuffled and cross-stimulus autocorrelograms, and reverse correlations, from responses to 1 s noise bursts at 10–30 dB sensation level (dB above threshold). At comparable sensation levels, all measures showed that temporal coding was not altered in auditory nerve fibers of aging gerbils. Furthermore, both temporal fine structure and envelope coding remained unaffected. However, spontaneous rates were decreased in aging gerbils. Importantly, despite elevated pure tone thresholds, the frequency tuning of auditory nerve fibers was not affected. These results suggest that age-related temporal coding deficits arise more centrally, possibly due to a loss of auditory nerve fibers (or their peripheral synapses) but not due to qualitative changes in the responses of remaining auditory nerve fibers. The reduced spontaneous rate and elevated thresholds, but normal frequency tuning, of aged auditory nerve fibers can be explained by the well known reduction of endocochlear potential due to strial dysfunction in aged gerbils.

Key words: age-related hearing loss; discharge rate; frequency tuning; presbycusis; stimulus envelope; temporal fine structure

Significance Statement

As our society ages, age-related hearing deficits become ever more prevalent. Apart from decreased hearing sensitivity, elderly people often suffer from a reduced ability to communicate in daily settings, which is thought to be caused by known age-related deficits in auditory temporal processing. The current study demonstrated, using several different stimuli and analysis techniques, that these putative temporal processing deficits are not apparent in responses of single-unit auditory nerve fibers of quiet-aged gerbils. This suggests that age-related temporal processing deficits may develop more central to the auditory nerve, possibly due to a reduced population of active auditory nerve fibers, which will be of importance for the development of treatments for age-related hearing disorders.

Introduction

Age-related hearing loss is a highly common sensory disorder among elderly people. Approximately two-thirds of the population over seventy years old suffer from hearing problems, and the absolute numbers will only increase further as our society ages (Lin et al., 2011). People with age-related hearing loss face not only degraded hearing sensitivity, that is, elevated hearing thresholds, but also deficits in various temporal processing tasks (Plack et al., 2014; Ozmeral et al., 2016). These are typically evident in daily life as a reduced ability to communicate, resulting in social isolation, decreased quality of life, and even dementia in some severe cases (Strawbridge et al., 2000; Gurgel et al., 2014).

A variety of pathological changes within the cochlea are associated with age-related hearing deficits, and include degeneration of hair cells (*sensory presbyacusis*), neurons (*neural presbyacusis*), and stria vascularis (*strial presbyacusis*; Schuknecht and Gacek, 1993; Heeringa and Köppl, 2019). The quiet-aged Mongolian

Received Oct. 27, 2018; revised Oct. 25, 2019; accepted Nov. 4, 2019.
Author contributions: L.Z. and C.K. designed research; A.N.H., L.Z., and F.S. performed research; G.A. and R.B. contributed unpublished reagents/analytic tools; A.N.H. and L.Z. analyzed data; A.N.H., L.Z., G.A., R.B., F.S., and C.K. wrote the paper.
This work was supported by the DFG Cluster of Excellence EXC 1077/1 "Hearing4all". We thank Philip X. Joris from the K.U. Leuven for generously providing the code developed in his laboratory for the SAC/XAC analysis, and Amin Saremi and Helge Ahrens for providing technical assistance.
The authors declare no competing financial interests.
*A.N.H. and L.Z. contributed equally as co-first authors.
Correspondence should be addressed to Christine Köppl at christine.koeppl@uni-oldenburg.de.
https://doi.org/10.1523/JNEUROSCI.2784-18.2019
Copyright © 2020 the authors

gerbil, a commonly used animal model for age-related hearing loss, typically presents with strial presbycusis. The cochlear lateral wall and stria vascularis are degenerated (Schulte and Schmiedt, 1992; Gratton et al., 1995), which results in a reduced endocochlear potential (EP; Schmiedt, 1996). Largely because of the dependence of outer hair-cell amplification on a high EP, loss of EP results in elevated hearing thresholds (Schmiedt, 1993; Schmiedt et al., 2002). Sensory presbycusis is more likely the result of otologic insults, such as exposure to loud noise or ototoxic compounds (Gates and Mills, 2005). Consistent with that, quiet-aged gerbils show only minimal inner hair-cell loss (Tarnowski et al., 1991). Recent studies have drawn attention to synaptopathy, which is a loss of ribbon synapses between inner hair cells and auditory nerve fibers (ANFs), as an ongoing effect of aging (Sergeyenko et al., 2013; Liberman and Kujawa, 2017). Functional consequences of synaptopathy are largely unclear and not detected by standard audiometric procedures (Kujawa and Liberman, 2015). Quiet-aged gerbils also show synapse loss toward the end of their lifespan (Gleich et al., 2016).

Studies addressing the effects of these age-related cochlear pathologies on coding of sounds in the auditory nerve at the single-unit level are scarce (Heeringa and Köppl, 2019). It has been shown in gerbils that rate-level functions are shifted toward higher levels, that is, have higher thresholds but are otherwise unaltered (Hellstrom and Schmiedt, 1991). Furthermore, a significant reduction of the number of low spontaneous rate (SR) fibers is encountered only among ANFs tuned to high frequencies (>6 kHz; Schmiedt et al., 1996). It is unknown whether temporal coding by ANFs is affected by age, as suggested from human psychophysical studies (Fitzgibbons and Gordon-Salant, 1996; Gordon-Salant et al., 2011).

ANFs temporally align their spiking activity to the phase of low frequencies in the acoustic signal, called phase locking. Phase locking faces a species-specific upper frequency limit (Heil and Peterson, 2017). Gerbil ANFs are able to phase lock to pure tones as high as 3 kHz (Versteegh et al., 2011). Temporal coding can be divided between coding of the envelope (ENV) and of the temporal fine structure (TFS), i.e., phase locking to the slow and fast amplitude fluctuations of the acoustic signal, respectively. Both TFS and ENV cues are important for speech understanding (Rosen, 1992). Low-pass filtered speech, containing only ENV information, can still be understood under quiet conditions (Shannon et al., 1995), while the TFS is critical for accurate perception of speech under degraded listening conditions (Hopkins and Moore, 2007; Swaminathan et al., 2016).

In this study, we aimed to understand whether phase locking and coding of TFS and ENV information is affected in ANFs of quiet-aged gerbils with age-related hearing loss. Furthermore, additional properties of spiking activity in the auditory nerve, including spontaneous and evoked firing rates, sharpness of tuning, and thresholds, were investigated.

Materials and Methods

Animals. Forty-one Mongolian gerbils (*Meriones unguiculatus*) of either sex (weight 51–103 g) were used in this study. Animals were divided into three groups: young animals (YO; age range 3–14 months, $n = 26$), middle-aged animals (MA; 23–33 months, $n = 6$), and old animals (OL; 37–42 months, $n = 9$). Experiments were conducted in a custom-built sound-attenuating chamber. Hearing thresholds were determined before surgery using auditory brainstem responses (ABRs) and were monitored at various time points throughout the experiment to assess the condition of the middle and inner ear. All animals were born at the University of Oldenburg animal house, raised and maintained in a controlled, quiet environment (average sound levels of 48 and 55 dB A outside and during working hours, respectively), and were free of middle-ear infections. All experimental procedures were approved by the ethics authorities of Lower Saxony, Germany (permit numbers AZ 33.9-42502-04-11/0337 and AZ 33.19-42502-04-15/1990).

Surgical preparation. Animals were anesthetized by intraperitoneal injection of a ketamine (135 mg/kg; Ketamin 10%, bela-pharm) and xylazine (6 mg/kg; Xylazin 2%, Ceva Tiergesundheit) mixture diluted in saline (0.9% NaCl). Anesthesia was maintained with subcutaneous injections of the same mixture containing one-third of the initial dose (45 mg/kg ketamine, 2 mg/kg xylazine) hourly or upon presence of a positive hindpaw reflex. In addition, a nonsteroidal antiphlogistic agent (meloxicam, 0.2 mg/kg) was injected at the beginning of the experiment, only when the animal was sensitive to the surgical procedures. The depth of anesthesia was constantly monitored by electrocardiogram recordings using intramuscular needle electrodes in the front leg and the contralateral hind leg, and by checking the absence of a muscle reflex upon a hindpaw pinch. Rectal body temperature was maintained at 38°C by a homeothermic blanket (Harvard Apparatus). To avoid airway obstruction during the experiment, middle-aged and old gerbils were tracheotomized but still breathed unaided. Some of the gerbils received additional oxygen (flow 1.5 L/min) in front of the tracheotomy or snout throughout the experiment. The head of the animal was fixed by using a bite bar, with the head mount, in addition, glued to the exposed frontal skull using dental cement (Kopf Instruments). After fixation of the head, the right pinna was removed to expose the bony ear canal. Subsequently, the ear bar, in which the speaker and the calibration microphone were sealed, was placed directly onto the bony ear canal. To avoid damage to the eardrum, the diameter of the ear bar's front end was a bit larger than the ear canal. The ear bar was sealed to the ear canal using petroleum jelly, to obtain a closed system from speaker to eardrum. A small opening was made in the bulla to prevent buildup of negative pressure in the middle ear.

To visualize the auditory nerve, a craniotomy of the right occipital bone was performed, followed by a duratomy and aspiration of cerebellar tissue until the brainstem and vestibular nerve were exposed. A few very small balls of paper tissue drenched in saline, with a maximal diameter <0.5 mm, were placed between the temporal bone and the brainstem to expose the auditory nerve. The auditory nerve could be discriminated from the cochlear nucleus using visual cues, including a distinct difference in color. To further ascertain that units were recorded from the ANF bundle, waveforms, response properties, and click delays were inspected carefully (see Data analysis).

Auditory brainstem responses. Two platinum needle electrodes (Grass Technologies) were placed subdermally: an active electrode ventral of the ear canal and a reference electrode in the neck close to the bulla to record ABRs evoked by chirps (see Acoustic stimuli to evoke auditory brainstem responses). The necessary surgeries did not leave any skin on the vertex to allow for a classical vertex placement of the reference electrode. ABRs were amplified (10,000 times) and bandpass filtered (0.3–3 kHz) using an amplifier (ISO 80, World Precision Instruments), and recorded using a Hammerfall DSP Multiface II (RME Audio; 48 kHz sampling rate) controlled by custom-written MATLAB software (MathWorks).

Acoustic stimuli to evoke auditory brainstem responses. Acoustic stimuli were generated and calibrated to the individual animal's ear using custom-written software in MATLAB and a Hammerfall DSP Multiface II. Stimuli were preamplified (HB7, TDT), and presented through a small speaker (ER-2, Etymotic Research, or IE 800, Sennheiser) that was sealed into the ear bar. Stimuli were calibrated after each placement of the ear bar by measuring SPL near the eardrum with a miniature microphone (FG-23329, Knowles Electronics, or ER7-C, Etymotic Research in combination with the ER-2 or IE 800 speaker, respectively) sealed in the same ear bar, amplified by a microphone amplifier (MA3, TDT). ABRs were measured during the presentation of custom-generated chirps to compensate for the frequency-dependent group delays along the gerbil cochlea (Dau et al., 2000; Versteegh et al., 2011; 0.3–19 kHz, 4.2 ms duration). Stimulus levels were typically separated by 5 dB and were presented randomly (300–500 repetitions). ABR thresholds were visually defined, as the lowest sound level at which clear ABR waves were still distinguishable.

Auditory-nerve single-unit recordings. Single units in the ANF bundle were recorded using glass micropipette electrodes (GB120F-10, Science Products; pulled using a P-2000, Sutter Instruments), filled with a 3M-KCl solution and impedances typically between 10 and 60 MΩ. Electrodes were placed just above the ANF bundle under visual control with a micromanipulator and then advanced remotely via a piezo microdriver (6000 ULN inchworm motor controller and 6005 ULN handset, Burleigh). Neural signals were amplified (WPI 767, World Precision Instruments), filtered for line frequency noise (50/60 Hz; Hum Bug, Quest Scientific), played over a speaker (MS2, TDT), visualized on an oscilloscope (SDS 1102CNL, SIGLENT Technologies), and digitized (RX6, TDT; 48,828 Hz sampling rate) before storage on a personal computer using custom-written MATLAB software. Spike triggering was defined interactively during the experiment and was more carefully manually revisited offline on a trial-by-trial basis (see Data analysis).

Acoustic stimuli for single-unit recordings. As the glass electrode was advanced through the ANF bundle, a broadband noise search stimulus was presented (1–9 kHz, 50–70 dB SPL) until a single unit was isolated, as judged on the oscilloscope by spike amplitude and interspike interval. After a quick audiovisual estimate of the fiber's sensitive range, best frequency (BF) was determined by recording neural responses to tone bursts at ~10 dB above threshold (range 0–30 dB above threshold, 50 ms duration, including 5 ms cosine rise/fall times, 5–10 repetitions). Next, tone bursts at BF (50 ms duration, 5 ms rise/fall time, 10 repetitions) were presented at levels ranging from 10 to 79 dB SPL (3 dB step size) to derive a rate-level function and determine the unit's threshold. If the fiber had a BF < 10 kHz, more repetitions of tone bursts at BF (50 ms duration, 5 ms rise/fall time, 40 repetitions) were presented at several levels below and above threshold (10 dB step size), to test for phase locking. To estimate temporal coding in response to noise, a stimulus consisting of two 1 s noise bursts (separated by 200 ms, 10 ms cosine ramps, 60 repetitions) was presented at 10–30 dB above the unit's threshold. Noise bursts had a frequency range of 0.2–12 kHz and were identical between repetitions (frozen noise). The second burst of each stimulus pair was 180° phase inverted relative to the first (Joris, 2003; Louage et al., 2004). Noise bursts were filtered to compensate for the frequency response of the hardware, according to the individual ear's calibration. If the unit was still stably isolated, pure tones from a matrix of a broader range of frequencies (100–250 Hz step size) and levels (3–5 dB step size, 50 ms durations, 5 ms rise/fall time, 5 repetitions) were presented randomly, to determine the receptive field and derive a tuning curve, and 80 dB clicks were presented (5 ms delay, 20 ms acquisition time, condensation click, 500 repetitions) to determine response latency. All stimuli were calibrated before presentation according to the latest calibration. A new calibration was obtained after each new placement of the ear bar, using a miniature microphone (either the FG-23329, Knowles Electronics, or the ER7-C, Etymotic Research) sealed near the speaker in the same ear bar, a microphone amplifier (MA3, TDT; set at 40 dB amplification), and custom-made MATLAB software.

Data analysis. As our testing protocols were quite prolonged, typically >30 min if all recordings were acquired, spike amplitude could vary within and between single recordings. Therefore, threshold for spike detection was set offline for each individual trial using custom-written MATLAB software. Single-unit isolation was confirmed by checking the interspike intervals, of which a large majority should be >1 ms and none should be <0.6 ms based on the absolute ANF refractoriness (Heil et al., 2007). Recordings from 16 of a total of 463 units were excluded based on this criterion. Furthermore, spike waveforms were carefully inspected to exclude the presence of a pre-potential, which would indicate that the unit was recorded from the ventral cochlear nucleus instead of from the ANF bundle (Keine and Rübsamen, 2015). There were no units recorded in which a pre-potential was observed. In addition, when responses to clicks were recorded, a click latency <2 ms gave an additional confirmation that the unit was recorded from the ANF bundle (FitzGerald et al., 2001). The click latency was determined by two consecutive bins (0.05 ms) in the peristimulus time histogram (PSTH) being higher than the highest bin before the onset of the click (spontaneous rate). Three units were excluded based on having a click latency that was unlikely to be derived from the auditory nerve. Last, the shape of the PSTH at 20 and 30 dB above threshold and the shape of the rate-level function to BF tones were inspected. Three additional units were excluded based on non-primary like PSTH (e.g., chopper) or rate-level function (e.g., non-monotonic).

To determine BF, mean spike rates in responses to tone bursts at a fixed level of ~10 dB above threshold were fitted using a smoothing spline and the frequency at which the fitted line reached maximum firing rate was defined as BF. Bandwidth of the frequency-response curve was determined at the half-maximum evoked rate (relative to mean SR) from the fitted function only from recordings that were collected at a level between 5 and 15 dB above threshold. Threshold was determined from the rate-level function, defined as the tone level evoking a firing rate larger than the SR + 2.5 × SD of the SR and at least 15 spikes/s above the SR. Characteristic frequency (CF) and threshold were also determined from the threshold-tuning curve that could be interpolated from the receptive field, whenever these data were recorded (see Fig. 8*A*). These values were used as BF and threshold when data from the rate-frequency and rate-level curve were unavailable (in $n = 6$ and $n = 4$ units, respectively). Furthermore, the $Q_{10\ dB}$ value was derived from the tuning curve, which is calculated by dividing CF by the tuning-curve bandwidth at 10 dB above threshold. SRs were calculated from randomly presented silent trials throughout the tone presentations. Noise-evoked firing rates were calculated from responses to both noise bursts.

To determine temporal coding in response to pure tones, the vector strength (VS) was calculated (Goldberg and Brown, 1969), which represents the tendency of a unit to phase lock to the period of the tone:

$$VS = \frac{1}{N}\left|\sum_{j=1}^{N} e^{i\varphi(j)}\right|,$$

where N represents the total number of spikes and $\varphi(j)$ is the phase of the jth spike relative to the period of the tone. A p value of the VS was calculated by $p = e\text{^}(-N \times VS^2)$, where $p < 0.001$ and $N > 50$, was considered a significant VS (Mardia and Jupp, 2000).

More extensive temporal coding properties of single units were determined by analyzing responses to the noise bursts. Noise-evoked responses of units were analyzed only when >25 repetitions and >1000 noise-evoked spikes were recorded. Shuffled autocorrelograms (SACs) and cross-stimulus autocorrelograms (XACs) were constructed using a bin width of 20 μs, according to procedures established by Joris (2003) and Louage et al. (2004). SACs and XACs were normalized for firing rate, number of repetitions, bin width, and stimulus duration. The ratio between the XAC and the SAC at $t = 0$ ms delay was calculated, which represents a metric for the transition from predominantly TFS to predominantly ENV phase locking. Subsequently, the DifCor was calculated by a bin per bin subtraction of the XAC from the SAC, and the SumCor was calculated by taking the bin per bin average of the SAC and the XAC. Leakage of locking to the TFS into the SumCor was minimized by applying a low-pass Chebyshev filter (6th order, type II, 30 dB stopband ripple attenuation) with a cutoff frequency at the BF of the unit (Heinz and Swaminathan, 2009). The peak height of the DifCor and the SumCor was used as a measure for temporal coding of the TFS and the ENV, respectively, whereas the peak width of the DifCor and SumCor represents temporal precision (jitter) of the phase locking (Louage et al., 2004). Units in which the SAC peak height (correlation index) was not significant for either of the two noise bursts, as determined by a bootstrap method on random permutations of the interspike intervals ($p > 0.01$; Joris et al., 2006), were excluded from the XAC/SAC ratio, DifCor, and SumCor analyses.

Responses to the noise bursts, subjected to the same inclusion criteria as for the SAC/XAC analysis, were also used to calculate the reverse correlation (*revcor*; de Boer and Kuyper, 1968; de Boer and de Jongh, 1978). The *revcor* function equals the cross-correlation of the acoustical input and the neural spike signal, and is proportional to the normalized average noise stimulus preceding the spikes. Oscillations in the *revcor* function appear when the unit phase locks to a frequency within its receptive field that is present in the noise stimulus (see Fig. 3*A*). The noise that was presented at the eardrum of the gerbil was reconstructed by

reversing the compensation that was applied to the noise to account for the frequency response of the hardware. Unfortunately, it turned out *post hoc* that not all calibrations had been correctly performed and applied to the noises. However, the system response typically did not vary more than ± 5 dB in the 0.5–3.5 kHz frequency range, the frequency range of interest for temporal coding of the TFS. After carefully going over the data, unit responses from one young animal were excluded from the *revcor* analysis based on outlying noise properties that could not be corrected for. Because the absolute amplitude of the noise differed depending on the threshold of the unit, the noise that was used to calculate the *revcor* was normalized to have an RMS value of 1. Subsequently, the *revcor* function was calculated as follows:

$$revcor(\tau) = \frac{1}{N}\sum_{i=1}^{N} x(t_i - \tau),$$

in which τ is the time before the spike, $x(t)$ is the normalized input noise signal, N is the total number of spikes, and t_i (with $i = 1,\ldots,N$) are the spike times. Oscillations in the *revcor* were considered significant if the maximal *revcor* amplitude exceeded five times the RMS of the *revcor* function, calculated from a time window where no significant oscillations were expected (between $t = -20$ ms and $t = -8$ ms relative to t_i). If the *revcor* was significant, the magnitude of the highest spectral peak was used as an additional measure to quantify temporal coding (see Fig. 3*B*). The *revcor* spectrum was also used to determine the *revcor* frequency (at highest spectral peak) and the 10 dB filter bandwidth, which is very similar to the unit's tuning curve (de Boer and de Jongh, 1978).

Experimental design and statistical analysis. Differences between measures of young, middle-aged, and old gerbils were tested for significance preferentially with the nonparametric Kruskal–Wallis test, followed by pairwise comparisons using the Mann–Whitney *U* test. If assumptions of normality were not violated, the ANOVA and *post hoc* Tukey–Kramer's test were used. Metrics that typically varied as a function of BF were tested for significance using an analysis of covariance (ANCOVA), with BF as the covariate. Significant correlations were detected using the nonparametric Spearman's rank test. *P* values were Holm–Bonferroni corrected for multiple comparisons. All statistical tests were done in MATLAB (R2017b) using the Statistics and Machine Learning Toolbox v11.2. The criterion *p* value for significance was conservatively chosen at 0.01. For analyses with inconclusive results (null hypothesis retained) that were of critical importance, power analyses were performed based on the sample and effect sizes actually observed, using $\alpha = 0.01$ and taking the covariate BF into account when necessary. The power calculations were performed with the PASS Software v16.0.4 (PASS 16 Power Analysis and Sample Size Software, 2018, NCSS).

Results

Gerbils were divided into three age groups: YO (3–14 months, $n = 26$), MA (23–33 months, $n = 6$), and OL (37–42 months, $n = 9$).

Old gerbils exhibited variable hearing loss

Overall hearing sensitivity was determined using ABRs evoked by chirps. Middle-aged and old gerbils had significantly higher thresholds than young gerbils but did not significantly differ from each other (Kruskal–Wallis test: $H_{(2)} = 21.69$, $p = 1.95 \times 10^{-5}$; Mann–Whitney *U* tests: YO vs MA, $p = 1.60 \times 10^{-3}$, YO vs OL, $p = 1.50 \times 10^{-4}$, MA vs OL, $p = 0.23$). The median threshold shifts of the middle-aged and old animals were 25 and 40 dB, respectively (Fig. 1*A*). Furthermore, there was substantial variation in the threshold shift among old gerbils (range 10–55 dB relative to the median threshold of young gerbils), suggesting that not all old gerbils experienced the same amount of age-related hearing loss. Plotting individual threshold against the animal's age confirmed that, although there is a general effect of age on hearing threshold, the variation increases with age as well (Fig. 1*B*).

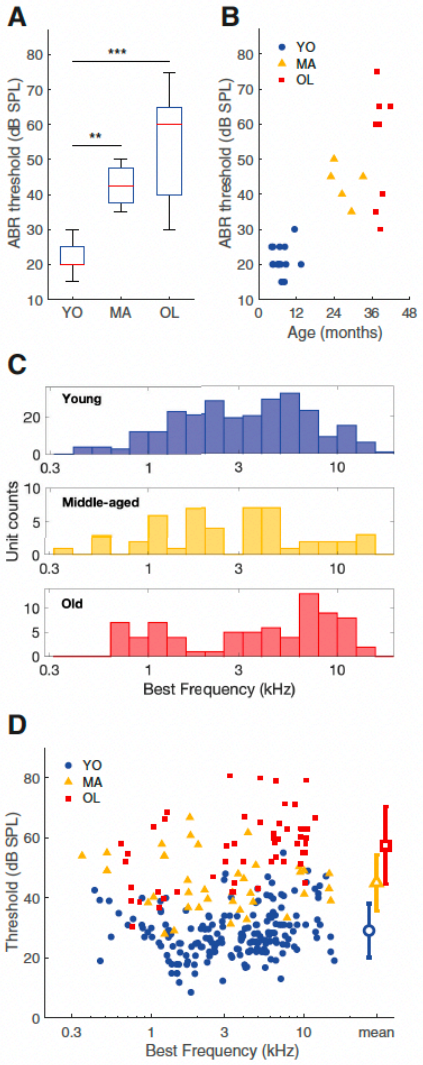


Figure 1. Quiet-aged gerbils presented variable degrees of age-related hearing loss. ***A***, Box plots of ABR thresholds elicited by chirps in YO ($n = 15$), MA ($n = 5$), and OL ($n = 9$) gerbils. Stars indicate a significant difference between two groups after *post hoc* comparisons. $^{**}p < 0.01$, $^{***}p < 0.001$, Bonferroni–Holm corrected. Box plots show the median (horizontal red line), 25th and 75th percentile (blue box), and more extreme data points not considered outliers (whiskers). Data points are considered outliers if they are higher than the 75th percentile + 1.5 × (75–25th percentile) or lower than the 25th percentile–1.5 × (75–25th percentile), which approximates ±2.7 × SD. For the ABR thresholds of the young gerbils, the median and 25th percentiles are the same value and are therefore on top of each other. ***B***, The ABR threshold to chirps of each animal, as a function of its age in months. ***C***, The BF distribution of all auditory nerve single units recorded from young animals ($n = 261$, blue), middle-aged animals ($n = 48$, yellow), and old ($n = 76$, red) animals. ***D***, Threshold as a function of the fiber's BF in young (blue circles; $n = 186$), middle-aged (yellow triangles; $n = 39$), and old (red squares; $n = 54$) animals. Mean thresholds ± SD are shown with large open symbols on the right.

The BF distribution of recorded auditory-nerve single units is shown for each group in Figure 1*C* and showed evidence of bimodality, particularly in the young and old group. A bimodal BF distribution with a notch near 3.5 kHz is typical for the gerbil

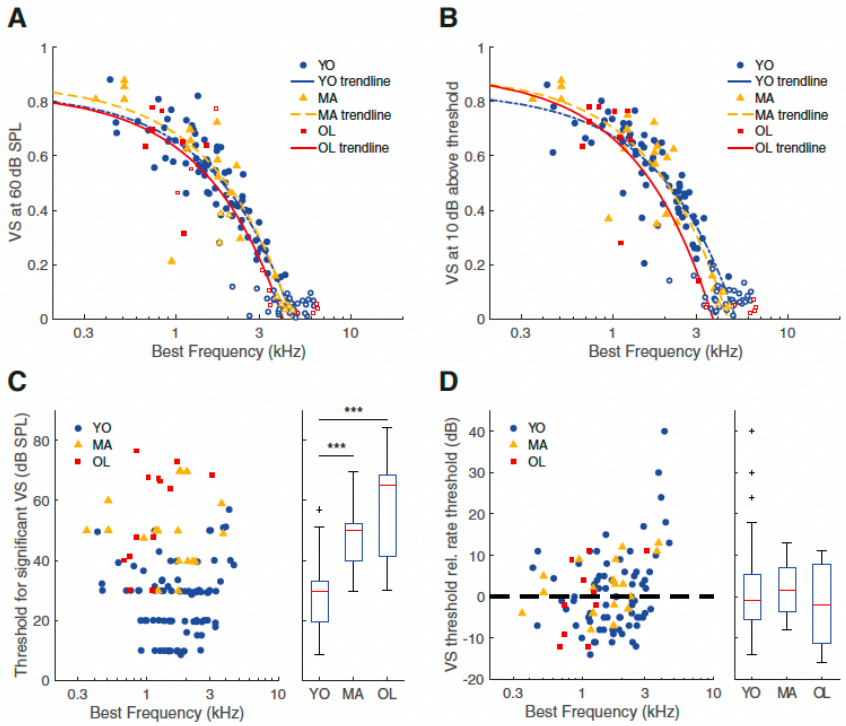


Figure 2. Phase locking to pure tones was not affected by aging. ***A***, VS of the units' response to a BF tone at 60 dB SPL, as a function of BF, for young ($n = 74$), middle-aged ($n = 16$), and old ($n = 7$) gerbils. Open symbols indicate VS values that were not significant ($p > 0.001$ or $N < 50$; see Materials and Methods), which were not included in the analysis. The few high, yet nonsignificant VS values in the middle-aged and old gerbil group come from units with a high threshold and thus a small number of spikes ($N < 50$). VS values from units with a firing rate <5 spikes/s at 60 dB SPL are not shown (MA: $n = 1$, OL: $n = 5$). The trend lines show linear regressions, separately for young, middle-aged, and old gerbils (note the logarithmic scale of the horizontal axis). ***B***, Same format as in ***A***, but here VS is examined for BF tones at 10 dB above threshold (YO: $n = 69$, MA: $n = 20$, OL: $n = 10$). ***C***, The lowest sound level where VS was significant, as a function of BF. To the right, the population data are presented as a box plot in the same format as in Figure 1*A* (YO: $n = 86$, MA: $n = 20$, OL: $n = 13$). Outliers are presented as black crosses. ***D***, Same format as in ***C*** but VS threshold is now shown relative to the rate threshold (VS threshold − rate threshold; YO: $n = 73$, MA: $n = 20$, OL: $n = 10$). The dotted reference line indicates where the VS threshold is equal to the rate threshold, data points below this line represent significant phase locking at sound levels that did not elicit a significant increase in firing rate. In all panels, blue circles indicate data from young gerbils, yellow triangles from middle-aged gerbils, and red squares from old gerbils. ***$p < 0.001$. Outliers are presented as black crosses (+).

auditory nerve (Huet et al., 2016). Thresholds to BF tone bursts differed significantly with age (one-way ANOVA: $F_{(2)} = 194$, $p = 3.81 \times 10^{-54}$). Single-unit thresholds of middle-aged gerbils had a significant mean elevation of 16 dB relative to the mean threshold of young animals [95% confidence interval (CI): 12–20 dB difference, Tukey–Kramer's test: $p = 9.56 \times 10^{-10}$]; thresholds of old gerbils were elevated by 28 dB relative to controls (95% CI: 25–32 dB difference, Tukey–Kramer's test: $p = 9.56 \times 10^{-10}$). At the single-unit level, thresholds differed also significantly between the middle-aged and the old group (mean elevation: 12 dB; 95% CI: 8–17 dB; Tukey–Kramer's test: $p = 7.51 \times 10^{-9}$; Fig. 1*D*).

Phase locking to pure tones was not altered with age

Temporal coding in ANFs was studied using various measures. First, VS, a measure for synchronization to the period of a BF tone, i.e., TFS coding, was studied at different sound levels. Figure 2*A* shows VS of young, middle-aged, and old gerbils in response to BF tones of a fixed level (60 dB SPL). Analysis of covariance did not reveal a significant difference in VS between age groups (effect of group, $F_{(2)} = 0.58$, $p = 0.56$; estimated power = 80%; Fig. 2*A*). Because rate thresholds between age groups differed significantly (Fig. 1*D*) and VS varies as a function of level relative to threshold (Huet et al., 2018), we also compared VS at a fixed sensation level (10 dB above the individual unit's rate threshold). At this level, VS also did not differ between the age groups (ANCOVA: effect of group, $F_{(2)} = 0.48$, $p = 0.62$; Fig. 2*B*). Here, the estimated test power was low (17%), however the differences between the trendlines were small and unsystematic (effect size (Cohen's f) = 0.09). Next, we determined the lowest sound level at which the VS was significant ($p < 0.001$), which was termed the VS threshold. VS thresholds were significantly higher in middle-aged and old gerbils than in young gerbils, with median elevations of 20 and 36 dB, respectively (Kruskal–Wallis test: $H_{(2)} = 51.26$, $p = 7.40 \times 10^{-12}$; Mann–Whitney *U* tests: YO vs MA, $p = 3.82 \times 10^{-8}$, YO vs OL, $p = 4.84 \times 10^{-7}$, MA vs OL, $p = 0.23$; Fig. 2*C*). However, this threshold is conceivably confounded by the rate threshold. Therefore, we calculated the VS threshold relative to the rate threshold. A negative value means that significant phase locking to the tone was present at a level where no significant rate change was yet observed. This relative threshold did not differ significantly between the age groups (Kruskal–Wallis test: $H_{(2)} = 1.75$, $p = 0.42$; Fig. 2*D*). Together, these results show that the absolute sound level at which significant phase locking emerges in ANFs was increased in middle-aged and old gerbils, further indicative of age-related hearing loss, whereas the qualitative properties of phase locking to BF tones in quiet did not differ with increasing age.

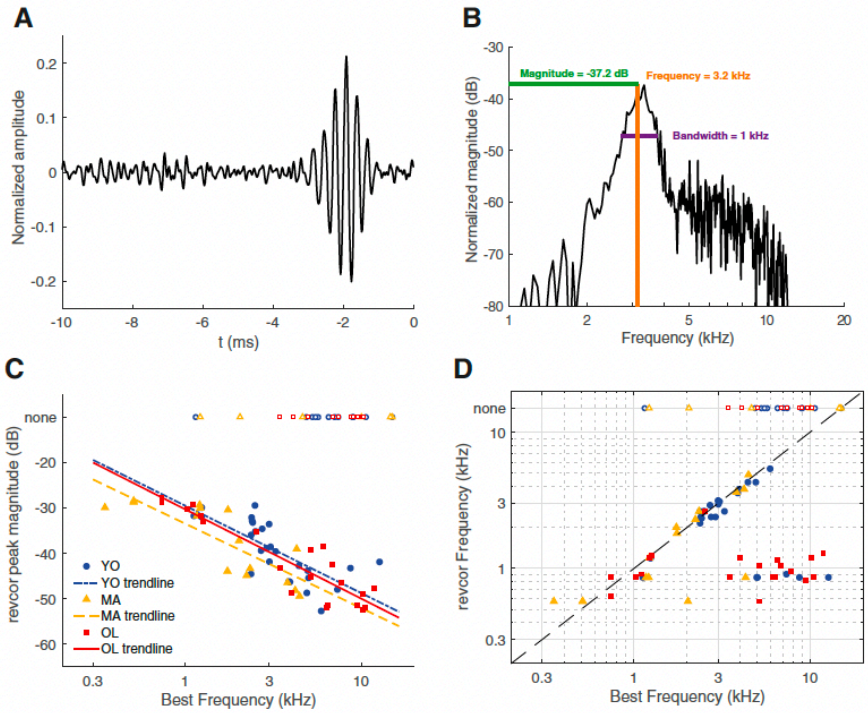


Figure 3. Temporal coding measures derived from the revcor were not affected by aging. ***A***, An example of a *revcor*, with a significant oscillation occurring ~−2 ms relative to the spike (t = 0 ms). BF of this unit was 3.0 kHz. ***B***, Spectrum of the *revcor* function shown in ***A***. Peak magnitude, *revcor* frequency at peak magnitude, and bandwidth at 10 dB below peak magnitude are indicated in the plot. ***C***, *Revcor* peak magnitude as a function of BF for young (blue circles), middle-aged (yellow triangles), and old gerbils (red squares). Magnitudes were similar between groups but decreased with increasing BF. Logarithmic regression lines are shown as visual aids, separately for the different groups (YO: n = 27, MA: n = 15, OL: n = 21). ***D***, *Revcor* frequency as a function of BF for young, middle-aged, and old gerbils. The dashed line represents $y = x$. Open symbols at the top of the graph in ***C*** and ***D*** indicate the BF of units that had no significant *revcor* oscillation (none).

Peak magnitude of the reverse correlation was not affected by aging

Single-unit responses to noise bursts were analyzed using a *revcor* paradigm, which shows a significant oscillation when the unit phase locks to a frequency present in the noise stimulus, typically its BF. The *revcor* can be considered to represent the normalized average stimulus that elicited a spike, with $t = 0$ ms indicating the time of the spike. An example of a *revcor* from a unit of a young gerbil is shown in Figure 3*A*. The frequency to which the unit responded (3.2 kHz) can be derived from the spectrum of the *revcor* and was close to its BF at 3.0 kHz (Fig. 3*B*). The peak magnitude in the *revcor* spectrum is considered a measure for robustness of temporal coding of the TFS (analogous to VS and DifCor peak height). For a given ANF unit, *revcor* magnitude typically decreases with increasing sound level (Recio-Spinoso et al., 2005). The levels of the noise stimuli were therefore selected following online sensitivity measures during the experiment, aiming for similar sensation levels between units (between 10–30 dB above threshold). Indeed, noise-evoked firing rates did not differ between the different age groups (Kruskal–Wallis test: $H_{(2)} = 3.83$, $p = 0.15$; YO: $n = 39$, MA: $n = 21$, OL: $n = 31$). Average absolute noise levels were 53.6, 66.2, and 79.7 dB SPL for the young, middle-aged, and old gerbils, respectively, and these did differ significantly between the groups (Kruskal–Wallis test: $H_{(2)} = 52.18$, $p = 4.94 \times 10^{-12}$), which mirrors the increased thresholds in the middle-aged and old gerbils (Fig. 1*D*).

Strength of temporal coding of the TFS clearly decreased with increasing BF and there was no significant difference in *revcor* magnitude between the different age groups when controlling for BF (ANCOVA: effect of group, $F_{(2)} = 3.43$, $p = 0.04$; Fig. 3*C*). Although the estimated test power was low (11%), the observed effects were so small (effect size = 0.1) that we would not consider them biologically relevant even if a much larger sample showed them to be statistically significant. Plotting the *revcor* frequency against the unit's BF showed that most units with a BF <3.5 kHz had a *revcor* frequency similar to BF (Fig. 3*D*). Note that some units with a BF > 3.5 kHz still showed a significant *revcor*, but the *revcor* frequency was considerably lower, suggesting that they phase locked to frequencies far below BF (~1 kHz). This is a well known phenomenon in mammalian ANFs if the stimulus level is high enough to excite units at frequencies in the tail regions of their frequency-threshold curves (Heil and Peterson, 2017). Units from gerbils of all age groups showed a similar correspondence between BF and *revcor* frequency and a similar incidence of insignificant *revcors* (43%, 40%, and 45% for young, middle-aged, and old gerbils, respectively).

TFS and ENV coding, at comparable sensation levels, were unaffected by aging

To study temporal coding more in depth and to be able to distinguish TFS coding from ENV coding, responses to noise bursts were also analyzed by constructing SACs from responses to different trials of the same noise bursts and XACs from responses to trials of noise bursts of opposite polarity (Louage et al., 2004). A total of six units (YO: n = 1/39, MA: n = 2/19, OL: n = 3/29) did not show any locking to either TFS or ENV, as determined by a

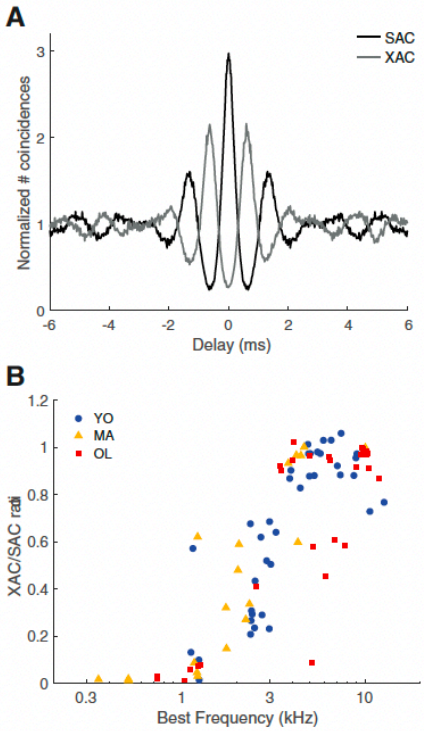


Figure 4. Transition from predominantly fine structure coding to predominantly envelope coding with increasing BF. ***A***, Example of the SAC (black line) and XAC (gray line) of noise responses from a unit of a young gerbil (BF = 900 Hz). The XAC/SAC ratio at 0 ms delay of this unit was 0.09. ***B***, The XAC/SAC ratio at delay = 0 ms, as a function of BF for young (blue circles), middle-aged (yellow triangles), and old gerbils (red squares).

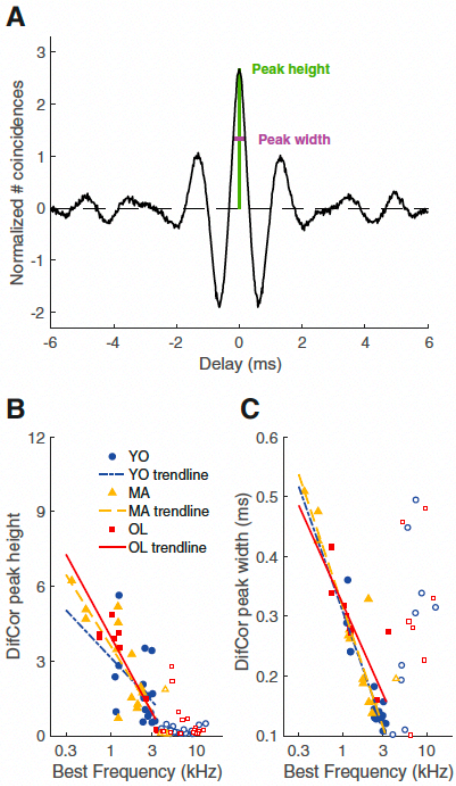


Figure 5. DifCor peak height and width were not affected by aging. ***A***, Example of the DifCor, for the same unit shown in Figure 4*A*. Peak height (at delay = 0 ms, from dotted reference line) was 2.67 (represented in green) and peak width was 0.38 ms (represented in magenta). ***B***, DifCor peak height as a function of BF for young (blue circles; $n = 18$), middle-aged (yellow triangles; $n = 13$), and old gerbils (red squares; $n = 9$). Peak heights were similar between the different age groups, but decreased with increasing BF. Logarithmic regressions are shown as visual aids. Open symbols in ***B*** and ***C*** indicate units with a BF > 3.5 kHz and were not included in the regression analyses. ***C***, Same data and format as in ***B*** but now plotting DifCor peak width.

bootstrap method on interspike intervals on the SAC (Joris et al., 2006), and were therefore not included in subsequent analyses. Figure 4*A* depicts an example of the SAC (black) and XAC (gray) from one unit of a young gerbil (BF = 0.9 kHz). The ratio between the XAC and the SAC at delay = 0 ms was calculated to determine whether the fiber was predominantly locking to the TFS or to the ENV of the stimulus. All included units with a BF < 3.5 kHz showed XAC/SAC ratios <0.7 (Fig. 4*B*) and were thus primarily phase locking to the TFS (Fig. 4*A*). In contrast, units with a BF > 3.5 kHz generally showed high XAC/SAC ratios and were thus primarily phase locking to the ENV of the stimulus, consistent with previous data by Louage et al. (2004).

The DifCor was calculated by subtracting the XAC from the SAC, and displays regular oscillations separated by ~half the period of BF if the unit phase locked to the TFS of the acoustic signal (Fig. 5*A* shows an example of the DifCor derived from the SAC and XAC in Fig. 4*A*). DifCor peak height is then a measure of the strength of phase locking to the TFS (analogous to VS and *revcor* peak magnitude) and DifCor peak width represents the amount of spike jitter of phase locking. DifCor peak height did not differ between young, middle-aged, and old gerbils when controlling for BF (ANCOVA: effect of group, $F_{(2)} = 0.102$, $p = 0.90$; estimated power = 74%; Fig. 5*B*). DifCor peak width also did not differ between the different age groups (ANCOVA: effect of group, $F_{(2)} = 1.14$, $p = 0.33$; Fig. 5*C*). Because the high-frequency units with a XAC/SAC ratio <0.7 likely showed TFS phase locking to tail frequencies of their tuning curve (see previous section; Fig. 3*D*), only fibers with a BF < 3.5 kHz were included in the statistical analyses of the DifCor (Fig. 5*B*,*C*, filled symbols).

The SumCor was calculated by taking the average of the XAC and SAC and shows a simple peak if the unit locked to ENV features of the acoustic signal (Fig. 6*A*). The SumCor peak height, representing strength of ENV coding, did not vary with BF [ANCOVA: effect of group, $F_{(2)} = 0.07$, $p = 0.93$; effect of log(BF), $F_{(2)} = 0.35$, $p = 0.56$; Fig. 6*B*] and were therefore further analyzed with the Kruskal–Wallis test. This showed no significant effect of age on SumCor peak height (Kruskal–Wallis test: $H_{(2)} = 1.92$, $p = 0.38$; Fig. 6*B*). The estimated test power was very low (<10%) but, again, the observed differences between age groups were extremely small and probably not biologically relevant. Likewise, the SumCor peak width, representing the jitter of ENV coding, showed only minimal, insignificant differences between young, middle-aged, and old gerbils (ANCOVA: effect of group, $F_{(2)} = 1.05$, $p = 0.35$; Fig. 6*C*).

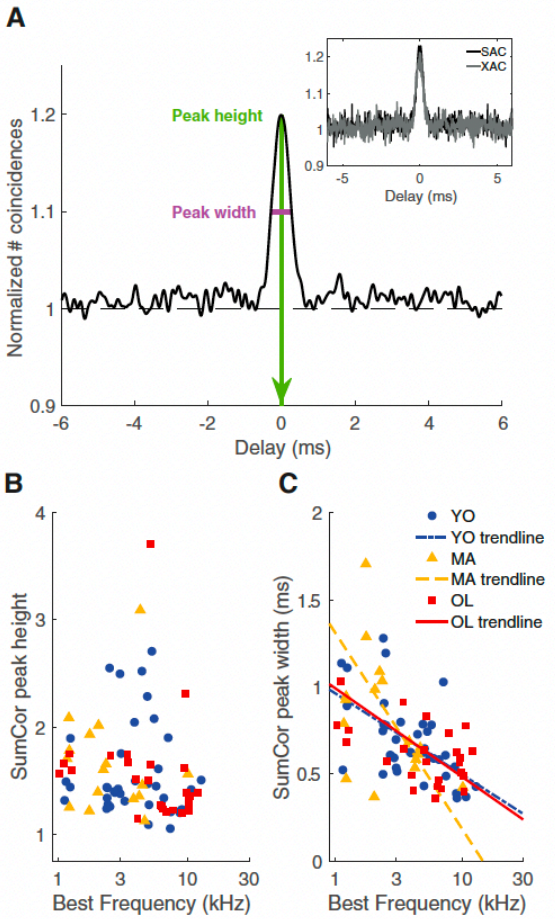


Figure 6. SumCor peak height and width were not affected by aging. ***A***, Example of the SumCor of a unit of a young gerbil (BF = 7.5 kHz). Inset, The SAC and XAC of the same unit (XAC/SAC ratio = 1.02). Peak height (from 0) was 1.22 (green) and peak width was 0.53 ms (magenta). ***B***, SumCor peak height as a function of BF for young (blue circles; $n = 38$), middle-aged (yellow triangles; $n = 19$), and old gerbils (red squares; $n = 28$). ***C***, SumCor peak width as a function of BF for the different age groups. Logarithmic regressions are shown as visual aids.

Auditory nerve spontaneous firing rates were decreased with aging

SR was significantly decreased in ANFs of both middle-aged and old gerbils, compared with young gerbils (Kruskal–Wallis test: $H_{(2)} = 64.34$, $p = 1.07 \times 10^{-14}$; Mann–Whitney U tests: YO vs MA, $p = 4.50 \times 10^{-11}$, YO vs OL, $p = 5{,}90 \times 10^{-8}$, MA vs OL, $p = 0.15$; Fig. 7*A*). This difference between age groups was intriguing and prompted us to further differentiate between the low- and high-frequency parts of the cochlea. Separate Kruskal–Wallis tests showed that there was a significant effect of group in both the low- and the high-BF units (Kruskal–Wallis test: $H_{(2)} = 51.43$, $p = 6.79 \times 10^{-12}$, for fibers with a BF < 3.5 kHz; $H_{(2)} = 21.86$, $p = 1.79 \times 10^{-5}$, for fibers with a BF ≥ 3.5 kHz). *Post hoc* pairwise comparisons revealed a significant decrease of SR in low-BF units of the middle-aged and old animals (Mann–Whitney *U* tests: YO vs MA, $p = 6.04 \times 10^{-8}$, YO vs OL, $p = 1.22 \times 10^{-7}$, MA vs OL, $p = 0.64$; Fig. 7*C*) and a significant SR decrease in high-BF units in the middle-aged animals (Mann–Whitney *U* tests: YO vs MA, $p = 5.31 \times 10^{-5}$, YO vs OL, $p = 0.02$, MA vs OL, $p = 0.03$; Fig. 7*D*).

We wondered whether the decreased SR might reflect some association with age-related hearing loss, since the age of onset and the extent of age-related hearing loss were quite variable across different animals (Fig. 1*B*). Therefore, the SR was plotted as a function of the ABR threshold in response to chirps (Fig. 7*E*). Single-unit SRs negatively correlated with the individual's ABR threshold (Spearman's rank correlation: $\rho = -0.34$, $p = 1.70 \times 10^{-8}$), indicating that a larger extent of age-related hearing loss was accompanied by lower SRs in the single-unit auditory nerve fibers.

Tuning of auditory nerve fibers was not altered with aging

For a subset of units, we obtained receptive fields from which a frequency threshold curve, or tuning curve could be derived (Fig. 8*A*). From the tuning curve, $Q_{10\ dB}$ was calculated as a measure for tuning sharpness. $Q_{10\ dB}$ increased logarithmically with increasing CF for young, middle-aged, and old gerbils, but there was no significant difference in $Q_{10\ dB}$ between the different age groups (ANCOVA: effect of group, $F_{(2)} = 0.89$, $p = 0.42$; Fig. 8*B*). A second measure of ANF frequency tuning was derived from the frequency-response curves, where the bandwidth at the half-maximum rate was determined. Again, the log(bandwidth) correlated positively with log(BF), but no significant effect of group was observed ($F_{(2)} = 2.68$, $p = 0.07$; Fig. 8*C*). As a third measure, ANF tuning was derived from the spectrum of the *revcor* (Fig. 3*B*), which is commonly determined at 10 dB below the maximum magnitude and also represents frequency selectivity (Henry et al., 2016). Only units in which the *revcor* frequency corresponded to the BF (Fig. 3*D*) were analyzed for bandwidth. 10 dB bandwidth did not differ between the different groups (Kruskal–Wallis test: $H_{(2)} = 1.24$, $p = 0.54$; Fig. 8*D*). Note that estimated test power was low (<10%) for all three tuning metrics explored, such that we cannot exclude minor changes with age. However, as for similar cases above, the power estimates refer to the detectability of the very small differences that we actually observed and that are unlikely to have biological relevance (effect sizes <0.1). Together these data strongly suggest that, despite thresholds being increased in old gerbils, this did not affect tuning sharpness of their ANFs to a relevant degree.

Discussion

Our study demonstrated that temporal coding in ANFs of quiet-aged gerbils was not altered relative to young gerbils, at comparable sensation levels. This was shown using several different measures of temporal coding of responses to pure tones and to noise. Specifically, responses to noise revealed that both TFS and ENV coding remained unaffected in old gerbils. In addition, ANF SRs were significantly decreased, especially in low-frequency ANFs. Because these data were obtained from gerbils that were not exposed to noise damage or to any ototoxic events, the changes in spontaneous rates are likely the result of natural aging processes. This is further supported by the observation that despite elevated thresholds, ANF frequency tuning was not affected in middle-aged and old gerbils, in contrast to the typical loss of frequency tuning after noise trauma that causes a permanent threshold shift of similar magnitude (chinchilla; Henry et al., 2016).

Age-related temporal coding deficits likely arise central to the auditory nerve

Previous studies in animals judged to be of geriatric age for the respective species have shown temporal coding degradations at

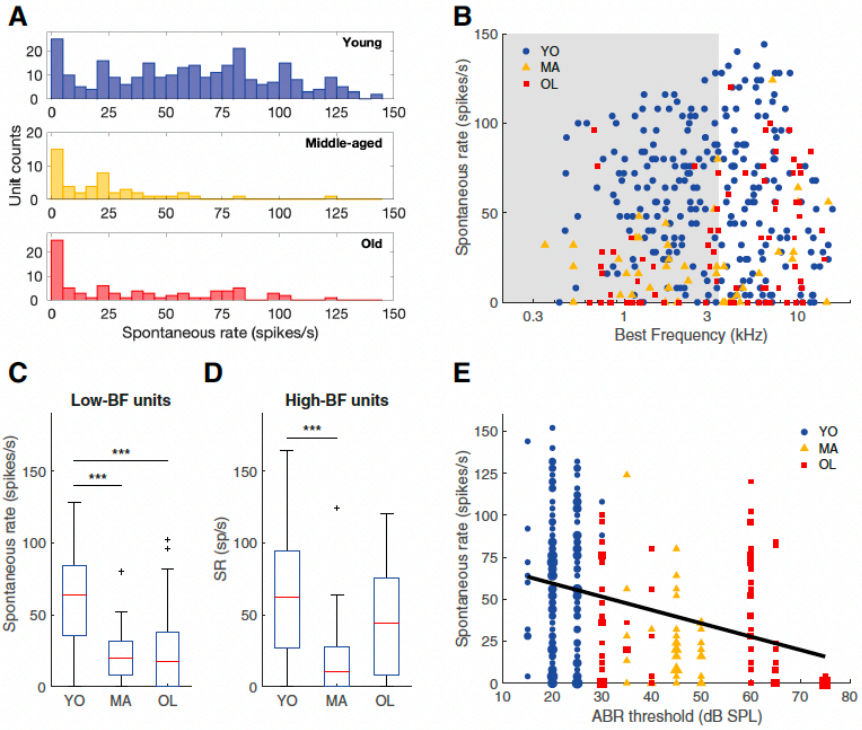


Figure 7. Auditory nerve SR decreased with age-related hearing loss. ***A***, The SR distribution of all auditory nerve single units recorded from young ($n = 272$; blue), middle-aged ($n = 48$; yellow), and old gerbils ($n = 78$; red). ***B***, SR plotted against BF in young (blue circles), middle-aged (yellow triangles), and old (red squares) animals. The gray shaded area indicates units with a BF < 3.5 kHz. ***C***, ***D***, Boxplots of SRs, separately for low-BF (***C***; YO: $n = 146$, MA: $n = 28$, OL: $n = 36$) and high-BF units (***D***; YO: $n = 137$, MA: $n = 20$, OL: $n = 44$), and for YO, MA, and OL gerbils in each graph. ***E***, SR plotted as a function of the ABR threshold to chirps of that animal (YO: $n = 149$, MA: $n = 37$, OL: $n = 78$). The black trend line represents the linear regression between ABR threshold and SR. Marker size represents the number of overlapping data points. ***$p < 0.001$. Outliers are presented as black crosses (+).

the level of the auditory brainstem (cochlear nucleus), midbrain (inferior colliculus), and cortex (Walton, 2010). Specifically, the minimal gap threshold is increased in the inferior colliculus (mice; Walton et al., 1998) and responses to amplitude modulated tones and noise are deteriorated in the dorsal cochlear nucleus (rats), inferior colliculus (mice), and primary auditory cortex (Rhesus macaque monkeys; Walton et al., 2002; Schatteman et al., 2008; Overton and Recanzone, 2016). Furthermore, humans with age-related hearing loss often present with deficits in various temporal processing tasks (Hopkins and Moore, 2011; Plack et al., 2014; Ozmeral et al., 2016). Therefore, it may seem surprising that temporal coding was not deteriorated in auditory-nerve single units of quiet-aged gerbils.

There are several possible explanations for this apparent discrepancy. First, temporal coding deficits central to the auditory nerve can be explained by a local age-related decrease in inhibition (Caspary et al., 1995; Gleich et al., 2003; Canlon et al., 2010; Rabang et al., 2012), and thus do not require any changes in the auditory-nerve input. Second, temporal coding deficits may develop, for example, at the endbulb of Held: the large axosomatic central synapse between ANFs and ventral cochlear nucleus neurons. The complexity of the endbulb of Held decreases with age in mice, even before thresholds are elevated (Muniak et al., 2018), corresponding to a functional decline of the synapse, as measured with patch-clamping (Xie, 2016; Xie and Manis, 2017). Last, the size of the ANF population, rather than the functional properties of the remaining individual units, may change as a function of age. Aging is associated with synaptopathy and neuropathy in mammals, i.e., a substantial decline in the number of inner hair cell–ANF synapses and spiral ganglion neurons, respectively (for reviews, see Liberman and Kujawa, 2017; Heeringa and Köppl, 2019). It is thought that the convergence of multiple ANFs on their postsynaptic targets in the cochlear nucleus contributes to enhanced phase locking in the auditory brainstem (Joris and Smith, 2008). Therefore, a decrease in ANF population size, as shown for the gerbil starting from 24–30 months of age (Keithley et al., 1989; Gleich et al., 2016), would be expected to affect temporal coding. Indeed, studies on envelope following responses (EFRs), which represent the electrophysiological responses of populations of brainstem and midbrain auditory neurons, showed decreased response amplitudes in aged rats and mice (Parthasarathy and Bartlett, 2011; Parthasarathy and Kujawa, 2018). When the sound level is matched for wave I amplitude, and thus activating equivalent numbers of ANFs (Parthasarathy and Kujawa, 2018), the effect of age is eliminated (Lai et al., 2017). Moreover, EFR amplitude also decreases following noise-induced synapse loss (Shaheen et al., 2015). Therefore, a decrease in auditory nerve population size, rather than degraded temporal coding abilities of single ANFs, may be the predominant peripheral contribution to central age-related temporal coding deficits.

Threshold loss combined with normal frequency tuning is consistent with age-related strial dysfunction

Quiet-aged gerbils present a mixture of strial presbyacusis and synaptopathy at 34–39 months of age, with minimal sensory presbycusis (Heeringa and Köppl, 2019). Elevated single-unit

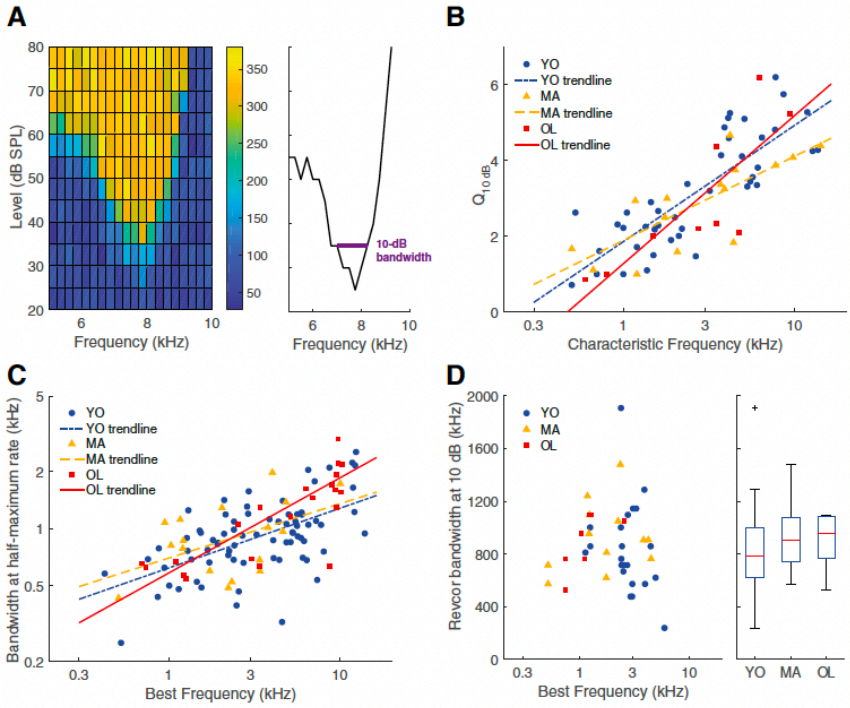


Figure 8. Frequency tuning of ANFs did not deteriorate with age. ***A***, Example of a receptive field (left) which shows the firing rate in spikes/s (mean over 50 ms stimulus) as a color code for all presented combinations of sound level (*y*-axis) and frequency (*x*-axis). From the receptive field, a tuning curve was derived (right), from which the $Q_{10\ dB}$ was calculated at 10 dB above threshold. ***B***, $Q_{10\ dB}$ as a function of CF. There was no difference between units recorded from young (blue circles; $n = 42$), middle-aged (yellow triangles; $n = 15$), and old gerbils (red squares; $n = 10$) but $Q_{10\ dB}$ generally increased with increasing CF. Exponential regression lines are shown as a visual aid. ***C***, Bandwidth of the iso-level response curve, at the half-maximum tone-evoked firing rate, shown in the same format as ***B*** (YO: $n = 75$, MA: $n = 17$, OL: $n = 22$). ***D***, Bandwidth of the *revcor* spectrum at 10 dB below the maximum magnitude, shown in the same format as ***B***. In addition, a boxplot shows the distribution of the *revcor* bandwidths for each group (YO: $n = 22$, MA: $n = 12$, OL: $n = 7$). Outliers are presented as black crosses (+).

and ABR thresholds are likely results of EP loss due to strial dysfunction (Schmiedt et al., 2002), which in turn affects cochlear amplification by outer hair cells (Ruggero and Rich, 1991). Consistently, experimentally induced EP loss, using furosemide injections, results in elevated single-unit and ABR thresholds (Sewell, 1984a; Schmiedt et al., 2002; Lang et al., 2010). In contrast, experimentally induced synaptopathy is typically not reflected in elevated thresholds; thresholds can remain normal in the face of synapse losses of up to 60% (Kujawa and Liberman, 2009; Bourien et al., 2014).

Despite elevated thresholds, tuning sharpness remained unaltered in ANFs of old gerbils. This is in marked contrast to noise-induced hearing loss, which is typically associated with broadened frequency selectivity and hypersensitivity of the low-frequency tuning-curve tail. Noise-induced hearing loss is associated predominantly with hair cell damage and loss (Liberman and Dodds, 1984), whereas hair-cell loss remains minimal in quiet-aged gerbils (Tarnowski et al., 1991). A recent study showed that auditory-nerve fiber's tip-to-tail ratios are much less affected in experimentally-induced strial dysfunction compared with noise-induced hearing loss of similar magnitude. Interestingly, the tip-to-tail ratio was likely the primary factor in temporal coding deficits accompanying the noise-induced hearing loss (Henry et al., 2019). Whereas noise trauma that causes permanent threshold shifts of similar magnitude as in our old gerbils resulted in enhanced temporal ENV coding, and distorted tonotopic coding of TFS and ENV (Kale and Heinz, 2010; Henry et al., 2016), these changes did not occur following experimentally-induced strial dysfunction with similar threshold shifts (Henry et al., 2019). In addition, experimentally-induced synaptopathy has no effect on auditory-nerve-fiber frequency tuning (Furman et al., 2013). Thus, the absence of both tuning deficits and temporal coding deficits are consistent with the typical pathologies in quiet-aged gerbils: strial dysfunction and synaptopathy (Heeringa and Köppl, 2019).

In summary, the single-unit phenotype of our quiet-aged gerbils, with threshold loss but unaltered frequency selectivity, is best explained by age-related strial dysfunction. Synaptopathy was likely present (Gleich et al., 2016) but is expected to affect neither threshold nor tuning measures.

Changes in spontaneous rates likely represent the mixed consequences of strial dysfunction and selective degeneration of fibers

Our study showed that SRs were decreased in both low- and high-frequency ANFs of quiet-aged gerbils and that this decrease was proportional to the extent of age-related hearing loss. A previous study on ANFs in quiet-aged gerbils (36–40 months old) found a reduced proportion of low-SR fibers (Schmiedt et al., 1996; Lang et al., 2010), apparently at odds with our results. However, this change was only significant for high-frequency ANFs (BFs > 6 kHz), with a trend in the opposite direction at lower BFs (Schmiedt et al., 1996). Thus, both studies agree on similar trends of decreased mean SRs at low

BFs in quiet-aged gerbils but found conflicting results for high-BF fibers that are currently unexplained.

ANFs are commonly classified based on their SR because it was shown that SR correlates with other fiber properties, both morphological and physiological, and thus defines two to three ANF types, depending on species (Heil and Peterson, 2015). The SR decrease observed in the present study may in principle be explained either by a specific loss of high-SR fibers or by a general reduction of SR in ANFs, leading to a change in individual fiber typology relative to that in young animals. It has been shown that furosemide-induced and hypoxia-induced EP loss decreases the SR of a unit (Manley and Robertson, 1976; Sewell, 1984b), suggesting a similar mechanism at work with age-related EP loss. In contrast to that, noise- and ouabain-induced synaptopathy is known to specifically target the low-SR fibers, resulting in an increase of mean SR (Furman et al., 2013; Bourien et al., 2014). Furthermore, in mice, spiral ganglion cells with the molecular signature of the likely low-SR type degenerate disproportionately as a function of age (Shrestha et al., 2018).

In summary, synaptopathy may specifically target low-SR fibers, whereas age-related EP loss may decrease the firing rates of remaining ANFs and blur the distinction of ANF types compared with young animals. The relative contributions of these two cochlear pathologies in a given animal, or even in different cochlear regions of the same animal, will then determine the distribution of spontaneous firing rates. Variable individual extents of synaptic loss and strial pathology in quiet-aged gerbils conceivably explain the minor conflicts between studies. Note that it is a common assumption that low-SR ANFs are crucial for signal-in-noise perception and that loss of the low-SR fibers thus results in problems with understanding speech in difficult listening conditions (Bharadwaj et al., 2014; Liberman, 2017). Recent papers have questioned this assumption and the relative importance of low- and high-SR fibers in complex auditory processing tasks is still under debate (Carney, 2018; Huet et al., 2018). Therefore, the consequences of age-related synaptopathy and reductions of intrinsic spontaneous rates in individual ANFs remain largely unknown.

References

Bharadwaj HM, Verhulst S, Shaheen L, Liberman MC, Shinn-Cunningham BG (2014) Cochlear neuropathy and the coding of supra-threshold sound. Front Syst Neurosci 8:26.

Bourien J, Tang Y, Batrel C, Huet A, Lenoir M, Ladrech S, Desmadryl G, Nouvian R, Puel JL, Wang J (2014) Contribution of auditory nerve fibers to compound action potential of the auditory nerve. J Neurophysiol 112:1025–1039.

Canlon B, Illing RB, Walton J (2010) Cell biology and physiology of the aging central auditory pathway. In: The aging auditory system (Gordon-Salant S, Frisina RD, Popper AN, Fay RR, eds), pp 39–74. New York: Springer.

Carney LH (2018) Supra-threshold hearing and fluctuation profiles: implications for sensorineural and hidden hearing loss. J Assoc Res Otolaryngol 19:331–352.

Caspary DM, Milbrandt JC, Helfert RH (1995) Central auditory aging: GABA changes in the inferior colliculus. Exp Gerontol 30:349–360.

Dau T, Wegner O, Mellert V, Kollmeier B (2000) Auditory brainstem responses with optimized chirp signals compensating basilar-membrane dispersion. J Acoust Soc Am 107:1530–1540.

de Boer E, de Jongh HR (1978) On cochlear encoding: potentialities and limitations of the reverse-correlation technique. J Acoust Soc Am 63:115–135.

de Boer R, Kuyper P (1968) Triggered correlation. IEEE Trans Biomed Eng 15:169–179.

FitzGerald JV, Burkitt AN, Clark GM, Paolini AG (2001) Delay analysis in the auditory brainstem of the rat: comparison with click latency. Hear Res 159:85–100.

Fitzgibbons PJ, Gordon-Salant S (1996) Auditory temporal processing in elderly listeners. J Am Acad Audiol 7:183–189.

Furman AC, Kujawa SG, Liberman MC (2013) Noise-induced cochlear neuropathy is selective for fibers with low spontaneous rates. J Neurophysiol 110:577–586.

Gates GA, Mills JH (2005) Presbycusis. Lancet 366:1111–1120.

Gleich O, Hamann I, Klump GM, Kittel M, Strutz J (2003) Boosting GABA improves impaired auditory temporal resolution in the gerbil. Neuroreport 14:1877–1880.

Gleich O, Semmler P, Strutz J (2016) Behavioral auditory thresholds and loss of ribbon synapses at inner hair cells in aged gerbils. Exp Gerontol 84:61–70.

Goldberg JM, Brown PB (1969) Response of binaural neurons of dog superior olivary complex to dichotic tonal stimuli: some physiological mechanisms of sound localization. J Neurophysiol 32:613–636.

Gordon-Salant S, Fitzgibbons PJ, Yeni-Komshian GH (2011) Auditory temporal processing and aging: implications for speech understanding of older people. Audiol Res 1:e4.

Gratton MA, Smyth BJ, Schulte BA, Vincent DA Jr (1995) Na, K-ATPase activity decreases in the cochlear lateral wall of quiet-aged gerbils. Hear Res 83:43–50.

Gurgel RK, Ward PD, Schwartz S, Norton MC, Foster NL, Tschanz JT (2014) Relationship of hearing loss and dementia: a prospective, population-based study. Otol Neurotol 35:775–781.

Heeringa AN, Köppl C (2019) The aging cochlea: towards unraveling the functional contributions of strial dysfunction and synaptopathy. Hear Res 376:111–124.

Heil P, Peterson AJ (2015) Basic response properties of auditory nerve fibers: a review. Cell Tissue Res 361:129–158.

Heil P, Peterson AJ (2017) Spike timing in auditory-nerve fibers during spontaneous activity and phase locking. Synapse 71:5–36.

Heil P, Neubauer H, Irvine DR, Brown M (2007) Spontaneous activity of auditory-nerve fibers: insights into stochastic processes at ribbon synapses. J Neurosci 27:8457–8474.

Heinz MG, Swaminathan J (2009) Quantifying envelope and fine-structure coding in auditory nerve responses to chimaeric speech. JARO 10:407–423.

Hellstrom LI, Schmiedt RA (1991) Rate/level functions of auditory-nerve fibers in young and quiet-aged gerbils. Hear Res 53:217–222.

Henry KS, Kale S, Heinz MG (2016) Distorted tonotopic coding of temporal envelope and fine structure with noise-induced hearing loss. J Neurosci 36:2227–2237.

Henry KS, Sayles M, Hickox AE, Heinz MG (2019) Divergent auditory nerve encoding deficits between two common etiologies of sensorineural hearing loss. J Neurosci 39:6879–6887.

Hopkins K, Moore BC (2007) Moderate cochlear hearing loss leads to a reduced ability to use temporal fine structure information. J Acoust Soc Am 122:1055–1068.

Hopkins K, Moore BC (2011) The effects of age and cochlear hearing loss on temporal fine structure sensitivity, frequency selectivity, and speech reception in noise. J Acoust Soc Am 130:334–349.

Huet A, Batrel C, Tang Y, Desmadryl G, Wang J, Puel JL, Bourien J (2016) Sound coding in the auditory nerve of gerbils. Hear Res 338:32–39.

Huet A, Desmadryl G, Justal T, Nouvian R, Puel JL, Bourien J (2018) The interplay between spike-time and spike-rate modes in the auditory nerve encodes tone-in-noise threshold. J Neurosci 38:5727–5738.

Joris PX (2003) Interaural time sensitivity dominated by cochlea-induced envelope patterns. J Neurosci 23:6345–6350.

Joris PX, Smith PH (2008) The volley theory and the spherical cell puzzle. Neuroscience 154:65–76.

Joris PX, Louage DH, Cardoen L, van der Heijden M (2006) Correlation index: a new metric to quantify temporal coding. Hear Res 216–217:19–30.

Kale S, Heinz MG (2010) Envelope coding in auditory nerve fibers following noise-induced hearing loss. J Assoc Res Otolaryngol 11:657–673.

Keine C, Rübsamen R (2015) Inhibition shapes acoustic responsiveness in spherical bushy cells. J Neurosci 35:8579–8592.

Keithley EM, Ryan AF, Woolf NK (1989) Spiral ganglion cell density in young and old gerbils. Hear Res 38:125–133.

Kujawa SG, Liberman MC (2009) Adding insult to injury: cochlear nerve degeneration after "temporary" noise-induced hearing loss. J Neurosci 29:14077–14085.

Kujawa SG, Liberman MC (2015) Synaptopathy in the noise-exposed and aging cochlea: primary neural degeneration in acquired sensorineural hearing loss. Hear Res 330:191–199.
Lai J, Sommer AL, Bartlett EL (2017) Age-related changes in envelope-following responses at equalized peripheral or central activation. Neurobiol Aging 58:191–200.
Lang H, Jyothi V, Smythe NM, Dubno JR, Schulte BA, Schmiedt RA (2010) Chronic reduction of endocochlear potential reduces auditory nerve activity: further confirmation of an animal model of metabolic presbyacusis. J Assoc Res Otolaryngol 11:419–434.
Liberman MC (2017) Noise-induced and age-related hearing loss: new perspectives and potential therapies. F1000Res 6:927.
Liberman MC, Dodds LW (1984) Single-neuron labeling and chronic cochlear pathology: III. Stereocilia damage and alterations of threshold tuning curves. Hear Res 16:55–74.
Liberman MC, Kujawa SG (2017) Cochlear synaptopathy in acquired sensorineural hearing loss: manifestations and mechanisms. Hear Res 349:138–147.
Lin FR, Thorpe R, Gordon-Salant S, Ferrucci L (2011) Hearing loss prevalence and risk factors among older adults in the united states. J Gerontol A Biol Sci Med Sci 66:582–590.
Louage DH, van der Heijden M, Joris PX (2004) Temporal properties of responses to broadband noise in the auditory nerve. J Neurophysiol 91:2051–2065.
Manley GA, Robertson D (1976) Analysis of spontaneous activity of auditory neurons in spiral ganglion of guinea-pig cochlea. J Physiol 258:323–336.
Mardia KV, Jupp PE (2000) Directional statistics. New York:Wiley.
Muniak MA, Ayeni FE, Ryugo DK (2018) Hidden hearing loss and endbulbs of held: evidence for central pathology before detection of ABR threshold increases. Hear Res 364:104–117.
Overton JA, Recanzone GH (2016) Effects of aging on the response of single neurons to amplitude-modulated noise in primary auditory cortex of rhesus macaque. J Neurophysiol 115:2911–2923.
Ozmeral EJ, Eddins AC, Frisina DR Sr, Eddins DA (2016) Large cross-sectional study of presbycusis reveals rapid progressive decline in auditory temporal acuity. Neurobiol Aging 43:72–78.
Parthasarathy A, Bartlett EL (2011) Age-related auditory deficits in temporal processing in F-344 rats. Neuroscience 192:619–630.
Parthasarathy A, Kujawa SG (2018) Synaptopathy in the aging cochlea: characterizing early-neural deficits in auditory temporal envelope processing. J Neurosci 38:7108–7119.
Plack CJ, Barker D, Prendergast G (2014) Perceptual consequences of "hidden" hearing loss. Trends Hear 18:1–11.
Rabang CF, Parthasarathy A, Venkataraman Y, Fisher ZL, Gardner SM, Bartlett EL (2012) A computational model of inferior colliculus responses to amplitude modulated sounds in young and aged rats. Front Neural Circuits 6:77.
Recio-Spinoso A, Temchin AN, van Dijk P, Fan YH, Ruggero MA (2005) Wiener-kernel analysis of responses to noise of chinchilla auditory-nerve fibers. J Neurophysiol 93:3615–3634.
Rosen S (1992) Temporal information in speech: acoustic, auditory and linguistic aspects. Philos Trans R Soc Lond B Biol Sci 336:367–373.
Ruggero MA, Rich NC (1991) Furosemide alters organ of corti mechanics: evidence for feedback of outer hair cells upon the basilar membrane. J Neurosci 11:1057–1067.
Schatteman TA, Hughes LF, Caspary DM (2008) Aged-related loss of temporal processing: altered responses to amplitude modulated tones in rat dorsal cochlear nucleus. Neuroscience 154:329–337.
Schmiedt RA (1993) Cochlear potentials in quiet-aged gerbils: does the aging cochlea need a jump start? In: Sensory research: multimodal perspectives. (Verrillo RT, ed), pp 91–103. Hillsdale, NJ: Lawrence Erlbaum.
Schmiedt RA (1996) Effects of aging on potassium homeostasis and the endocochlear potential in the gerbil cochlea. Hear Res 102:125–132.
Schmiedt RA, Mills JH, Boettcher FA (1996) Age-related loss of activity of auditory-nerve fibers. J Neurophysiol 76:2799–2803.
Schmiedt RA, Lang H, Okamura HO, Schulte BA (2002) Effects of furosemide applied chronically to the round window: a model of metabolic presbyacusis. J Neurosci 22:9643–9650.
Schuknecht HF, Gacek MR (1993) Cochlear pathology in presbycusis. Ann Otol Rhinol Laryngol 102:1–16.
Schulte BA, Schmiedt RA (1992) Lateral wall na, K-ATPase and endocochlear potentials decline with age in quiet-reared gerbils. Hear Res 61:35–46.
Sergeyenko Y, Lall K, Liberman MC, Kujawa SG (2013) Age-related cochlear synaptopathy: an early-onset contributor to auditory functional decline. J Neurosci 33:13686–13694.
Sewell WF (1984a) The effects of furosemide on the endocochlear potential and auditory-nerve fiber tuning curves in cats. Hear Res 14:305–314.
Sewell WF (1984b) The relation between the endocochlear potential and spontaneous activity in auditory nerve fibres of the cat. J Physiol 347:685–696.
Shaheen LA, Valero MD, Liberman MC (2015) Towards a diagnosis of cochlear neuropathy with envelope following responses. J Assoc Res Otolaryngol 16:727–745.
Shannon RV, Zeng FG, Kamath V, Wygonski J, Ekelid M (1995) Speech recognition with primarily temporal cues. Science 270:303–304.
Shrestha BR, Chia C, Wu L, Kujawa SG, Liberman MC, Goodrich LV (2018) Sensory neuron diversity in the inner ear is shaped by activity. Cell 174:1229–1246.e17.
Strawbridge WJ, Wallhagen MI, Shema SJ, Kaplan GA (2000) Negative consequences of hearing impairment in old age: a longitudinal analysis. Gerontologist 40:320–326.
Swaminathan J, Mason CR, Streeter TM, Best V, Roverud E, Kidd G Jr (2016) Role of binaural temporal fine structure and envelope cues in cocktail-party listening. J Neurosci 36:8250–8257.
Tarnowski BI, Schmiedt RA, Hellstrom LI, Lee FS, Adams JC (1991) Age-related changes in cochleas of Mongolian gerbils. Hear Res 54:123–134.
Versteegh CP, Meenderink SW, van der Heijden M (2011) Response characteristics in the apex of the gerbil cochlea studied through auditory nerve recordings. J Assoc Res Otolaryngol 12:301–316.
Walton JP (2010) Timing is everything: temporal processing deficits in the aged auditory brainstem. Hear Res 264:63–69.
Walton JP, Frisina RD, O'Neill WE (1998) Age-related alteration in processing of temporal sound features in the auditory midbrain of the CBA mouse. J Neurosci 18:2764–2776.
Walton JP, Simon H, Frisina RD (2002) Age-related alterations in the neural coding of envelope periodicities. J Neurophysiol 88:565–578.
Xie R (2016) Transmission of auditory sensory information decreases in rate and temporal precision at the endbulb of held synapse during age-related hearing loss. J Neurophysiol 116:2695–2705.
Xie R, Manis PB (2017) Synaptic transmission at the endbulb of held deteriorates during age-related hearing loss. J Physiol 595:919–934.

Arbeit 3:

European Archives of Oto-Rhino-Laryngology
https://doi.org/10.1007/s00405-024-08699-6

OTOLOGY

The curvature quantification of wave I in auditory brainstem responses detects cochlear synaptopathy in human beings

Florian Herrmann Schmidt[1] · Alexander Dörmann[1] · Karsten Ehrt[1] · Wilma Grossmann[1] · Robert Mlynski[1] · Lichun Zhang[1]

Received: 19 January 2024 / Accepted: 18 April 2024
© The Author(s), under exclusive licence to Springer-Verlag GmbH Germany, part of Springer Nature 2024

Abstract

Purpose Patients with age-related hearing loss complain often about reduced speech perception in adverse listening environment. Studies on animals have suggested that cochlear synaptopathy may be one of the primary mechanisms responsible for this phenomenon. A decreased wave I amplitude in supra-threshold auditory brainstem response (ABR) can diagnose this pathology non-invasively. However, the interpretation of the wave I amplitude in humans remains controversial. Recent studies in mice have established a robust and reliable mathematic algorithm, i.e., curve curvature quantification, for detecting cochlear synaptopathy. This study aimed to determine whether the curve curvature has sufficient test–retest reliability to detect cochlear synaptopathy in aging humans.

Methods Healthy participants were recruited into this prospective study. All subjects underwent an audiogram examination with standard and extended high frequencies ranging from 0.125 to 16 kHz and an ABR with a stimulus of 80 dB nHL click. The peak amplitude, peak latency, curvature at the peak, and the area under the curve of wave I were calculated and analyzed.

Results A total of 80 individuals with normal hearing, aged 18 to 61 years, participated in this study, with a mean age of 26.4 years. Pearson correlation analysis showed a significant negative correlation between curvature and age, as well as between curvature and extended high frequency (EHF) threshold (10–16 kHz). Additionally, the same correlation was observed between age and area as well as age and EHF threshold. The model comparison demonstrated that the curvature at the peak of wave I is the best metric to correlate with EHF threshold.

Conclusion The curvature at the peak of wave I is the most sensitive metric for detecting cochlear synaptopathy in humans and may be applied in routine diagnostics to detect early degenerations of the auditory nerve.

Keywords Age-related hearing loss · Hidden hearing loss · Cochlear synaptopathy · ABR · Curve curvature · Extended high frequency threshold

✉ Lichun Zhang
lichun.zhang@med.uni-rostock.de

Florian Herrmann Schmidt
florian.schmidt@med.uni-rostock.de

Alexander Dörmann
alexander.doermann@uni-rostock.de

Karsten Ehrt
karsten.ehrt@med.uni-rostock.de

Wilma Grossmann
Wilma.grossmann@med.uni-rostock.de

Robert Mlynski
RobertArndt.mlynski@med.uni-rostock.de

[1] Department of Otorhinolaryngology, Head and Neck Surgery, Otto Körner, Rostock University Medical Center, Doberaner Strasse 137-139, 18057 Rostock, Germany

Introduction

Age-related hearing loss is a common sensory disorder among elderly humans [9]. Patients typically report reduced auditory function, which includes a decrease in threshold sensitivity and speech discrimination, especially in the presence of background noise. In the early stages, listeners often experience degraded speech perception in adverse listening environments, but display no clinical threshold shift in their audiogram [45]. This phenomenon, in which the reduced hearing ability hides behind a normal audiogram, was first termed as 'hidden hearing loss' by Schaette and McAlpine [46].

Previous animal studies have suggested that the specific synaptic loss between inner hair cells (IHCs) and spiral

Published online: 04 May 2024

Content courtesy of Springer Nature, terms of use apply. Rights reserved.

ganglion neurons (SGNs) in the cochlea, referred to as cochlear synaptopathy, often occurs prior to sensorineural hearing threshold change and may be a cause for 'hidden hearing loss' [7, 17, 46, 47]. Additionally, physiological data from several animal studies suggests that the auditory nerve (AN consists of different fiber types according to their spontaneous rate (SR, namely high-SR fibers (SR > 18 spikes/s, medium-SR (0.5 < SR < 18 spikes/s, and low-SR ones (SR < 0.5 spikes/s [10, 26]). Low-SR fibers have higher response thresholds, larger dynamic ranges, and greater vulnerability to external events (such as noise, aging, ototoxic drugs and so on) than medium-to-high SR fibers [3, 28, 34]. Therefore, synaptopathy at the low-SR fibers occurs earlier under external influences and results in 'hidden hearing loss' [31]. Likewise, age-related synaptopathy in humans has also been detected through analyzing temporal bones harvested post-mortem. In this human temporal bone study, the authors have applied immunostaining protocol in five temporal bones, harvested within 9-h post-mortem and directly counted the number of the synapses. [53].

To date, although a wide variety of non-invasive metrics have been attempted to detect cochlear synaptopathy in living humans including those based on the auditory brainstem response (ABR), envelope-following response (EFR), and acoustic middle-ear-muscle reflex (MEMR), none of them have been validated as a reliable standard tool [6]. In contrast to the studies on human beings, the most applied metric in animal models is ABR wave I amplitude. The ABR wave I amplitude reflects the summated activities of auditory nerve fibers [35], which significantly decreases in animals with age-related and noise-induced synaptopathy [22, 23, 47, 48]. However, the use of wave I amplitude analysis in humans remains controversial [6]. Some studies report correlations between reduced ABR wave I amplitude and possible auditory nerve (AN) deficits, i.e., synaptopathy during aging [2, 20]. However, other researchers found no significant correlation between them [14, 49]. The primary reason for this discrepancy may be the large variations and very small amplitude of ABR wave I in humans (review in [7]), which are attributable to many factors unrelated to synaptopathy, such as head size, sex, cochlear dispersion, physiological noise and pre-neural dysfunction [43], as well as electrode montage [40].

Recently, Bao et al. [8] employed a novel mathematic method called curvature quantification, which is based on ABR wave I, to detect cochlear synaptopathy in mice. In their study, they compared the curvature with amplitude and latency measurements in a cochlear synaptopathy mouse model and found that this approach yielded robust and reliable results. Mathematically, the curvature quantification measures the degree of deviation of a curve from a straight line by quantifying the change in tangent (T). If a curve has a sharp turn and so T changes rapidly, the curvature value will be large [42]. The shape of ABR wave I depends primarily on the conduction velocity and fiber diameter of the contributing neurons, which vary depending on the fiber type and cochlea location [27]. Thus, it is theoretically possible to detect even minor changes in the AN using the curvature quantification. Furthermore, this method is less affected by background noise than traditional wave peak amplitude analysis. Thus, curvature quantification may also be a suitable metric for detecting cochlear synaptopathy in humans.

In this study, the aim was to first apply the curvature quantification to humans of different ages to evaluate its ability to detect the suspected early degenerative changes in the AN, particularly cochlear synaptopathy. Additionally, the area under the curve from the wave I will be calculated and its potential application in detecting suspected cochlear synaptopathy shall be explored. Finally, all the metrics will be compared with each other to find the best metric, which might be used in the clinic for the future.

Materials and methods

Participants

Recruitment underwent from our university and outpatient during the period from 28.06.2022 to 20.12.2022, which included students, colleagues and also patients that had other complains except ear. All the participants had no previous history of ear issues and did not report any subjective hearing loss. Upon recruitment, each participant underwent a physical examination by an ENT-Consultant at the clinic. Subsequently, all participants underwent audiometric tests in both ears using a clinically calibrated audiometer (AT900, Auritec GmbH Hamburg, Germany). Pure tones were presented at frequencies of 0.125, 0.25, 0.5, 0.75, 1, 2, 3, 4, 6, 8, 10, 11.2, 12.5, 14 and 16 kHz. The stimuli at frequencies ranging from 0.125 to 8 kHz were delivered through DT48 headphones, while the extended high-frequency regions (EHF), i.e.,10, 11.2, 12.5, 14 and 16 kHz, were delivered through HDA200 (Sennheiser, Wedemark-Wennebostel, Germany) circum-aural headphones.

The physical examinations revealed normal eardrums and ear canals upon otoscopy. Additionally, 40 of the young participants (≤ 30 years old) completed the 1-min noise screening questionnaire to assess the impact of noise exposure [19]. All those young probands were classified into a low-risk group (total score ≤ 4) and a high-risk (total score ≥ 5) one [19]. Participants were excluded from the study if their hearing threshold in the test ear exceeded 30 dB HL at any conventional audiometric frequencies between 0.125 and 8 kHz or the average hearing threshold levels at 0.25, 0.5, 1, 2 and

Content courtesy of Springer Nature, terms of use apply. Rights reserved.

4 kHz more than 20 dB HL [4]. The study protocol received approval from our ethical committee (A 2022-0127).

ABR-measurements

ABRs were recorded using the Eclipse ERA-system (Interacoustics A/S, Middelfart, Denmark) at a sampling rate of 30 kHz. Active electrodes (Ambu BlueSensor N, Ambu GmbH, Bad Nauheim, Germany) were placed prefrontal on the midline sagittal plane of the skull (Fpz) and on the mastoid behind the ear where acoustic stimulation was applied. Meanwhile, the ground electrode serving as a reference was positioned on the central forehead. To ensure electrode contact, the skin area was prepared with alcohol and conductive gel, maintaining contact impedance less than 3 kΩ.

A monaural click stimulus was presented at a level of 80 dB nHL through unshielded insert earphones (E-A-RTONE Insert Earphone, 3 M, USA) in rarefaction polarity at a rate of 9.1 s^{-1}. During the recording session, participants were comfortably positioned on an examination bed in a sound isolated room, with their eyes closed and neck and shoulder muscles relaxed.

Online analysis included artifact rejection at 40 µV and digital filtering from 10 to 4000 Hz. A residual noise of smaller than 40 nV was targeted in the average signal, and a minimum of 6000 artifact-free samples were acquired from each ear within a recording window of 0–16 ms relative to stimulus onset. The recording session lasted approximately 15 min. All recorded ABR waveforms were imported into Matlab (Version 2014a, MathWorks, Natick, MA, USA) for additional offline processing. The raw data were filtered using a second-order Butterworth filter, with a low-pass cut-off at 3000 Hz and a high-pass cutoff at 150 Hz, ensuring zero-phase digital filtering.

Peak evaluation: latency and amplitude

The peak latencies were automatically determined by identifying the highest point within each designated time range (Fig. 1A). The ABR wave I was measured in microvolts, calculated as voltage difference between the peak of wave I and preceding onset [13].

Area of wave I

The sampling rate of the ABR wave was increased tenfold by interpolation. To determine the amplitude and latency of the wave peak, the signal's region of interest was set to 1.2-2.1 ms, as this range consistently exhibited a wave I peak in all cases, which were individually double-checked by us. If multiple peaks were found within this range, the peak with the higher amplitude was selected. The onsets and offsets of wave I were determined by identifying the nearest valleys

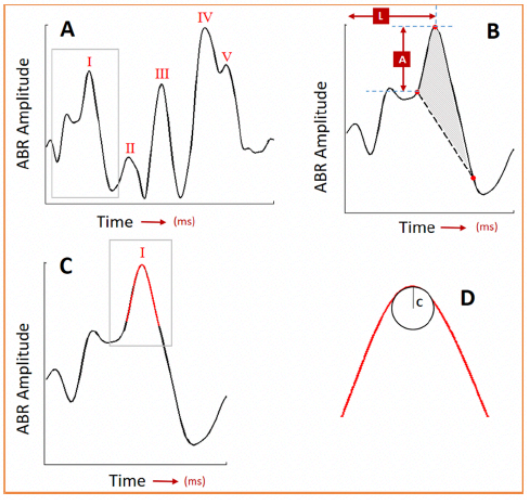


Fig. 1 Examples of quantification of wave I in ABR Recording. **A** ABR recording from one subject, all the waves (I-V) are labeled. The gray square was used to label the wave I. **B** Wave I from the same subject is picked out for the calculation of the amplitude (**A**), peak latency (L) and area under the curve (grey area). **C** Polynominal fit is applied on the same wave I for curvature quantification. **D** Curvature quantification is calculated at the peak of the wave I

prior to and after the peak. Previous studies demonstrated that adjusting the positions of the onsets and offsets at 10% peak amplitude, yields more reliable results [16, 32, 39]. Consequently, the peak amplitude between the valleys and the peak in each case was calculated and 90% of this difference used to determine the positions of the onsets and offsets.

Onset and offset were further used to determine the area under the curve of the signal "y" representing wave I (Fig. 1B). The line "b" connecting these two points defines the lower boundary of the area (Eqs. 1–4).

$$b = a_1 \cdot t + a_2, \text{with} \tag{1}$$

$$b(t_{onset}) = y(t_{onset}) \text{ and} \tag{2}$$

$$b(t_{offset}) = y(t_{offset}) \tag{3}$$

The calculation of the area is done by numerical integration, i.e. the product of the increment Δt with the difference of the signal y and b (Eq. 4).

$$\text{Area} = \sum_{onset}^{offset} \Delta t \cdot (y - b) \tag{4}$$

Content courtesy of Springer Nature, terms of use apply. Rights reserved.

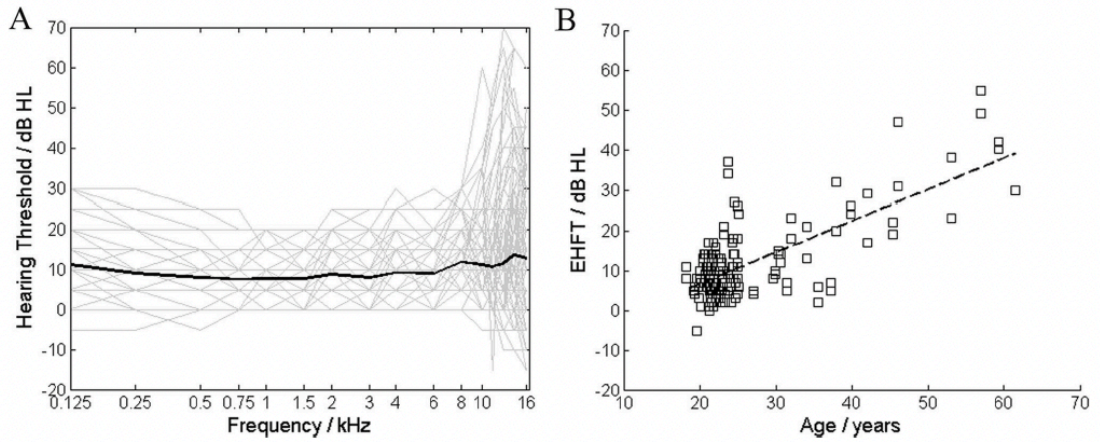


Fig. 2 **A** Hearing thresholds of all the patients (gray color) and the average (black) at the frequency range from 0.125 kHz to 16 kHz, showing the hearing threshold at the normal range from 0.125 to 8 kHz, i.e. no more than 30 dB, however increased up 10 kHz. **B** Scatter plot of average high frequency threshold (from 10 to 16 kHz) versus age from all the ears of the probands. The Pearson correlation analysis showing a positive correlation with R = 0.73

Curvature quantification

The time range of the ABR response was narrowed down to a specific domain where wave I was measured, specifically between 1.2 and 2.1 ms. A 7th order polynomial fit was applied, and the signal was then calculated with a high sampling rate of 10,000 samples per domain, using the determined fit parameters to generate a smooth curve (Fig. 1C, D). The curvature of the polynomial was computed using the following formula (Eq. 5).

$$k = \frac{|x' \cdot y'' - y' \cdot x''|}{\left(x'^2 + y'^2\right)^{3/2}} \quad (5)$$

The curvature value at the time sample corresponding to the peak of wave I was utilized for further analysis.

Analysis

Data analysis was performed using Matlab software (Matlab, version 2014a, Massachusetts: The MathWorks Inc, USA). Pearson correlation was used to determine the relationships between various metrics of ABR wave I (such as curvature quantification, area, peak amplitude, and latencies) and the average EHFT as well as the age of the patients. The Kruskal–Wallis test was applied to compare the prediction error estimates based on Root-Mean-Squares derived from repeated k-folded cross validation (k = 5; repetitions = 500), followed by post-hoc analysis using Dunn test. Additionally, the Kruskal–Wallis test and in case of normal distributed samples (Kolmogorov–Smirnov test) a two-sided t-test were conducted to evaluate the influence of noise exposure and sex on the metrics.

Results

A total of 80 participants, aged from 18 to 61 years old, with a mean of 26.4 years, were initially recruited in this study. Among them, 47 were female and 33 were male. The tone audiograms are presented in Fig. 2A. All ears had normal hearing thresholds, with average hearing threshold levels at 0.25, 0.5, 1, 2, and 4 kHz not exceeding 20 dB HL (British Society of Audiology, 2004), and the hearing threshold at every single frequency ranging from 0.125 to 8 kHz not exceeding 30 dB HL. However, the EHFTs exhibited a notably larger variance, with hearing thresholds reaching up to 70 dB HL.

The correlation between EHFT and age (Fig. 2B) was investigated and a significant positive correlation (R = 0.73, $p < 0.001$) found. The evaluation of the wave I metrics and their correlations with EHFT and age are presented in Figs. 3 and 4, and is summarized in Table 1. Two typical samples demonstrating the correlation between EHFT and wave I metrics are presented in Fig. 5. All metrics showed significant correlations with age and EHFTs, with the highest correlation observed between curvature and age (R = -0.34, p = 0.007) as well as between the curvature and EHFT (R = -0.24, p = 0.002). The metrics were compared

Content courtesy of Springer Nature, terms of use apply. Rights reserved.

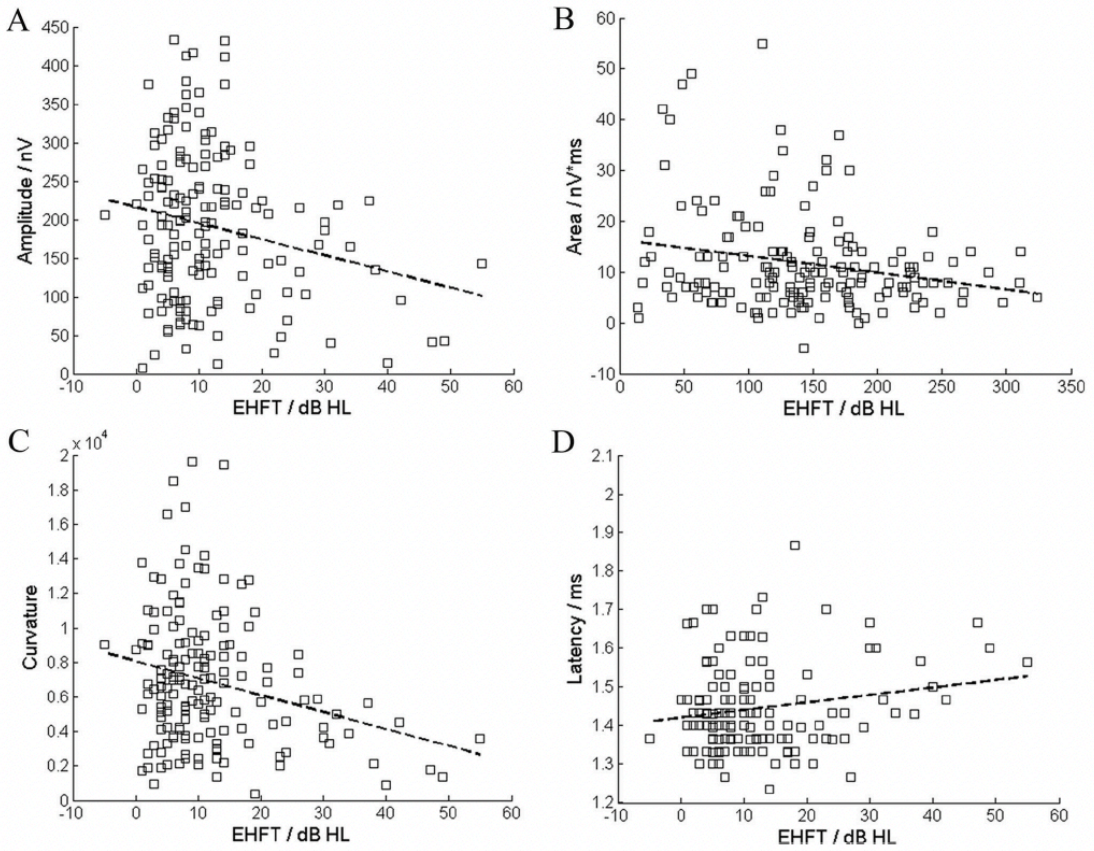


Fig. 3 The Correlation analyses of the amplitude (**A**), area (**B**), curve curvature (**C**) and peak latency (**D**) with EHFT, showing statistical negative correlations between Amplitude and EHFT, between area and EHFT as well as between Curvature and EHFT; and a significant positive correlation between peak latency and EHFT

by examining the Root-Mean-Square-Errors (RMSE) using k-folded cross validation (Fig. 6). The RMSE represents the mean prediction error as the difference of the estimated values from the actual observations. The curvature quantification outperformed the other metrics for both EHFT and age ($RMSE_{curvature,EHFT} = 9.63 \pm 0.10$, $RMSE_{others,\ EHFT} > 9.85 \pm 0.11$;Kruskal–Wallis test: $\chi^2 = 117.37$; post-hoc Dunn test: $p_{curvature,amplitude} = 0.014$, $p_{curvature,area} = 0.083$, $p_{curvature,latency} < 0.001$; Kruskal–Wallis test: $\chi^2 = 105.44$, $p < 0.01$; post-hoc Dunn test: $p_{curvature,amplitude} = 0.022$, $p_{curvature,area} < 0.001$, $p_{curvature,latency} < 0.001$).

Upon further examination of the scatter plots in Fig. 4 wide variations in all metrics of ABR wave I, including amplitude, curvature quantification and area, among the younger probands (< 30 years old) were observed. This suggests the presence of factors other than the aging process that may be related to cochlear synaptopathy. One well-known factor is the noise exposure. To disambiguate this factor, the wave I metrics and EHFTs were compared with the perceived noise exposure from the collected survey but no significant differences were found between the low- and high-risk groups.

Furthermore, the influence of sex as a factor on EHFT in humans and ABR wave I responses was examined. The EHFT between male and female probands were compared and it was found that EHFT was significantly higher in male than in female subjects ($T = -3.8$, $p < 0.001$). Additionally, the amplitude, area, curve curvatures and peak latency between male and female subjects (Fig. 7A-D) was analyzed. Statistically, women exhibited larger amplitude ($T = 4.30$, $p < 0.001$), area ($T = 4.59$, $p < 0.001$) and curve curvature ($T = 3.74$, $p < 0.001$) than men. To further

Content courtesy of Springer Nature, terms of use apply. Rights reserved.

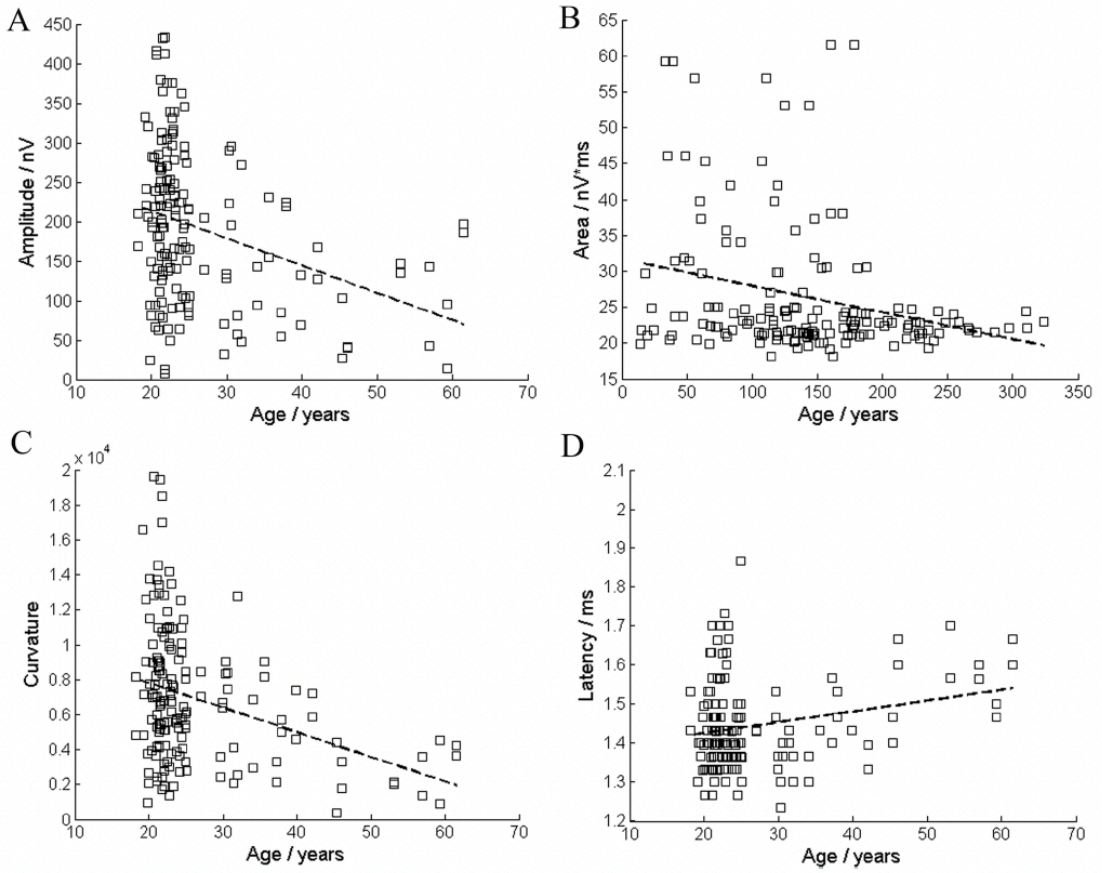


Fig. 4 Correlation analyses of the amplitude (**A**), area (**B**), curve curvature (**C**) and peak latency (**D**) with the age, showing statistical negative correlations between amplitude and age, area and age as well as curvature and age; and a statistical positive correlation between peak latency and age

Table 1 Wave I metrics and their correlations with age and EHFT; (**p < 0.001, *p < 0.01)

	Mean	Standard-deviation	R_{age}	R_{EHFT}
Amplitude	197.3 nV	96.1 nV	−0.30**	−0.21*
Latency	1.44 ms	0.11 ms	0.23*	0.18*
Area	142.7 nV × ms	69.1 nV × ms	−0.27**	−0.23*
Curvature	6908.5 cu	3858.4 cu	−0.34**	−0.25*

isolate the influence of sex on cochlear synaptopathy, focus was set on comparing these metrics in young subjects (< 30 years old). In this subgroup, the EHFT was significantly higher in males than in females (T = −3.32, p = 0.002), and the amplitude (T = 3.2, p = 0.002), curve curvature (T = 3.1, p = 0.003) and area (T = 3.31, p = 0.001) were significantly smaller in males compared to females. In terms of peak Latency, however, there was no significant differences between male and female probands (p = 0.20) even in young age group (< 30 years old) (p = 0.23) (Fig. 7A–D).

Discussion

'Hidden hearing loss', 'Synaptopathy' and EHF thereshold

The term 'hidden hearing loss' refers to hearing deficits that are not detectable by standard pure-tone audiometry (PTA) [46]. In animal models, cochlear synaptopathy has been observed even in the absence of any elevation in hearing

Content courtesy of Springer Nature, terms of use apply. Rights reserved.

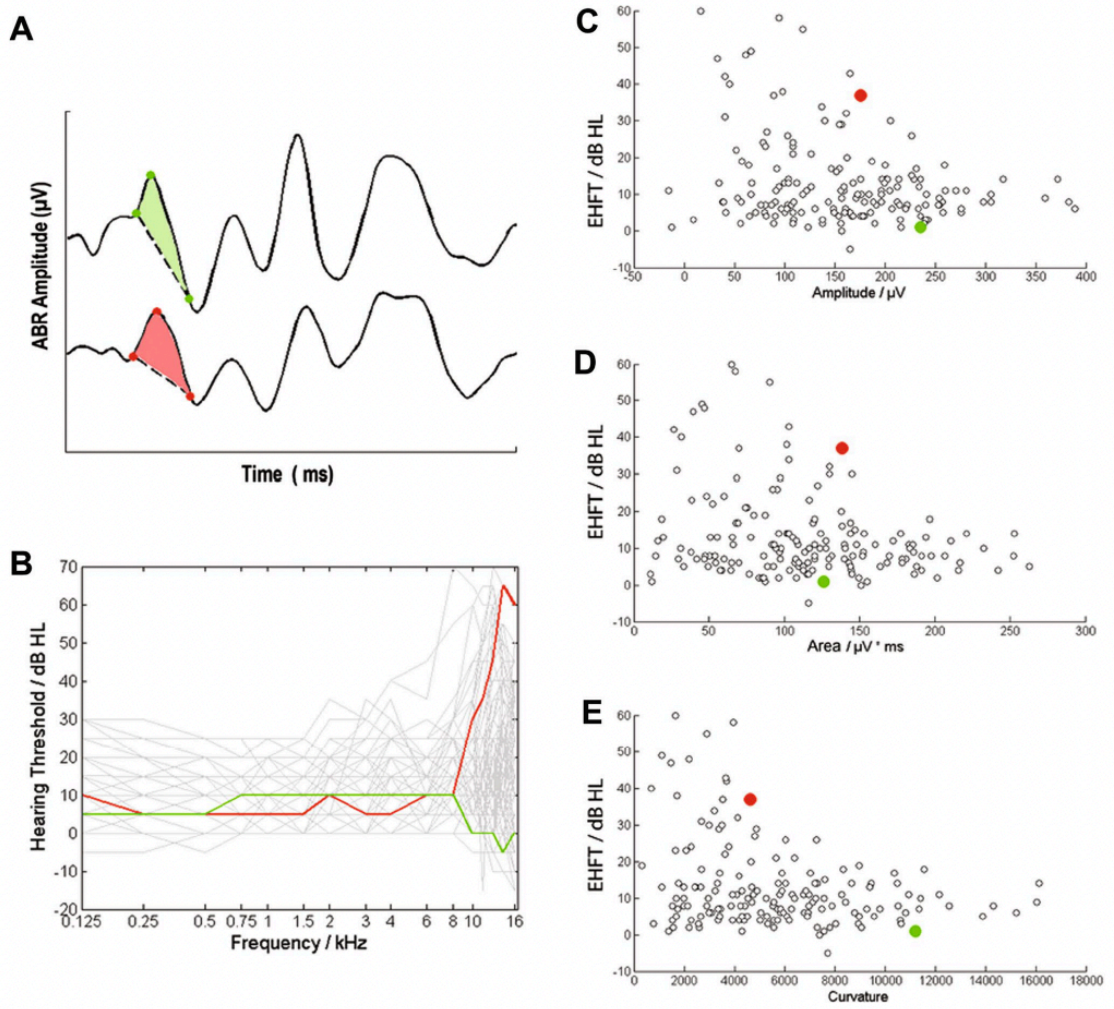


Fig. 5 Examples of two subjects are selected and marked by different colors (Green: low EHFT; Red: high EHFT). **A** ABR waves showing area of the wave I. **B** Hearing thresholds from 0.125 to 16 kHz. **C** Scatter plot of EHFT against amplitude. **D** Scatter plot of EHFT against area. **E** Scatter plot of EHFT against curvature

threshold (i.e., the loss would be sub-clinical in human) (Fernandez et al. 2019, [25]). Histopathological temporal bone studies in humans have also provided direct evidence of cochlear synaptopathy [53]. However, it is unclear whether cochlear synaptopathy is already present in humans with 'hidden hearing loss' (i.e., the young people with normal standard PTA). A direct study of cochlear synaptopathy in a living human is not feasible. Elevated EHF threshold has been shown to be a possible marker for cochlear synaptopathy in a lower frequency region [5, 30]. Direct evidence from some animal studies, including those by Maison et al. [38] and Liberman et al. [29], has shown that synapses in the mid and/or apical parts of the cochlea are more vulnerable than the outer hair cells in the far base [29, 38]. This suggests that the cochlear synaptopathy occurs in the mid and/or apical region as long as the EHF threshold increases. In this study, a significant positive correlation between EHF threshold and age in the individuals with normal standard PTA was found. In another words, the EHF threshold increases significantly as individual age. These results provide further evidence that the elevation of EHF threshold could be used to diagnose cochlear synaptopathy in humans with hidden hearing loss. Therefore, the reduction of EHF threshold as an indicator of cochlear synaptopathy was used for the further analysis.

Content courtesy of Springer Nature, terms of use apply. Rights reserved.

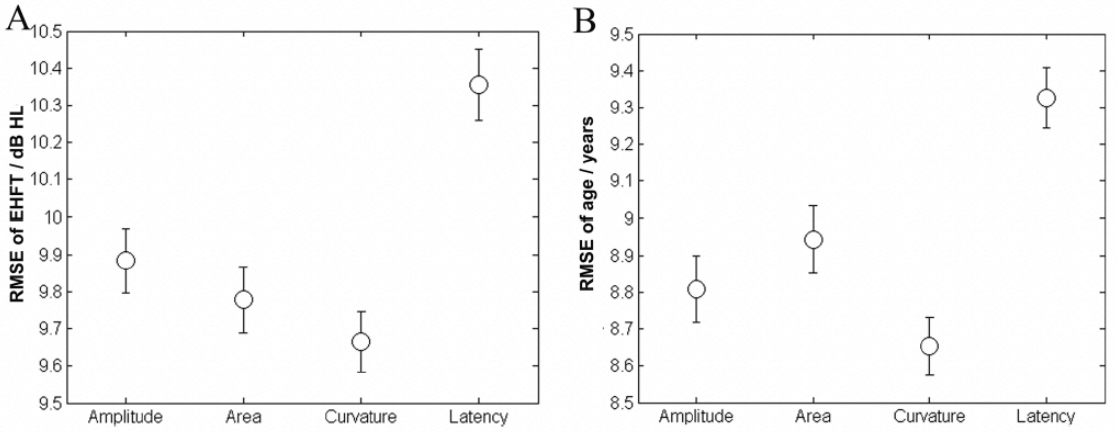


Fig. 6 Comparison of the different parameters from the wave I via repeated k-fold cross validation, showing the curve curvature is the best metric to correlate with EHFT (**A**) and age (**B**)

Different metrics from wave I in ABR: Amplitude, latency, curve curvature and area.

As mentioned in the introduction, ABR wave I is generated by AN fibers and reflects their summed activities [35]. Therefore, all kinds of deficits in AN, including cochlear synaptopathy, should be revealed in ABR wave I. The diagnosis of cochlear synaptopathy requires finding a sensitive and appropriate metric to reveal such pathology. In animal studies, suprathreshold ABR wave I amplitude was associated with synaptopathy in both noise and aging models [10, 11, 33]. However, applying such metrics in humans is inconclusive, partly due to the greater between-subject variability [43]. One potential reason is that the human ABRs are often recorded using surface electrodes instead of subcutaneous electrodes used in animals, which are positioned much closer to the AN [18]. The far-field responses of surface electrodes reduce the signal strength and increase the recording's susceptibility to noise and electrical interference, causing larger variability in peak amplitude [18, 24, 43]. The other factors that affect recording quality might include head size and application of anesthesia [51, 52]. The present wave I results surprisingly detected the assumed cochlear synaptopathy in aging humans. Specifically, there were negative correlations between ABR wave I amplitude and age as well as between wave I amplitude and the EHFT. This may be due to the large samples and recording techniques of this study, which recorded the ABR response at 80 dB HL and repeated at least 6000 time for each recording. Therefore, the variation was dramatically reduced.

The latency of ABR wave I has received less attention in detecting cochlear synaptopathy compared to amplitude. However, Harris et al. [16] suggests that the different latencies of ABR wave I, including onset, offset, peak and wave width, may also have some value in identifying AN deficit. Therefore, the correlation between different latencies, age, and as EHF threshold was investigated to detect cochlear synaptopathy. Unfortunately, no evidence was found that the latencies of ABR wave I could detect cochlear synaptopathy (only the peak latency data in this paper are presented). It can be suspect that current method of determining latencies is not sensitive enough to detect tiny changes in the wave I.

Compared to traditional metrics, curve curvature was proven to be more sensitive and consistent in identifying individual mice with cochlear synaptic loss (Bao et al., 2021). To the best of our knowledge, this is the first and only application of this metric in ABR analysis to date. Therefore, the use of this metric was extended to aging humans. Additionally, the area of wave I was applied for the first time to quantify cochlear synaptopathy. Both metrics were significantly correlated with age and EHFT, which supports the initial assumptions that both metrics could detect cochlear synaptopathy in aging humans. To answer the question of which metric is the best one a model comparison was conducted and it was found that the curve curvature is the most sensitive metric to detect cochlear synaptopathy in aging human, which may be attributed to the following advantages as mentioned by Bao et al. (2021): (1) The curve curvature is less affected by background noise than traditional wave peak amplitude analyses and (2) The curvature is potentially more sensitive to cochlear synaptic loss of low-SR spiral ganglion neurons.

Content courtesy of Springer Nature, terms of use apply. Rights reserved.

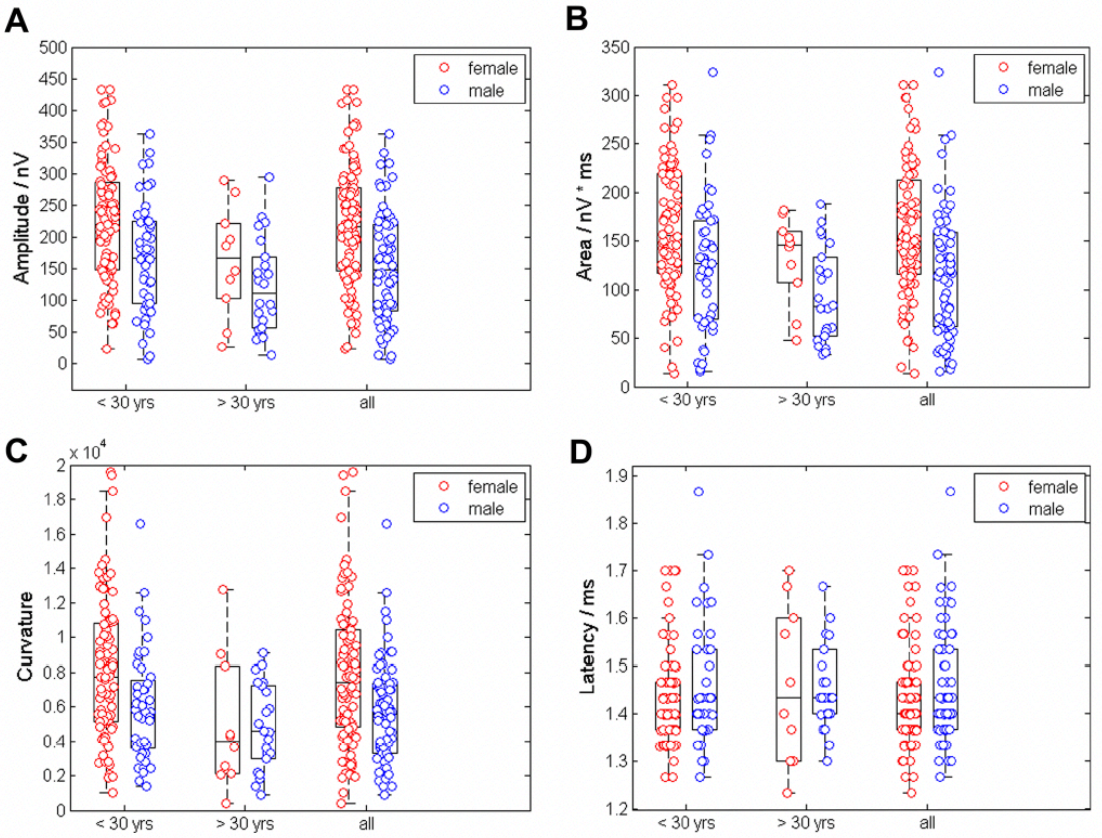


Fig. 7 Box plots, comparing amplitude of wave I (**A**), area of wave I (**B**), curve curvature of wave I (**C**) and peak latency (**D**) in ABR recordings between different sexes both in all participants and in young probands (≤ 30), show female have higher amplitude, higher curvature bigger area than male; however, there is no significant difference between male and femal in term of peak latency

Other unavoidable co-factors affect cochlear synaptopathy during the aging: noise-exposure and sex

Noise exposure has a significant impact on the hearing system in all species, with overexposure leading to synaptopathy and hair cell loss in the animal cochlea. In animal models, noise overexposure initially induces cochlear synaptopathy and then damages the hair cells when the exposure reaches a certain level [12, 21, 31]. However, the current study did not find any significant differences in terms of EHF threshold, ABR wave I amplitude, curve curvature and area. One possible reason for the negative results is the difficulty in reliably estimating lifetime noise exposure [55]. Estimations are largely based on self-report and depend on how noise levels are calculated [15]. The use of a comprehensive questionnaire may improve results and should be explored in the future studies.

Sex-based differences in the hearing system of non-human primates have produced mixed findings [54]. In humans, however, it has been demonstrated that age-related hearing loss occur earlier, more often, and more severely in men [1, 41, 44]. Although these observations have historically been attributed to differential noise exposure, some studies have still shown sex differences even when taking noise exposure history into account [56]. In this study, it was also found that there are sex differences, specifically, that women had higher amplitude of wave I, higher curvature at the peak of wave I and larger area from wave I than men. As suggested by other investigations, it can be assumed that these sex differences in hearing result from hormonal differences between males and females. Specifically, estrogen plays a significant role in both the development of the inner ear and the hearing process [36, 37, 50].

Content courtesy of Springer Nature, terms of use apply. Rights reserved.

Limitation

There is no direct evidence of cochlear synaptopathy in this study. Unfortunately, there is no non-invasive direct method that can be used to detect cochlear synaptopathy in living human beings.

Conclusion

In conclusion all metrics derived from ABR recordings, including wave I amplitude, curvature at the peak of wave I and area of the wave I, might be used clinically to detect cochlear synaptopathy in humans. However, the curvature at the peak of wave I is the most sensitive metric to detect cochlear synaptopathy in humans. This metric could be used in future clinical applications.

Acknowledgements we would like to thank all the participants to take part in the study. We also want to thank the FORUN-Program 2022/2023 (Project-number:889028) from Rostock University Medical Center providing financial support for presenting this work in ARO 2023 in Orlando USA.

Author contributions L.Z. and F.H.S. designed research; A.D., K.E. performed research; F.H.S. and L.Z. analyzed data; L.Z., F.H.S. W.G. and R.M. wrote and corrected the paper.

Data availability The data that support the findings of this study are available from the corresponding author, [LZ], upon reasonable request.

Declarations

Conflict of interest The authors declare no competing interest.

Ethical statement The study protocol received approval from our ethical committee (A 2022-0127).

References

1. Agrawal Y, Platz EA, Niparko JK (2008) Prevalence of hearing loss and differences by demographic characteristics among US adults: data from the national health and nutrition examination survey, 1999–2004. Arch Inten Med 168(14):1522–1530. https://doi.org/10.1001/archinte.168.14.1522
2. Burkard RF, Sims D (2002) A comparison of the effects of broadband masking noise on the auditory brainstem response in young and older adults. Am J Audiol 11(1):12–22. https://doi.org/10.1044/1059-0889(2002/004)
3. Bourien J, Tang Y, Batrel C, Huet A, Lenoir M, Ladrech S, Desmadryl G, Nouvian R, Puel JL, Wang J (2014) Contribution of auditory nerve fibers to compound action potential of the auditory nerve. J Neurophysiol 112:1025–1039. https://doi.org/10.1152/jn.00738.2013
4. British Society of Audiology (2004) Recommended procedure: pure tone air and bone conduction threshold audiometry with and without masking and determination of uncomfortable loudness levels
5. Bharadwaj HM, Mai AR, Simpson JM, Choi I, Heinz MG, Shinn-Cunnigham BG (2019) Non-invasive assays of cochlear synaptopathy-candidates and considerations. Neuroscience 407:53–66. https://doi.org/10.1016/j.neuroscience.2019.02.031
6. Bramhall N, Beach EF, Epp B, Le Prell CG, Lopez-Poveda EA, Plack CJ, Schaette R, Verhulst S, Canlon B (2019) The search for noise-induced cochlear synaptopathy in humans: mission impossible? Hear Res 377:88–103. https://doi.org/10.1016/j.heares.2019.02.016
7. Bramhall NF (2021) Use of the auditory brainstem response for assessment of cochlear synaptopathy in humans. J Acoust Soc Am 150(6):4440. https://doi.org/10.1121/10.0007484
8. Bao J, Jegede SL, Hawks JW, Dade B, Guan Q, Middaugh S, Qiu Z, Levina A, Tsai TH (2022) Detecting cochlear synaptopathy through curvature quantification of the auditory brainstem response. Front Cell Neurosci 16:851500. https://doi.org/10.3389/fncel.2022.851500
9. Ciorba A, Bianchini C, Pelucchi S, Pastore A (2012) The impact of hearing loss on the quality of lie of elderly adults. Clin Interv Aging 7:159–163. https://doi.org/10.2147/CIA.S26059
10. Furman AC, Kujawa SG, Liberman MC (2013) Noise-induced cochlear neuropathy is selective for fibers with low spontaneous rates. J Neurophysiol 110(3):577–586. https://doi.org/10.1152/jn.00164.2013
11. Fernandez KA, Jeffers PWC, Lall K, Liberman MC (2015) Aging after noise exposure: acceleration of cochlear synaptopathy in 'recovered' ears. J Neurosci 35(19):7509–7520. https://doi.org/10.1523/JNEUROSCI.5138-14.2015
12. Fernandez KA, Guo D, Micucci S, Gruttola VD, Liberman MC, Kujawa SG (2020) Noise-induced cochlear synaptopathy with and without sensory cell loss. Neuroscience 427:43–57. https://doi.org/10.1016/j.neuroscience.2019.11.051
13. Gu JW, Herrmann BS, Levine RA, Melcher JR (2012) Brainstem auditory evoked potentials suggest a role for the ventral cochlear nucleus in tinnitus. J Assoc Res Otolaryngol 13(6):819–833. https://doi.org/10.1007/s10162-012-0344-1
14. Grinn SK, Wisemann KB, Baker JA, Le Prell CG (2017) Hidden Hearing loss? No effect of commen recreational noise exposure on cochlear nerve response amplitude in humans. Front Neurosci 11:465. https://doi.org/10.3389/fnins.2017.00465
15. Guest H, Munro KJ, Prendergast G, Millman RE, Plack CJ (2018) Impaired speech perception in noise with a normal audiogram: no evidence for cochlear synaptopahty and no relation to lifetime noise exposure. Hear Res 364:142–151. https://doi.org/10.1016/j.heares.2018.03.008
16. Harris KC, Vaden KI Jr, McClaskey CM, Dias JW, Dubno JR (2018) Complementary metrics of human auditory nerve function derived from compound action potentials. J Neurophysiol 119(3):1019–1028. https://doi.org/10.1152/jn.00638.2017
17. Harris KC, Ahlstrom JB, Dias JW, Kerouac LB, McClaskey CM, Dubno JR, Eckert MA (2021) Neural presbyacusis in humans inferred from aged-related differences in auditory nerve function and structure. J Neurosci 41(50):10293–10304. https://doi.org/10.1523/JNEUROSCI.1747-21.2021
18. Harris KC, Bao J (2022) Optimizing non-invasive functional markers for cochlear deafferentation based on electrocochleography and auditory brainstem responses. J Acoust Soc Am 151(4):2802. https://doi.org/10.1121/10.0010317
19. Johnson TA, Cooper S, Stamper GC, Chertoff M (2017) Noise exposure questionnaire: a tool for quantifying annual noise exposure. J Am Acad Audiol 28(1):14–35. https://doi.org/10.3766/jaaa.15070
20. Johannesen PT, Buzo BC, Lopez-Poveda EA (2019) Evidence for aged-related cochlear synaptopathy in humans unconnected

Content courtesy of Springer Nature, terms of use apply. Rights reserved.

to speech-in-noise intelligibility deficits. Hear Res 374:35–48. https://doi.org/10.1016/j.heares.2019.01.017
21. Kobel M, Le Prell CG, Liu J, Hawks JW, Bao J (2017) Noise-induced cochlear synaptopathy: past findings and future studies. Hear Res 349:148–154. https://doi.org/10.1016/j.heares.2016.12.008
22. Kujawa SG, Libermann MC (2009) Adding insult to injury: cochlear nerve degeneration after 'temporary' noise-induced hearing loss. J Neurosci 29(45):14077–14085. https://doi.org/10.1523/JNEUROSCI.2845-09.2009
23. Kujawa SG, Liberman MC (2015) Synaptopathy in the noise-exposed and aging cochlea: primary neural degeneration in acquired sensorineural hearing loss. Hear Res 330(Pt B):191–199. https://doi.org/10.1016/j.heares.2015.02.009
24. Kujawa SG, Liberman MC (2019) Translating animal models to human therapeutics in noise-induced and age-related hearing loss. Hear Res 377:44–52. https://doi.org/10.1016/j.heares.2019.03.003
25. Kohrman DC, Wan G, Cassinotti L, Corfas G (2020) Hidden hearing loss: a disorder with multiple etiologies and mechanisms. Cold Spring Harb Persepect Med 10(1):a035493. https://doi.org/10.1101/cshperspect.a035493
26. Libermann MC (1982) The cochlear frequency map for the cat: labeling auditory-nerve fibers of known characteristic frequency. J Acoust Soc Am 72(5):1441–1449. https://doi.org/10.1121/1.388677
27. Liberman MC (1982) Single-neuron labeling in the cat auditory nerve. Science 216:1239–1241. https://doi.org/10.1126/science.7079757
28. Liberman MC (1988) Physiology of cochlear efferent and afferent neurons: direct comparisons in the same animal. Hear Res 34:179–192. https://doi.org/10.1016/0378-5955(88)90105-0
29. Liberman MC, Liberman LD, Maison SF (2014) Effect feedback slows cochlear aging. J Neurosci 34(13):4599–4607. https://doi.org/10.1523/JNEUROSCI.4923-13.2014
30. Liberman MC, Epstein MJ, Cleveland SS, Wang H, Maison SF (2016) Toward a differential diagnosis of hidden hearing loss in humans. PLoS ONE 11(9):e0162726. https://doi.org/10.1371/journal.pone.0162726
31. Liberman MC, Kujawa SG (2017) Cochlear synaptopathy in acquired sensorineural hearing loss: manifestations and mechanisms. Hear Res 349:138–147. https://doi.org/10.1016/j.heares.2017.01.003
32. Luck SJ (2014) An introduction to the event-related potential technique, Second Edition. Cambridge, Massachusetts, MIT Press
33. Lobarinas E, Spankovich C, Le Prell GC (2017) Evidence of , hidden hearing loss' following noise exposures that produce robust TTS and ABR wave-I amplitude reductions. Hear Res 349:155–163. https://doi.org/10.1016/j.heares.2016.12.009
34. Merchan-Perez A, Liberman MC (1996) Ultrastructural differences among afferent synapses on cochlear hair cells: correlations with spontaneous discharge rate. J Comp Neurol 371:208–221. https://doi.org/10.1002/(SICI)1096-9861(19960722)371:2%3c208::AIDF-CNE2%3e3.0.CO;2-6
35. Melcher JR, Kiang NY (1996) Generators of the brainstem auditory evoked potential in cat. III: identified cell populations. Hear Res 93(1–2):52–71. https://doi.org/10.1016/0378-5955(95)00200-6
36. Motohashi R, Takumida M, Shimizu A, Konomi J, Fujita K, Hirakawa K, Suzuki M, Anniko M (2010) Effects of age and sex on the expression of estrogen receptor alpha and beta in the mouse inner ear. Acta Otolaryngol 130(2):204–214. https://doi.org/10.3109/00016480903016570
37. Marano RJ, Tickner J, Redmond SL (2013) Prolactin expression in the cochlea of aged BALB/c mice is gender biased and correlates to loss of bone mineral density and hearing loss. PLoS ONE 8(5):e63952. https://doi.org/10.1371/journal.pone.0063952
38. Maison SF, Usubuchi H, Liberman MC (2013) Efferent feedback minimizes cochlear neuropathy from moderate noise exposure. J Neurosci 33(13):5542–5552. https://doi.org/10.1523/JNEUROSCI.5027-12.2013
39. McClaskey CM, Panganiban CH, Noble KV, Dias JW, Lang H, Harris KC (2020) A multi-metric approach to characterizing mouse peripheral audiotry nerve fuction using the auditory brainstem response. J Neurosci Methods 346:108937
40. McFarlane KA, Sanchez JT (2023) Exploring electrode placements to optimize the identification and measurement of early auditory evoked potentials. Audio Res 13(6):978–988. https://doi.org/10.3390/audiolres13060085
41. Nolan LS (2020) Age-related hearing loss: why we need to think about sex as a biological variable. J Neurosci Res 98(9):1705–1720
42. Osborne J.M., Cook W., Bossé M.J., 2019. Quantifying the curvature of curves: an intuitive introduction to differential geometry. PRIMUS. 0(0): 1–21. Doi: https://doi.org/10.1080/10511970.2019.1636432.
43. Plack CJ, Leger A, Prendergast G, Kluk K, Guest H, Munro KJ (2016) Toward a diagnostic test for hidden hearing loss. Trends Hear. https://doi.org/10.1177/2331216516657466
44. Park C, Kim SJ, Lee WK, Moon SK, Kwak S, Choe SK, Park R (2016) Tetrabromobisphenol-A induces apoptotic death of auditory cells and hearing loss. Biochem Biophys Res Commun 478(4):1667–1673. https://doi.org/10.1016/j.bbrc.2016.09.001
45. Starr A, Sininger YS, Pratt H (2000) The varieties of auditory neuropathy. J Basic Clin Physiol Pharmacol 11:215–230. https://doi.org/10.1515/jbcpp.2000.11.2.215
46. Schaette R, McAlpine D (2011) Tinnitus with a normal audiogram: physiological evidence for hidden hearing loss and computational model. J Neurosci Off J Soc Nurosci 31:13452–13457. https://doi.org/10.1523/JNEUROSCI.2156-11.2011
47. Sergeyenko Y, Lall K, Liberman MC, Kujawa SG (2013) Age-related cochlear synaptopathy: an early-onset contributor to auditory functional decline. J Neurosci 33(34):13686–13694. https://doi.org/10.1523/JNEUROSCI.1783-13.2013
48. Shaheen LA, Valero MD, Liberman MC (2015) Towards a diagnosis of cochlear neuropathy with envelope following responses. J Assoc Res Otolaryngol 16(6):727–745. https://doi.org/10.1007/s10162-015-0539-3
49. Spankovich C, Le Prell CG, Lobarinas E, Hood LJ (2017) Noise history and auditory function in young adults with and without type 1 diabetes mellitus. Ear Hear 38(6):724–735. https://doi.org/10.1097/AUD.0000000000000457
50. Shuster BZ, Depireux DA, Mong JA, Hertzano R (2019) Sex differences in hearing: Probing the role of estrogen signaling. J Acoust Soc Am 145(6):3656. https://doi.org/10.1121/1.5111870
51. Trune DR, Mitchell C, Phillips DS (1988) The relative importance of head size, gender and age on the auditory brainstem response. Hear Res 32(2–3):165–174. https://doi.org/10.1016/0378-5955(88)90088-3
52. van Looji MAJ, Liem S, van der Burg H, van der Wees J, De Zeeuw CI, van Zanten BGA (2004) Impact of conventional anesthesia on auditory brainstem responses in mice. Hear Res 193(1–2):75–82. https://doi.org/10.1016/j.heares.2004.02.009
53. Viana LM, O'Malley JT, Burgess BJ, Jones DD, Oliveria CA, Santos F, Merchant SN, Liberman LD, Liberman MC (2015) Cochlear neuropathy in human presbycusis: Confocal analysis of hidden hearing loss in post-mortem tissue. Hear Res 327:78–88. https://doi.org/10.1016/j.heares.2015.04.014
54. Villavisanis DF, Berson ER, Lauer AM, Cosetti MK, Schrode KM (2020) Sex-based differences in hearing loss: perspectives from non-clinical research to clinical outcomes. Oto Neurotol 41(3):290–298. https://doi.org/10.1097/MAO.0000000000002507

Content courtesy of Springer Nature, terms of use apply. Rights reserved.

55. Wei W, Heinze S, Gerstner DG, Walser SM, Twardella D, Reiter C, Weilnhammer V, Perez-Alvarez C, Steffens T, Herr EWC (2017) Audiometric notch and extended high-frequency hearing threhold shift in relation to total leisure noise exposure: an exploratory analysis. Noise Health. 19(91):263–269. https://doi.org/10.4103/nah.NAH_28_17
56. Wang Q, Wang X, Yang L, Han K, Huang Z, Wu H (2021) Sex differences in noise-induced hearing loss: a cross-sectional study in China. Biol Sex Differ 12(1):24. https://doi.org/10.1186/s13293-021-00369-0

Publisher's Note Springer Nature remains neutral with regard to jurisdictional claims in published maps and institutional affiliations.

Springer Nature or its licensor (e.g. a society or other partner) holds exclusive rights to this article under a publishing agreement with the author(s) or other rightsholder(s); author self-archiving of the accepted manuscript version of this article is solely governed by the terms of such publishing agreement and applicable law.

Content courtesy of Springer Nature, terms of use apply. Rights reserved.

Arbeit 4:

audiology research

MDPI

Article

Can Mismatch Negativity Be Used as an Indicator to Predict Central Auditory Deficits in Individuals with Normal Hearing?

Lichun Zhang *, David Mißler, Karsten Ehrt, Wilma Großmann, Robert Mlynski and Florian Herrmann Schmidt

Department of Otorhinolaryngology, Head and Neck Surgery, 'Otto Körner', Rostock University Medical Center, Doberaner Straße 137–139, D-18507 Rostock, Germany; david.missler@uni-rostock.de (D.M.); karsten.ehrt@med.uni-rostock.de (K.E.); wilma.grossmann@med.uni-rostock.de (W.G.); robert.mlynski@med.uni-rostock.de (R.M.); florian.schmidt@med.uni-rostock.de (F.H.S.)
* Correspondence: lichun.zhang@med.uni-rostock.de; Tel.: +49-381-494-8372

Abstract: Background/Objectives: In the early stage of presbycusis, patients experience reduced speech perception in noisy environments despite normal audiometry, normally known as hidden hearing loss. Diagnostic indicators like the reduced amplitude of ABR wave I, elevated extended high-frequency threshold (EHT), and decreased middle ear muscle reflex (MEMR) amplitude aim to identify biomarkers of peripheral auditory pathology but remain inconsistent. Mismatch negativity (MMN) is a cortical auditory evoked potential generated when the brain detects sound changes. This study aimed to assess MMN as a diagnostic tool for hidden hearing loss in adults. **Methods**: Seventy-three subjects with normal hearing underwent an extended pure-tone audiogram examination ranging from 0.125 to 16 kHz and a subsequent MMN assessment with two different paradigms: a speech (ba/da) and a tone (1/2 kHz) paradigm. The MMN's amplitude and latency were measured and analyzed. **Results**: The outcome shows a significant age-related effect on MMN amplitude in the speech condition ($\chi^2 = 13.0$, $p = 0.002$). Specifically, the MMN amplitude in the 25–30-year-old group was significantly smaller than in the 20–25-year-old group ($p = 0.0015$, Cohen's d = 0.63). Additionally, no further effects of age were observed on the cortical potentials examined. Also, neither tone nor speech paradigms showed a significant influence of EHT on the amplitude or latency of either MMN or P300. **Conclusions**: The application of MMN as an electrophysiological tool to diagnose hidden hearing loss in normal hearing adults has limitations. However, in contrast to MMN responses to tonal stimuli, the present study reveals that MMN amplitude obtained with speech stimuli may indicate early signs of central auditory deficits.

Keywords: cochlear synaptopathy; mismatch negativity; age related hearing loss; presbyacusis

check for updates

Academic Editor: Andy J. Beynon

Received: 12 February 2025
Revised: 9 April 2025
Accepted: 14 April 2025
Published: 16 April 2025

Citation: Zhang, L.; Mißler, D.; Ehrt, K.; Großmann, W.; Mlynski, R.; Schmidt, F.H. Can Mismatch Negativity Be Used as an Indicator to Predict Central Auditory Deficits in Individuals with Normal Hearing? *Audiol. Res.* **2025**, *15*, 43. https://doi.org/10.3390/audiolres15020043

Copyright: © 2025 by the authors. Licensee MDPI, Basel, Switzerland. This article is an open access article distributed under the terms and conditions of the Creative Commons Attribution (CC BY) license (https://creativecommons.org/licenses/by/4.0/).

1. Introduction

Age-related hearing loss (ARHL), also known as presbycusis, is the most common sensory deficit affecting adults, which increases with age and can reach a prevalence of 84.3% among people over 80 years old [1,2]. The estimated prevalence is that more than 500 million individuals over 60 will be affected by 2025 [3]. Typical patients exhibit progressive, irreversible sensorineural hearing loss that deteriorates with age, mainly involving the high-frequency range and gradually spreading to the low-frequency range [4]. ARHL affects not only the cochlear structures but also the central nervous system, leading to a reduced ability to process auditory information [5].

Recent studies predominantly focused on the early stage of ARHL and its potential mechanisms [6–8]. At this stage, patients mainly experience difficulties in speech percep-

tion, especially in challenging listening situations like environments with background noise. A typical example is the "cocktail party phenomenon". This issue often goes unnoticed in routine clinical practice because standard hearing tests fail to detect changes in hearing thresholds in such cases. Consequently, Schaette and McAlpine (2011) referred to this condition as "hidden hearing loss" [9]. Animal studies suggest that cochlear synaptopathy may be the primary pathological mechanism underlying hidden hearing loss [10,11]. In these studies, a reduction in wave I amplitude has been proven to be a useful diagnostic marker [10,12–14]. However, in humans, ABR wave I is typically small and highly variable, limiting its diagnostic value for cochlear synaptopathy [15]. As a result, several alternative diagnostic metrics have been developed and studied, such as envelop-following response (EFR), acoustic middle ear muscle reflex (MEMR), and ABR wave I curvature [15–18]. Additionally, Electrocochleography (ECochG) has been explored using the ratio of summation potential (SP) to action potential (AP), as well as the amplitude of cochlear microphonics (CM) [19–22]. Extended high-frequency threshold (EHT) measurements have also been investigated [16,18]. Among these metrics, EHT is considered a highly sensitive biomarker for detecting early changes in the peripheral auditory pathway and may serve as an indirect indicator of cochlear synaptopathy [16,18]. Animal studies have shown that cochlear synapses in the mid and apical regions are more vulnerable than the outer hair cells (OHCs) in the far base [23,24]. Therefore, an increase in EHT may indicate cochlear synaptopathy occurring at least in the mid and/or apical region. Additionally, EHT can easily be performed in a clinical setting and is both faster and easier to analyze compared to the aforementioned measurements [18]. Therefore, this study aims to use EHT as a marker of the earliest changes in the peripheral auditory pathway.

How does the central nervous system change at the early stage of ARHL? Pathological changes in the peripheral auditory pathway lead to reduced signal input to the central nervous system, causing compensatory downregulation of inhibitory processing. This mechanism is known as central gain. While central gain can restore perception of sounds in quiet environments, it cannot recover the processing of temporal details [25]. Previous studies proved that the consequences of central gain extend beyond merely increasing central responses and may also contribute to tinnitus and/or hyperacusis [26–29]. All this evidence highlights that sensory deficits, specifically pathological changes in the peripheral auditory pathway, have complex effects that extend beyond central gain alone [30]. Currently, there is no clear understanding of the mechanisms by which central gain influences target sound processing in background noise.

Mismatch negativity (MMN), the cognitive component of the auditory evoked brain response, is a late latency response that provides an objective and non-invasive electrophysiological measure of cortical potential that reflects the brain's automatic detection of stimulus differences [31–33]. MMN represents the capability of auditory discrimination and provides reliable results in evaluating the central auditory system. MMN is recorded using an oddball paradigm, in which a deviant or rare stimulus is presented within a series of homogenous or standard stimuli [31,34]. This study aims to record MMN responses using different types of stimuli across various age groups to investigate how these responses change with age, especially in the early stage of ARHL. Additionally, it examines how potential peripheral cochlear synaptopathy affects central auditory processing by analyzing the correlation between MMN and EHT. This approach may offer more reliable and objective diagnostic metrics for hidden hearing loss in the future.

2. Materials and Methods

The local ethics committee approved this prospective study (A 2023-0010). Written information was provided to the participants of the study group, and their consent was given. All personal data were anonymized and de-identified prior to the analysis.

2.1. Subjects

This prospective study included adults with normal hearing. Recruitment took place at the local university from January to June 2023 and involved students and staff members. All participants were young and healthy, without a medical history or regular medication use. In particular, none of the participants had a history of ear problems or reported subjective hearing loss. Additionally, we inquired about their history of noise exposure by asking them to recall significant experiences from their lives. Upon recruitment, each participant underwent a physical examination by an ENT consultant. After that, all participants underwent audiometric tests by qualified personnel in both ears using a clinically calibrated audiometer (AT900, Auritec GmbH, Hamburg, Germany). Pure-tone stimuli were presented at frequencies of 0.125 to 16 kHz. Frequencies from 0.125 to 8 kHz were presented by DT48 headphones, while extended high-frequency regions (10, 11.2, 12.5, 14, and 16 kHz) were presented by HDA200 circum-aural headphones (Sennheiser, Wedemark-Wennebostel, Germany). Otoscopy revealed that all participants had normal eardrums and ear canals. Participants were excluded from the study if their hearing threshold exceeded 30 dB HL at any conventional frequencies between 0.125 and 8 kHz or if their average hearing threshold at 0.25, 0.5, 1, 2, and 4 kHz exceeded 20 dB HL [35]. Furthermore, we excluded ears that did not exhibit a measurable MMN response in at least one of the two measurement paradigms.

2.2. Stimulation and Recording

Two MMN experiments were carried out: one based on a tone paradigm and another on a speech paradigm. In the tone paradigm, 100 ms tone pulses were used, featuring a 40 ms plateau and 30 ms onset and offset. The standard stimulus was a 1 kHz tone pulse. The deviant stimulus was a 2 kHz tone pulse. The stimuli and the measurement procedure are part of the standard repertoire of the ERA system. In the speech paradigm, the syllables b'a' and d'a' were used to trigger an MMN. The b'a' stimulus, used as the standard, had a duration of 150 ms at a sample rate of 30 kHz. Conversely, the deviant, represented by the d'a' stimulus, also operated at a sample rate of 30 kHz but with a duration of 40 ms. The probability of the deviant stimulus was 16%. All stimuli were presented monaurally at a level of 70 dB nHL for each ear in randomized order. The stimuli were presented through earphones calibrated for unshielded insert by a technician from Diatec Diagnostics GmbH, the company responsible for the regular clinical maintenance of the ERA system. The stimuli were presented in identical conditions using insert earphones (E-A-RTONE Insert Earphone, 3M, USA).

The electrophysiological measurements were performed using the Eclipse ERA-system (Interacoustics A/S, Middelfart, Denmark) at a sampling rate of 500 Hz. AgCl electrodes (Ambu BlueSensor N, Ambu GmbH, Bad Nauheim, Germany) were placed prefrontally on the midline sagittal plane of the skull (Fpz) and on the ipsilateral mastoids (TP9 or TP10), and the ground electrode was positioned on the central forehead. To ensure electrode contact, the skin area was prepared with alcohol and conductive gel, maintaining a contact impedance of less than 3 kΩ. During the recording session, participants lay on an examination bed in a sound-isolated room (GTA < 40). They were instructed to minimize blinking as much as possible, to fixate their eyes on a cross positioned on the opposite wall, and to keep their neck and shoulder muscles relaxed.

2.3. Data Processing and Analysis

The online analysis included digital filtering from 1 to 33 Hz. The oddball paradigm involved presenting a sequence of standard and deviant stimuli. On average, there were 336 trials for the standard stimulus and 64 trials for the deviant stimulus, corresponding to probabilities of 84% and 16%, respectively. The cortical responses were recorded within a recording window of −85 to 850 ms relative to stimulus onset. The recording session lasted approximately 20 min. All recorded data were imported into MATLAB (Version 2014a, Massachusetts: The MathWorks Inc., Natick, MA, USA) for additional offline processing. The samples of the raw data were excluded if they exceeded an artifact threshold of 30 µV to minimize eye artifacts. Afterward, the data were filtered using a second-order butter worth filter design, with a low-pass cutoff at 25 Hz and a high-pass cutoff at 1 Hz, ensuring zero-phase digital filtering. The baseline was adjusted by subtracting the mean EEG response before stimulus onset, sample by sample. The samples were averaged using an iterated weighted averaging procedure [36] with two iterations. This procedure provided weights for each epoch according to its estimated amount of noise contamination.

Our study investigates the differences in amplitudes and latencies of the cortical components MMN and P300. We established appropriate time windows for analyzing these potentials based on grand averages. These windows were both physiologically relevant and consistent with the latencies of both potentials in the literature. The time windows were set at 70 to 180 ms for MMN and 300 to 500 ms for P300.

To measure the amplitude of the potentials, the average amplitude was calculated within a time window that covered the critical duration of each potential. Within these windows, the peak of the potential was centered and the boundaries defined where the amplitude decreased to half its peak relative to both the peak and the baseline. This approach allowed us to represent the potential's amplitude as the mean amplitude within this specified window (Figure 1).

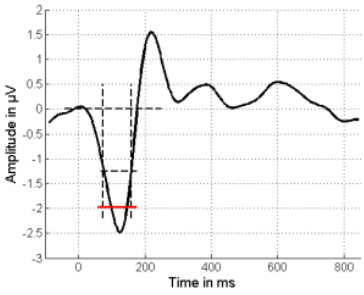


Figure 1. Measurement of the amplitude of the potentials. Long horizontal dashed line: baseline; short horizontal dashed line: 50% amplitude between peak and baseline; vertical dashed lines: time window of the critical duration, defined by the 50% amplitude values of the rising and the falling slope; red line: average amplitude across the critical time window.

Pearson correlation was performed on the electrophysiological measures, ears, age, and the mean EHT. To further investigate the effects of age and EHT, participants were divided into subgroups based on these factors for better comparison. For analyzing the impact of age, we used five-year increments, resulting in the following three groups: (1) 20–25 years old, (2) 25–30 years old, and (3) 30–35 years old. Similar, participants were grouped based on EHT into the following categories: (1) EHT < 0 dB HL, (2) 0 dB HL $\leq$ EHT $\leq$ 15 dB HL, and (3) EHT > 15 dB HL. The 'Grand Average', calculated as the arithmetic mean, was used to represent the overall EEG response across all measurements,

reflecting total neural activity. The median was not used due to potential discontinuities in the temporal signal. However, for statistical analysis, non-parametric tests were employed, as the assumption of a normal distribution of the samples cannot be reliably verified. The Kruskal–Wallis Test was used to compare the amplitudes and latencies of the cortical components across these groups. For further analysis after the initial tests, the Dunn test was applied in the post-hoc phase.

3. Results

A total of seventy-three participants with normal hearing status were recruited in this study: 33 females and 40 males, with an average age of 25.8 ± 3.6 years, ranging from 21 to 35 years old. All 146 ears had normal hearing thresholds, with average hearing thresholds levels at 0.25, 0.5, 1, 2, and 4 kHz recorded at 5.5 ± 3.8 dB HL (Figure 2A). The hearing threshold at frequencies ranging from 0.125 to 8 kHz did not exceed 30 dB HL and was recorded at 6.1 ± 3.5 dB HL. Fourteen ears were excluded from further analysis because they did not show a measurable MMN response in at least one of the two stimulation paradigms (among them are four ears from two female participants, while the remaining ten excluded ears comprised four right ears and six left ears from ten different participants).

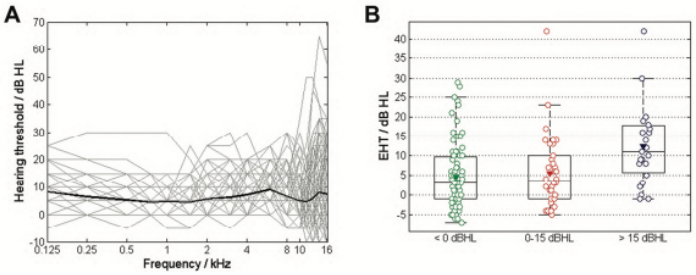


Figure 2. The hearing thresholds from 0.125 to 16 kHz for all participants are shown as gray lines, with the average threshold presented by a dark line (**A**). The boxplot (**B**) illustrates the average hearing threshold in the extended high-frequency range (EHT), categorized into three age groups: 20–25 years, 25–30 years, and 30–35 years. The mean values are indicated by triangles.

3.1. Age and EHT

In the selected ears, the average EHT at 10, 11.2, 12.5, 14, and 16 kHz was 6.5 ± 9.4 dB HL, with values ranging from −7 to 42 dB HL. After applying the exclusion criteria, the mean age of the participants whose ears were analyzed was 25.3 ± 3.5 years, with an age range of 21 to 35 years. The demographic distribution of ears according to age and EHT is summarized in Table 1. The EHT of three groups differed significantly ($\chi^2 = 11.9$, $p = 0.03$) as seen in Figure 2B. The post-hoc analysis revealed that the EHT for the 30–35-year age group was significantly higher than for those of the other two groups ($p < 0.02$, Cohen's d = 0.88).

Table 1. Demographic table for participants. EHT for each group is presented as mean and standard deviation.

Group		20–25 Years	25–30 Years	30–35 Years	Total
Number of subjects		40	19	12	71
Number of ears		75	34	23	132
Sex	M	43	16	11	72
	F	32	18	12	62
EHT in dB HL		4.8 ± 8.4	5.6 ± 9.6	12.4 ± 10.1	6.5 ± 9.4

3.2. Cortical Response of the MMN Paradigms

We conducted two mismatch negativity (MMN) paradigms, each employing different acoustic stimuli: tonal and speech. After artifact reduction, the average number of recorded epochs was 165 for the standard stimulus (range: 50 to 194) and 43 for the deviant stimulus (range: 13 to 67). This corresponds to the exclusion of 17% of epochs for the standard stimulus and 32% for the deviant stimulus due to artifacts.

The responses to the standard stimulus, the deviant stimulus, and the difference between them are depicted as the grand average response for both conditions (Figure 3A,B).

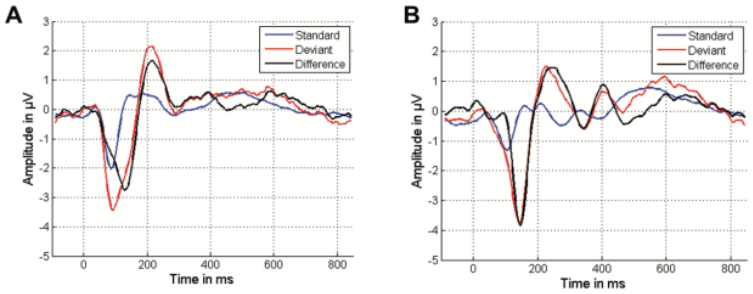


Figure 3. The grand average response to the standard stimulus (blue), the deviant stimulus (red), and the difference between the two stimuli (black) in the tone paradigm (**A**) and the speech paradigm (**B**). Both the standard and deviant stimuli elicit similar cortical reactions, characterized by pronounced negative N1 and positive P2 deflections. However, the response to the deviant stimulus is marked by a substantial negative deflection known as Mismatch Negativity (MMN), which is identifiable by examining the difference between the standard and deviant responses. The cortical response to the speech stimuli exhibits delayed latencies for N1, P2, and MMN compared to the tone stimulus paradigm. Additionally, a P300 component is elicited in the speech paradigm.

In the tone paradigm (Figure 3A), two distinct potentials in the cortical response to the standard stimulus were identified (Figure 3A, blue). The first was a pronounced negative deflection with an amplitude of 2.01 µV occurring at a latency of 88 ms, associated with the N1 component. This was followed by a pronounced positive deflection, observed at a latency of 160 ms with an amplitude of 0.1 µV, corresponding to the P2 component. Considering the difference between the cortical response to the deviant and standard stimuli (Figure 3A, black), the MMN was successfully identified as a pronounced negative deflection with an amplitude of 2.75 µV at a latency of 130 ms.

In the speech paradigm (Figure 3B), the cortical response to the standard stimulus (Figure 3B, blue) displayed a pronounced negative deflection with an amplitude of 1.32 µV at a latency of 104 ms, indicative of the N1 component. This was followed by a double-peaked positive deflection reaching a maximum amplitude of 0.25 µV at a latency of 210 ms, associated with the P2 component. Regarding the difference of the cortical responses (Figure 3B, black), a distinct MMN was noted with an amplitude of 3.84 µV at 146 ms, accompanied by a pronounced positive deflection of 0.88 µV at a latency of 404 ms. This latter positive potential is attributed to the P300 component, reflecting attentional processes.

3.3. Comparison of the MMN Responses Grouped by Age and EHT

We found no significant correlation between MMN responses of the left and right ear, MMN responses and age, or MMN responses and EHT. However, significant effects were found when participants were grouped based on the effect being investigated. Figure 4 (on the left) displays the grand averages of these groups for both effects in the different responses across the two MMN paradigms (Speech: A–D, Tone: E–H); on the right side,

the amplitudes per subject are compared using a boxplot. The comprehensive analysis encompassed not only the comparison of MMN amplitude but also the evaluation of MMN peak latency and the analysis of both amplitude and latency for the P300 potential within the speech paradigm (refer to Table 2). A significant age-related effect on the MMN amplitude in the speech condition was found (χ^2 = 13.0, p = 0.002)m with mean amplitudes and corresponding confidence intervals of $A_{20\text{-}25} = -3.51 \pm 0.33$ µV, $A_{25\text{-}30} = -2.54 \pm 0.60$ µV, and $A_{30\text{-}35} = -2.8 \pm 0.65$ µV in each group. The post-hoc analysis showed a significant difference between the 20–25 yrs and 25–30 yrs groups (p = 0.0015, Cohen's d = 0.63). Apart from that, no further effects of age were observed on the cortical potentials examined. Also, no significant influence of EHT on the amplitude or latency of the MMN or the P300 was detected for either the tone or speech paradigms.

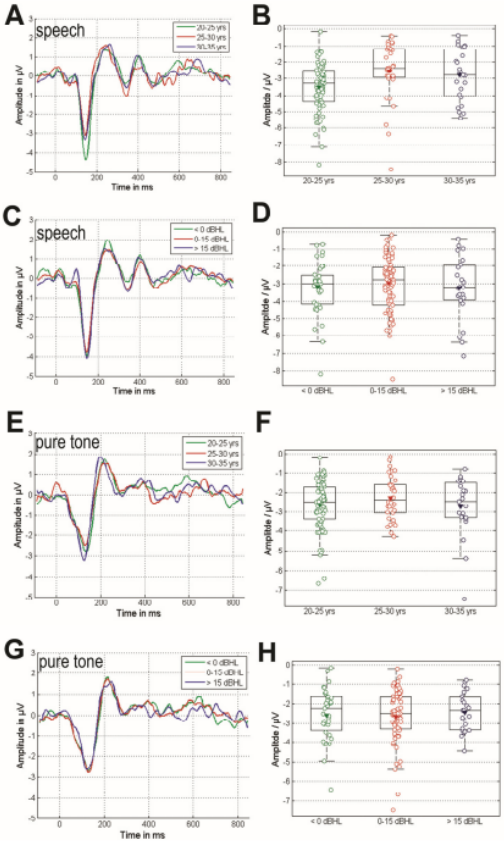


Figure 4. Comparison of cortical responses to difference between deviant and standard stimuli in speech (**A**–**D**) and tone (**E**–**H**) conditions. (**A**) Averaged cortical responses to speech stimuli across groups, categorized by participant ages: 20–25, 25–30, and 30–35 years old. (**B**) Age-based comparison of MMN amplitudes for grouped speech response data. (**C**) Averaged cortical responses to speech stimuli across groups, categorized by participants' EHT: <0 dB HL, 0–15 dB HL, >15 dB HL and (**D**) corresponding MMN amplitude. (**E**) Averaged cortical responses to tone stimuli across groups, categorized by age and (**F**) corresponding MMN amplitude. (**G**) Averaged cortical responses to tone stimuli across groups, categorized by participants' EHT and (**H**) corresponding MMN amplitudes. The mean values are indicated by triangles in all boxplots.

Table 2. Kruskal–Wallis test to analyze the relationship between age and EHT and electrophysiological metrics: Amplitude and Latency of MMN and P300.

Categorical Group	Metric	$\chi^2_{Amplitude}$	$P_{Amplitude}$	$\chi^2_{Latency}$	$P_{Latency}$
Age	MMN_{Tone}	1.29	0.53	4.64	0.10
	MMN_{Speech}	13.0	0.002	1.87	0.39
	$P300_{Speech}$	4.24	0.12	0.19	0.91
EHT	MMN_{Tone}	0.12	0.94	0.94	0.62
	MMN_{Speech}	0.69	0.71	2.86	0.24
	$P300_{Speech}$	0.21	0.90	0.96	0.62

4. Discussion

4.1. Summary of Findings of EHT and Cortical Potentials in Response to Tone and Speech Stimuli

Direct measurement of early changes in the peripheral auditory pathways, particularly cochlear synaptopathy, requires invasive methods that are not feasible in humans. As a non-invasive alternative, EHT has been considered a biomarker for early changes in the peripheral auditory pathway and may serve as an indirect marker for cochlear synaptopathy in humans [16,18]. This study found that individuals over 30 exhibited significantly higher EHT compared to younger groups, suggesting that early changes in the peripheral auditory pathway, potentially including cochlear synaptopathy, may already be present in these individuals. This finding aligns with previous research [18].

The aim of this study was to examine individual differences in central auditory processing in relation to age and EHT. The MMN, which is a marker of auditory discrimination ability, was chosen as a key measure since it is elicited even by small differences between two stimuli. To achieve this, oddball paradigms consisting of a standard stimulus and a deviant were employed, using two different stimulus pairs: a tone-based paradigm (1 kHz and 2 kHz) and a speech-based paradigm ("ba" and "da"). In both paradigms, the MMN component was successfully extracted by calculating the difference between cortical responses to the standard and deviant stimuli (Figure 3).

Notably, in both paradigms, the MMN amplitude was larger than the N1 amplitude for both deviant and standard stimuli. This may be attributed to the electrode placement at Fpz, where MMN amplitudes tend to be higher [37], whereas the N1–P2 complex typically exhibits higher amplitudes when recorded at Cz [38].

In the tone paradigm, it was unexpectedly found that subtracting the standard stimulus did not fully eliminate the N1–P2 complex of the deviant stimulus. The reason for this incomplete regression remains unclear but may be related to the properties of the stimuli and not with the recording setup, as both were recorded with the same electrode positions. The N1–P2 complex is known to be sensitive to loudness effects [39]. However, it is unlikely that differences in perceived loudness contributed to this effect, as both stimuli were calibrated to 70 dB nHL, and participants' hearing thresholds at 1 kHz and 2 kHz showed only minimal variation. A more plausible explanation are differences in the frequency dependent interstimulus interval (ISI) between the deviant and standard stimulus. Longer ISI has been shown to specifically reduce P2 component amplitudes due to loudness adaptation [40]. For the N1 component, this regression approach is considered a robust method for isolating the MMN component [41]. In our data, this approach successfully regressed out the N1 component in the speech paradigm, as expected. Although this issue does not significantly affect the interpretation of our results—since the regression artifact equally impacts all groups—further data collection would be valuable to explore this effect in greater detail. Future studies utilizing EEG recordings with multiple channels, which enable higher spatial resolution analyses and the possibility to localize dipole sources in

the brain, along with additional cortical responses for each stimulus, would allow for a more thorough examination of this aspect.

Furthermore, a distinct endogenous P300 potential was successfully recorded in the speech paradigm without the need for an additional task, whereas it was absent in the tone paradigm. This unexpected finding contrasts with previous studies [42,43] and may be due to the substantial spectral and temporal differences between the stimuli "da" and "ba" used in this study, which could have involuntarily captured the participants' attention [44].

4.2. The Relation of MMN and EHT

When participants were classified into different EHT-based groups and compared in terms of MMN responses, no significant differences were found in amplitude or latency for either pure-tone or speech stimuli. However, previous studies suggest that high-frequency audiometric thresholds can influence cortical auditory evoked potentials [45–47], including the MMN. For example, Chen et al. (2016) showed that increasing high-frequency hearing thresholds correlate with prolonged speech-evoked MMN latency in noisy environments [45]. Zeng et al. (2020) found that hearing loss across the frequency range between 125 Hz and 8 kHz impairs suprathreshold processing and interferes with speech perception [47]. We believe that the differences in results may be attributed to variations in hearing threshold deterioration across different frequency ranges. In this study, the focus was set on EHT in a frequency range from 10 to 16 kHz, while the other study examined frequencies from 4 to 8 kHz. As we know, the stimulus of 'da/ba' is primarily located within frequencies up to around 4 kHz [48]. Therefore, differencing between these stimuli may not engage a central processing area above 8 kHz.

As mentioned previously, animal studies have shown that OHCs in the basal turn exhibit lower sensitivity compared to cochlear synapses in the apical and middle turns. In animals, OHC loss at the basal turn, particularly in the high-frequency range, is strongly associated with cochlear synaptopathy in the apical and middle turns. Consequently, high-frequency threshold deterioration in animals can serve as an indirect indicator of cochlear synaptopathy [23,24]. While animal data cannot be directly extrapolated to humans, these findings suggest that EHT elevation, as an early sign of peripheral auditory pathway changes, could similarly serve as an indirect biomarker for cochlear synaptopathy, particularly in the apical and middle turns of the cochlea in humans. Based on these assumptions, our findings suggest that the early changes in the peripheral auditory pathway, including potential cochlear synaptopathy in the apical and middle turns, may not significantly impact central auditory processing. However, a major limitation of this study is the absence of a direct approach to verify early auditory pathway changes in the participants histologically, including potential cochlear synaptopathy.

4.3. The Relation Between MMN and Aging

Previous studies have reported that aging not only reduces the amplitude of the MMN response but also prolongs its latency [49–54]. However, the work by Kisley et al. (2005) compared only older adults (over 55 years old) with young individuals aged 18–23 years old [52]. Since aging is often associated with high-frequency hearing loss, it is unclear whether the observed MMN effect is due to age-related changes or high-frequency hearing loss. The study's criteria only considered hearing thresholds at 1 kHz with a limit of 10 dB HL, without accounting for other frequencies. In another study by Ruzzoli et al. (2012), MMN was compared across three age groups: (1) 21–40 years, (2) 41–60 years, and (3) 61–80 years, revealing that MMN was diminished in the oldest group but showing no difference between the young and middle-aged groups [53]. However, the study only briefly mentioned conducting a hearing test to exclude sensorineural hearing loss, without

specifying the test frequencies or criteria. In contrast, the present study enrolled young adults aged 21–35 years with normal hearing thresholds from 0.125 kHz to 8 kHz only. Here, MMN amplitudes decrease with age.

Another aspect is that most previous studies used pure tones as stimuli and observed aged-related changes in MMN [52,53]. Pure-tone and speech stimuli applied to all the participants in this study led to the observation of age-related changes only in response to speech stimuli. This finding suggests that early changes in the central nervous system during aging, similar to hidden hearing loss in the peripheral auditory system, may affect complex listening situations or the capacity to understand complex speech stimuli, while leaving simple tone differentiation unaffected [55,56].

Finally, this study found no age-related effect on MMN latency in response to either speech or pure-tone stimuli. This suggests that the speed of signal propagation in the nervous system may remain largely unaffected in the early phase of aging, indicating that significant demyelination in the central auditory system has not yet occurred. This indicates that MMN latency is a less sensitive and appropriate biomarker for evaluating central speech recognition. Similar findings have been reported in studies involving cochlear implant patients [37].

5. Limitations

The measurement of MMN in this study has several limitations. Firstly, we used only three active electrodes, which limits the ability to differentiate distinct MMN generators. Secondly, the differentiation between standard and deviant stimuli is imprecise when using speech stimuli. Specifically, the 'da' deviant response is a superposition of the 'da' cortical response and the MMN. Regarding the 'da' cortical response, the paradigm must be repeated with 'da' as the standard stimulus. However, this was not implemented in the present study due to time constraints. Moreover, there is currently no direct evidence of cochlear synaptopathy in humans. The possibility of pathological changes in the peripheral and central nervous systems was not directly observed or confirmed in the participants. Additionally, the age range in this study was limited to only 20–35 years old. Future studies recruiting a broader age range may reveal clearer age-related effects. Furthermore, we did not use a professional questionnaire to assess noise exposure; instead, we asked participants to actively recall their history of noise exposure. This method may introduce bias and does not fully eliminate the potential effects of noise exposure. Moreover, a limited number of repetitions were conducted for both the standard stimulus and, in particular, the deviant stimulus, which may have increased variability in amplitude and introduced bias in the conclusions. The resulting differences in the signal-to-noise ratio between subjects can lead to smearing the EEG signal when averaging across participants. This limitation will need to be addressed in future studies.

6. Conclusions

During the early stages of age-related hearing loss, pathological changes occur in the peripheral and central auditory systems. EHT was used as an indirect biomarker to detect pathology, potentially associated with cochlear synaptopathy in the peripheral auditory system; however, it is not suitable for detecting changes in the central auditory system. The application of using MMN as an electrophysiological tool to diagnose hidden hearing loss in normal hearing adults has limitations. However, in contrast to MMN responses to tonal stimuli, the present study reveals that MMN amplitudes obtained with speech stimuli may indicate early signs of central auditory deficits.

Author Contributions: L.Z. and F.H.S. designed research; D.M. performed research; F.H.S. and L.Z. analyzed data; L.Z., F.H.S., K.E., W.G. and R.M. wrote and corrected the paper. All authors have read and agreed to the published version of the manuscript.

Funding: This research received no financial support or funding.

Institutional Review Board Statement: The study was conducted in accordance with the Declaration of Helsinki and approved by the Institutional Review Board (or Ethics Committee) of Rostock University Medical Center (protocol code A 2023-0010 and approved on 12 January 2023).

Informed Consent Statement: Informed consent was obtained from all subjects involved in the study.

Data Availability Statement: The data that support the findings of this study are available from the corresponding author, (L.Z.) upon reasonable request.

Acknowledgments: We would like to thank all the participants that took part in the study. We would also like to thank Gesa Schmidt, an English teacher, for her linguistic revision of the manuscript.

Conflicts of Interest: The authors declare no conflicts of interest.

Abbreviations

The following abbreviations are used in this manuscript:

ARHL	age-related hearing loss
EFR	envelop-following response
EHT	extended high-frequency threshold
MEMR	acoustic middle ear muscle reflex
MMN	mismatch negativity
OHC	outer hair cell

References

1. Agrawal, Y.; Platz, E.A.; Niparko, J.K. Prevalence of hearing loss and differences by demographic characteristics among US adultsdata from the national health and nutrition examination survey, 1999–2004. *Arch. Intern. Med.* **2008**, *168*, 1522–1530. [CrossRef] [PubMed]
2. Yamasoba, T.; Lin, F.R.; Someya, S.; Kashio, A.; Sakamoto, T.; Kondo, K. Current concepts in age-related hearing loss: Epidemiology and mechanistic pathways. *Hear. Res.* **2013**, *303*, 30–38. [CrossRef] [PubMed]
3. *Addressing the Rising Prevalence of Hearing Loss*; World Health Organization: Geneva, Switzerland, 2018.
4. Wang, J.; Puel, J.-L. Presbycusis: An update on cochlear mechanisms and therapies. *J. Clin. Med.* **2020**, *9*, 218. [CrossRef] [PubMed]
5. Basner, M.; Babisch, W.; Davis, A.; Brink, M.; Clark, C.; Janssen, S.; Stansfeld, S. Auditory and non-auditory effects of noise on health. *Lancet* **2014**, *383*, 1325–1332. [CrossRef]
6. Liberman, M.C.; Kujawa, S.G. Cochlear synaptopathy in acquired sensorineural hearing loss: Manifestations and mechanisms. *Hear. Res.* **2017**, *349*, 138–147. [CrossRef]
7. Long, P.; Wan, G.; Roberts, M.T.; Corfas, G. Myelin development, plasticity, and pathology in the auditory system. *Dev. Neurobiol.* **2018**, *78*, 80–92. [CrossRef]
8. Mulders, W.H.; Chin, I.L.; Robertson, D. Persistent hair cell malfunction contributes to hidden hearing loss. *Hear. Res.* **2018**, *361*, 45–51. [CrossRef]
9. Schaette, R.; McAlpine, D. Tinnitus with a normal audiogram: Physiological evidence for hidden hearing loss and computational model. *J. Neurosci. Off. J. Soc. Neurosci.* **2011**, *31*, 13452–13457. [CrossRef]
10. Sergeyenko, Y.; Lall, K.; Liberman, M.C.; Kujawa, S.G. Age-related cochlear synaptopathy: An early-onset contributor to auditory functional decline. *J. Neurosci.* **2013**, *33*, 13686–13694. [CrossRef]
11. Moser, T.; Predoehl, F.; Starr, A. Review of hair cell synapse defects in sensorineural hearing impairment. *Otol. Neurotol.* **2013**, *34*, 995–1004. [CrossRef]
12. Kujawa, S.G.; Liberman, M.C. Adding insult to injury: Cochlear nerve degeneration after "temporary" noise-induced hearing loss. *J. Neurosci.* **2009**, *29*, 14077–14085. [CrossRef] [PubMed]
13. Kujawa, S.G.; Liberman, M.C. Synaptopathy in the noise-exposed and aging cochlea: Primary neural degeneration in acquired sensorineural hearing loss. *Hear. Res.* **2015**, *330 Pt B*, 191–199. [CrossRef]

14. Shaheen, L.A.; Valero, M.D.; Liberman, M.C. Towards a diagnosis of cochlear neuropathy with envelope following responses. *J. Assoc. Res. Otolaryngol.* **2015**, *16*, 727–745. [CrossRef] [PubMed]
15. Bramhall, N.; Beach, E.F.; Epp, B.; Le Prell, C.G.; Lopez-Poveda, E.A.; Plack, C.J.; Schaette, R.; Verlust, S.; Canlon, B. The search for noise-induced cochlear synaptopathy in humans: Mission impossible? *Hear. Res.* **2019**, *377*, 88–103. [CrossRef] [PubMed]
16. Liberman, M.C.; Epstein, M.J.; Cleveland, S.S.; Wang, H.; Maison, S.F. Toward a differential diagnosis of hidden hearing loss in humans. *PLoS ONE* **2016**, *11*, e0162726. [CrossRef]
17. Bramhall, N.F. Use of the auditory brainstem response for assessment of cochlear synaptopathy in humans. *J. Acoust. Soc. Am.* **2021**, *150*, 4440. [CrossRef]
18. Schmidt, F.H.; Dörmann, A.; Ehrt, K.; Grossmann, W.; Mlynski, R.; Zhang, L. The curvature quantification of wave I in auditory brainstem responses detects cochlear synaptopathy in human beings. *Eur. Arch. Otorhnilaryngol.* **2024**, *281*, 4735–4746. [CrossRef]
19. James, J.A.; Park, J.H.; Smith, E.M.; Johnson, C.E.; Clifton, S.; Danhauer, J.L.; Barbee, C.M. Effectiveness of auditory measures for detecting hidden hearing loss and/or cochlear synaptopathy: A systematic review. *Semin. Hear.* **2018**, *39*, 172–209. [CrossRef]
20. Pappa, A.K.; Hutson, K.A.; Scott, W.C.; Wilson, J.D.; Fox, K.E.; Masood, M.M.; Giardina, C.K.; Pulver, S.H.; Grana, G.D.; Askew, C.; et al. Hair cell and Neural contributions to the cochlear summating potential. *J. Neurophysiol.* **2019**, *121*, 2163–2180. [CrossRef]
21. Yaşar, M.; Öner, F.; Atalay, F.; Anbar, S.S. Cochlear synaptopathy evaluation with Electrocochleography in patients with hearing difficulty in noise despite normal hearing levels. *Clin. Otolaryngol.* **2025**, *50*, 75–81. [CrossRef]
22. Haggerty, R.A.; Hutson, K.A.; Riggs, W.J.; Brown, K.D.; Pillsbury, H.C.; Adunka, O.F.; Buchman, C.A.; Fitzpatrick, D.C. Assessment of cochlear synaptopathy by electrocochleography to low frequencies in a preclinical model and human subjects. *Front. Neurol.* **2023**, *14*, 1104574. [CrossRef] [PubMed]
23. Maison, S.F.; Usubuchi, H.; Liberman, M.C. Efferent feedback minimizes cochlear neuropathy from moderate noise exposure. *J. Neurosci.* **2013**, *33*, 5542–5552. [CrossRef] [PubMed]
24. Liberman, M.C.; Liberman, L.D.; Maison, S.F. Efferent feedback slows cochlear aging. *J. Neurosci.* **2014**, *34*, 4599–4607. [CrossRef] [PubMed]
25. Chambers, A.R.; Resnik, J.; Yuan, Y.; Whitton, J.P.; Edge, A.S.; Liberman, M.C.; Polley, D.B. Central gain restores auditory processing following near-complete cochlear denervation. *Neuron* **2016**, *89*, 867–879. [CrossRef]
26. Gu, J.W.; Halpin, C.F.; Nam, E.-C.; Levine, R.A.; Melcher, J.R. Tinnitus, diminished sound-level tolerance, and elevated auditory activity in humans with clinically normal hearing sensitivity. *J. Neurophysiol.* **2010**, *104*, 3361–3370. [CrossRef]
27. Sun, W.; Deng, A.; Jayaram, A.; Gibson, B. Noise exposure enhances auditory cortex responses related to hyperacusis behavior. *Brain Res.* **2012**, *1485*, 108–116. [CrossRef]
28. Chen, G.-D.; Radziwon, K.E.; Kashanian, N.; Manohar, S.; Salvi, R. Salicylate-induced auditory perceptual disorders and plastic changes in nonclassical auditory centers in rats. *Neural. Plast.* **2014**, *2014*, 658741. [CrossRef]
29. Noreña, A.J. An integrative model of tinnitus based on a central gain controlling neural sensitivity. *Neurosci. Biobehav. Rev.* **2011**, *35*, 1089–1109. [CrossRef]
30. Auerbach, B.D.; Rodrigues, P.V.; Salvi, R.J. Central gain control in tinnitus and hyperacusis. *Front. Neurol.* **2014**, *5*, 206. [CrossRef]
31. Näätänen, R.; Gaillard, A.; Mäntysalo, S. Early selective-attention effect on evoked potential reinterpreted. *Acta Psychol.* **1978**, *42*, 313–329. [CrossRef]
32. Näätänen, R. The mismatch negativity: A powerful tool for cognitive neuroscience. *Ear Hear.* **1995**, *16*, 6–18. [CrossRef] [PubMed]
33. Näätänen, R.; Petersen, B.; Torppa, R.; Lonka, E.; Vuust, P. The MMN as a viable and objective marker of auditory development in CI users. *Hear. Res.* **2017**, *353*, 57–75. [CrossRef] [PubMed]
34. Lonka, E.; Kujala, T.; Lehtokoski, A.; Johansson, R.; Rimmanen, S.; Alho, K.; Näätänen, R. Mismatch negativity brain response as an index of speech perception recovery in cochlear-implant recipients. *Audiol. Neurotol.* **2004**, *9*, 160–162. [CrossRef] [PubMed]
35. British Society of Audiology. Recommended Procedure: Pure Tone Air and Bone Conduction Threshold Audiometry with and Without Masking and Determination of Uncomfortable Loudness Levels. 2004. Available online: https://www.thebsa.org.uk/ (accessed on 2 February 2025).
36. Riedel, H.; Granzow, M.; Kollmeier. Single-sweep-based methods to improve the quality of auditory brain stem responses Part II: Averaging methods. *Z. Audiol.* **2001**, *40*, 62–85.
37. Turgeon, C.; Lazzouni, L.; Lepore, F.; Ellemberg, D. An objective auditory measure to assess speech recognition in adult cochlear implant users. *Clin. Neurophysiol.* **2014**, *125*, 827–835. [CrossRef]
38. Näätänen, R.; Picton, T. The N1 Wave of the human electric and magnetic response to sound: A review and an analysis of the component structure. *Psychophysiology* **1987**, *24*, 375–425. [CrossRef]
39. Schmidt, F.H.; Mauermann, M.; Kollmeier, B. Neural representation of loudness: Cortical evoked potentials in an induced loudness reduction experiment. *Trends Hear.* **2020**, *24*, 2331216519900595. [CrossRef]
40. Lanting, C.P.; Briley, P.M.; Sumner, C.J.; Krumbholz, K. Mechanisms of adaption in human auditory cortex. *J. Neurophysiol.* **2013**, *110*, 973–983. [CrossRef]

41. Näätänen, R.; Paavilainen, P.; Rinne, T.; Alho, K. The mismatch negativity (MMN) in basic research of central audiotry processing: A review. *Clin. Neurophyiol.* **2007**, *118*, 2544–2590. [CrossRef]
42. Tao, D.; Zhang, Y.; Liu, H.; Zhang, W.; Xu, M.; Galvin, J.J., 3rd; Zhang, D.; Liu, J. The P300 auditory event-related potential may predict segregation of competing speech by bimodal cochlear implant listeners. *Front. Neurosci.* **2022**, *16*, 8888596. [CrossRef]
43. Polich, J. Updating P300: An integrative theory of P3a and P3b. *Clin. Neurophysiol.* **2007**, *118*, 2128–2148. [CrossRef] [PubMed]
44. Tervaniemi, M.; Lehtokoski, A.; Sinkkonen, J.; Virtanen, J.; Ilmoniemi, R.; Näätänen, R. Test–retest reliability of mismatch negativity for duration, frequency and intensity changes. *Clin. Neurophysiol.* **1999**, *110*, 1388–1393. [CrossRef] [PubMed]
45. Chen, J.; Chen, S.; Zheng, Y.; Ou, Y. The effect of aging and the high-frequency auditory threshold on speech-evoked mismatch negativity in a nosiy background. *Audiol. Neurootol.* **2016**, *21*, 1–11. [CrossRef] [PubMed]
46. Chen, J.; Zhao, Y.; Zou, T.; Wen, X.; Zhou, X.; Yu, Y.; Liu, Z.; Li, M. Sensorineural hearing loss affects functional connectivity of auditory cortex, parahipocampal gyrus and inferior prefrontal gyrus in tinnitus patients. *Front. Neurosci.* **2022**, *16*, 816712. [CrossRef]
47. Zeng, F.-G.; Richardson, M.; Turner, K. Tinnitus does not interfere with auditory and speech perception. *J. Neurosci.* **2020**, *40*, 6007–6017. [CrossRef]
48. Berthommier, F.; Girin, L.; Boe, L.J. A simple hybrid acoustic/morphologically constrained technique for the synthesis of stop consonants in various vocalic contexts. In Proceedings of the Interspeech 2012—13th Annual Conference of the International Speech Communication Association, Portland, OR, USA, 9–13 September 2012; p. Thu.P10a.05. hal-00807519.
49. Pekkonen, E.; Jousmäki, V.; Partanen, J.; Karhu, J. Mismatch negativity area and age-related auditory memory. *Electroencephalogr. Clin. Neurophysiol.* **1993**, *87*, 321–325. [CrossRef]
50. Pekkonen, E.; Rinne, T.; Reinikainen, K.; Kujala, T.; Alho, K.; Naatanen, R. Aging effects on auditory processing: An event-related potential study. *Exp. Aging Res.* **1996**, *22*, 171–184. [CrossRef]
51. Cooper, R.J.; Todd, J.; McGill, K.; Michie, P.T. Auditory sensory memory and the aging brain: A mismatch negativity study. *Neurobiol. Aging* **2006**, *27*, 752–762. [CrossRef]
52. Kisley, M.A.; Davalos, D.B.; Engleman, L.L.; Guinther, P.M.; Davis, H.P. Age-related change in neural processing of time-dependent stimulus features. *Cogn. Brain Res.* **2005**, *25*, 913–925. [CrossRef]
53. Ruzzoli, M.; Pirulli, C.; Brignani, D.; Maioli, C.; Miniussi, C. Sensory memory during physiological aging indexed by mismatch negativity (MMN). *Neurobiol. Aging* **2012**, *33*, 625.e21–625.e30. [CrossRef]
54. Näätänen, R.; Kujala, T.; Escera, C.; Baldeweg, T.; Kreegipuu, K.; Carlson, S.; Ponton, C. The mismatch negativity (MMN)—A unique window to disturbed central auditory processing in aging and different clinical conditions. *Clin. Neurophysiol.* **2012**, *123*, 424–458. [CrossRef] [PubMed]
55. Maddox, J. Cocktail party effect made tolerable. *Nature* **1994**, *369*, 517. [CrossRef] [PubMed]
56. Starr, A.; Sininger, Y.; Pratt, H. The varieties of auditory neuropathy. *J. Basic Clin. Physiol. Pharmacol.* **2000**, *11*, 215–230. [CrossRef] [PubMed]

Disclaimer/Publisher's Note: The statements, opinions and data contained in all publications are solely those of the individual author(s) and contributor(s) and not of MDPI and/or the editor(s). MDPI and/or the editor(s) disclaim responsibility for any injury to people or property resulting from any ideas, methods, instructions or products referred to in the content.

Arbeit 5:

Invited Original Study

The Predictive Value of Preoperative Measurements of Cochlear Nerve Diameters From MRT and Postoperative Speech Perception in Adult Patients With Cochlear Implant

*Lichun Zhang, *Florian Herrmann Schmidt, †Daniel Cantré, *Robert Brenzel, *Karsten Ehrt, *Wilma Großmann, †Sönke Langner, and *Robert Mlynski

*Department of Otorhinolaryngology, Head and Neck surgery, "Otto Körner," Rostock University Medical Center; and †Institute of Diagnostic and Interventional Radiology, Pediatric Radiology and Neuroradiology, University Medical Center Rostock, Rostock, Germany

Downloaded from http://journals.lww.com/otology-neurotology by BhDMf5ePHKav1zEoum1tQfN4a+kJLhEZgbsIHo4XMi0hCywCX1AWnYQp/IlQrHD3i3D0OdRyi7TvSFl4Cf3VC4/OAVpDDa8K2+Ya6H515kE= on 09/16/2024

Objective: The current study aims to investigate whether objective measurements of the cochlear nerve (CN), derived from preoperative MRI images, correlate with postoperative speech perception in CI patients.
Study Design: Retrospective cohort study.
Setting: University Medical Center, tertiary academic referral center.
Patients: Patients undergoing a cochlear implant surgery including MED-EL (Synchrony 2, FLEX electrode series; MED-EL, Innsbruck, Austria) Cochlear (slim straight electrodes; Cochlear Ltd., Sydney, Australia), Advanced Bionics (HiRes Ultra 3D CI, HiFocus SlimJ electrodes; Sonova, Zürich, Switzerland), and Oticon (Neuro Zti EVO; Oticon A/S, Smørum, Denmark) between 2020 and 2023.
Intervention: Preoperative MRI images were utilized to measure the volume of the modiolus (VM), the cross-sectional areas of the CN (ACN), and for normalization, the area of the facial nerve (AFN) and the area of the internal ear canal (AIEC). Postoperative speech perceptions were assessed through word recognition scores (WRS) at several stages following the first fitting (FF) of the CI processor: immediately after FF, 1 month, 3 months, and 6 months after FF.
Main Outcome Measures: Sixty-eight patients were enrolled in this study. A statistically significant positive correlation between the ratio between ACN and AFN (ACN/AFN) and WRS_{FF} was identified ($R = 0.36$, $p < 0.003$). However, this correlation disappeared in subsequent follow-up tests. Moreover, upon grouping patients based on their degree of asymmetrical hearing loss, it was observed that the correlation was primarily driven by patients with moderate to severe asymmetrical hearing loss (AHLm) on the contralateral side ($R = 0.62$, $p = 0.0003$).
Conclusion: The present results suggest that assessing the size of the CN through MRI has limited predictive utility for postoperative speech perceptions during CI consultations. This limitation seems to be particularly relevant for AHLm patients and is confined to the initial activation period.
Key words: Cochlear implant—Cochlear nerve—Magnetic resonance imaging (MRI)—Speech perception.

Otol Neurotol **00**:00–00, 2024.

INTRODUCTION

The cochlear implant (CI) electrically stimulates spiral ganglion neurons (SGN) and generates nerve impulse, which are then transmitted through the vestibulocochlear nerve to the auditory brainstem. Clinically, CI has been successfully implanted in a very broad patient spectrum ranging from infants to elderly, who exhibit severe-to-profound sensorineural hearing loss (SNHL) (1,2). In general, postoperative speech perception is highly promising and satisfying. However, there are often significant individual variabilities among patients (1). Previous studies have identified various demographic factors that affect the outcome of CIs, including the age at implantation, history of hearing aid use, cognitive ability, parental socioeconomic status, language training, and the status of cochlear nerve (CN) (1,3–6). Among these factors, the integrity of the CN is particularly crucial (5,6). Thus, the accurate preoperative evaluation of the degree of CN impairment could potentially facilitate appropriate counseling regarding the outcomes of cochlear implantation.

The promontory stimulation test (PST) assesses the integrity of the CN by inserting a needle electrode through the tympanic membrane into the cochlear vicinity. However, this method is invasive, and its significance has been questioned due to the fact that negative results do not necessarily rule out the function use of a CI (7–10). In contrast, the ear canal stimulation test (ECST) offers a noninvasive alternative. It utilizes a silver ball ear canal electrode positioned close to the tympanic membrane. However, this method typically requires higher electric stimulation intensity to elicit auditory sensation, potentially leading to a higher incidence of

Address correspondence and reprint requests to Lichun Zhang, M.D., Ph.D., Department of Otorhinolaryngology, Head and Neck surgery, "Otto Körner," Rostock University Medical Center, Doberaner Strasse 137-139, D-18057, Rostock, Germany; E-mail: lichun.zhang@med.uni-rostock.de
Conflict of interest: The authors declare no competing interest.
Lichun Zhang and Florian Herrmann Schmidt provided equal contribution.
DOI: 10.1097/MAO.0000000000004293

© 2024, Otology & Neurotology, Inc.

Copyright © 2024 Otology & Neurotology, Inc. Unauthorized reproduction of this article is prohibited.

Downloaded from http://journals.lww.com/otology-neurotology by BhDMf5ePHKav1zEoum1tQfN4a+kJLhEZgbsIHo4XMi0hCywCX1AWnYQp/IlQrHD3i3D0OdRyi7TvSFl4Cf3VC4/OAVpDDa8K2+Ya6H515kE= on 09/16/2024

unwanted somatosensory sensation (10–14). In contrast to these physiological tests, the most commonly employed non-invasive methods for preoperative assessment of the status of the CN involve a combination of computed tomography (CT) and magnetic resonance imaging (MRI). By analyzing CT and MRI images, CN deficiency (CND), encompassing CN hypoplasia and aplasia, can be detected. According to existing literature, CN hypoplasia is characterized by bony cochlear nerve canal (BCNC) diameter of <1.5 mm and an internal auditory canal of <2 mm (15,16). Aplasia, on the other hand, is determined when the CN is not observable in MRI (17,18). Regarding the postoperative benefits of CIs, several studies have demonstrated that patients with aplastic CNs tend to exhibit poorer outcomes compared to those with hypoplastic CNs after CI implantations (19,20). Besides, comparative studies have shown that the benefits of CIs in patients with CND were inferior to those in other children with SNHL who possessed normal-sized CNs (21,22). In 2015, Yamazaki et al. analyzed the correlation between the preoperative relative diameter of the vestibulocochlear nerve in the CPA as observed on the preoperative MRI scans, and the postoperative auditory performance with CI in congenitally deaf children with CND (23). Their findings revealed a statistically significant positive correlation (23). Collectively, these pieces of evidence suggest that the size of the CN serves as a potential biomarker for congenital hearing loss in these patients. However, a question arises regarding the results in adults with postlingual deafness. Given that most of these adult patients should have a normally developed size of CN at birth, further investigation is needed to understand how this factor may influence outcomes in this specific population. As directly presented in the human anatomical study, the diameter of the CN is smaller in patients with profound deafness throughout their lives compared to those with normal hearing (24)

This study aimed to measure the diameters of the CNs in adult patients with postlingual deafness and to investigate the correlation between these diameters and postoperative speech perception following CI surgery.

MATERIALS AND METHODS

The local ethics committee approved this retrospective study (A 2023-0022). All patient data were anonymized and deidentified prior to the retrospective analysis.

Subjects

All patients who underwent a CI including MED-EL (Synchrony 2, FLEX electrode series; MED-EL, Innsbruck, Austria), Cochlear (slim straight electrodes; Cochlear Ltd., Sydney, Australia), Advanced Bionics (HiRes Ultra 3D CI, HiFocus SlimJ electrodes; Sonova, Zürich, Switzerland), and Oticon (Neuro Zti EVO; Oticon A/S, Smørum, Denmark) between 2020 and 2023 were retrospectively included in this study. Exclusion criteria comprised congenital deafness, cochlear malformation, patients with vestibular schwannoma, labyrinthitis, trauma, incomplete insertion of CI array (none), and noninformative speech tests due to patient age or language origin, as well as missing or inadequate preoperative MRI examinations, missing high-resolution T2-weighted 3D sequences. Patient selection based on these criteria was conducted retrospectively utilizing operation reports, physician letters, processor fitting records, and in-clinic progress documents.

MRT Protocol and Measurement of the CN

Each patient received a dedicated MRI examination before the CI surgery based on the guidelines (ZITAT S2k-LL CI-Implantation). MRI was acquired from different clinical MRI systems (1.5 or 3.0 T), with slight adjustments to the protocols depending on the department and individual MRI scanner on which the studies were done (1.5 T Avanto fit, 3.0 Skyra fit, or 3.0 T Vida MRI; Siemens Healthineers, Erlangen, Germany; 1.5 T Signa Artist or 3.0 T Signa Premier MRI; General Electric, California, USA). Assignment of patients to different MRI scanners was determined by appointment capacities. All dedicated protocols included pre- and postcontrast 3D T1-weighted sequences, as well as axial FLAIR and DWI whole brain, and heavily T2-weighted 3D sequences of the internal ear canal (IEC) and inner ear. Three-dimensional T2-weighted sequences with isotropic voxel size of less than 1 mm were obtained in all cases. Mainly, Fast (Turbo) spin echo sequences, optimized for isotropic 3D imaging, were used. For the 3.0 T Siemens scanners, the so-called sampling perfection with application optimized contrasts using different flip angle evolution (SPACE-) sequences with 0.5-mm voxel size was chosen. For the GE scanners, the respective 3D Fast spin echo sequence technique (CUBE) with 0.6-mm voxel size at the 1.5 T Signa Artist MRI and 0.4-mm voxel size at the 3.0 T Signa Premier scanner were used. Only at the Siemens 1.5 T Avanto fit MRI, a gradient echo sequence was used, i.e., 3D constructive interference in steady state (CISS) with 0.6-mm voxel size. The 3D T2-weighted sequences were exported from the PACS in DICOM format for the following measurements.

Measurements of the CN were obtained on the software 3D Slicer (www.slicer.org, Federov et al., 2012)(25). The DICOM files of the MRI pictures were transferred to the software. Based on axial pictures of the IEC, a plane perpendicular to the long axle of IEC was placed to build the parasagittal image. By moving the plane slowly from the cochlea to the CPA, the sectional image of the nerve in the IEC will be clearly displayed. Among all the sectional images, there is at least one section, at which all four nerves, CN, facial nerve (FN), vestibular nerve superior, and vestibular nerve inferior, are clearly demarcated. If multiple sections contain the four aforementioned structures, the analysis will focus on the first encountered section. Based on the section, the boundary lines of the CN and FN was outlined for the measurement of the area (Fig. 1). In order to measure the volume of the modiolus (VM), the axial images of the cochlea were analyzed. The boundary line of the modiolus was clearly demarcated slice by slice. Then the volume was automatically calculated by 3D Slicer. All the measurements were conducted by one ENT resident. Subsequently, each measurement was reviewed by one ENT senior consultant and one senior neuroradiologist. In cases where there was disagreement regarding the measurements, all three

Copyright © 2024 Otology & Neurotology, Inc. Unauthorized reproduction of this article is prohibited.

Downloaded from http://journals.lww.com/otology-neurotology by BhDMf5ePHKav1zEoum1tQfN4a+kJLhEZgbsIHo4XMi0hCywCX1AWnYQp/IlQrHD3i3D0OdRyi7TvSFl4Cf3VC4/OAVpDDa8K2+Ya6H515kE= on 09/16/2024

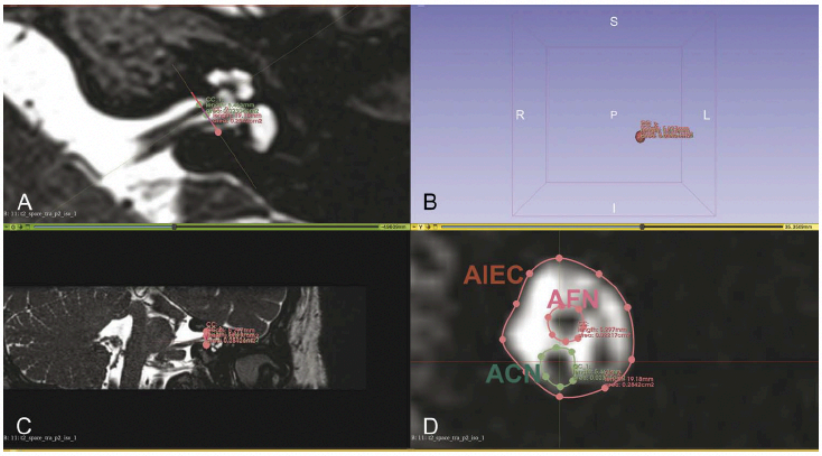


FIG. 1. Screenshot of 3D Slicer showing the measurement of the areas of the CN (ACN), facial nerve (AFN), and inner ear canal (AIEC) from the parasagittal section.

individuals would convene for discussion and repeat the measurement process.

Audiological Parameters

All participants underwent audiometric tests before CI surgery in both ears by skilled staff using a calibrated clinical audiometer (AT900; Auritec GmbH, Hamburg, Germany). Pure tones were presented at frequencies of 0.125, 0.25, 0.5, 0.75, 1, 2, 3, 4, 6, and 8 kHz through a headphone (DT48; Beyer, Heilbronn, Germany).

After CI surgery, speech recognition was evaluated by measuring the word recognition score (WRS) at 65 dB in a quiet environment at various stages after the initial fitting of the CI processor: initial fitting (FF), and 1, 3, and 6 months. The speech-test signal (Freiburg monosyllable test) was presented frontally in a soundproof room (1 × 2 × 44 m).

Statistical Analysis

The investigation of the CN encompassed four metrics: the VM, the area of the CN (ACN), the area of the CN normalized to the area of FN (ACN/AFN), and the area of the CN normalized to the area of IEC (ACN/AIEC). Subsequently, these metrics underwent examination for relationships with physiological and audiological variables. The physiological variables included in the analysis are sex, ear side, contralateral ear, and age. The audiological variables considered are preoperative hearing loss of the affected ear, asymmetrical hearing loss, and postoperative speech intelligibility throughout the follow-up care period. Differences in sex, ear side, and the contralateral ear were analyzed using a *t* test. Correlations with age, preoperative hearing loss, and postoperative speech intelligibility were examined using Pearson correlation. Differences in asymmetrical hearing loss were analyzed using a one-way ANOVA, followed by post hoc analysis using the Tukey test. The correlations between the CN size and speech recognition post-cochlear implant (CI) surgery at various stages—first fitting (FF), and 1, 3, as well as 6 months after FF—were examined.

RESULTS

Sixty-eight patients were included in the study, comprising 25 males and 43 females. The mean age of the participants was 63.0 years, ranging from 22.7 to 89.8 years. Among them, 10 bilateral implanted subjects had both ears included, resulting in a total of 38 left ears and 40 right ears. The demographic data were presented in Table 1.

TABLE 1. *Demographic table for participants*

Group		SSD	AHLm	AHLh	Overall
Patient numbers		16	32	20	68
Age		52.7 ± 16.3	65.0 ± 15.9	68.0 ± 13.4	63.0 ± 16.3
Sex	M	4	15	6	25
	F	12	17	14	43
Company	MED-EL	9	26	17	52
	Cochlear	6	8	9	23
	Advanced Bionics	1	0	0	1
	Oticon	0	2	0	2
Bilateral CI		0 (0%)	4 (12.5%)	6 (30%)	10 (14.7%)

CI indicates cochlear implant; SSD, single-sided deafness; AHLm, moderate asymmetric hearing loss; AHLh, high asymmetric hearing loss.

Copyright © 2024 Otology & Neurotology, Inc. Unauthorized reproduction of this article is prohibited.

Downloaded from http://journals.lww.com/otology-neurotology by BhDMf5ePHKav1zEoum1tQfN4a+kJLhEZgbsIHo4XMi0hCywCX1AWnYQp/IlQrHD3i3D0OdRyi7TvSFl4Cf3VC4/OAVpDDa8K2+Ya6H515kE= on 09/16/2024

All ears underwent CI surgery and had an average 4FPTA of 98.2 ± 17.9 dB HL (mean ± standard deviation). The contralateral ear exhibited an average 4FPTA of 58.3 ± 27.5 dB HL. Sixteen patients were categorized as having single-sided deafness (SSD: the contralateral ear had an average 4FPTA ≤30 dB HL), 32 had moderate asymmetric hearing loss (AHLm: the contralateral ear had an average 4FPTA >30 dB HL and ≤80 dB HL), and 20 were classified as high asymmetric hearing loss (AHLh: the contralateral ear had an average 4FPTA >80 dB HL).

Modiolus and CN

The mean VM measured 4.35 ± 0.62 mm^3, while the average ACN was 0.0178 ± 0.0057 cm^2. Similarly, the average AFN was 0.0174 ± 0.0051 cm^2, and the average AIEC was 0.23 ± 0.063 cm^2. Notably, the CN's area represented approximately 7.6% of the IEC.

The investigation of the CN involved four metrics: the VM, the ACN, the ACN/AFN, and the ACN/AIEC. Following this, these metrics underwent analyses for correlations with physiological and audiological variables (Table 2). No age-related effects or influence from preoperative hearing loss on nerve size parameters were identified in the Pearson correlation. Moreover, no impact was observed on these parameters based on sex and ear side from the *t* test. Similarly, no relationship was found between asymmetric hearing loss in the ANOVA. Furthermore, no significant differences in the parameters were observed when comparing the cochlear implant ear with its corresponding contralateral ear (Fig. 2).

CN and Speech Recognition

Pearson correlations were conducted between word recognition scores (WRS) and the VM, the ACN, the ACN/AFN, and the ACN/AIEC (Table 3). Only one significant correlation emerged between WRS_{FF} and ACN/AFN (R = 0.36, p = 0.003). At all other time points, no clear correlation was identified between the CN and WRS. Moreover, no significant correlation was identified between VM, ACN, ACN/AIEC, and WRS.

$$WRSFF = 67.2 \bullet \frac{ACN}{AFN} - 34.2 \qquad (1)$$

Subsequently, the relationship between ACN/AFN and WRS_{FF} in the aforementioned subgroup was separately examined. This correlation analysis revealed that only the AHLm group exhibited a significant correlation with WRS_{FF} (R = 0.62, p = 0.0003) (Fig. 3). The relationship between WRS_{FF} and ACN/AFN can be expressed as a linear model for prediction, as indicated in Eq. (1). The predictive accuracy of this model was estimated at 16.1 ± 10.8%.

DISCUSSION

MRI Did Not Detect CN Size Change in Patients With Postlingual Deafness

Deafness is reported to lead to changes in the CN, specifically reduce the number of spiral ganglion cells (26). The counts of the remaining spiral ganglion cell have been reported to correlate significantly with the maximum diameter

TABLE 2. *Statistical analysis of the relationship between physiological and audiological factors and CN metric*

Physiological /Audiological Variable		CN Metric	Statistical Test	Statistical Measure	p
Age		VM	Pearson correlation	$R = -0.01$	0.87
		ACN		$R = -0.04$	0.64
		ACN/AFN		$R = -0.08$	0.41
		ACN/AIEC		$R = -0.10$	0.24
Sex		VM	*t* test	$T = 1.20$	0.23
		ACN		$T = 0.05$	0.95
		ACN/AFN		$T = 1.01$	0.31
		ACN/AIEC		$T = 0.03$	0.98
Asymmetric hearing loss		VM	ANOVA	$F = 0.60$	0.55
		ACN		$F = 0.11$	0.90
		ACN/AFN		$F = 0.21$	0.81
		ACN/AIEC		$F = 0.05$	0.95
Contralateral ear (SSD)	VM	VM	*t* test	$T = 0.01$	0.99
	ACN	ACN		$T = 0.16$	0.88
	ACN/AFN	ACN/AFN		$T = 1.20$	0.24
	ACN/AIEC	ACN/AIEC		$T = 0.06$	0.78
Contralateral ear (AHLm)	VM	VM	*t* test	$T = 0.53$	0.60
	ACN	ACN		$T = 0.34$	0.73
	ACN/AFN	ACN/AFN		$T = 0.94$	0.35
	ACN/AIEC	ACN/AIEC		$T = 0.28$	0.78
Contralateral ear (AHLh)	VM	VM	*t* test	$T = 0.52$	0.60
	ACN	ACN		$T = 0.91$	0.37
	ACN/AFN	ACN/AFN		$T = 1.03$	0.31
	ACN/AIEC	ACN/AIEC		$T = 0.36$	0.72

CN indicates cochlear nerve; VM, volume of the modiolus; ACN, area of the cochlear nerve; ACN/AFN, area of the cochlear nerve normalized to the area of the facial nerve; ACN/AIEC, area of the cochlear nerve normalized to the inner ear canal area; SSD, single-sided deafness; AHLm, moderate asymmetric hearing loss; AHLh, high asymmetric hearing loss.

Copyright © 2024 Otology & Neurotology, Inc. Unauthorized reproduction of this article is prohibited.

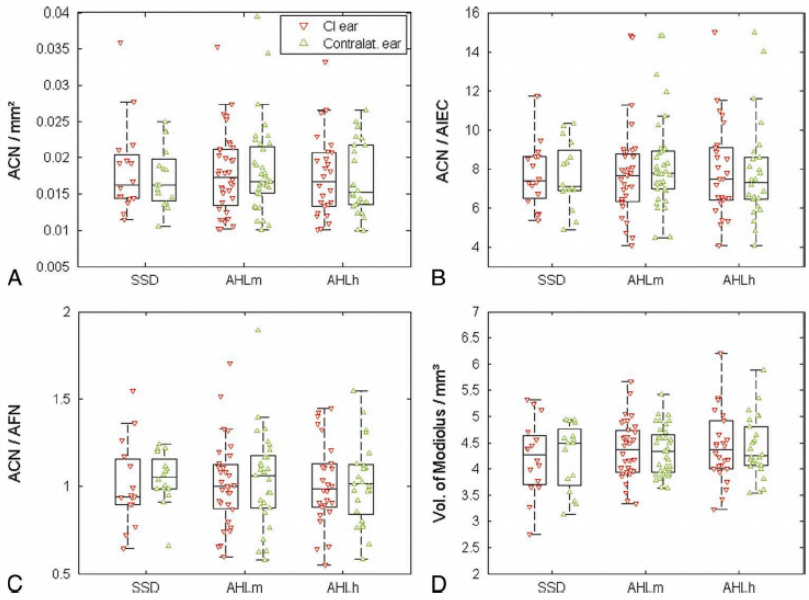


FIG. 2. Comparison of the CN between the ear with cochlear implant (CI) and the contralateral ear across the four groups with different degrees of asymmetrical hearing loss.

of the cochlear and eighth cranial nerve (27). Another study on human temporal bones has directly measured the maximum diameter of the AN in deaf patients and found that the diameter is significantly smaller than in normal hearing population (24). However, conducting histological studies in living human beings is not feasible. This raises the question whether advanced radiological techniques can detect subtle changes in the AN in the human population. In the early stages, some researchers measured the length and width of the bony CN canal using high-resolution temporal bone computed tomography (HRCT) and found them to be significantly smaller in ears with congenital hearing loss (28,29). In comparison, current MRI can directly visualize the CN, providing a more precise and accurate assessment (26,30). Despite attempts to analyze CN size with MRI in patients with hearing loss, the results are inconclusive. Russo et al. (31) reported mild hypoplasia in the CN in children with sensorineural hearing loss. Sildiroglu et al. (30) found no

TABLE 3. *Statistical analysis of the relationship between CN metric and WRS in different groups at different time points after activation of CI*

		Pearson Correlation				*p*			
WRS at Time Point	CN metric	SSD	AHLm	AHLh	Total	SSD	AHLm	AHLh	Total
First fitting	VM	0.15	−0.06	0.07	0.04	0.60	0.74	0.76	0.73
	ACN	0.22	0.03	0.10	0.09	0.44	0.87	0.67	0.47
	ACN/AFN	0.24	**0.62****	0.14	**0.36***	0.44	**0.0003**	0.533	**0.003**
	ACN/AIEC	−0.05	0.04	0.18	0.07	0.86	0.84	0.43	0.58
1 mo	VM	−0.33	−0.08	0.29	0.04	0.26	0.65	0.16	0.72
	ACN	0.22	−0.07	0.15	0.07	0.48	0.70	0.48	0.58
	ACN/AFN	−0.3	0.34	0.03	0.08	0.34	0.08	0.89	0.70
	ACN/AIEC	−0.03	−0.04	0.08	0.01	0.91	0.81	0.72	0.91
3 mo	VM	−0.21	−0.09	0.35	0.04	0.46	0.62	0.15	0.76
	ACN	0.07	−0.21	0	−0.08	0.82	0.27	0.98	0.56
	ACN/AFN	−0.43	0.11	0.29	0.05	0.14	0.60	0.24	0.70
	ACN/AIEC	−0.24	−0.15	0.13	−0.06	0.41	0.44	0.59	0.66
6 mo	VM	−0.02	0.13	0.25	0.14	0.95	0.56	0.35	0.31
	ACN	0.18	−0.09	−0.01	0.01	0.57	0.66	0.96	0.95
	ACN/AFN	−0.05	0.30	0.11	0.14	0.88	0.20	0.70	0.36
	ACN/AIEC	−0.05	−0.29	0.08	−0.10	0.89	0.17	0.76	0.48

CI indicates cochlear implant; CN, cochlear nerve; WRS, word recognition scores; VM, volume of the modiolus; ACN, area of the cochlear nerve; ACN/AFN, area of the cochlear nerve normalized to the area of the facial nerve; ACN/AIEC, area of the cochlear nerve normalized to the inner ear canal area; SSD, single-sided deafness; AHLm, moderate asymmetric hearing loss; AHLh, high asymmetric hearing loss.

Copyright © 2024 Otology & Neurotology, Inc. Unauthorized reproduction of this article is prohibited.

Downloaded from http://journals.lww.com/otology-neurotology by BhDMf5ePHKav1zEoum1tQfN4a+kJLhEZgbsIH04XMI0hCywCX1AWnYQp/IlQrHD3i3D0OdRyi7TvSFl4Cf3VC4/OAVpDDa8K2+Ya6H515kE= on 09/16/2024

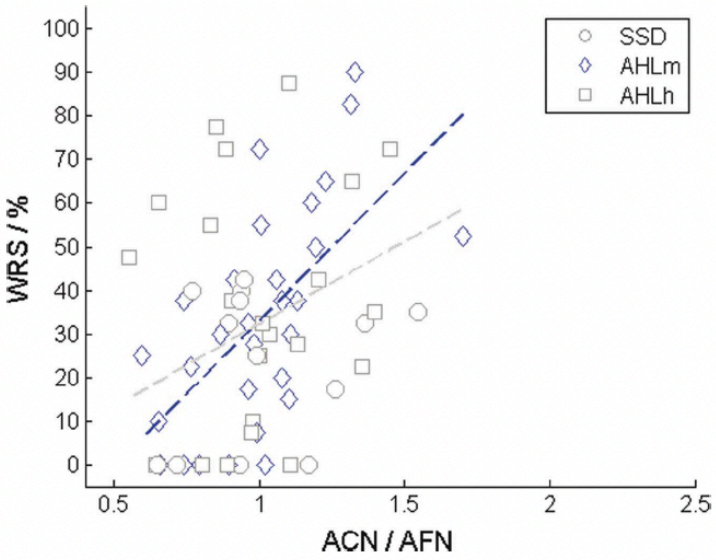


FIG. 3. Area of the CN normalized to the area of the facial nerve (ACN/AFN) and the word recognition score after the initial fitting for four groups with different degrees of asymmetrical hearing loss: single-sided deaf (gray circles), moderate asymmetric hearing loss (dark blue diamonds), and high asymmetrical hearing loss (gray squares). The Pearson correlation analyses showing a positive correlation with $R = 0.36$ in the whole group (gray dotted line) and an enhanced correlation with $R = 0.62$ in the subgroup of AHLm (dark blue dotted line).

Downloaded from http://journals.lww.com/otology-neurotology by BhDMf5ePHKav1zEoum1tQfN4a+kJLhEZgbsIHo4XMi0hCywCX1AWnYQp/IlQrHD3i3D0OdRyi7TvSFl4Cf3VC4/OAVpDDa8K2+Ya6H515kE= on 09/16/2024

significant change in CN size on MRI in patients with sensorineural hearing loss. Kim et al. (26) discovered a negative correlation between CN size and both the duration of deafness and the degree of hearing loss.

In this study, the cross-section of the CN on both sides of the same patient was measured and compared to the CN size on CI side to the contralateral one. Additionally, patients were classified into three different groups based on the degree of hearing loss on the contralateral side. The results revealed no significant differences between the two sides, considering both the absolute values and various normalized measurements, across all three groups. Therefore, it can be presumed that deviations in CN diameter are lost in the noise of the natural variation of the CN or the MRI may not be sensitive enough to detect subtle changes in the CN following postlingual deafness. One limitation of our study is the absence of clear reconstruction of the duration of deafness. It is well established that the degeneration process of the CN system takes years. To observe morphological changes in the CN through MRI, a significant amount of time may be required. This may also explain, why differences in the subgroup with single-side deafness (SSD) could not be observed. In the SSD subgroup, all patients suffered a sudden hearing loss and most underwent CI surgery approximately 6 months after the onset of deafness.

MRT Predicts Postoperative Speech Perception in CI Patients at the First Fitting Process

It is well known that the CN status directly affects the postoperative speech perception. In this study, a positive correlation between CN size and postoperative speech perception in CI patients at the first fitting process was found. Similar findings were also reported by Kim et al. (26). However, in their study, a weaker correlation was identified, possibly attributed to the lack of a precise definition of the exact time when the postoperative speech tests were conducted. In this study, it was also noted that this correlation diminished during the follow-up period. Therefore, if speech tests were administered a few weeks after CI activation, this observation might have been overlooked.

The second point that should be discussed is that the correlation was only evident in the subgroup of AHLm and not in the other groups. This may be explained by the following factors 1) In the SSD group, despite using masking noise for the normal hearing ear during the speech test of the CI ear, the normal ear may still pick up the signal sounds in the free field speech test. This suggests a potential issue with the accuracy of the speech test results for the CI ears in SSD users. 2) In the AHLh group, challenges were encountered often during the fitting process. Patients faced difficulties in performing the task, particularly due to communication difficulties during the fitting process. This issue arises because the CI processor has not been adjusted yet, and patients with AHLh also struggle with understanding speech through the contralateral ear. Therefore, it may be that the fitting process in these patients cannot always be accurately performed. Specifically, the threshold and comfortable levels might not be correctly defined, leading to suboptimal postoperative speech performance.

The main limitation of this study lies in its retrospective design. Consequently, the consistency of measurement conditions could not be maintained throughout the period under review. Factors such as variations in MRI image quality, differences

Copyright © 2024 Otology & Neurotology, Inc. Unauthorized reproduction of this article is prohibited.

in adaptation strategies, and updates to manufacturers' processors contributed to variability in this data. Additionally, standard clinical diagnostics and care evolve over time, which could have affected the interpretation of results. These limitations could be addressed more effectively in a prospective study.

Finally, it is noteworthy that the correlation, observed in both the entire group and the AHLm subgroup, diminished in the subsequent follow-up tests. A plausible explanation for this phenomenon could be attributed to the inherent plasticity of the central nervous system (32,33). A typical example involves patients with short intracochlear electrode arrays. In these cases, their implants are programed to provide electrical stimulation based on acoustic signals, extending up to two octaves below the frequencies that would typically activate that cochlear region. Over the course of several years of device usage, the patients' perceptions of electrode pitch align with the programed frequencies, deviating from those predicted based on cochlear position (34). Additionally, numerous researchers have documented that postlingually deaf implant patients exhibit normal pitch percepts (35–37).

CONCLUSION

In conclusion, the findings of this study indicate that measuring the CN size from MRI has limited predictive value for postoperative speech perceptions during CI consultations. This limitation appears to be applicable specifically to patients with moderate hearing loss on the contralateral side and only for the time of activation.

REFERENCES

1. Lee J, Nadol JB Jr., Eddington DK. Depth of electrode insertion and postoperative performance in humans with cochlear implants: a histopathologic study. *Audiol Neurootol* 2010;15:323–31.
2. Bruijnzeel H, Draaisma K, van Grootel R, et al. Systematic review on surgical outcomes and hearing preservation for cochlear implantation in children and adults. *Otolaryngol Head Neck Surg* 2016;154:586–96.
3. Blamey P, Artieres F, Başkent D, et al. Factors affecting auditory performance of postlinguistically deaf adults using cochlear implants: an update with 2251 patients. *Audiol Neurootol* 2013;18:36–47.
4. Pisoni DB, Kronenberger WG, Harris MS, Moberly AC. Three challenges for future research on cochlear implants. *World J Otorhinolaryngol Head Neck Surg* 2018;23:240–54.
5. Peng KA, Kuan EC, Hagan S, Wilkinson EP, Miller ME. Cochlear nerve aplasia and hypoplasia: predictors of cochlear implant success. *Otolaryngol Head Neck Surg* 2017;157:392–400.
6. Chung J, Jang JH, Chang SO, et al. Does the width of the bony cochlear nerve canal predict the outcomes of cochlear implantation? *Biomed Res Int* 2018;21:5675848.
7. House WV, Brackman DE. Electrical promontory testing in differential diagnosis of sensori-neural hearing impairment. *Laryngoscope* 1974;84: 2163–71.
8. Gantz BJ, Tyler RS, Knutson JF, et al. Evaluation of five different cochlear implant designs: audiologic assessment and predictors of performance. *Laryngoscope* 1988;98:1100–6.
9. Savvas E, Heslinga K, Sudermann B, et al. Prognostic factors in cochlear implantation in adults: determining central process integrity. *Am J Otolaryngol* 2020;41:102435.
10. Spies TH, Snik AF, Mens LH, van den Broek P. Ear canal electrodes versus promontory electrodes in preoperative electrical stimulation for cochlear implantation selection. *Adv Otorhinolaryngol* 1993;48:108–13.
11. Takanami T, Ito K, Yamasoba T, Kaga K. Comparison of electro-audiometry with cochlear implant in children with inner ear anomaly. *Int J Pediatr Otorhinolaryngol* 2009;73:153–8.
12. Khan S, Raine CH, Becconsall K. Comparison of a promontory stimulation test using a transtympanic needle electrode with a test using an ear canal electrode. *Ann Oto Rhinol Laryngol Suppl* 1995;166:190–2.
13. Kelly EA, Levine S, Gravel KE, Hart DL, Huang T. Utilization of nerve integrity monitor for promontory stimulation testing prior to cochlear implant. *Otol Neurotol* 2018;39:e60–2.
14. Kurasawa M, Nakamura T, Ganaha A, Nakashima T, Tono T. Electrical promontory stimulation test using a portable peripheral nerve stimulator with an ear canal electode. *Auris Nasus Larynx* 2023;51:76–81.
15. Miyasaka M, Nosaka S, Morimoto N, Taiji H, Masaki H. CT and MR imaging for pediatric cochlear implantation: emphasis on the relationship between the cochlear nerve canal and the cochlear nerve. *Pediatr Radiol* 2010;40:1509–16.
16. Yan F, Li J, Xian J, Wang Z, Mo L. The cochlear nerve canal and internal auditory canal in children with normal cochlea but cochlear nerve deficiency. *Acta Radiol* 2013;54:292–8.
17. Casselman JW, Offeciers FE, Govaerts PJ, et al. Aplasia and hypoplasia of the vestibulocochlear nerve: diagnosis with MR imaging. *Radiology* 1997;202:773–81.
18. Sennaroglu L, Bajin MD. Classification and current management of inner ear malformations. *Balkan Med J* 2017;34:397–411.
19. Valero J, Blaser S, Papsin BC, James AL, Gordon KA. Electrophysiologic and behavioral outcomes of cochlear implantation in children with auditory nerve hypoplasia. *Ear Hear* 2012;33:3–18.
20. Kutz JW Jr., Lee KH, Isaacson B, et al. Cochlear implantation in children with cochlear nerve absence or deficiency. *Otol Neurotol* 2011;32:956–61.
21. Ehrmann-Müller D, Kühn H, Matthies C, Hagen R, Shehata-Dieler W. Outcomes after cochlear implant provision in children with cochlear nerve hypoplasia or aplasia. *Int J Pediatr Otorhinolaryngol* 2018; 112:132–40.
22. Arumugam SV, Nair G, Paramasivan VK, et al. A study of outcome of pediatric cochlear implantation in patients with cochleovestibular nerve deficiency. *J Int Adv Otol* 2020;16:147–52.
23. Yamazaki H, Jaime L, Robert B, Yasushi N. Usefulness of MRI and EBAR testing for predicting CI outcomes immediately after cochlear implantation in cases with cochlear nerve deficiency. *Otol Neurotol* 2015;36:977–84.
24. Nadol JB Jr., Xu WZ. Diameter of the cochlear nerve in deaf humans: implications for cochlear implantation. *Ann Otol Rhinol Laryngol* 1992;101:988–93.
25. Fedorov A, Beichel R, Kalpathy-Cramer J, Finet J, Fillion-Robin J-C, Pujol S, Bauer C, Jennings D, Fennessy FM, Sonka M, Buatti J, Aylward SR, Miller JV, Pieper S, Kikinis R. 3D Slicer as an Image Computing Platform for the Quantitative Imaging Network. *Magn Reson Imaging* 2012;30(9):1323–41
26. Kim BG, Chung HJ, Park JJ, et al. Correlation of cochlear nerve size and auditory performance after cochlear implantation in postlingually deaf patients. *JAMA Otolaryngol Head Neck Surg* 2013;139:604–9.
27. Nadol JB Jr. Patterns of neural degeneration in the human cochlea and auditory nerve: implications for cochlear implantation. *Otolaryngol Head Neck Surg* 1997;117:220–8.
28. Teissier N, Van Den Abbeele T, Sebag G, Elmaleh-Berges M. Computed tomography measurements oft he normal and the pathologic cochlea in children. *Pediatr Radiol* 2010;40:275–83.
29. Fatterpaekar GM, Mukherji SK, Alley J, Lin Y, Castillo M. Hypoplasia of the bony canal for the cochlear nerve in patients with congenital sensorineural hearing loss: intial observations. *Radiology* 2000;215: 243–6.
30. Sildiroglu O, Cincik H, Sonmez G, et al. Evaluation of cochlear nerve size by magnetic resonance imaging in elderly patients with sensorineural hearing loss. *Radiol Med* 2010;115:483–7.
31. Russo EE, Manolidis S, Morriss MC. Cochlear nerve size evaluation in children with sensorineural hearing loss by high-resolution magnetic resonance imaging. *Am J Otolaryngol* 2006;27:166–72.
32. Irvine DR. Auditory cortical plasticity: does it provide evidence for cognitive processing in the auditory cortex? *Hear Res* 2007;229:158–70.

Copyright © 2024 Otology & Neurotology, Inc. Unauthorized reproduction of this article is prohibited.

Downloaded from http://journals.lww.com/otology-neurotology by BhDMf5ePHKav1zEoum1tQfN4a+kJLhEZgbsIHo4XMi0hCywCX1AWnYQp/IlQrHD3i3D0OdRyi7TvSFl4Cf3VC4/OAVpDDa8K2+Ya6H515kE= on 09/16/2024

33. Weinberger NM. Auditory associative memory and representational plasticity in the primary auditory cortex. *Hear Res* 2007;229(1–2):54–68.
34. Fallon JB, Irvine DR, Shepherd RK. Cochlear implants and brain plasticity. *Hear Res* 2008;238(1–2):110–7.
35. Cohen LT, Saunders E, Clark GM. Psychophysics of a prototype perimodiolar cochlear implant electrode array. *Hear Res* 2001;155:63–81.
36. Fu QJ, Shannon RV. Frequency mapping in cochlear implants. *Ear Hear* 2002;23:339–48.
37. Pfingst BE, Franck KH, Xu L, Bauer EM, Zwolan TA. Effects of electrode configuration and place of stimulation on speech perception with cochlear prostheses. *J Assoc Res Otolaryngol* 2001; 2:87–103.

Downloaded from http://journals.lww.com/otology-neurotology by BhDMf5ePHKav1zEoum1tQfN4a+kJLhEZgbsIHo4XMi0hCywCX1AWnYQp/IlQrHD3i3D0OdRyi7TvSFl4Cf3VC4/OAVpDDa8K2+Ya6H515kE= on 09/16/2024

Copyright © 2024 Otology & Neurotology, Inc. Unauthorized reproduction of this article is prohibited.

Arbeit 6:

Invited Original Study

Systematic Overestimation of the Angular Insertion Depth of Electrode Arrays in Cochlear Implantation (CI) Patients with Small Cochlea by Imaging Processing Software

*Florian Herrmann Schmidt, *Lichun Zhang, *Mats Wilhelm Glabasnia, †Daniel Schurzig, *Karsten Ehrt, ‡Daniel Cantré, *Sara Maria van Bonn-Ytrehus, *Wilma Großmann, and *Robert Mlynski

*Department of Otorhinolaryngology, Head and Neck surgery, 'Otto Körner', Rostock University Medical Center, Rostock, Germany; †MED-EL Research Center, Hannover, Germany; and ‡Institute of Diagnostic and Interventional Radiology, Pediatric Radiology and Neuroradiology, University Medical Center Rostock, Rostock, Germany

Downloaded from http://journals.lww.com/otology-neurotology by BhDMf5ePHKav1zEoum1tQfN4a+kJLhEZgbsIHo4XMi0hCywCX1AWnYQp/IlQrHD3i3D0OdRyi7TvSFl4Cf3VC1y0abggQZXdtwnfKZBYtws= on 08/04/2024

Objective: By estimating the length of the cochlear duct, commercial software algorithms intend to support CI teams by the selection of the suitable electrode array length prior to cochlear implant (CI) surgery. In the present study center, predominantly 31.5 mm flexible electrode arrays are used for patients with radiologically regular cochleae. Routinely performed postoperative Stenvers x-ray detects complete insertion in all cases. The aim of this study was to test the accuracy of the commercial software algorithm in predicting the angular insertion depths for this specific CI group with deeply inserted electrodes.
Study Design: Retrospective cohort study.
Setting: University medical center, tertiary academic referral center.
Patients: Patients undergoing a cochlear implant surgery MED-EL FLEXsoft electrode array (Synchrony2, MED-EL, Innsbruck, Austria) between January 2019 and December 2022.
Intervention: Preoperative CT images for 72 CI ears with 31.5 mm flexible electrode arrays were examined using OTOPLAN, and the maximum insertion depth (maxAID) was estimated. Postoperatively, the actual maxAID was determined through Stenvers x-ray images.
Main Outcome Measures: The preoperatively estimated maxAID demonstrated a correlation with the postoperatively measured maxAID ($R = 0.45$, $p < 0.001$) but deviated by 44.8° ± 8.4°. There is a systematic overestimation by OTOPLAN of the insertion depths for estimated values exceeding 720°. To address this, an optimal offset of 2.4 mm is identified when considering this parameter in estimating maxAID for depths exceeding 720°.
Conclusion: OTOPLAN predicts AID outcomes in CI patients but may deviate in small cochleae (CDL < 35 mm).
Key words: Angular insertion depth—Cochlear implant—Overestimation—Speech perception.

Otol Neurotol **00**:00–00, 2024.

INTRODUCTION

Cochlear implant (CI) surgery restores the hearing capability for patients with severe sensorineural hearing loss via insertion a CI array into the cochlea. The CI array stimulates spiral ganglions and/or nerve fibers, which enables the recipient to understand speech. Although the CI can significantly improve speech, some CI recipients do not achieve optimal speech recognition even after many years (1). Previous studies have shown that several demographic factors such as etiology, duration of deafness, history of hearing aid usage, age at the time of implantation, and CI experience affect the patient's postoperative speech perception (2–4). In addition, more recent studies support the hypothesis that the selection of the electrode array and the resulting insertion depth/cochlea coverage (CC) affect postoperative outcomes as well (5–19). However, the results remain inconclusive. While numerous researchers have identified a positive correlation between postoperative speech perception and insertion depth (8–18), other studies have failed to demonstrate such a correlation (5–7,16,19). In cases where deeper insertion depths were associated with better hearing outcomes, the authors mainly ascribed the better performance to the fact that the perception of low-pitched sounds could be improved by activation of the entire spiral ganglion (14,20,21). Nevertheless, it is crucial to acknowledge another factor that cannot be ignored: deep insertion can be associated with overinsertion, potentially causing an intracochlear trauma that leads to reduced speech perception (22). The question arises: which is the optimal percentage of CC leading to the optimal postoperative performances? Based on the available findings until now, both MistrÍk and Jolly (23) as well as Timm et al.

Address correspondence and reprint requests to Dr. Florian Herrmann Schmidt, Ph.D., Department of Otorhinolaryngology, Head and Neck surgery, 'Otto Körner', Rostock University Medical Center, Doberaner Strasse 137-139, D-18057, Rostock, Germany; E-mail: florian.schmidt@med.uni-rostock.de
Conflict of interest: The authors disclose no conflicts of interest.
Florian Herrmann Schmidt and Lichun Zhang equal contribution.
DOI: 10.1097/MAO.0000000000004294

© 2024, Otology & Neurotology, Inc.

Copyright © 2024 Otology & Neurotology, Inc. Unauthorized reproduction of this article is prohibited.

Downloaded from http://journals.lww.com/otology-neurotology by BhDMf5ePHKav1zEoum1tQfN4a+kJLhEZgbsIHo4XMi0hCywCX1AWnYQp/IlQrHD3i3D0OdRyi7TvSFl4Cf3VC1y0abggQZXdtwnfKZBYtws= on 08/04/2024

(24) suggested that the optimal CC should be around 80%. In those studies, however, they even do not have patients inserted with flexible 31.5-mm electrode arrays. In contrast to these studies, the majority of patients in the study center, excluding those with cochlear malformation, labyrinthitis, schwannomas, or other cochlear irregularities receive flexible 31.5-mm electrode arrays. The insertion depth reaches up to 90%, and the majority of patients achieve the expected speech perception targets of the local guideline (unpublished result feedback of the local registry). Therefore, the goal of this study is to work out the optimal CC based on the analysis of data from patients implanted with a 31.5-mm flexible electrode array.

One way to test a specific cochlear coverage for an individual patient preoperatively is the analysis of preoperative imaging data using OTOPLAN, which is a software developed by CAScination AG (Bern, Switzerland) in collaboration with MED-EL Corporation (Innsbruck, Austria). (25) The software algorithm uses the location of the user-identified modiolus (defined as the center of the modiolus in the three-dimensionally rendered cochlear view), round window and individual electrode array, individually selected by the user, to determine the angular insertion depth (AID) for each electrode plus the cochlear duct length (CDL). The AID from the most apical electrode also called maximum AID (maxAID). Based on these results, the surgeon can select an appropriate length of the electrode array preoperatively to reach a certain cochlear coverage.

The goal of the present study was to evaluate the prediction accuracy for maxAID and CDL of OTOPLAN in a population of patients with particularly deep insertions (specifically, small cochlea was inserted with a FLEXsoft array). To date, there has been limited experience in this area, as the studies known to us have only examined a small number of deeply inserted electrode arrays, with the primary focus not solely on these cases (26,27). To do so, preoperative CT images were analyzed with OTOPLAN to predict the maxAID and CC for these CI patients. The reliability of the predictions made by OTOPLAN was then checked by comparing them with the data from postoperative radiological images (x-ray in Stenvers view). Last but not least, we compared the postoperative speech perceptions at different maxAIDs and CCs were compared.

METHODS

The study was managed according to the 1964 Declaration of Helsinki. Consecutive patients of diverse age, gender, and treatments were eligible for inclusion. The local ethics committee approved this retrospective study (A 2023–0011).

Subjects

Patients were recruited out of a total of 264 CI from the local cochlear implant program at a tertiary hospital in a university medical center between January 2019 and December 2022. All patients who underwent a CI surgery in which they received a MED-EL FLEXsoft electrode array (Synchrony2, MED-EL, Innsbruck, Austria) were included in this study. Patients with comprised cochlear malformation, incomplete insertion (none), fitting after vestibular schwannoma or long-term deafness, as well as noninformative speech tests due to patient age or origin were excluded. Patient selection based on these criteria was conducted retrospectively utilizing surgery reports, physician letters, processor fitting records, and in-clinic progress documents.

OTOPLAN Predictions

The diameter (d) and the width (w) of the cochlea were measured manually in preoperatively acquired computed tomographic (CT) sequences of the temporal bone using OTOPLAN (version 1.5.0). It was shown that these parameters can be used to reliably compute the length of the lateral wall (BTL) within the basal cochlear turn according to

$$\mathrm{BTL}(d,w) = 1.18 \cdot d + 2.69 \cdot w - \sqrt{0.72 \cdot d \cdot w} \quad (1)$$

By making use of the average offset between lateral wall and organ of Corti of $\Delta r_{OC} = 0.5$ mm as well as the linear relationship between the organ of Corti's basal turn length (BTL_{OC}) and the total CDL (28), Eq. 1 is utilized within OTOPLAN to estimate the length of the cochlear duct (estCDL) according to

$$\mathrm{estCDL} = 1.71 \cdot \mathrm{BTL}(d - 2 \cdot \Delta r_{oc}, w - 2 \cdot \Delta r_{oc}) + 0.18 + \mathrm{HRL} \quad (2)$$

where HRL describes the average hook region length of 2.5 mm (29). The maxAID of a specific electrode array is then being calculated assuming that the trajectory of the electrode array runs directly adjacent to the lateral wall, with a distance equal to the average radius of the electrode array $r_E = 0.35$ mm (28). Furthermore, the length of the array needs to be taken into account: the FLEXsoft, which was the electrode array we focused on in this study, has a total length of $L_E = 31.5$ mm; however, it must be considered that the electrode tip is neither responsible for electrical stimulation nor can it be identified in clinical imaging data because of that the tip length L_{tip} is commonly subtracted for coverage calculations (30). In case of the FLEXsoft array, this tip length 1.2 mm. Based on these requirements, OTOPLAN calculates a "percent basal turn length" ($p_{\mathrm{BTL,c1}}$) value according to

$$p_{\mathrm{BTL,c1}} = \frac{L_E - L_{tip}}{\mathrm{BTL}(d - 2 \cdot \Delta r_E, w - 2 \cdot \Delta r_E)} \quad (3)$$

The final key to derive the maxAID and CC values is a correlation between pBTL values and cochlear angular values Θ incorporated in OTOPLAN, which can also be approximately defined by using the following polynomial function (25):

Copyright © 2024 Otology & Neurotology, Inc. Unauthorized reproduction of this article is prohibited.

$$p_{BTL} = 8.3 \cdot 10^{-8}\theta^3 - 2.4 \cdot 10^{-4}\theta^2 + 3.4 \cdot 10^{-1}\theta + 3.7 \quad (4)$$

Using this correlation, OTOPLAN can look up which angular value Θ corresponds to the previously calculated value of $p_{BTL,cl}$. That specific value corresponds to the predicted maxAID of the array. Furthermore, the value is used to predict the CC achieved by the array according to the following equation (25):

$$\text{estCC} = \frac{p_{BTL,cl}\,\text{BTL}(d - 2 \cdot \Delta r_{oc}, w - 2 \cdot \Delta r_{oc})}{\text{estCDL}}. \quad (5)$$

Evaluation of the X-ray Images According to Stenvers

The via OTOPLAN estimated maxAID was validated by comparing it with the maxAID_{post} determined from postoperatively acquired x-ray imaging using the Stenvers method (31,32). Initially, the positions of the electrodes were determined, followed by estimating the position of the modiolus at the center of the resulting spiral. The position of the round window (RW) was defined based on the orientation of the vestibular organ. Subsequently, the maxAID was calculated by summing the angles relative to the modiolus, starting from RW = 0° (Fig. 1).

In order to convert this maxAID_{post} value into CC, the correlation of pBTL and cochlear angular values Θ (Eq. 5) was employed to derive the $p_{BTL,post}$ value corresponding to the postoperatively assessed angular insertion depth maxAID_{post}. Finally, the actual CC of the inserted electrode array could be calculated as

$$\text{CC} = \frac{p_{BTL,post}\text{BTL}}{\text{estCDL}} \quad (7)$$

Model Optimization

The dataset investigated in this study focuses on fully inserted electrode flex electrode arrays where the insertion depth extends far into the second and in some cases even into the third turn of the cochlea. This is highly relevant as development and validation of the models implemented into OTOPLAN were mostly conducted within an insertion angle range of up to 1.5 cochlear turns only (25,33,34). Consequently, there is a likelihood of deviations in the estimation of electrode positions above 1.5 turns. While adjustments to the model are reasonable, they should primarily address the parameters related to electrode position rather than the cochlea-scaling model itself. The position of the electrode array within the model is significantly affected by two factors: the distance of the electrode array from the lateral wall (r_E) and the length of the electrode array within the cochlea (L_E). In OTOPLAN, as indicated in the study by Alexiades et al. (28), the recommended position for the electrode array is presumed to be as lateral as feasible. Specifically, the distance from the lateral wall to the center of the electrode array is restricted to the mean radius r_E of the electrode array. It is essential to note that deviations in the estimated insertion depths determined by OTOPLAN may only be underestimated due to this initial assumption. If there is an overestimation in the insertion depth, the distance to the lateral wall can be ruled out as the contributing factor. As a result, both the distance to the lateral wall and the round window off sett can be modified to achieve a better fitting model (Eq. 5).

$$p_{BTL} = \frac{L_E - \alpha}{\text{BTL}(d - 2 \cdot r_E, w - 2 \cdot r_E)} \quad (5)$$

The parameter α in this context represents the offset between the occlusion ring of the electrode array and the round window (RW). A negative value of α indicates that the occlusion ring is positioned inside the cochlea, while a positive value of α indicates that the occlusion ring does not directly close onto the RW. This offset is influenced by surgical parameters, i.e., the extend of drilling the bony overhangs of the round window niche plainly to the level of the round window membrane or not (Fig. 2) or the position of a cochleostomy.

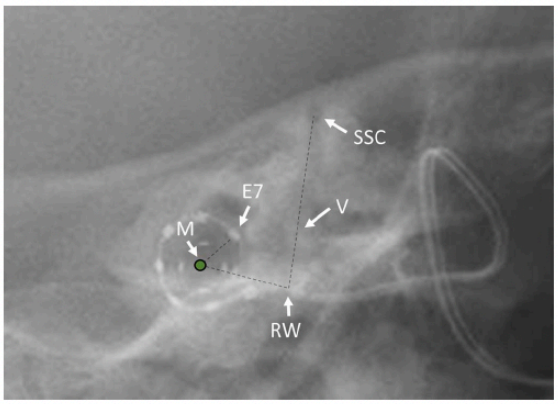


FIG. 1. Postoperative x-ray image (Stenvers) to determine the insertion angle illustrated with the example of electrode 6 from a FLEXsoft electrode array; SSC indicates superior semicircular canal; V, vestibule; M, modiolus; 0°, position round window (RW).

Copyright © 2024 Otology & Neurotology, Inc. Unauthorized reproduction of this article is prohibited.

Downloaded from http://journals.lww.com/otology-neurotology by BhDMf5ePHKav1zEoum1tQfN4a+kJLhEZgbsIHo4XMi0hCywCX1AWnYQp/IlQrHD3i3D0OdRyi7TvSFl4Cf3VC1y0abggQZXdtwnfKZBYtws= on 08/04/2024

Downloaded from http://journals.lww.com/otology-neurotology by BhDMf5ePHKav1zEoum1tQfN4a+kJLhEZgbsIHo4XMi0hCywCX1AWnYQp/IlQrHD3i3D0OdRyi7TvSFl4Cf3VC1y0abggQZXdtwnfKZBYtws= on 08/04/2024

Audiological Parameters

For all ears, speech recognition was evaluated 6 months after the initial fitting of the processor by measuring the word recognition score (WRS_{65}(CI)) using the Freiburg monosyllable test at 65 dB [SPL] in a quiet environment. To assess the impact of the surgical intervention on the sense of balance, the clinical documents of each patient and the physician's letters from the postoperative period until the initial activation of the processor were carefully reviewed. The occurrence of nystagmus was used as a criterion to identify cases of vertigo associated with the surgical intervention.

Statistical Analysis

To assess the quality of the estimated maxAID, the Pearson correlation was initially calculated between the estimated maxAID obtained from OTOPLAN and the $maxAID_{post}$ obtained from the x-rays. Subsequently, the residuals were examined. The mean absolute value of the residuals was used as an indicator of the accuracy of the estimate. To test for potential over- or underestimation by OTOPLAN, a Kolmogorov–Smirnov test was conducted, assuming the null hypothesis of normally distributed residuals at a significance level of 0.05. If the null hypothesis was rejected, the skewness of the distribution was calculated. A skewness value greater than 0.5 or less than −0.5 was considered to indicate a measurable asymmetry in the distribution. In order to obtain a more accurate understanding of the variations in the estimated insertion depth provided by OTOPLAN, the differences between the estimated maxAID and the measured $maxAID_{post}$ were computed for each ear. The complete dataset was subsequently organized according to the estimated maxAID, with group intervals of 25° ranging from 625° to 775°. Two additional groups were formed to account for lower and higher insertion depths. Following this categorization, differences in deviations between estimation and measurement within each group were analyzed using the Kruskal–Wallis test. Post hoc comparisons between groups were then conducted using the Dunn test.

The model optimization was conducted by systematically adjusting the optimization parameters within a physiologically reasonable range. A range of 0 to 5 mm for the RW-offset α was selected throughout the parameter variation process. The root-mean-square-error (RMSE) between the estimated maxAID and the measured maxAID was collected as an indicator of the estimation quality.

To examine the impact of CC on speech understanding, the ears were divided into six groups based on estimated CC. Four of the groups ranged from 78.5% to 87.5% with a group width of 2.5%. The two extreme groups consisted of ears with CC values below 78.5% and above 85%. Group differences were analyzed using the Kruskal–Wallis test, followed by post hoc analysis using the Dunn test. The same procedure was applied to the maxAID determined from postoperative measurements.

RESULTS

Seventy-two ears were included in the analysis. The age of the patients ranged from 20.2 to 90.2 years, with a mean age of 64.9 years. Among them, 37 ears were from females and 35 ears were from males.

Comparison of Angular Insertion Depths

The cochlear size parameters (diameter d and width w) determined using OTOPLAN were $d = 9.17 \pm 0.47$ mm (mean ± standard deviation) and $w = 6.89 \pm 0.37$ mm (mean ± standard deviation). The estCDL calculated from this ranged from 31.6 to 41.1 mm, with a mean of 36.2 ± 1.93 mm. For maxAID, the estimation by OTOPLAN resulted in preoperative maxAID ($maxAID_{pre}$) = 689.6° ± 59.1°, and for the evaluated x-rays, $maxAID_{post}$ = 673.4° ± 43.7°. The preoperatively estimated maxAID showed a highly significant correlation with the postoperatively measured maxAID ($R = 0.45$, $p < 0.001$), with a difference of ΔmaxAID = 44.8° ± 8.4° (Fig. 3A). The distribution of the residuals indicated a non-normal distribution with a skewness of $s = -0.45$, suggesting a trend of overall overestimation in maxAID preoperatively. To further investigate this, the residuals were organized according to the estimated maxAID, with group intervals of 25° ranging from 625° to 775° (Fig. 3B). The Kruskal–Wallis test uncovered highly significant differences across the groups ($p < 0.001$). In the post hoc analysis employing the Dunn's test, noteworthy distinctions were identified, specifically between

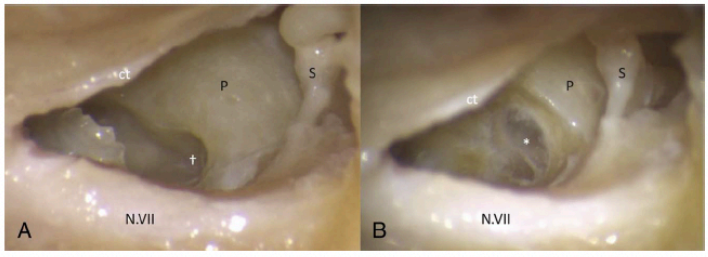


FIG. 2. Surgical access to the round window using a posterior tympanotomy (N.VII indicates facial nerve; ct, chorda tympani; P, promontory; †, round window niche; *, round window membrane). *(A)* Surgical situation with minimal exposure of the round window with the electrode occlusion ring (not visible) positioned offset the round window membrane approximately 1 diameter of the promontory wall. *(B)* Fully exposed round window membrane with the possibility to position the occlusion ring inside the round window without offset to the round window membrane.

Copyright © 2024 Otology & Neurotology, Inc. Unauthorized reproduction of this article is prohibited.

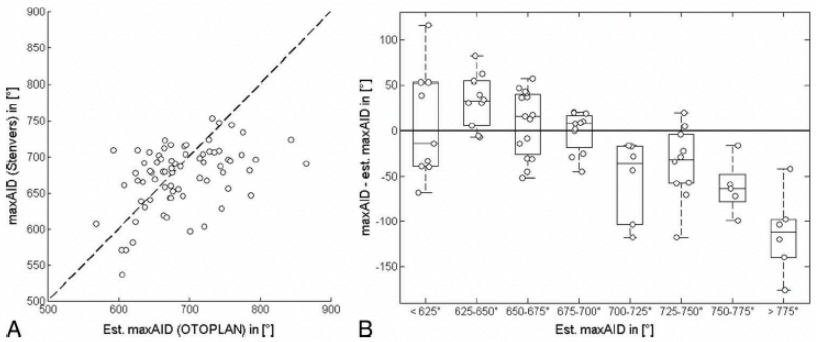


FIG. 3. (*A*) Scatter plot illustrating the relationship between estimated and measured maxAID. (*B*) Deviations of the estimated maxAID from the measured values, grouped by estimated insertion depth. Predictions within the 700°–725° range and at deeper insertion depths reveal a progressively greater deviation from the actually measured maxAID. The negative deviation signifies an overestimation.

the 625° and the 650° group and the groups with insertion depths surpassing 700° (see Table 1 for details). As deviations notably increase (in a negative direction) starting from the group with insertion depths between 700° and 725°, it suggests an overestimation by OTOPLAN, primarily due to estimated maxAID values exceeding second turn of the cochlea (i.e., maxAID >720°).

Model Optimization

In light of the present findings indicating OTOPLAN's propensity to overestimate rather than underestimate insertion depths, altering the distance of the electrode array to the lateral wall does not yield physiologically meaningful values. This limitation is attributed to OTOPLAN's aforementioned assumption of a minimum distance.

Hence, adjustments were made solely to the RW-offset. Based on the determined critical maxAID, adjusting the RW-offset for estimated maxAID >720° resulted in an optimal correction of correction of $\alpha = 2.4$ mm (Fig. 4A). The accuracy of the RW-corrected estimated maxAID related to the postoperatively measured maxAID and resulted in an improved accuracy of ΔmaxAID = 36° ± 5.8° (Fig. 4B).

Speech Recognition and vertigo

The patients obtained a WRS_{65}(CI) value of 71.74 ± 14.87%. When comparing the WRS_{65}(CI) between the divided groups (Fig. 5A), based on the CC, no significant differences in speech recognition were observed (Kruskal–Wallis: $\chi^2 = 4.6$, $p = 0.33$). Similarly, after dividing the groups based on the postoperatively determined maxAID (Fig. 5B), no significant difference was found (Kruskal–Wallis: $\chi^2 = 1.65$, $p = 0.80$). When investigating the impact of insertion depth on postoperative vertigo, there was no significant difference in maxAID between patients with and without vertigo ($T = 1.79$, $p = 0.08$).

DISCUSSION

Accuracy of Using OTOPLAN to Estimate the maxAID

OTOPLAN is a user-friendly commercial software designed for preoperative prediction of the insertion depth of the electrode arrays developed by MED-EL. This study presented two main findings: 1) OTOPLAN exhibits very high accuracy for the larger cochleae (i.e., CDL > 35 mm); 2) OTOPLAN consistently overestimates AID for the smaller cochleae (i.e., CDL < 35 mm). Nevertheless, overestimation was only observed in these data when the length of the basal turn was so small that the estimation by OTOPLAN for the AID extended beyond the second turn.

Currently, there are no standard criteria for preoperatively selecting the electrode array using OTOPLAN. However, it is generally suggested that when the tip of the electrode array extends beyond the second turn, a shorter electrode should be chosen. This suggestion coincidently aligns with the findings from previous studies that focus on the optimal insertion depth of the electrode array in CI patients. These studies have indicated that the optimal insertion depth should not exceed the second turns of the cochlea (18,35,36). This

TABLE 1. *Group comparisons between estimated and measured maxAID were conducted using a post hoc Dunn's test, and the p*-values were presented as follows: * $p < 0.05$; ** $p < 0.001$

Dunn's Test	<625°	625°–650°	650°–675°	675°–700°	700°–725°	725°–750°	750°–775°	>775°
<625°	–	0.83	0.99	1	0.53	0.73	0.29	0.02*
625°–650°	0.83	–	0.93	0.77	0.03*	0.03*	0.009*	0.0001**
650°–675°	0.99	0.93	–	0.99	0.22	0.32	0.09	0.002*
675°–700°	1	0.77	0.99	–	0.51	0.71	0.28	0.02*
700°–725°	0.53	0.03*	0.22	0.51	–	0.99	0.99	0.94
725°–750°	0.73	0.03*	0.32	0.71	0.99	–	0.98	0.59
750°–775°	0.29	0.009*	0.09	0.28	0.99	0.98	–	0.99
>775°	0.02*	0.0001**	0.002*	0.02*	0.94	0.59	0.99	–

Copyright © 2024 Otology & Neurotology, Inc. Unauthorized reproduction of this article is prohibited.

Downloaded from http://journals.lww.com/otology-neurotology by BhDMf5ePHKav1zEoum1tQfN4a+kJLhEZgbsIHo4XMi0hCywCX1AWnYQp/IlQrHD3i3D0OdRyi7TvSFl4Cf3VC1y0abggQZXdtwnfKZBYtws= on 08/04/2024

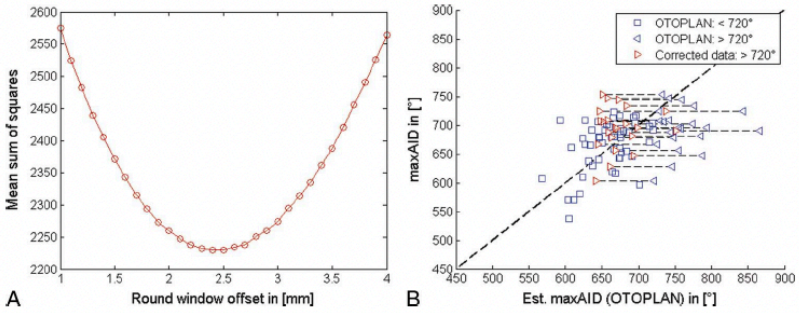


FIG. 4. Optimization of the estimation of maximum insertion depth (maxAID) using OTOPLAN involved adjusting the offset on the round window (RW). (*A*) Depicts the deviation between estimated and measured maxAID after fine-tuning the RW-offset, with the optimum at 2.4 mm. (*B*) Presents a scatter plot illustrating the relationship between estimated and measured maxAID, categorized as Est. maxAID <720° (*blue squares*), Est. maxAID >720° (*blue triangles* pointing left), and maxAID >720° after correction using the optimal RW-offset (*red triangles* pointing right).

recommendation might be based on the consideration that deeper insertions challenge the surgeon's surgical technique and may carry the risk of damaging spiral neurons in the cochlea, as also presumed in aforementioned studies (18,22). However, this assumption fails to address the question of why OTOPLAN is not suitable for predicting AID when the electrode array extends beyond the second turn of the cochlea—specifically, why OTOPLAN overestimates the insertion depth in small cochlear. Where does the system make faulty predictions?

The primary reason for this phenomenon could be the lack of precision in postoperative imaging in our study, mainly due to the two-dimensional representation of the electrode array in x-ray imaging. This is indeed a valid concern, which is why computed tomography imaging is considered the gold standard in such cases. Factors such as head rotation (37) or interobserver variability (38) introduce bias into the measured AIDs. The notable difference between the preoperative AID estimate by OTOPLAN and the postoperatively determined AID from x-rays is likely not solely due to the preoperative estimate but also to the postoperative measurement. However, the measurement error from x-rays does not fully explain the consistent overestimation observed in cases with small cochleae; it merely contributes to general variability regardless of insertion depth. Therefore, it is unlikely that postoperative imaging alone is the decisive factor for the overestimation of insertion depth identified in this study.

It can be posited that one possible explanation for the overestimation could be attributed to the distance between occlusion ring of the electrode array and the round window, which could be referred to as round window offset (RW-offset). In a smaller cochlea, the diameter of the round window may be smaller than the diameter of the occlusion ring of the electrode array. Therefore, even with the electrode array fully inserted during surgery, the occlusion ring may still remain outside the round window niche, increasing the distance between occlusion ring and the round window membrane. This slight extension of the electrode array beyond the cochlea is not taken into account in the AID calculation by OTOPLAN, therefore maybe resulting in an overestimation.

Regarding the accuracy of OTOPLAN in predicting the AID in CI patients, a previous study has also identified predictive deviations that increased from the base to the apex, particularly noting larger deviations for longer electrode arrays (33). This observation can be attributed to the spiral shape of the cochlea because the radius of the cochlea decreases from the base to the apex, causing small changes in length to be more prominently reflected angularly (33).

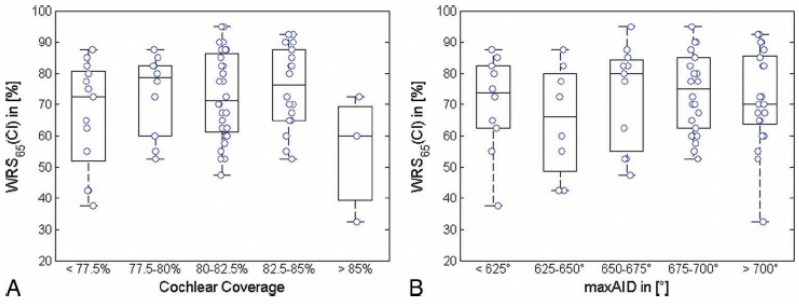


FIG. 5. Box plots depict the WRS across cochlear coverage (*A*) and maxAID (*B*), each subdivided into smaller sections according to the corresponding coverage or insertion depth.

Copyright © 2024 Otology & Neurotology, Inc. Unauthorized reproduction of this article is prohibited.

Downloaded from http://journals.lww.com/otology-neurotology by BhDMf5ePHKav1zEoum1tQfN4a+kJLhEZgbsIHo4XMi0hCywCX1AWnYQp/IlQrHD3i3D0OdRyi7TvSFl4Cf3VC1y0abggQZXdtwnfKZBYtws= on 08/04/2024

Downloaded from http://journals.lww.com/otology-neurotology by BhDMf5ePHKav1zEoum1tQfN4a+kJLhEZgbsIHo4XMi0hCywCX1AWnYQp/IlQrHD3i3D0OdRyi7TvSFl4Cf3VC1y0abggQZXdtwnfKZBYtws= on 08/04/2024

In their study, the longest electrode array that was examined had a length of 28 mm. By contrast, this present study has exclusively involved CI patients with FLEXsoft electrode arrays (31.5 mm). Hence, here insertion depth regions where the sensitivity of the AID estimation is significantly greater are explored. A mere 1-mm alteration in insertion depth can lead to an apical change in AID exceeding 40° (39). This substantiates the hypothesis that minor shifts at the RW can exert a substantial influence on the AID, particularly in a smaller cochlea.

Another theory regarding the suspected increase in RW-offset could be possible postoperative electrode migration out of the cochlea after insertion. However, this possibility can be ruled out by the surgical technique: all electrode carriers were fixed using a fixation clip (MED-EL, Innsbruck, Austria) between the buttress and the electrode intraoperatively, which was demonstrated previously (40).

To address the overestimation of AID by OTOPLAN in a small cochlea, a revised RW-offset of 2.4 mm was identified and implemented in the model for cochleae with a CDL < 35 mm. Consequently, the preoperative deviation significantly decreased after integrating this new value. However, it is important to note that the assumption regarding the RW-offset has not been validated in this study. A study specifically designed to measure the RW-offset should be conducted in prospective settings to validate this hypothesis. In addition to high-resolution postoperative radiological imaging, this study could incorporate intraoperative position measurements of the occlusion ring using 3D microscopy.

Another potential explanation for the overestimation could be the lateral wall offset. The estimation of the electrode position by OTOPLAN is based on the assumption that the electrode array is positioned directly adjacent to the lateral wall, and the software applies a constant value of 0.35 mm for AID calculation. However, a previous study found that the intracochlear position of the electrode array in relation to the lateral wall is not consistently aligned: electrode contact with the lateral wall starts approximately at 180° insertion depth, and the tip of the electrode array consistently faces the modiolar wall (41). Therefore, a fixed value of 0.35 mm as it was assumed in OTOPLAN is imprecise and may lead to predictive AID deviations. A model incorporating the real trajectory of the CI array, specifically a variable offset to the lateral wall, would reduce the predictive deviation (42). This aspect requires further investigation in future studies.

Last but not least, Schurzig et al. (43) have revealed that while the first turns of two cochleae may be very similar, significant variability exists in the second turns. This implies the fact that OTOPLAN is solely relying on information from the first turn may lead to considerable predictive deviations. To minimize such deviations, a more effective model based on individual cochlear anatomy should be employed.

Speech Perception in Patients with High Cochlear Coverage

According to previous publications, improvements in speech perception among CI patients are associated with increased insertion depth and electrode length (8,17,44). Deeper insertions lead to a smaller mismatch between the natural tonotopic frequency distribution in the cochlea and that imposed by the implanted electrode array (21,31). However, in this study, there were no significant differences in postoperative speech perception among the various groups, classified either with CC or max AID. Upon closer examination of the data, certain trends emerge: 1) the best performances were observed in patients with a CC around 80–85%; 2) postoperative performances declined when the CC exceeded 85%. These findings align with those of previous publications (23,24). In their reports, optimal CC values were found around 80%, and performance declined with further deep insertion (23,24). Many previous investigations attributed the reduced postoperative speech perception in more deeply inserted CIs to damage to intracochlear neuron structures, often encountered when surgeons faced challenges or resistance during the insertion of longer electrode arrays (22). By contrast, the present surgical technique in the study center did not encounter any issues when inserting the 31.5-mm flexible electrode array (FLEXsoft) during surgery for those patients. Therefore, surgical damage to intracochlear neuron structures seems unlikely. On the other hand, it is also known that the scala tympani is very narrow in the apical region. Clearly, the electrode array in this area makes very close contact to the intracochlear neuron structures. In the Salcher model, it can be observed how this close contact potentially causes the electrode to migrate away from the lateral wall toward the modiolus (41). This might indeed lead the changes in intracochlear neuron structures, affecting the performance. A temporal bone study focusing on changes in intracochlear neuron structures after the implantation of the FLEXsoft electrode array could provide answers to this question.

Moreover, a recent study utilizing synchrotron radiation phase-contrast imaging of the cochlea revealed that the spiral ganglion cells converge and form a strand in the modiolus toward the end of the second cochlear turn (45). In CI patients with deeply inserted electrode arrays, the neurons in this strand make multiple contacts with the electrodes simultaneously. If the electrodes fire concurrently, it can lead to pitch confusion for CI patients and result in a reduction in speech perception. Particular focus on pitch fitting apical electrodes might be necessary.

CONCLUSION

OTOPLAN can be used to predict AID in CI Patients. However, it exhibits a systematic deviation in individuals with small cochleae, i.e., CDL <35 mm. The potential cause for this overestimation could be the increased distance between the closely positioned ring of the CI electrode array and the round window, specifically the RW-offset. Postoperative speech perception for CI arrays with deeper insertion did not show any statistically significant differences in the current study setting. Nevertheless, the trend indicates that the optimal performance for CI patients is around 80–85%, with the speech perception decreasing with deeper insertion.

Copyright © 2024 Otology & Neurotology, Inc. Unauthorized reproduction of this article is prohibited.

REFERENCES

1. Boisvert I, Reis M, Au A, Cowan R, Dowell RC. Cochlear implantation outcomes in adults: a scoping review. *PLoS One* 2020;15:e0232421.
2. Lee J, Nadol JB Jr., Eddington DK. Depth of electrode insertion and postoperative performance in humans with cochlear implants: a histopathologic study. *Audiol Neurootol* 2010;15:323–31.
3. Blamey P, Artieres F, Başkent D, et al. Factors affecting auditory performance of postlinguistically deaf adults using cochlear implants: an update with 2251 patients. *Audiol Neurootol* 2013;18:36–47.
4. Pisoni DB, Kronenberger WG, Harris MS, Moberly AC. Three challenges for future research on cochlear implants. *World J Otorhinolaryngol Head Neck Surg* 2018;23:240–54.
5. Holden LK, Finley CC, Firszt JB, et al. Factor affecting open-set word recognition in adults with cochlear implants. *Ear Hear* 2013;34: 342–60.
6. Lazard DS, Vincent C, Venail F, et al. Pre-, per- and postoperative factors affecting performance of postlinguistically deaf adults using cochlear implants: a new conceptual model over time. *PLoS One* 2012;7:e48739.
7. Finley CC, Holden TA, Holden LK, et al. Role of electrode placement as a contributor to variability in cochlear implant outcomes. *Otol Neurotol* 2008;29:920–8.
8. O'Connell BP, Hunter JB, Haynes DS, et al. Insertion depth impacts speech perception and hearing preservation for lateral wall electrodes. *Laryngoscope* 2017;127:2352–7.
9. Morrel WG, Holder JT, Dawant BM, Noble JH, Labadie RF. Effect of scala tympani height on insertion depth of straight cochlear implant electrodes. *Otolaryngol Head Neck Surg* 2020;162:718–24.
10. Buchman CA, Dillon MT, King ER, et al. Influence of cochlear implant insertion depth on performance: a prospective randomized trial. *Otol Neurotol* 2014;35:1773–9.
11. Hochmair I, Arnold W, Nopp P, et al. Deep electrode insertion in cochlear implants: apical morphology, electrodes and speech perception results. *Acta Otolaryngol* 2003;123:612–7.
12. O'Connell BP, Cakir A, Hunter JB, et al. Electrode location and angular insertion depth are predictors of audiologic outcomes in cochlear implantation. *Otol Neurotol* 2016;37:1016–23.
13. Yukawa K, Cohen L, Blamey P, et al. Effects of insertion depth of cochlear implant electrodes upon speech perception. *Audiol Neurootol* 2004;9:163–72.
14. Canfarotta MW, Dillon MT, Buss E, et al. Frequency-to-place mismatch: characterizing variability and the influence on speech perception outcomes in cochlear implant recipients. *Ear Hear* 2020; 41:1349–61.
15. Hamzavi J, Arnoldner C. Effect of deep insertion of the cochlear implant electrode array on pitch estimation and speech perception. *Acta Otolaryngol* 2006;126:1182–7.
16. Helbig S, Adel Y, Rader T, Stöver T, Baumann U. Long-term hearing preservation outcomes after cochlear implantation for electric-acoustic stimulation. *Otol Neurotol* 2016;37:e353–9.
17. Büchner A, Illg A, Majdani O, Lenarz T. Investigation of the effect of cochlear implant electrode length on speech comprehension in quiet and noise compared with the results with users of electro-acoustic-stimulation, a retrospective analysis. *PLoS One* 2017;12:e0174900.
18. Weller T, Timm ME, Lenarz T, Büchner A. Cochlear coverage with lateral wall cochlear implant electrode arrays affects post-operative speech recognition. *PLoS One* 2023;18:e0287450.
19. Mlynski R, Luesebrink A, Oberhoffner T, Langner S, Weiss NM. Mapping cochlear duct length to electrically evoked compound action potentials in cochlear implantation. *Otol Neurotol* 2021;42:e254–60.
20. Faulkner A, Rosen S, Norman C. The right information may matter more than frequency-place alignment: simulations of frequency-aligned and upward shifting cochlear implant processors for a shallow electrode array insertion. *Ear Hear* 2006;27:139–52.
21. Landsberger DM, Svrakic M, Roland T Jr., Svirsky M. The relationship between insertion angles, default frequency allocations and spiral ganglion place pitch in cochlear implants. *Ear Hear* 2015;36:e207–13.
22. Kamakura T, Nadol JB. Correlation between word recognition score and intracochlear new bone and fibrous tissue after cochlear implantation in the human. *Hear Res* 2016;339:132–41.
23. Mistrík P, Jolly C. Optimal electrode length to match patient specific cochlear anatomy. *Eur Ann Otorhinolaryngol Head Neck Dis* 2016; 133:S68–71.
24. Timm ME, Majdani O, Weller T, et al. Patient specific selection of lateral wall cochlear implant electrodes based on anatomical indication ranges. *PLoS One* 2018;13:e0206435.
25. Schurzig D, Timm ME, Batsoulis C, et al. A novel method for clinical cochlear duct length estimation toward patient-specific cochlear implant selection. *OTO Open* 2018;2:2473974X18800238.
26. Yoshimura H, Watanabe K, Nishio S, Takumi Y, Usami S. Determining optimal cochlear implant electrode array with OTOPLAN. *Acta Otolaryngol* 2023;143:748–52.
27. Breitsprecher T, Mlynski R, Voelter C, et al. Accuracy of preoperative cochlear duct length estimation and angular insertion depth prediction. *Otol Neurotol* 2023;44:e566–71.
28. Alexiades G, Dhanasingh A, Jolly C. Method to estimate the complete and two-turn cochlear duct length. *Otol Neurotol* 2015;36:904–7.
29. Helpard L, Li H, Rohani SA, et al. Three-dimensional modeling and measurement of the human cochlear hook region: considerations for tonotopic mapping. *Otol Neurotol* 2021;42:e658–65.
30. Schurzig D, Timm ME, Batsoulis C, John S, Lenarz T. Analysis of different approaches for clinical cochlear coverage evaluation after cochlear implantation. *Otol Neurotol* 2018;39:e642–50.
31. Rader T, Döge J, Adel Y, Weissgerber T, Baumann U. Place dependent stimulation rates improve pitch perception in cochlear implantees with single-sided deafness. *Hear Res* 2016;339:94–103.
32. Xu J, Xu SA, Cohen LT, Clark GM. Cochlear view: postoperative radiography for cochlear implantation. *Am J Otol* 2000;21:49–56.
33. Avallone E, Lenarz T, Timm ME. On the accuracy of clinical insertion angle predictions with a surgical planning platform for cochlear implantation. *Otol Neurotol* 2021;42:e1242–9.
34. Mertens G, Van Rompaey V, Van de Heyning P, Gorris E, Topsakal V. Prediction of the cochlear implant electrode insertion depth: clinical applicability of two analytical cochlear models. *Sci Rep* 2020;10:3340.
35. Canfarotta MW, Dillon MT, Brown KD, et al. Insertion depth and cochlear implant speech recognition outcomes: a comparative study of 28- and 31.5-mm lateral wall arrays. *Otol Neurotol* 2022;43:183–9.
36. Helbig S, Adel Y, Leinung M, et al. Hearing preservation outcomes after cochlear implantation depending on the angle of insertion: indication for electric or electric-acoustic stimulation. *Otol Neurotol* 2018;39:834–41.
37. Svrakic M, Friedmann DR, Berman PM, et al. Measurement of cochlear implant electrode position from intraoperative post-insertion skull radiographs: a validation study. *Otol Neurotol* 2015;36:1486–91.
38. Sokolov M, Zavdy O, Raveh E, et al. Assessment of angular insertion-depth of bilateral cochlear implants using plain x-ray scans. *Otol Neurotol* 2020;41:1363–8.
39. Escudé B, James C, Deguine O, et al. The size of the cochlea and predictions of insertion depth angles for cochlear implant electrodes. *Audiol Neurootol* 2006;11(Suppl 1):27–33.
40. Zhang L, Schmidt F, Oberhoffner T, et al. Transimpedance matrix can be used to estimate electrode positions intraoperatively and to monitor their positional changes postoperatively in cochlear implant patients. *Otol Neurotol* 2024;45:e289–96.
41. Salcher R, Boruchov A, Timm M, et al. On the intracochlear location of straight electrode arrays after cochlear implantation: how lateral are lateral wall electrodes? *Otol Neurotol* 2021;42:242–50.
42. Schurzig D, Repp F, Timm ME, et al. Virtual cochlear implantation for personalized rehabilitation of profound hearing loss. *Hear Res* 2023; 429:108687.
43. Schurzig D, Pietsch M, Erfurt P, et al. A cochlear scaling model for accurate anatomy evaluation and frequency allocation in cochlear implantation. *Hear Res* 2021;403:108166.
44. Roy AT, Penninger RT, Pearl MS, et al. Deeper cochlear implant electrode insertion angle improves detection of musical sound quality deterioration related to bass frequency removal. *Otol Neurotol* 2016;37:146–51.
45. Li H, Helpard L, Ekeroot J, et al. Three-dimensional tonotopic mapping of the human cochlea based on synchrotron radiation phase-contrast imaging. *Sci Rep* 2021;11:4437.

Copyright © 2024 Otology & Neurotology, Inc. Unauthorized reproduction of this article is prohibited.

Downloaded from http://journals.lww.com/otology-neurotology by BhDMf5ePHKav1zEoum1tQfN4a+kJLhEZgbsIHo4XMi0hCywCX1AWnYQp/IlQrHD3i3D0OdRyi7TvSFl4Cf3VC1y0abggQZXdtwnfKZBYtws= on 08/04/2024

Arbeit 7:

frontiers | Frontiers in Neuroscience

TYPE Original Research
PUBLISHED 26 February 2025
DOI 10.3389/fnins.2025.1559141

Check for updates

OPEN ACCESS

EDITED BY
Achim Klug,
University of Colorado Anschutz Medical Campus, United States

REVIEWED BY
András Bálint,
University of Bern, Switzerland
Geetha Chinnaraj,
All India Institute of Speech and Hearing, India

*CORRESPONDENCE
Lichun Zhang
lichun.zhang@med.uni-rostock.de

RECEIVED 11 January 2025
ACCEPTED 13 February 2025
PUBLISHED 26 February 2025

CITATION
Zhang L, Stauga P, Mißler D, Ehrt K, Großmann W, Mlynski R and Schmidt FH (2025) Electrically evoked mismatch negativity from speech stimuli as an objective measure of cochlear implant performance.
Front. Neurosci. 19:1559141.
doi: 10.3389/fnins.2025.1559141

COPYRIGHT
© 2025 Zhang, Stauga, Mißler, Ehrt, Großmann, Mlynski and Schmidt. This is an open-access article distributed under the terms of the Creative Commons Attribution License (CC BY). The use, distribution or reproduction in other forums is permitted, provided the original author(s) and the copyright owner(s) are credited and that the original publication in this journal is cited, in accordance with accepted academic practice. No use, distribution or reproduction is permitted which does not comply with these terms.

Electrically evoked mismatch negativity from speech stimuli as an objective measure of cochlear implant performance

Lichun Zhang*, Pattric Stauga, David Mißler, Karsten Ehrt, Wilma Großmann, Robert Mlynski and Florian Herrmann Schmidt

Department of Otorhinolaryngology, Head and Neck Surgery, 'Otto Körner', Rostock University Medical Center, Rostock, Germany

Introduction: Cochlear implant (CI) success is often assessed using subjective tests like word recognition scores (WRS). However, these tests are unsuitable for children, non-native speakers, and individuals with cognitive impairments. Mismatch negativity (MMN), an objective measure of cortical auditory processing, offers a promising alternative for evaluating speech perception. This study aimed to assess speech perception in CI patients using MMN and examine its correlation with WRS.

Methods: The study included 23 ears from CI users fitted for at least six months. Speech stimuli were presented via direct audio input to the CI processor at 70 dB nHL using an MMN paradigm. The syllables 'ba' (standard) and 'da' (deviant) served as stimuli. MMN amplitude and latency were analyzed, and their correlation with WRS was examined.

Results: A significant correlation was observed between WRS and MMN responses. CI users with lower WRS scores exhibited reduced MMN amplitudes and prolonged latencies compared to those with higher scores, indicating impaired cortical speech processing.

Discussion: These findings suggest that speech-induced MMN could serve as an objective tool for assessing speech perception in CI users. MMN provides valuable insights for optimizing CI fitting, particularly for patients unable to undergo subjective testing. Integrating MMN into clinical practice could improve speech perception outcomes and enhance the quality of life for CI users.

KEYWORDS

cochlear implantation, mismatch negativity, cortical potentials, word recognition scores, speech perception

1 Introduction

Cochlear implants (CIs) restore hearing by directly stimulating the auditory nerve (Lee et al., 2010; Bruijnzeel et al., 2016; Lonka et al., 2013). Generally, postoperative speech perception outcomes are promising. However, performance varies significantly among users (Lee et al., 2010; Osberger et al., 2000; Garnham et al., 2002). Some patients achieve near-normal speech perception, including musical appreciation, while others can only detect sounds (Won et al., 2010; Fowler et al., 2021).

Currently, the evaluation of postoperative performance is mainly based on behavioral methods such as speech audiometry (Turgeon et al., 2014). However, these tests are not always

suitable for all patients. This is particularly true for patients who are unable to complete behavioral speech testing, such as infants with limited communication abilities or patients with cognitive deficits. Therefore, objective electrophysiological measures might be more appropriate for those patients, as it does not require their attention, cooperation or a certain level of speech and language skills (Turgeon et al., 2014; Wagner et al., 2023; Table 1).

For quite some time, there has been a growing use of objective electrophysiological measurement methods to evaluate the quality of stimulation provided by CI (Zhang et al., 2024a; Grolman et al., 2009). For the objective assessment of speech perception, examining auditory evoked potentials, especially the best derivable early latency responses, is particularly popular (Rocha-Muniz et al., 2012). Although examining the electrically evoked auditory brainstem responses (ABR) can effectively evaluate the peripheral nerves and device functionality, it does not assess the status of the central nervous system (Kileny and Kemink, 1987; Kileny et al., 1994; Shallop et al., 1990). While peripheral processing affects postoperative speech comprehension immediately after CI implantation, central processes dominate the patient's performance within just a few weeks (Zhang et al., 2024b). Highly specific processing of the auditory stimulus, such as temporal changes in loudness, has been associated with late auditory evoked potentials (LAEP), represented by the P1-N1-P2-N2 complex (Schmidt et al., 2020). It is assumed that the spectral processing of the stimulus is distributed across various cortical regions—at least up to N1 (Woods et al., 2009). Spectral interaction processes, such as those occurring in speech, are difficult to assess at this level of processing. A more promising approach involves deriving cortical auditory event-related potentials (cERPs) that reflect cognitive processes, such as mismatch negativity (MMN), as well as more central stages like P300 or N400, though these potentials are linked to more complex processes like attention or semantic incongruence (Hahne et al., 2024) Compared to ABR, MMN, also called the cognitive component, reflects the brain's automatic detection of stimulus differences, representing the auditory discrimination (Näätänen et al., 1978; Näätänen et al., 2017). MMN is elicited using an oddball paradigm, in which a deviant or rare stimulus is presented within a series of homogenous or standard stimuli. When using speech stimuli as standard or deviant, the MMN results can indicate how well-defined, electrically encoded speech parameters are subcortically and cortically discriminated, thereby enhancing the understanding of minimal cues required for processing speech in implant recipients (Näätänen et al., 1978; Näätänen, 1995; Lonka et al., 2004).

To date, several studies have focused on measuring MMN in CI patients and analyzing the relationship between amplitude and latency of these responses and postoperative speech performance (Kraus et al., 1993; Groenen et al., 1996; Wable et al., 2000). The results show a tendency but are not statistically compelling. Kraus et al. (1993) were the first to measure MMN in 9 CI patients. Eight of the subjects were good performers and demonstrated a clear MMN response, whereas the only poor performer did not show an MMN. They concluded that MMN was a useful method for the objective evaluation of CI functions (Kraus et al., 1993). Groenen et al. (1996) recorded MMN in seven CI patients, including three good performers and four poor ones. Group average analysis of the good performers revealed a MMN, whereas that of the poor performers did not (Groenen et al., 1996). Wable et al. (2000) investigated MMN in eight adult CI patients and did not find a relationship between MMN and speech performance (Wable et al., 2000). In 2014, Turgeon et al. analyzed the amplitude and latency of MMN in patients with CIs and found that the amplitude of MMN in normal-hearing patients was significantly larger than that in CI patients with poor performance. However, there was no significant difference between good and poor performers. In terms of MMN latency, the normal-hearing patients had significantly shorter latency compared to CI patients, regardless of their performance. When comparing CI patients with different performance levels, there was no significant difference (Turgeon et al., 2014).

TABLE 1 Overview of inclusion and exclusion criteria for CI participants.

Category	Inclusion criteria	Exclusion criteria
Age	• ≥ 18 years	• < 18 years
CI activation	• ≥ 6 months	• < 6 months
Preoperative hearing status	• Healthy cochlea and auditory nerve at the time of implantation	• Cochlear malformation • Vestibular schwannoma
Implant functionality	• Completely inserted electrode array • Auditory perception at each electrode	• Incomplete insertion
Speech ability	• Consistent word recognition scores	• German as second language • Cognitive impairment • Absence of sound and speech perception

Besides the inconclusive results, as far as we know, all the aforementioned studies have applied stimuli through a free-field system. The free-field system theoretically increases the risk of interference from acoustic preprocessing or the influence of microphone and audio processor characteristics (Turgeon et al., 2014; Kraus et al., 1993; Groenen et al., 1996; Wable et al., 2000). Even though some studies have tried to control the stimulus intensity for the test (Lonka et al., 2013), they could not ensure that the patients remained in one position throughout the entire process. As is known, the recording process takes a long time. If patients move their heads even slightly, the stimulus input will change. To avoid this risk, Wagner et al. (2023) have applied the channel-specific stimuli by directly stimulating each single electrode (Wagner et al., 2023). However, with this method, speech stimuli, cannot be delivered to the patients because the frequency range of speech is electrically coded across multiple channels. The present study aims to determine if MMN can provide an objective measure of postoperative speech perception in patients with CIs for the future applications by delivering the stimuli directly to the CI processor.

2 Materials and methods

The local ethics committee approved this prospective study (A 2023–0012). A written information was provided to the participants of the study group, and their consent given. All personal data were anonymized and de-identified prior to the analysis.

2.1 Subjects

Twenty-three participants who received a cochlear implant by the company Med-EL were included in this prospective study: 11 females and 12 males. Their mean age was 64.8 ± 19.0 years, ranging from 23 to 92 years. Two subjects were implanted bilaterally with a CI. For both

patients, only one ear was randomly selected by the investigator for inclusion in the study. Patients were only included in this study if they had activated their CI for at least 6 months. This criterion was implemented to ensure that patients had acclimated to hearing with their CIs and that the CI processors were optimally adjusted for each patient. At this point, the patients' results in speech recognition tests should no longer significantly change over time (Ma et al., 2023). Exclusion criteria comprised cochlear malformation, incomplete insertion or vestibular schwannoma, as well as noninformative speech tests due to patient age, origin, cognitive impairment or absence of sound and speech perception. The inclusion and exclusion criteria are summarized in Table 1.

Additionally, a control group of 35 normal hearing participants (18 females, 17 males), aged from 21.5 to 28.9, with the mean of 24.1 were enrolled. Totally, there are 53 ears. None of the participants with normal hearing had a history of ear problems or reported subjective hearing loss. Upon recruitment, each participant underwent a physical examination conducted by an ENT consultant. Following this, all participants underwent audiometric testing performed by qualified personnel on both ears using a clinically calibrated audiometer (AT900, Auritec GmbH, Hamburg, Germany). Pure-tone stimuli were presented at frequencies ranging from 0.125 to 8 kHz delivered by using DT48 headphones. Physical examinations confirmed that all participants had normal eardrums and ear canals as observed during otoscopy. Participants were excluded from the study if their hearing threshold in the test ear exceeded 30 dB HL at any frequencies between 0.125 and 8 kHz, or if their average hearing thresholds at 0.25, 0.5, 1, 2, and 4 kHz exceeded 20 dB HL (British Society of Audiology, 2004). Additionally, ears were excluded from the study if they did not exhibit a measurable MMN response in at least one of the two measurement paradigms.

2.2 Speech audiometry

All participants underwent speech audiometric testing in the CI ear using a calibrated clinically audiometer (AT900, Auritec GmbH, Hamburg, Germany). At our clinic, three audiologists with expertise in cochlear implants are responsible for diagnosing CI patients. The measurements were carried out by one of these specialists. Speech recognition was evaluated by measuring the word recognition score (WRS). The test was conducted unilaterally in a quiet environment, with a presentation level set at 65 dB sound pressure level (SPL) in free field. The contralateral ear was masked, if necessary, appropriately through a headphone (DT48; Beyer, Heilbronn, Germany). The speech test signal (Freiburg Monosyllable Test) was presented frontally in a soundproof room (5 × 6 × 2.5 m) Before the test begins, the procedure is explained to the patient. The patient is asked to repeat the word they have understood and is encouraged to make guesses if necessary (Mrowinski and Scholz, 2017). The test comprises 20 lists, each containing 20 words. Two lists are selected and presented to the patient consecutively. If a word is understood correctly, the audiologist records the response. The WRS is calculated by determining the average of the correct answers from both lists. The test takes approximately 4 min to complete.

2.3 Stimulation and recording

Following the experiment conducted by Turgeon et al. (2014), two stimuli 'da' and 'ba' were employed for the MMN paradigm (Turgeon et al., 2014). This selection was based on their finding of the highest correlation between MMN amplitude and speech recognition among cochlear implant (CI) patients for these two syllables. The 'ba' stimulus, serving as the standard, has a duration of 150 ms at a sample rate of 30 kHz. Conversely, the deviant, represented by the 'da' stimulus, also operates at a sample rate of 30 kHz but with a duration of 40 ms. The probability of occurrence for the deviant stimulus was 16%. Both stimuli were presented at a level of 70 dB nHL through calibrated for unshielded insert earphones by a technician from Diatec Diagnostics GmbH, the company responsible for regular clinical maintenance of the ERA system. The stimulus was directly transmitted from the ERA-System to the Sonnet or Sonnet 2 audioprocessor using an audio-in adapter integrated in a specialized battery sleeve from MED-EL (MA070103, Ref. 165,182). To facilitate this, the EA Cable Ext transmission cable (Ref. 04439) was employed to link the Eclipse to the battery sleeve. Nevertheless, the stimulus volume is slightly attenuated to ensure concurrent hearing through the processor microphones. The input mixing ratio via cable and microphone was set at 90% / 10%. For the normal-hearing control group, stimuli were presented acoustically under identical conditions using insert earphones (E-A-RTONE Insert Earphone, 3 M, United States).

The electrophysiological measurements were performed using the Eclipse ERA-system (Interacoustics A/S, Middelfart, Denmark) at a sampling rate of 500 Hz. Active electrodes (Ambu BlueSensor N, Ambu GmbH, Bad Nauheim, Germany) were placed prefrontally on the midline sagittal plane of the skull (Fpz) and on the contralateral mastoids (TP9 and TP10) to avoid the artifact of CI stimulation, while the ground electrode was positioned on the central forehead. To ensure electrode contact, the skin area was prepared with alcohol and conductive gel, maintaining contact impedance less than 3 kΩ. During the recording session, participants were comfortably positioned on an examination bed in a sound isolated room (GTA < 40). They were instructed to minimize blinking as much as possible, to fixate their eyes on a cross positioned on the opposite wall and to keep their neck and shoulder muscles relaxed. The measurement duration of the MMN paradigm is approximately 10 min.

2.4 Data processing and analysis

The online analysis included digital filtering from 1 to 33 Hz. A total of 240 cortical response samples to the standard stimuli and 80 to the deviant stimuli were recorded within a recording window of −85 to 850 ms relative to stimulus onset. The recording session lasted approximately 20 min. All recorded data were imported into MATLAB (Version 2024a, Massachusetts: The MathWorks Inc., United States) for additional offline processing. The samples of the raw data were excluded if they exceeded an artifact threshold of 30 μV in order to minimize eye artifacts. Afterwards, the data were filtered using a second-order butter worth filter design, with a low-pass cutoff at 15 Hz of and a high-pass cutoff at 2 Hz, ensuring zero-phase digital filtering. The baseline was adjusted by subtracting the mean EEG response before stimulus onset, sample by sample. To achieve an optimal signal-to-noise ratio (SNR) during averaging, each epoch was weighted by the inverse of its noise power. To enhance noise estimation, two iterative steps were performed,

utilizing the residual noise from the previous steps (Riedel et al., 2001).

Our study focused on the differences in amplitudes and latencies of the cortical components N1, P2, and MMN. The peak-to-peak amplitude between the N1 and P2 deflections and between the MMN and the peak of the subsequent positive deflection were used. Peak-to-peak amplitudes of the components were extracted by selecting the minimum amplitude for the negative components (N1 and MMN) or the maximum for the positive component (P2, positive deflection subsequent to the MMN), each within physiologically reasonable time windows. The selection of time windows was broadly based on the known latencies observed in normal hearing with acoustic stimulation (Martin et al., 1999). However, it is anticipated that the latencies of the potentials may vary due to hearing loss and the use of electrical stimulation via the audio-in adapter. Consequently, the center and width of the time windows were slightly adjusted based on the measured temporal occurrence of the components in the mean EEG response of the grand average response. The respective time windows were chosen for N1 from 100 to 210 ms, for P2 from 180 to 350 ms, for MMN from 140 to 250 ms and its subsequent positive deflection from 210 to 310 ms. The position of each peak was used as a representation of the latency of the respective cortical component.

Pearson correlation was employed to assess the relationship between the electrophysiological parameters and WRS. Additionally, consistent with the approach by Turgeon et al. (2014), participants were divided into two groups: poor performers and good performers (Turgeon et al., 2014). The WRS served as the discrimination criterion. Participants with a WRS $\leq$ 65% were classified as poor performers, while those with a WRS higher than 65% were categorized as good performers. A Kruskal-Wallis Test was employed to compare amplitudes and latencies of the examined cortical component of these two groups. Additionally, the electrophysiological parameters of the CI group were compared with those of the control group comprising normal-hearing listeners.

2.5 Audio processor settings

The processor settings for each patient were checked immediately before measurement. The noise-reduction algorithms were disabled, and the directional microphone was set to an omnidirectional mode. Below is a brief overview of the standard procedure for configuring CI processors at our clinic. All patients included in this study were fitted following this protocol. The dynamic range of each electrode was assessed using single-channel stimulation. The upper stimulation levels were set to achieve the most comfortable loudness for continuously presented 500 ms bursts. The lower stimulation levels were adjusted to be a large increment of charge below the perception threshold. All patients used the FS4 speech coding strategy at the maximum available stimulation rate. Biphasic pulses with minimal interphase gaps were employed, with triphasic pulses being used only in exceptional cases where secondary facial nerve stimulation occurred at certain electrodes. The frequency range spanned from 70 to 8,500 Hz. The distribution of this frequency range across the bands was logarithmic in all cases, ensuring equal energy distribution for white noise across all bands. A logarithmic characteristic of the dynamic range was applied, with a compression coefficient between 500 and 750.

3 Results

The demographic and audiometric data of the study patients are displayed in Table 2. The word recognition score at 65 dB with CI [WRS65 (CI)] was 65.2% ± 20.0% resulting in 9 poor performers and 14 good performers.

After artifact reduction, the average number of recorded epochs for the standard stimulus was 194, ranging from 100 to 240, and for the deviant stimulus, the average was 59, ranging from 36 to 80. This indicates that 19% of the epochs for the standard stimulus and 26% for the deviant stimulus were excluded due to artifacts.

The epidemiological characteristics of the patients did not exhibit any correlation with WRS or the measures characterizing the cortical components. Examined factors were such as age, sex, and ear side, CI processor, compared with WRS65 (CI) and the amplitudes and latencies of the cortical components (N1 and MMN). No significant correlation was identified between age and either WRS65 (CI), or and the amplitudes and latencies of the cortical components. Similarly, a Mann Whitney U-Test for ear, CI processor and sex characteristics revealed no significant differences.

3.1 Cortical response of the MMN paradigm

The cortical responses of the CI group to the standard stimulus, the deviant, and their difference are illustrated as the Grand Average in Figure 1A. Typical P1, N1, and P2 potentials are discernible for both the standard stimulus and the deviant. Specifically, for the standard stimulus, the N1 deflection peaks at 134 ms and the P2 at 284 ms. Conversely, for the deviant, the N1 peak occurs at 146 ms and the P2 at 268 ms. The MMN is clearly identifiable within the disparity between the cortical responses to the standard and deviant stimuli, with the MMN deflection peaking at 206 ms.

Compared to the control group with normal hearing, as shown in Figure 1B, the cochlear implant (CI) group exhibits delayed latencies and reduced amplitudes of cortical potentials. For the standard stimulus (Figure 2, top), the N1-P2 peak-to-peak amplitude significantly decreases in the CI group ($\chi^2 = 6.27$, $p < 0.001$), and N1 latencies are notably increased ($\chi^2 = 44.88$, $p < 0.001$). A similar pattern is observed in the cortical response to the difference signal between the standard and deviant (Figure 2, bottom), where the MMN peak-to-peak amplitude markedly decreases ($\chi^2 = 35.98$, $p < 0.001$) and MMN latencies are prolonged ($\chi^2 = 26.41$, $p < 0.001$) in the CI group. Additionally, the P300 potential is not measurable in the CI group.

Investigating the relationship between speech performance and electrophysiological parameters, we found a significant correlation between WRS and MMN amplitude ($R = 0.50$, $p = 0.01$), a coefficient of determination of $R^2 = 0.25$, as well as between WRS and MMN latency ($R = -0.44$, $p = 0.036$). When analyzing the latencies and amplitudes of these potentials based on speech performance, a significant reduction in MMN amplitude

10.3389/fnins.2025.1559141

TABLE 2 Summary of participants' demographic and audiometric data.

Subject	Age	Sex	Ear	CI activation [months]	CI processor	WRS_{65}(CI) [%]	others
1	82	m	R	23	Sonnet 2	75	
2	66	m	L	60	Rondo 2	75	converted map
3	27	w	R	10	Sonnet 2	42.5	
4	71	w	R	6	Sonnet 2	77.5	
5	54	w	L	39	Rondo 2	70	converted map
6	23	w	R	94	Sonnet	82.5	
7	56	w	L	83	Sonnet	75	
8	73	m	R	159	Sonnet	95	triphasic
9	60	w	L	101	Sonnet	85	
10	79	m	R	51	Sonnet	82.5	
11	78	m	L	25	Sonnet 2	62.5	
12	69	m	R	141	Sonnet 2	20	
13	75	m	R	74	Sonnet	77.5	
14	92	m	L	84	Sonnet	20	
15	87	w	R	12	Sonnet 2	72.5	
16	53	m	L	13	Sonnet	57.5	
17	52	m	R	29	Sonnet 2	60	
18	57	w	L	48	Rondo 3	62.5	converted map
19	83	m	L	118	Sonnet 2	32.5	
20	82	w	L	7	Sonnet 2	52.5	
21	68	w	R	26	Sonnet 2	82.5	E12 deactivated
22	58	w	L	230	Sonnet	67.5	
23	80	m	R	7	Sonnet 2	72.5	

(Figures 3A,B) was observed in poor performers ($\chi^2 = 7.0$, $p = 0.008$), along with delayed latencies ($\chi^2 = 5.3$, $p = 0.02$). The analysis of the standard stimulus showed no significant correlation between WRS and N1 amplitude or latency, nor any difference between the two groups (Figures 3C,D).

4 Discussion

4.1 Comparison of cortical responses between normal hearing listener and CI patients

Cortical auditory event-related potentials (cERPs) reflect the brains' response to changes in an ongoing stimulus, such as deviant stimuli within a series of frequent stimuli in an oddball paradigm (Tao et al., 2022). Pre-attentive exogenous responses, including P1, N1, P2, N2 peaks, typically occur within the first 250 ms and do not reflect cognitive processing (Polich and Kok, 1995; Kok, 2001). The endogenous potential, P3 (also known as P300), typically presents between 250 and 400 ms and is thought to reflect attention and/or arousal (Polich and Kok, 1995; Kok, 2001). Recording P3 potentials usually requires participants to perform behavior tasks, such as counting deviant stimuli during the test (Tao et al., 2022).

Compared with the normal-hearing listeners (NHs), the CI patients in this study exhibited a similar typical pre-attentive response with P1, N1 and P2, although the amplitudes of these responses were reduced and latencies delayed. There are two potential explanations for the reduced amplitudes and prolonged latencies: (1) There is a technical delay in processing and information loss accompanying with reduced excitation due to the coding of the speech processor in CI devices. Similar concerns have been raised in previous studies, suggesting reduced activity in the central auditory system of CI patients (Farrar et al., 2024); (2) There might be some degree of degeneration in the central nervous system due to both hearing loss and aging. However, it cannot be distinguished between these two potential contributors with this study design. Further research is needed. Similar results were found evaluating the MMN. The amplitudes were reduced and latency delayed in CI patients compared to NHs, which is after all consistent with previous studies (Turgeon et al., 2014; Obuchi et al., 2012). Additionally, a clear endogenous potential, P3, was successfully recorded in NHs without an extra task, but not in the group of CI patients. The recording of the P3 potential in NH without performing any extra tasks is unexpected and differs from findings in previous studies (Tao et al., 2022; Polich, 2007). This might be attributed to the significant spectral and temporal differences between the stimuli 'da' and 'ba' used in this study, which could involuntarily capture participants' attentions (Tervaniemi et al., 1999). However, in CI patients, the P3 is not distinguishable. It might be that the difference between the two stimuli for CI users is reduced by the speech coding of the audio processor and the peripheral cochlear stimulation,

10.3389/fnins.2025.1559141

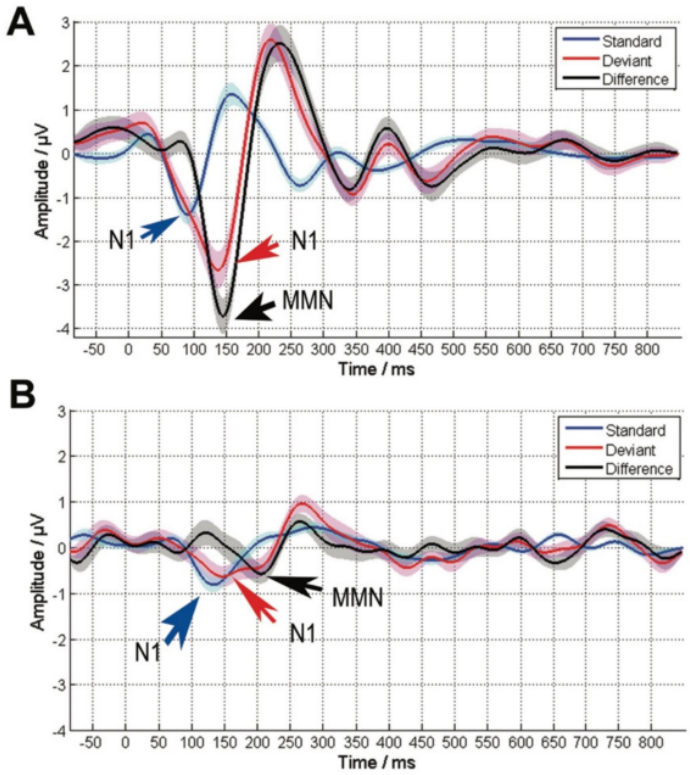


FIGURE 1
The average EEG response to the standard stimulus (blue), the deviant stimulus (red), and the difference between the two stimuli (black) for NH (control) **(A)** and the CI group **(B)**. The solid lines represent the average response, while the shaded area indicating the standard error. The arrows highlight the N1 responses to both the standard and deviant stimuli, as well as the MMN response to their difference. Both the standard and deviant exhibit a similar cortical response, typified by a pronounced N1 peaking between 120 ms and 150 ms, as well as a pronounced P2 with a peak between 250 ms and 300 ms. Nevertheless, the cortical response to the deviant stimulus (red) that includes N1 and P2 deflections is overshadowed by the MMN, which can be distinguished by analyzing the disparity between the standard and deviant (black), with the peak occurring between 140 and 210 ms.

which is than no longer sufficient to reach cortical awareness by the CI patients.

4.2 MMN is correlated to good and poor performance in CI patients

To our knowledge, this is the first study to demonstrate a significant correlation between WRS and MMN, showing that poor performers among CI patients have both significantly smaller MMN amplitudes and delayed latencies compared to good performers. The test duration in this study was just over twice the length of the speech test, which represents a highly efficient ratio for electrophysiological procedures. However, the explained variance by the coefficient of determination of 0.25 is likely insufficient for clinical application, but it provides insights into underlying physiological deficits. This finding might indicate that pre-attentive discrimination may be more severely compromised by long-term deafness in poor CI performers than in good performers. The question arises as to why a similar study by Turgeon in 2014 did not find a difference in MMN amplitude between good and poor CI performers (Turgeon et al., 2014). This discrepancy might be attributed to the considerable variation of implants used in previous investigations. Turgeon et al. included patients with implants from different companies (Turgeon et al., 2014), which likely introduced greater variability in the results. Different companies utilize distinct speech coding strategies, leading to variation in the differentiation between standard and deviant stimuli through their respective speech coding systems, thereby increasing variability in the input to the speech processors. Additionally, electrode designs differ among companies. Varied

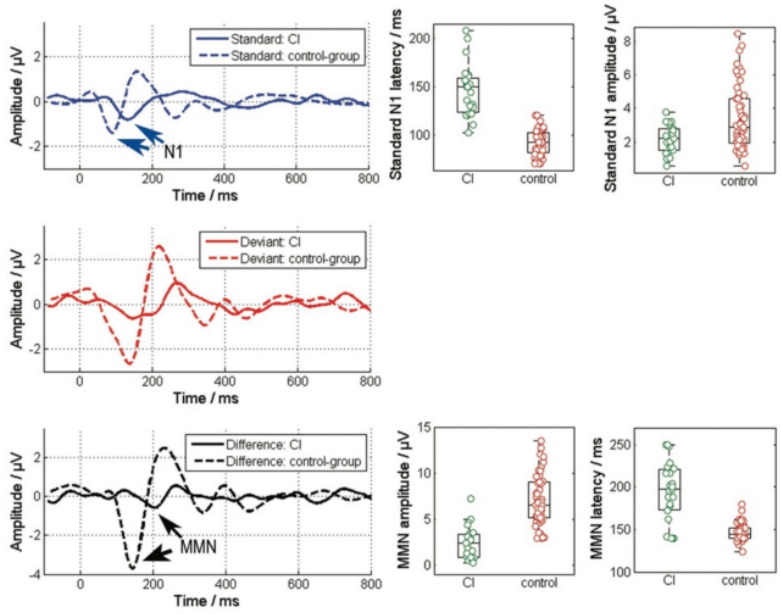


FIGURE 2
Comparison of the responses to the standard (blue), the deviant stimulus and the difference of their responses between the CI group and the control group. The left column depicts the grand average responses, while the right column details the amplitudes and latencies of specific potentials within these EEG responses. The N1 and MMN responses are highlight by the arrows. (Standard: N1-P2 amplitude and N1 peak latency; Difference: MMN amplitude from peak to peak and MMN peak latency).

electrode arrays possess differing numbers of electrodes, lengths and physical spacing, resulting in diverse insertion angles and distances from the modiolus. In particular, the insertion depth of the apical electrodes can vary the most, even with electrode arrays of the same length, due to cochlear anatomy and surgical placement (Schmidt et al., 2024). This variation of peripheral stimulation can lead to individual differences in the perception of fundamental frequencies. These factors have been demonstrated to influence pitch perception, potentially contributing to the absence of significant differences in MMN amplitude observed in their study (Turgeon et al., 2014; Ponton et al., 1997). In the present study, variability was minimized by exclusively enrolling patients with implants from the same company.

In terms of latency of MMN, the previous study has mentioned that the latency of the MMN is less sensitive and is a less appropriate indication of CI speech recognition (Turgeon et al., 2014). However, the current data showed that the latency is significantly delayed in poor performers compared to the good ones, which might suggest that the signal propagation speed in the nervous system significantly changes. This may be an indication that the number of neurons may degenerate during long-term deafness. However, further studies with focus on different factors affecting the above results should be performed in the future.

4.3 Limitations

One of the limitations of this study is that the stimuli used for MMN measurement differ from those used in the word recognition test. Patients might show very well speech recognition while are struggling to differentiate the stimuli from 'da/ba' sounds. This disparity can lead to confusing results. Additionally, the duration between CI activation and the MMN examination varied significantly, which could contribute to variability in the results. When comparing the MMN of the CI group to that of the NH group, differences exist in both hearing status and age. Since MMN morphology changes with age, this factor must be considered. However, finding a NH control group with an age comparable of that of CI patients presents a challenge. Furthermore, the postoperative performance of the subjects varied greatly, ranging from 6 to 230 months. This variability introduced uncertainty in the assessment of postoperative performance. Since we do not know the exact time point at which each patient reaches their best performance after CI activation, and give that every patient has a different adaptation process, the time required to reach peak performance varies for each individual. Lastly, due to the reduced objectivity of evaluation in the CI fitting process, even though the same audiologists performed the fitting process for each patient, variations may still exist among them.

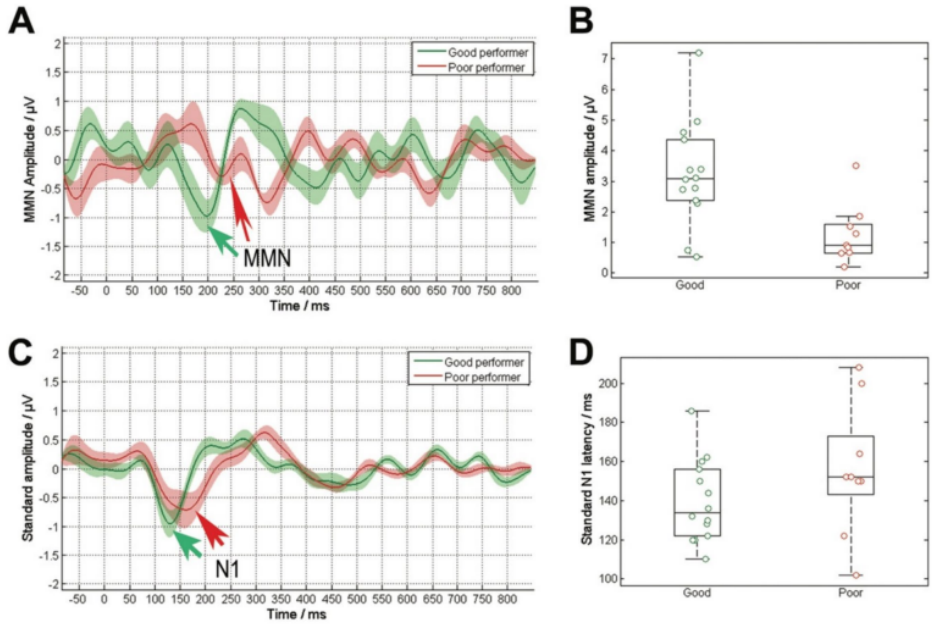


FIGURE 3
Comparison of cortical responses to the deviant stimulus **(A)** and the standard stimulus **(C)**, averaged across the grouped data based on speech comprehension (good performers: WRS ≥ 65%, poor performers: WRS < 65%). The solid lines represent the average response, while the shaded area indicating the standard error. The arrows highlight the N1 responses to both the standard stimuli and the MMN response to their difference. The deviant stimulus exhibited notable discrepancies in the amplitude of the MMN response **(B)**. Poor performers displayed a diminished MMN amplitude. The standard stimulus revealed no significant disparities in N1 latency **(D)**, with delayed latencies observed in poor performers.

5 Conclusion

This study demonstrated that the amplitude of MMN differs between good and poor performers among CI patients. Therefore, it might provide an objective evaluation criterion to differentiate CI performance in the future for clinical use, especially for those patients who are unable to complete behavioral speech testing, such as infants due to poor communication or patients with cognitive deficits.

Data availability statement

The raw data supporting the conclusions of this article will be made available by the authors, without undue reservation.

Ethics statement

The studies involving humans were approved by Medical College University Rostock. The studies were conducted in accordance with the local legislation and institutional requirements. The participants provided their written informed consent to participate in this study.

Author contributions

LZ: Conceptualization, Data curation, Formal analysis, Funding acquisition, Investigation, Methodology, Project administration, Resources, Software, Supervision, Validation, Visualization, Writing – original draft, Writing – review & editing. PS: Data curation, Investigation, Methodology, Writing – review & editing. DM: Data curation, Investigation, Methodology, Writing – review & editing. KE: Data curation, Writing – review & editing. WG: Writing – review & editing. RM: Resources, Supervision, Validation, Writing – review & editing. FS: Conceptualization, Data curation, Formal analysis, Funding acquisition, Investigation, Methodology, Project administration, Resources, Software, Supervision, Validation, Visualization, Writing – original draft, Writing – review & editing.

Funding

The author(s) declare that no financial support was received for the research, authorship, and/or publication of this article.

Acknowledgments

We would like to thank all the participants to take part in the study. We also want to thank MED-EL for providing a specialized battery sleeve (MA070103, Ref. 165182), which made it possible to directly transmit the stimulus from the ERA-System to the Sonnet or Sonnet 2 audio processor.

Conflict of interest

The authors declare that the research was conducted in the absence of any commercial or financial relationships that could be construed as a potential conflict of interest.

Generative AI statement

The authors declare that no Gen AI was used in the creation of this manuscript.

Publisher's note

All claims expressed in this article are solely those of the authors and do not necessarily represent those of their affiliated organizations, or those of the publisher, the editors and the reviewers. Any product that may be evaluated in this article, or claim that may be made by its manufacturer, is not guaranteed or endorsed by the publisher.

References

British Society of Audiology. (2004). Recommended procedure: pure tone air and bone conduction threshold audiometry with and without masking and determination of uncomfortable loudness levels.

Bruijnzeel, H., Draaisma, K., van Grootel, R., Stegeman, I., Topsakal, V., and Grolman, W. (2016). Systematic review on surgical outcomes and hearing preservation for cochlear implantation in children and adults. *Otolaryngol. Head Neck Surg.* 154, 586–596. doi: 10.1177/0194599815627146

Farrar, R., Ashjaei, S., and Arjmandi, M. K. (2024). Speech-evoked cortical activities and speech recognition in adult cochlear implant listeners: a review of functional near-infrared spectroscopy studies. *Exp. Brain Res.* 242, 2509–2530. doi: 10.1007/s00221-024-06921-9

Fowler, S. L., Calhoun, H., and Warner-Cyzy, A. D. (2021). Music perception and speech-in-noise skills of typical hearing and cochlear implant listeners. *Am. J. Audiol.* 30, 170–181. doi: 10.1044/2020_AJA-20-00116

Garnham, C., O'Driscoll, M., Ramsden, R., and Saeed, S. (2002). Speech understanding in noise with a med-El COMBI 40+ cochlear implant using reduced channels sets. *Ear Hear.* 23, 540–552. doi: 10.1097/00003446-200212000-00005

Groenen, P., Snik, A., and van den Broek, P. (1996). On the clinical relevance of mismatch negativity: results from subjects with normal hearing and cochlear implant users. *Audiol Neurotol.* 1, 112–124. doi: 10.1159/000259190

Grolman, W., Maat, A., Verdam, F., Simis, Y., Carelsen, B., Freling, N., et al. (2009). Spread of excitation measurements for the detection of electrode array foldovers: a prospective study comparing 3-dimensional rotational x-ray and intraoperative spread of excitation measurements. *Otol. Neurotol.* 30, 27–33. doi: 10.1097/MAO.0b013e31818f57ab

Hahne, A., Vavatzanidis, N. K., and Zahnert, T. (2024). The EEG N400 component as a marker of language acquisition and processing in cochlear implant users. *Laryngorhinootologie* 103, 252–260. doi: 10.1055/a-2246-2494

Kileny, P. R., and Kemink, J. (1987). Electrically evoked middle-latency auditory potentials in cochlear implant candidates. *Arch. Otolaryngol. Head Neck Surg.* 113, 1072–1077. doi: 10.1001/archotol.1987.01860100050020

Kileny, P. R., Zwolan, T. A., Zimmerman-Phillips, S., and Telian, S. A. (1994). Electrically evoked auditory brain-stem response in pediatric patients with cochlear implants. *Arch. Otolaryngol. Head Neck Surg.* 120, 1083–1090. doi: 10.1001/archotol.1994.01880340029006

Kok, A. (2001). On the utility of P3 amplitude as a measure of processing capacity. *Psychophysiology* 38, 557–577. doi: 10.1017/S0048577201990559

Kraus, N., Micco, A. G., Koch, D. B., McGee, T., Carell, T., Sharma, A., et al. (1993). The mismatch negativity cortical evoked potential elicited by speech in cochlear-implant users. *Hear. Res.* 65, 118–124. doi: 10.1016/0378-5955(93)90206-G

Lee, J., Nadol, J. B. Jr., and Eddington, D. K. (2010). Depth of electrode 287 insertion and postoperative performance in humans with cochlear implants: a histopathologic study. *Audiol. Neurootol.* 15, 323–331. doi: 10.1159/000289571

Lonka, E., Kujala, T., Lehtokoski, A., Johansson, R., Rimmanen, S., Alho, K., et al. (2004). Mismatch negativity brain response as an index of speech perception recovery in cochlear-implant recipients. *Audiol. Neurootol.* 9, 160–162. doi: 10.1159/000077265

Lonka, E., Relander-Syrjänen, K., Johansson, R., Näätänen, R., Alho, K., and Kujala, T. (2013). The mismatch negativity (MMN) brain response to sound frequency changes in adult cochlear implant recipeients: a follow-up study. *Acta Otolaryngol.* 133, 853–857. doi: 10.3109/00016489.2013.780293

Ma, C., Fried, J., Nguyen, S. A., Schvartz-Leyzac, K. C. S., Camposeo, E. L., Meyer, T. A., et al. (2023). Longitudinal speech recognition changes after cochlear implant: systematic review and Meta-analysis. *Laryngoscope* 133, 1014–1024. doi: 10.1002/lary.30354

Martin, B. A., Kurtzberg, D., and Stapells, D. (1999). The effects of decreased audibility produced by high-pass noise masking on N1 and the mismatch negativity to speech sounds /Ba/ and /da/. *J. Speech Lang. Hear. Res.* 42, 271–286. doi: 10.1044/jslhr.4202.271

Mrowinski, D., and Scholz, G. (2017). Audiometrie Eine Anleitung für Die Praktische Hörprüfung. *5th* Edn. Stuttgart, Germany: Georg Thieme Verlag, 58ff.

Näätänen, R. (1995). The mismatch negativity: a powerful tool for cognitive neuroscience. *Ear Hear.* 16, 6–18. doi: 10.1097/00003446-199502000-00002

Näätänen, R., Gaillard, A., and Mäntysalo, S. (1978). Early selective attention effect on evoked potential reinterpreted. *Acta Psychol.* 42, 313–329. doi: 10.1016/0001-6918(78)90006-9

Näätänen, R., Petersen, B., Torppa, R., Lonka, E., and Vuust, P. (2017). The MMN as a viable and objective marker of auditory development in CI users. *Hear. Res.* 353, 57–75. doi: 10.1016/j.heares.2017.07.007

Obuchi, C., Harashima, T., and Shiroma, M. (2012). Auditory evoked potentials under active and passive hearing conditions in adult cochlear implant users. *Clin Exp Otorhinolaryngol.* 5, S6–s9. doi: 10.3342/ceo.2012.5.S1.S6

Osberger, M. J., Fisher, L., and Kalberer, A. (2000). Speech perception results in adults implanted with the CLARION multi-strategy cochlear implants. *Adv. Otorhinolaryngol.* 57, 421–424. doi: 10.1159/000059195

Polich, J. (2007). Update P300: an integrative theory of P3a and P3b. *Clin. Neurophysiol.* 118, 2128–2148. doi: 10.1016/j.clinph.2007.04.019

Polich, J., and Kok, A. (1995). Cognitive and biological determinants of P300: an integrative review. *Biol. Psychiatry* 41, 103–146. doi: 10.1016/0301-0511(95)05130-9

Ponton, C. W., Dong, M., Eggermont, J. J., and Kwong, B. (1997). Integrated mismatch negativity (MMNi): A noise-free representation of evoked responses allowing single-point distribution-free statistical tests. *Electroencephalogr. Clin. Neurophysiol.* 104, 143–150. doi: 10.1016/S0168-5597(97)96104-9

Riedel, H., Granzow, M., and Kollmeier, B. (2001). Single-sweep-based methods to improve the quality of auditory brain stem responses part II: averaging methods. *Zeitschrift für Audiologie.* 40, 62–65.

Rocha-Muniz, C. N., Befi-Lopes, D. M., and Schochat, E. (2012). Investigation of auditory processing disorder and language impairment using the speech-evoked auditory brainstem response. *Hear. Res.* 294, 143–152. doi: 10.1016/j.heares.2012.08.008

Schmidt, F. H., Mauermann, M., and Kollmeier, B. (2020). Neural representation of loudness: cortical evoked potentials in an induced loudness reduction experiment. *Trends Hear.* 24:2331216519900595. doi: 10.1177/2331216519900595 (online ahead of print).

Schmidt, F. H., Zhang, L., Glabasnia, M. W., Schurzig, D., Ehrt, K., Cantré, D., et al. (2024). Systematic overestimation of the angular insertion depth of electrode arrays in Cochlear implantation (CI) patients with small cochlea by imaging processing software. *Otol. Neurotol.* doi: 10.1097/MAO.0000000000004294

Shallop, J. K., Beiter, A. L., Goin, D. W., and Meincke, R. E. (1990). Electrically evoked auditory brain stem responses (EABR) and middle latency responses (EMLR) obtained from patients with the nucleus multichannel cochlear implant. *Ear Hear.* 11, 5–15. doi: 10.1097/00003446-199002000-00004

Tao, D., Zhang, Y., Zhang, W., Xu, M., Galvin, J. J. III, Zhang, D., et al. (2022). The P300 auditory even-related potential may predict segregation of competing speech by bimodal cochlear implant listeners. *Front. Neurosci.* 16:888596. doi: 10.3389/fnins.2022.888596

Tervaniemi, M., Lehtokoski, A., Sinkkonen, J., Virtanen, J., Ilmoniemi, R. J., and Näätänen, R. (1999). Test-retest reliability of mismatch negativity for duration, frequency and intensity change. *Clin. Neurophysiol.* 110, 1388–1393. doi: 10.1016/S1388-2457(99)00108-X

Turgeon, C., Lazzouni, L., Lepore, F., and Ellemberg, D. (2014). An objective auditory measure to assess speech recognition in adult cochlear implant users. *Clin. Neurophysiol.* 125, 827–835. doi: 10.1016/j.clinph.2013.09.035

Wable, J., van den Abbeele, T., Gallego, S., and Frachet, B. (2000). Mismatch negativity: a tool for the assessment of stimuli discrimination in cochlear implant subjects. *Clin Neurophyisol.* 111, 743–751. doi: 10.1016/S1388-2457(99)00298-9

Wagner, L., Ladek, A. S., Plontke, S. K., and Torsten, R. (2023). Electrically evoked mismatch negativity responses to loudness and pitch cues in cochlear implant users. *Sci. Rep.* 13:2413. doi: 10.1038/s41598-023-29422-1

Won, J. H., Drennan, W. R., Kang, R. S., and Rubinstein, J. T. (2010). Psychoacoustic abilities associated with music perception in cochlear implant users. *Ear Hear.* 31, 796–805. doi: 10.1097/AUD.0b013e3181e8b7bd

Woods, D. L., Stecker, G. C., Rinne, T., Herron, T. J., Cate, A. D., Yund, E. W., et al. (2009). Functional maps of human auditory cortex: effects of acoustic features and attention. *PLoS One* 4:e5183. doi: 10.1371/journal.pone.0005183

Zhang, L., Schmidt, F. H., Cantré, D., Brenzel, R., Ehrt, K., Großmann, W., et al. (2024b). The predictive value of preoperative measurements of cochlear nerve diameters from MRT and postoperative speech perception in adult patients with cochlear implant (CI). *Otol Neurotol.* doi: 10.1097/MAO.0000000000004293 (Online ahead of print).

Zhang, L., Schmidt, F. H., Oberhoffner, T., Ehrt, K., Cantré, D., Großmann, W., et al. (2024a). Transimpedance matrix can be used to estimate electrode positions intraoperatively and to monitor their positional changes postoperatively in Cochlear implant patients. *Otol. Neurotol.* 45, e289–e296. doi: 10.1097/MAO.0000000000004145